Development of a Topical Formulation for the Treatment of Basal Cell Carcinoma

Caroline Searby

UMI Number: U571114

Dissertation Publishing

DECLARATION

This work has not previously been submitted in substance for any degree and is not concurrently submitted in candidature for any degree.

Signed.. (candidate)   Date...18-05-2011

STATEMENT 1

This thesis is being submitted in partial fulfilment of the requirements for the degree of PhD.

Signed.. (candidate)   Date..18-05-2011

STATEMENT 2

This thesis is a result of my own independent work/investigation, except where otherwise stated. Other sources are acknowledged by explicit references.

Signed.. (candidate)   Date..18-05-2011

STATEMENT 3

I hereby give consent for my thesis, if accepted, to be available for photocopying and for interlibrary loan, and for the title and the summary to be made available to outside organisations.

Signed.. (candidate)   Date..18-05-2011

Summary of Thesis

There is a need for a topical formulation for invasive forms of Basal cell carcinoma (BCC), a tumour caused by constitutive activation of the Sonic Hedgehog (SHH) signal transduction pathway. It has been shown that the expression of a subset of SHH target genes are augmented by EGF in GLI over-expressing keratinocytes suggesting inhibition of SHH and EGF signalling as potential targets.

Keratinocyte monolayer cultures in the presence of recombinant SHH and EGF were used to determine whether the subset of target genes would be increased when full SHH signalling was activated, a necessary requirement to test SHH inhibitors acting upstream of GLI. Activation of the SHH pathway was not fully achieved. Keratinocytes were therefore co-cultured with fibroblasts to find out if paracrine signalling was needed for SHH signalling induction. When this also did not activate the pathway, scanning electron microscopy was carried out to determine whether keratinocytes cultured under various conditions were capable of forming a primary cilium which is needed for SHH signalling activity. Only in co-cultures where keratinocytes were allowed to stratify at the air:liquid interface were primary cilia induced.

Franz-type diffusion cells were used to probe whether inhibitors to PI3K/AKT and MEK/ERK (LY294002 and PD98059 respectively) arms of the EGF pathway could successfully permeate through full thickness skin, which they were able to do. However, cyclopamine (SHH pathway inhibitor) proved to be highly insoluble and difficult to use in combination.

BCC samples were compared using immunohistochemistry of EGF pathway components to show whether the EGF pathway is important in BCC development in vivo. The results showed variable expression of EGF receptor and p-AKT but p-ERK was virtually absent from BCC tumours.

Despite the ability to modulate SHH signalling, EGF pathway inhibitors targeting p-AKT and p-ERK may not be useful for treating basal cell carcinoma. Alternative SHH signalling inhibitors such as those that target the formation of the primary cilium may be highly effective.

<u>Acknowledgements</u>

Abbreviations

A	Adenine
Ab	Antibody
ACTB/β-actin	Beta-actin
AKT	RAC-alpha serine/threonine-protein kinase
AP-1	Activator protein 1
APRT	Adenine phosphoribosyltransferase
APS	Ammonium persulphate
ARC	Activity-regulated cytoskeleton-associated protein
ARP	Actin-related protein
ATP	Adenosine triphosphate
Arrb2	Arrestin beta 2
BCC	Basal Cell Carcinoma
Bcl-2	B-cell CLL/lymphoma 2
BCN	Basal cell nevus syndrome
BMZ	Basement membrane zone
BPE	Bovine pituitary extract
BSA	Bovine serum albumin
C	Cytosine
cDNA	Complementary deoxyribonucleic acid
c-Jun	Jun proto-oncogene
CL	Companion Layer
CLSM	Confocal laser scanning microscopy
COX-1	Cyclooxygenase-1
COX-2	Cyclooxygenase-2
COXIBS	Cox inhibitors
CTG	Cell titer-glo reagent
DAB	3,3'-diaminobenzidine
DAG	Diacylglycerol
DAPI	4',6-diamidino-2-phenylindole
DF-K	DMEM/Ham's F12 (1:1, v/v)
dH$_2$O	Sterile water
DHA	Decosahexanoic acid
DHH	Desert Hedgehog
Disp	Dispatched
DMEM	Dulbecco's modified eagles medium
DMSO	Dimethyl sulfoxide
DNA	Deoxyribonucleic acid
dNTP	deoxyribonucleotide triphosphate
DP	Dermal Papilla
dPBS	Sterile phosphate buffered saline
DPX	Di-N-Butyle Phthalate in Xylene
dsDNA	Double stranded deoxyribonucleic acid
DTT	Dithiothreitol
ECL	Chemiluminescence reagent
ED50	Effective dosage producing therapeutic response in 50% of subjects
EDTA	Ethylenediaminetetraacetic acid
EGF	Epidermal Growth Factor

EGFR	Epidermal Growth Factor Receptor
EGR-3	Early growth response-3
Elk1	Ets LiKe gene1
EMT	Epithelial mesenchymal transition
EPA	Eicosapentanoic acid
ErbB1	Epidermal growth factor receptor 1
ErbB2-4	HER 2-4
ERK	Extracellular-signal-regulated kinase
FBS	Foetal Bovine serum
Fos	FBJ murine osteosarcoma viral oncogene homolog
FOXE1	Forkhead Box E1
FOXM1	Forkhead Box M1
G	Guanine
G2/M	Protein synthesis and mitosis in cell cycle
G418	Geneticin
GFP	Green Fluorescent Protein
GLI1	Glioma-associated oncogenes homologue 1
GLI2	Glioma-associated oncogenes homologue 2
GLI3	Glioma-associated oncogenes homologue 3
GLIA/GLIact	GLI activated
GLIR	Repressor form of GLI
Grk2	G protein–coupled receptor kinase 2
GSK3β	Glycogen synthase kinase 3 beta
HaCaT	Keratinocyte cell line
HCA2	Fibroblast cell line
HEPES	4-(2-hydroxyethyl)-1-piperazineethanesulfonic acid
HES-1	Hairy and enhancer of split 1
HHBBSS	Hepes modified Hank's balanced buffered salt solution
HH	Hedgehog
HIP	Heparin/Heparan sulphate-binding protein
HPLC	High performance liquid chromatography
HRP	Horseradish peroxidase
HS	Hair shaft
hTERT	Activity limiting component of telomerase enzyme
IFT88	Intraflagella transport protein 88
IgG	Immunoglobulin
IHC	Immunohistochemistry
IHH	Indian Hedgehog
IL1-R2	Interleukin-1 receptor, type II
IP3	Inositol triphosphate
IPTG	Isopropyl β-D-1-thiogalactopyranoside
IRS	Inner root sheath
JAG-2	Jagged 2
JNK	c-Jun N-terminal kinases
JUN	Forms the AP-1 early response transcription factor
K1-K17	Keratins 1- 17
KAPs	Keratin-associated proteins
kDa	Kilo Dalton
KHG	Keratohyalin granules
K-SFM	Keratinocyte serum free medium

LB	Luria-Bertani (broth or medium)
LogP	Lipophilicity
MAPK	Mitogen activated protein kinase
MEK	MAPK/ERK Kinase
MEKK1	Mitogen-activated protein kinase kinase kinase 1
MMP-9	Matrix metalloproteinase 9
mRNA	Messenger ribonucleic acid
n-3 PUFAs	n-3 Polyunsaturated acids
NS	Not significant
NSAIDS	Non-steroidal anti-imflammatory drugs
N/TERT1	Keratinocyte cell line
NTC	No tissue control
OCT	Optimal cutting temperature embedding medium
ORS	Outer root sheath
P16ink4a	Cyclin-dependent kinase inhibitor 2A
P53	Protein 53
PAGE	Polyacrylamide gel electrophoresis
P-AKT	Phosphorylated RAC-alpha serine/threonine-protein kinase
PBS	Phosphate buffered saline
PCR	Polymerase chain reaction
PDGFRα	Platelet-derived growth factor receptor α
PDK1	Pyruvate dehydrogenase kinase isozyme 1
PDVF	Polyvinylidene Fluoride
P-EGFR	Phosphorylated epidermal growth factor
P-ERK	Phosphorylated extracellular-signal-regulated kinase
PGE$_2$	Prostaglandin E2
PI3K	Phophoinositide 3 kinase
PIP	Plasma membrane intrinsic protein
PIP2	Phosphatidylinositol 4, 5-bisphosphate
PIP3	Phosphatidylinositol 3, 4, 5,-triphosphate
PKC	Protein kinase C
PLC	Phospholipase C
P-MAPK	Phosphorylated mitogen activated kinase
P-SHH-NC	Palmitoylated Sonic Hedgehog
PSU	Pilosebaceous unit
PTCH	Patched
PUFAs	Polyunsaturated fatty acids
qPCR	Quantitative Polymerase chain reaction
RAF	Proto-oncogene serine/threonine-protein kinase
Ras	RAt Sarcoma
RNA	Ribonucleic acid
RNAi	Interference ribonucleic acid
Rpm	Revolutions per minute
RT	Room temperature
RT-PCR	Reverse Transcription-Polymerase chain reaction
S	DNA synthesis in cell cycle
S100A7	S100 calcium binding protein A7
SCC	Squamous cell carcinoma
SDS	Sodium dodecyl sulphate
SEM	Scanning electron microscopy

SH2	Src (sarcoma) Homology 2 domain
SHH	Sonic Hedgehog
SHH-NC	Autoprocessed Sonic Hedgehog
shRNA	Small hairpin ribonucleic acid
SMO	Smoothened
S.O.C	Super optimal broth
S-S	Sulfide-sulfide
SUFU	Suppressor of Fused
T	Thymine
T75	75cm culture flask
TAE	Tris base, acetic acid and EDTA
TBST	Tris buffered saline Tween
TEMED	N, N, N', N'-tetramethyllethylenediamine
TF2H	Transcription factor IIH, polypeptide 1
Tris	Tris(hydroxymethyl)aminomethane
TT	Thymidine thymidine
UV	Ultraviolet
WB	Western blot
Wnt	Wingless/MMTV integration site factor
X-Gal	Bromo-chloro-indolyl-galactopyranoside
γ-ray	Gamma-ray

Presentations Arising from this Work

International meetings:

2007   Targets, Drugs and Carriers symposium, Freie Universität, Berlin 31 May – 2 June 2007. Topical delivery of epidermal growth factor signal transduction inhibitors as a novel therapeutic system for basal cell carcinoma (poster).

2008   Skin Forum, School of Pharmacy, University of London, London 25-26 June 2008. Development of a topical formulation for the treatment of basal cell carcinoma (poster).

2010   British Society for Investigative Dermatology, Edinburgh Sonic Hedgehog is not enough to create Basal Cell Carcinoma in vitro (talk).

Cardiff University:

2008   Welsh School of Pharmacy Postgraduate Research Day Development of a topical formulation for the treatment of basal cell carcinoma (poster)

2009   Metabolism, Regeneration & Repair Annual Science Meeting Development of a topical formulation for the treatment of basal cell carcinoma (poster)

2009   Cardiff University Postgraduate Research Day Development of a topical formulation for the treatment of basal cell carcinoma (poster)

2009   Cardiff Institute of Tissue Engineering and Repair Annual Meeting The importance of epithelial-mesenchymal interaction in sonic hedgehog signalling (talk).

2009   Welsh School of Pharmacy Postgraduate Research Day The role of epidermal growth factor signalling in basal cell carcinoma (talk).

Table of Contents

Contents

Table of Tables

Table of Figures

Chapter 1

General Introduction

1. Introduction

1.1 Skin Structure

The skin is a complex organ that protects the body from toxic substances and infection by micro-organisms, maintains its temperature, and regulates water loss (Williams, 2003). It also has immunological functions, protects against UV damage, synthesises vitamin D and is important for attraction and social interactions (Graham-Brown, 2007).

The skin has three main layers (**Figure 1.1**): epidermis, dermis and subcutaneous adipose (Candi et al, 2005). The epidermis and appendages are derived from embryonic ectoderm while the dermis is derived from mesoderm (Graham-Brown, 2007).

1.1.1 Subcutaneous Fat Layer (Hypodermis)

The subcutaneous fat layer is several millimetres thick and separates the skin from the underlying fascia and muscle. It insulates the body, provides physical protection, absorbs shock and stores energy (Graham-Brown, 2007; Young, 2006). It consists of loose connective tissue and adipose cells. It contains major blood vessels and long hair follicles (e.g. scalp) extend into this layer (Graham-Brown, 2007; Young, 2006).

1.1.2 Dermis

The dermis is 3-5mm thick, a major component of the skin and provides bulk and mechanical strength (Young, 2006). It consists of connective tissue made from interlacing fibres embedded in mucopolysaccharides and supports appendage structures such as hair follicles and sebaceous glands. The fibres are constructed from collagen and some elastin, which confer strength and elasticity to this tissue. The dermis is richly supplied with blood vessels, lymphatics, nerves and sensory receptors (Graham-Brown, 2007). The main cell types are fibroblasts (synthesize

2

connective tissue matrix), mast cells (specialised secretory cells) and macrophages (phagocytic cells from bone marrow that scavenge cell debris)
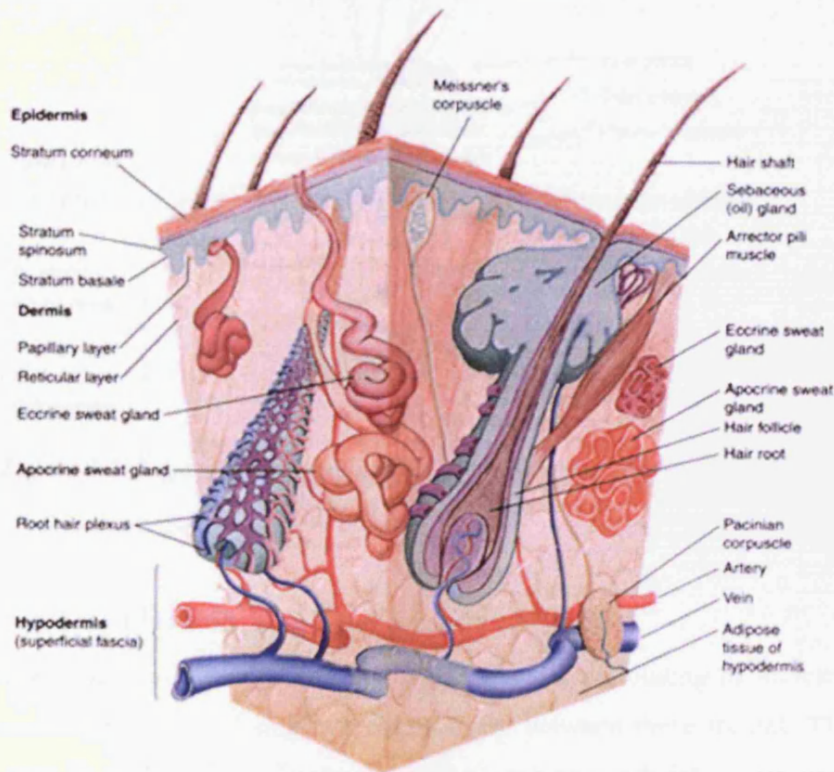
Figure 1.1: The Basic Structure of Skin (adapted from online source: University of Virginia, Cell Biology Handout: Skin, 2004).

1.1.3 Basement Membrane

The basement membrane lies immediately below the basal layer of the epidermis. It is made up of three layers: *lamina lucida, lamina densa* (hemidesmosomes attach to the lamina densa and dermal collagen) and *sublamina densa*. These layers are detailed in **Figure 1.2** (Graham-Brown, 2007).

Intracellular

Intermediate filaments (keratins 5 & 14

Inner plaque

Outer plaque

Plasma membrane

Lamina lucida

Lamina densa

Collagen and laminins

Anchoring fibrils

Sub-basal

Interstitial Collagen

lamina densa

Extracellular
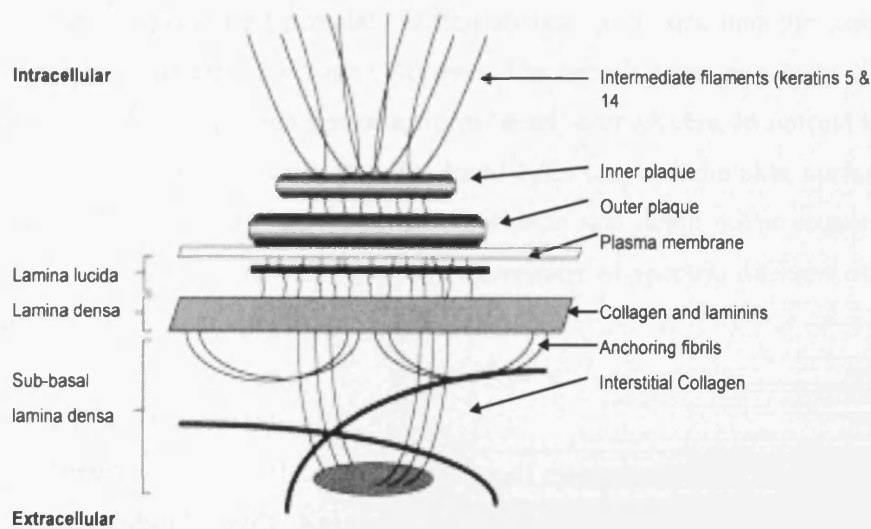
Figure 1.2: Layers of the Basement Membrane (from Nievers et al, 1999).

1.1.4 Epidermis

The epidermal-dermal interface is not flat but undulating to increase the surface area of contact and improve connectivity between these tissues. The dermis has cone-like projections ('dermal papillae') which reach into corresponding slots in the epidermis ('rete ridges') to form two sets of inter-locking cones. The epidermis has four well-defined sub-layers (**Figure 1.3**): *Stratum basale* (or basal layer), *stratum spinosum* (or spinous layer), *stratum granulosum* (or granular layer) and *stratum corneum* (or cornified layer). The thickness of the epidermis differs depending on body site, being thickest on the soles of the feet and palms of the hands (Graham-Brown, 2007). Intercellular adhesion and cohesion are mediated within the epidermis by adherens junctions, which connect the actin cytoskeleton of neighbouring cells together and by desmosomes, which connect keratin-filaments (cytoskeleton) within adjacent cells together to form a continuous network (Candi et al, 2005).

Keratinocytes move upwards from the proliferative basal layer through the spinous layer, where they lose their mitotic activity and alter their gene expression to

4

synthesise specialised proteins. Differentiation continues into the granular layer where the cornified envelope is formed. The cells become anucleate at this stage, lose their organelles and flatten to form 'dead' corneocytes. In normal human skin it takes approximately 30 days for basal cells to reach the skin surface (Young, 2006). Thus, cell proliferation, differentiation and death occur sequentially, and each process is characterised by the expression of specific differentiation-related proteins (Candi et al, 2005).

1.1.4.1 Stratum Basale

The stratum basale is the deepest portion of the epidermis and consists of a single layer of cuboidal cells. Keratinocytes are continuously produced in this layer by sufficient cell division to generate the overlying stratified epithelial strata (Young et al 2006). Basal keratinocytes are anchored to the basement membrane by hemidesmosomes, an interaction mediated by transmembrane proteins such as integrins (Graham-Brown, 2007; Candi et al., 2005; Young, 2006). The intermediate filaments (IF) within epidermal basal cells are formed by polymerisation of two keratin proteins, K5 and K14 in basal cells, which form a three-dimensional network within the cells. Keratins terminate at the hemidesmosome (BMZ surface) and at the desmosome (lateral and apical surfaces). These two keratins also persist as cells move into the suprabasal layers.

MERKel cells (associated with nerve endings in touch sensitive areas) occur on the dermal side of the basement membrane. Langerhans cells are also found in the epidermis and these present antigens to lymphocytes in the draining lymph nodes thus providing the skin with constant immune surveillance (Williams, 2003).

Melanocytes produce melanin in granules (melanosomes), which is transferred to keratinocytes and forms a cap over the nucleus to protect DNA from solar UV radiation. Two types of melanin are present in these granules in order to absorb UV irradiation: a brown/black pigment called eumelanin and a yellow/red pigment called phaeomelanin. Darker and lighter skin types contain the same number of

melanocytes, but darker skinned people have more active melanocytes which produce increased levels of pigment and a higher ratio of eumelanin. However, chronic exposure to sunlight can also induce an increase in melanocytes numbers (Candi et al., 2005; Williams, 2003).
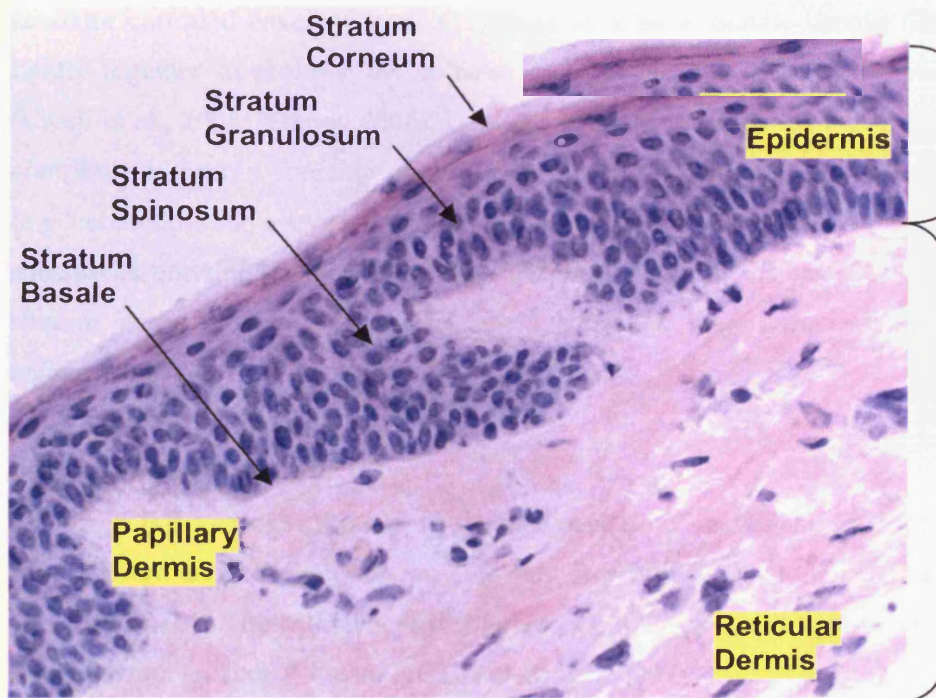
Figure 1.3: Section of Normal Human Skin stained with Haematoxylin and Eosin to Demonstrate the Different Layers and Cell Types.

1.1.4.2 Stratum Spinosum

The spinous or prickle cell layer is so named because of the spiky appearance of the cells, after histology processing. As well as keratinocytes, Langerhans cells are present in the spinous layer and are the first line of immunological defence against environmental antigens. These cells are probably modified macrophages and contain 'Birbeck' granules (Graham-Brown, 2007). Keratin intermediate filaments and desmosomes increase in number in these cells (Young et al., 2006), and the predominant keratins expressed in this layer (K1 and K10) are termed 'differentiation-related'.

6

1.1.4.3 Stratum Granulosum

The stratum granulosum consists of cells which acquire granular structures (keratohyalin and lamellar granules). The layer is so named because the keratohyalin granules (KHG) are visible by light microscopy. There are two types of KHG, F-granules that produce profilaggrin and L-granules that produce loricrin (a major cornified envelope protein). Filaggrin helps to bundle keratin filaments tightly together to promote the collapse of the cell into a flattened corneocyte (Candi et al., 2005; Young, 2006). Lamellar granules (also called Odland bodies) contribute to barrier function of the epidermis by discharging specialised lipids (e.g. ceramides) and enzymes into the spaces between granular cells. This prevents substances entering the tissue through channels between the dead cells of the stratum corneum (Graham-Brown, 2007) and is a major component of the epidermal barrier.

1.1.4.4 Stratum Lucidum

This layer is 3 to 5 cells thick and so-named because of its translucent appearance when viewed under the microscope. It is only present in areas of thick skin such as the soles of feet. The cell nucleus disintegrates in this layer and there is increased keratinisation and cell flattening (Graham-Brown, 2007).

1.1.4.5 Stratum Corneum

The stratum corneum is a horny layer of flattened keratinised cells, with no nuclei or cytoplasmic organelles. The keratin filaments have been cross-linked by formation of disulfide (S-S) bonds and tightly bundled by the action of filaggrin. Transglutaminase (a Ca^{2+} dependent enzyme) covalently links glutamine to lysine in adjacent polypeptides, forming isopeptide cross-links between envelope proteins to provide mechanical strength (Candi et al., 2005; Young, 2006). The cornified cell envelope provides further mechanical strength as well as forming an important part of the essential barrier function (Graham-Brown, 2007). Cells are locked together where adjacent cells overlap their margins and the high lipid content between the cells acts as a permeability barrier (Young, 2006). With

7

general wear and tear, as well as the activity of specialised proteases, the cells are sloughed off the skin surface in an active process called desquamation (Graham-Brown, 2007).

1.1.4.6 Epidermal Appendages

During embryonic development, the epidermis produces appendages by down-growth and specific re-programming of epithelial cells. During this time, molecular signalling between the epidermal cells (keratinocytes) and dermal cells (fibroblasts) is essential. These epithelial-mesenchymal interactions produce three main appendage structures: hair follicle, sebaceous gland and eccrine sweat gland (**Figures 1.4 and 1.5**). This region also contains an area termed the "bulge" that represents a stem cell niche and contains multipotent, slow cycling cells which act as a renewal source for the hair follicle, sebaceous gland and probably the sweat gland. In addition, during wound repair, these cells can also migrate to repopulate damaged epidermis.

The hair follicle is an invagination and down-growth of epidermal keratinocytes. This initially forms the infundibulum and then the outer root sheath (ORS) of the hair follicle. The sebaceous duct branches off the hair follicle below the infundibulum. Epithelial cell down-growth from the epidermis also forms the eccrine sweat gland and duct. Eccrine glands are innervated to regulate body temperature by secreting water containing NaCl to cool the body by evaporation. Apocrine glands in skin produce sweat and open into the hair follicle canal. They are larger than eccrine sweat glands and are only present in certain areas such as the arm pit and groin.

The pilosebaceous unit (PSU) is a term that describes the hair follicle, arrector pili muscle and sebaceous gland, as a single structural entity (**Figures 1.4 and 1.5**). While PSUs are present over most of the body, large PSUs are particularly prevalent on the face, chest and back and PSUs are absent from the hands and feet. The arrector pili muscle is a bundle of smooth muscle fibres, which attaches to the follicle below the sebaceous gland and just beneath the epidermis (BMZ of rete

8

ridges). Contraction produces erection of the hair as experienced during fright. The sebaceous gland discharges an oily secretion (sebum) into the hair follicle via the sebaceous duct, and this coats the hair fibre and skin surface with lipid (Young, 2006). PSU of the face, back and chest only have small vellus hair follicles and principally excrete sebum onto the skin surface.
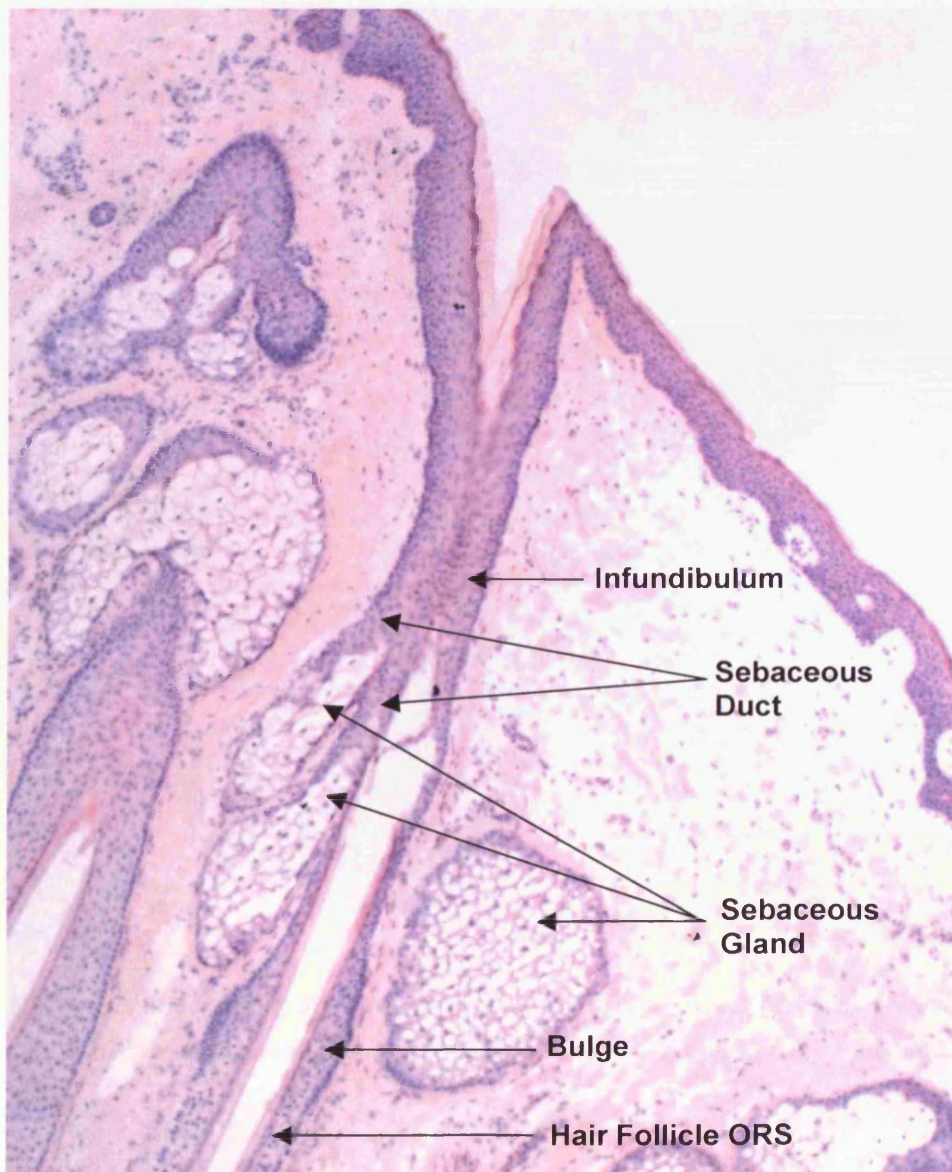
Figure 1.4: Haematoxylin and Eosin Stained Section of Normal Human Skin showing the Infundibulum, Upper Hair Follicle, Sebaceous Glands and Bulge.

9

Internal Root Sheath
Sheath cuticle
Huxley's layer
Henle's layer
External root sheath
Glassy membrane
Root hair plexus
Duct of sebaceous gland
Hair shaft
Hair papilla
Hair Root
Pore
Excretory duct
Myoepithelial cell
Dark cell
Clear cell
Secretory portion
Eccrine Sweat Gland
Sebaceous cell
Sebaceous Gland
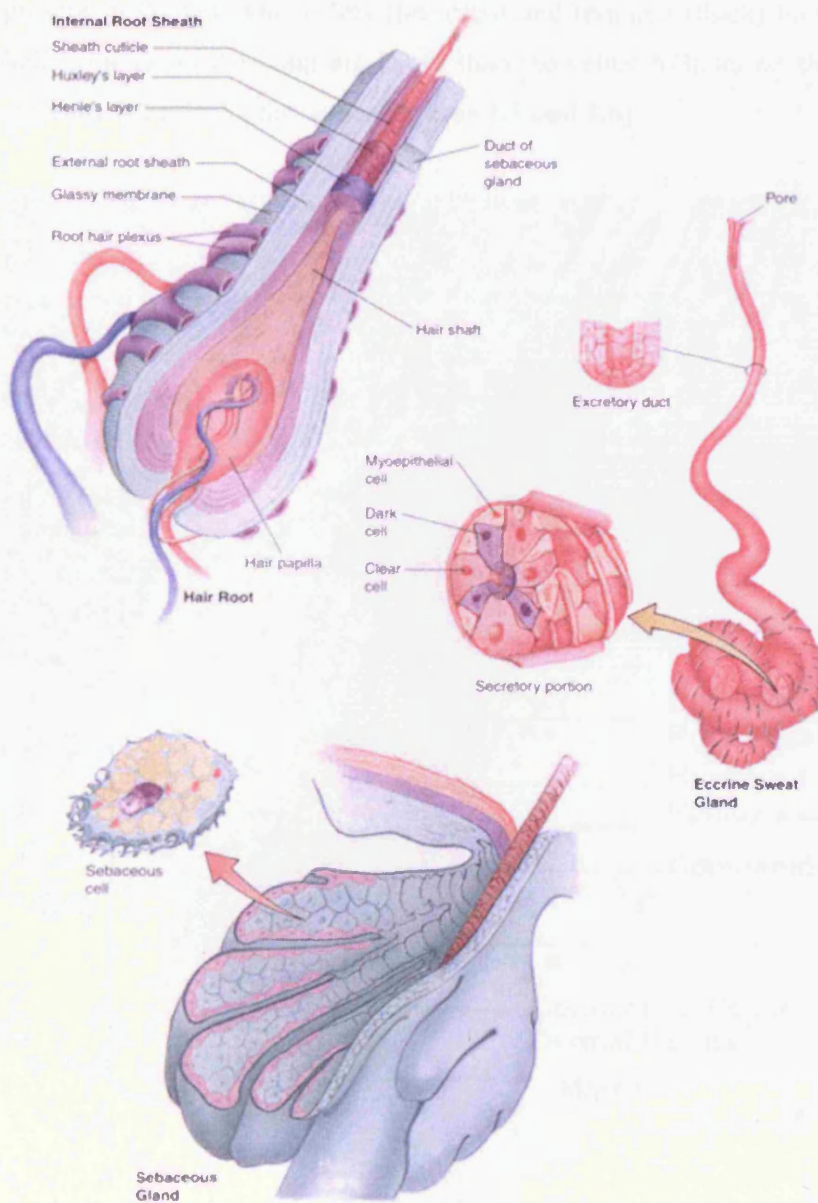
Figure 1.5: Diagrams of the Lower Hair Follicle, Eccrine Sweat Gland and Sebaceous Gland (adapted from online source: University of Virginia, Cell Biology Handout: Skin, 2004).

The hair follicle is continuous with the epidermis and separated from the dermis by a basement membrane and collagen capsule. There are two types of hair follicle

10

present in human skin: vellus (fine) hair and terminal (thick) hair. The terminal hair follicles on the scalp are larger than the vellus follicles on the body but the structure is basically the same (**Figures 1.5 and 1.6**).
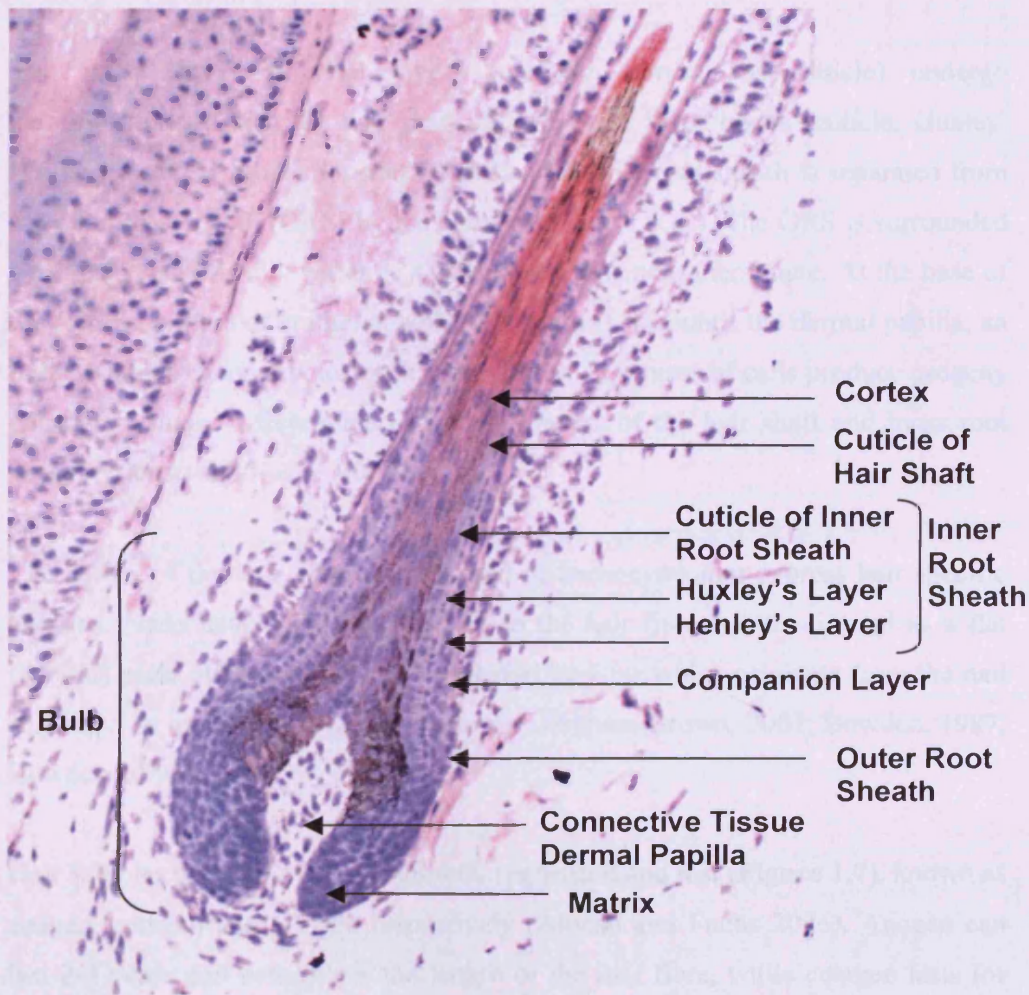
Figure 1.6: Haematoxylin and Eosin Stained Section of Normal Human Skin showing the Lower Hair Follicle.

There are 3 bumps on the original epidermal invagination during appendage formation, which form the sebaceous gland, apocrine sweat gland and bulge. Cells from the bulge produce the entire hair follicle including the hair fibre, inner root sheath (IRS) and companion layer (CL). Cells from the bulge move down the ORS

and populate the bulb matrix region. Epithelial-mesenchymal interactions between the dermal papilla and matrix induce all seven distinct lineages of specialised hair follicle cell layers which all have distinct differentiation programmes and are able to produce the hair fibre and the follicle.

The inner three epithelial layers (medulla, cortex and cuticle) undergo keratinisation to form the hair shaft and the outer three layers (cuticle, Huxley, Henley) form the inner root sheath (IRS). The inner root sheath is separated from the outer root sheath (ORS) by the companion layer (CL). The ORS is surrounded by a glassy membrane, which is a specialised basement membrane. At the base of the follicle, a mass of epithelial cells (hair matrix) surrounds the dermal papilla, an inductive mesenchymal cluster (Young, 2006). This mass of cells produce progeny which terminally differentiate to form all layers of the hair shaft and inner root sheath (Alonso and Fuchs, 2006).

The cortex of the hair fibre is composed of trichocytes that express hair specific keratins. Nails have a similar structure to the hair fibre but are formed as a flat (curved) plate of hair specific and epithelial keratins which originate from the nail fold, also an invagination of the epidermis (Graham-Brown, 2007; Bowden, 1987; Bowden, 1993).

Hair follicles undergo cycles of growth, regression and rest (**Figure 1.7**), known as anagen, catagen and telogen respectively (Alonso and Fuchs 2006). Anagen can last 2-3 years and determines the length of the hair fibre, while catagen lasts for approximately 2-3 weeks and telogen 2-3 months. During the early anagen phase, there is down-growth of the hair follicle and from mid anagen, proliferation in the bulb (matrix) produces the hair shaft (HS), inner root sheath (IRS) and companion layer (CL). The cells of the HS and IRS gain high tensile strength because they are packed with keratin filaments cross-linked to high sulphur matrix proteins (keratin-associated proteins or KAPs). The IRS supports the HS until the upper

follicle is reached where the cells of the IRS degenerate and allow the hair shaft (fibre) to protrude from the skin surface (Alonso and Fuchs, 2006).
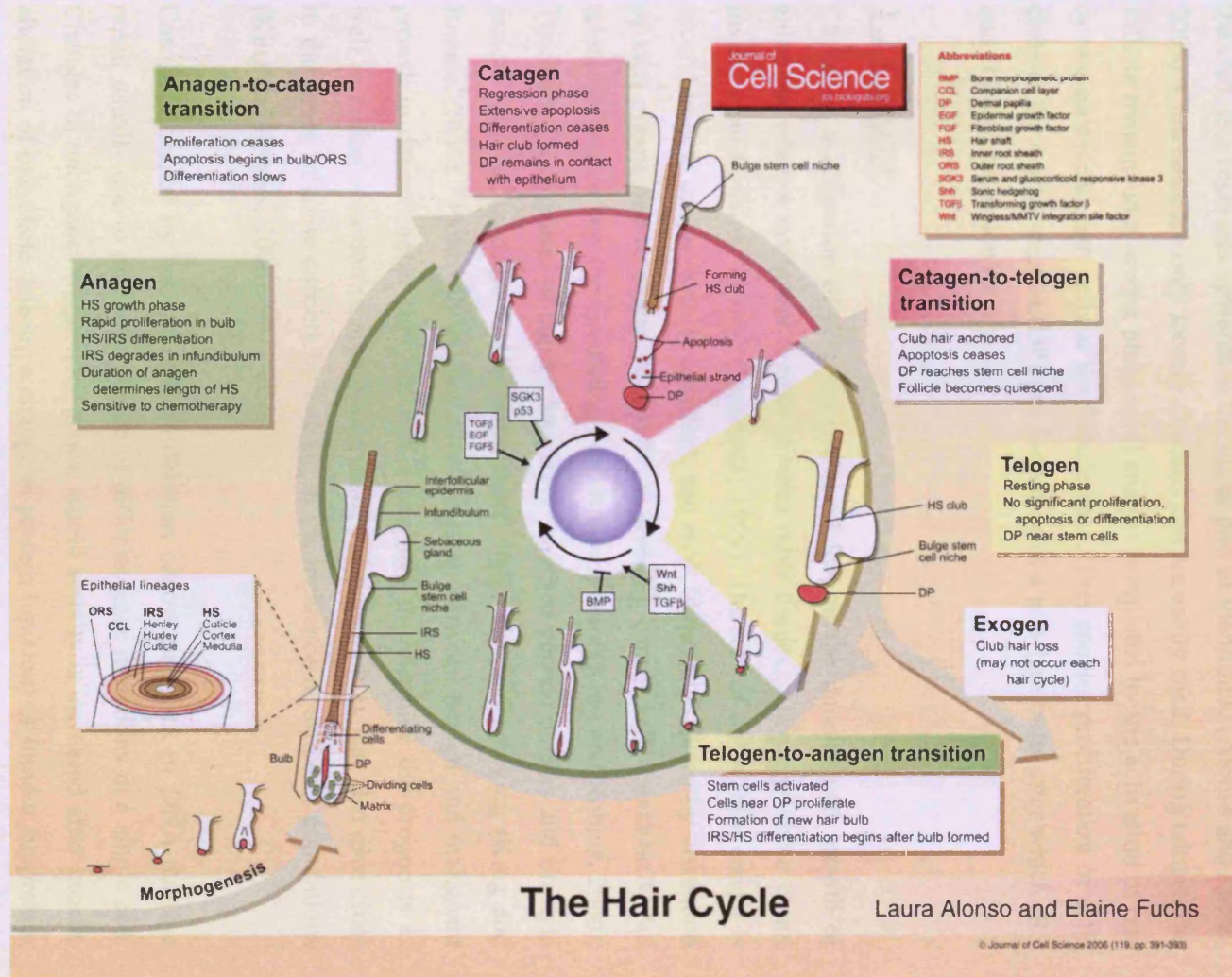
Figure 1.7: Stages of the Hair Cycle (Alonso and Fuchs, 2006)

During catagen, the lower part of the follicle regresses by apoptosis of the ORS and bulb epithelial cells. The bottom of the HS forms a rounded structure called the club, this regresses upwards to the upper part of the follicle (Alonso and Fuchs, 2006). Club hairs are only loosely attached and are easily shed. During telogen the follicle remains in a resting phase until anagen is initiated by the activation of one or two quiescent stem cells at the follicle base. This enables proliferation of cells close to the dermal papilla (DP) and formation of a new hair bulb, after which IRS and HS differentiation returns.

1.2 Cancer

Cancer is a collection of diseases which all feature the unrestrained growth of cells, but while a malignant tumour invades other tissues, a benign tumour is not invasive but remains "*in situ*" (Pasternak, 1999). The rate of death from cancer is second only to cardiovascular disorders, and most frequently caused by disruption of vital organs due to extensive growth of invading cancer cells (metastasis) but release of toxins into the circulation can also contribute (King and Robins, 2006). There are many causes of cancer, including inherited genetic defects and lifestyle factors such as exposure to UV (ultraviolet) light, diet and smoking (King and Robins, 2006). Pathology is used to distinguish between benign and malignant growth to define cancer subtypes which can help to determine the prognosis as well as aiding selection of appropriate therapy. Epidemiology can also give clues to the cause of some cancers by looking at the incidence in different populations (King and Robins, 2006).

Cancer is caused by loss of cell proliferation control and lack of DNA damage repair usually due to an accumulation of different gene mutations in a single cell. Changes in oncogenes (regulatory genes, whose activity is increased after genetic alteration of one allele causing a change in protein function) or tumour suppressor genes (encode inhibitory proteins) are major contributory factors. Thus, in simple terms, mutation of p53 affects the cell cycle check point, allows unrestricted growth of cells which then form a tumour (usually monoclonal in origin). Cancer

14

cells also continue to change their behaviour as they develop due to genetic instability. A tumour cell mass can be influenced by several factors including cell-cell contacts, immune attack, cell death, proliferation, differentiation, blood supply and the extracellular matrix.

1.2.1 Skin Cancers

Skin cancers, are generally classified into malignant melanoma and a collection of non-melanoma skin cancers, including squamous cell carcinoma (SCC) and basal cell carcinoma (BCC). Non-melanoma skin cancers tend to be less aggressive and are rarely lethal. BCC is the most common cancer in Caucasians (90% of all skin cancers indentified) and the major causative factor is UV light (Daya-Grosjean and Couve-Privat, 2005). Other causes include: X-rays, γ-rays, industrial oils, tars, bitumen and soot. UVB damage causes C to T (or CC to TT) structural changes in the DNA of epidermal basal cells (Athar et al., 2006). BCCs are thought to have a deeper origin in skin than SCCs and the most likely cause of this difference is based on wavelength dependent penetration of UV (Lacour, 2002).

Tumorigenesis usually requires an accumulation of changes that often involve more than one gene in a cell. Also, as these changes are usually required in both alleles, tumours are actually quite a rare occurrence, usually developing in later life probably due to accumulated age-related errors in DNA repair and long-term UV exposure. However, the risk is increased if one allele is already changed, such as in patients with Gorlins Syndrome (Basal Cell Nevus Syndrome) who are born with a mutation in one allele of either the patched (PTCH) or smoothened (SMO) gene. There is also a predisposition for those with some genetic conditions that affect repair mechanisms, such as xeroderma pigmentosm (an autosomal recessive genetic disorder of DNA repair in which the body's normal ability to remove damage caused by UV light is deficient) or in immunosuppressed individuals because the immune system normally removes defective cells (Graham-Brown, 2007).

While it is unusual for mutations in a single gene to cause a tumour, in the case of BCCs, homozygous mutations in PTCH, or occasionally SMO genes are sufficient to cause tumorigenesis, making BCCs a common tumour. Additional mutations may also occur (in p53 for example) but these are thought to affect tumour aggressiveness and growth patterns rather than initiating tumorigenesis.

1.2.2 Basal Cell Carcinoma

BCCs are malignant but not generally metastatic and often referred to as carcinoma *in situ*. They generally grow slowly, but can be unpleasant for the patient if not removed, because they can grow very large and may bleed (Daya-Grosjean and Couve-Privat, 2005). The incidence increases with age and most patients are over 50 years old when referred (Bastiaens et al., 1998).

There are 3 broad categories of BCC: nodular, morpheaform and superficial. Nodular lesions on the skin surface (60% of cases) appear smooth, round and waxy. The surrounding skin is thin, bleeds easily and lesions are generally slightly raised, red and ulcerated with a pearly border (**Figure 1.8A**). The histology of these tumours shows that they grow into a nodular morphology pushing down into the dermis (**Figure 1.8D**). Morpheaform BCCs (30% of cases) are fast growing and appear flat, shiny, and yellow on the surface (**Figure 1.8B**). Histology shows they extend deep into the skin with tiny root like projections (**Figure 1.8E**). Superficial BCCs (10% of cases) appear as a red mark on the skin surface (**Figure 1.8C**) and histology shows only superficial growth along the basement membrane (**Figure 1.8F**). Superficial BCCs are the most accessible to topical treatment.
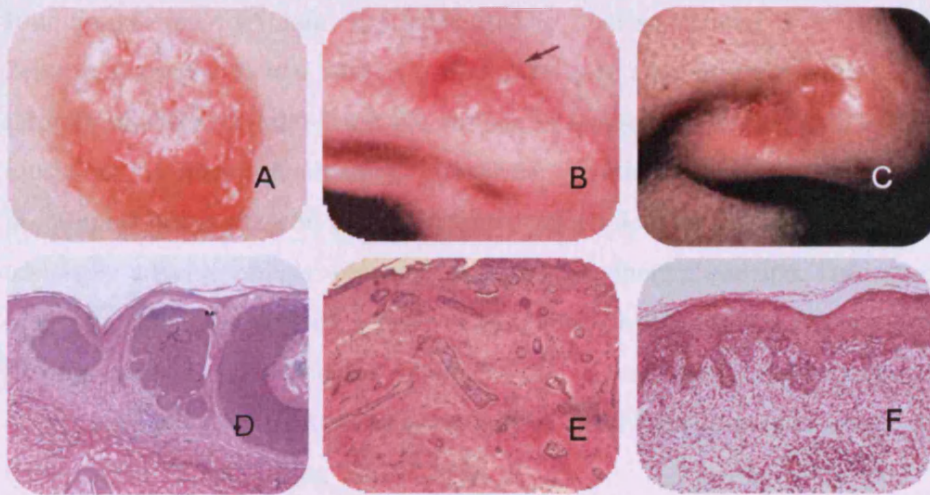
Figure 1.8: Three Broad Categories of Basal Cell Carcinoma (Nodular, Morpheaform and Superficial). Clinical appearance of BCC (A-C) and typical histology after staining with haematoxylin and eosin (D-F). Nodular BCC (A, D), morpheaform BCC (B, E) and superficial BCC (C, F). (Data from online sources:aafp, 2004; skin cancer guide, 2004; treat skin cancer: basal cell carcinoma, 2004; emedicine: Medscape: Basal Cell Carcinoma, 2004; Loyola University: Strith School of Medicine: Med Dean, 2004)

1.2.3 Surgical Treatment of BCC

Surgery is often the treatment of preference in order to remove the tumour prior to further growth. However, this leads to scarring, is inconvenient to the patient, and costly in terms of health care professional time and equipment requirements.

1.2.4 Drug Therapy

A topical formulation would be useful for treating BCCs on areas of skin where surgery is not advised (e.g. eyelids or close to the ear), for reducing the size of large tumours prior to excision, and to prevent tumour recurrence (possibly caused by altered stem cells that remain after surgery). A major benefit of topical formulations is that they are specific to the area of application and therefore any side effects caused by the drugs will be localised.

17

Imiquimod cream (Aldara) has been used to treat superficial BCCs of less than 2cm in diameter (Vidal and Alomar, 2004). It activates the immune system through toll-like receptor 7 (on the surface of antigen presenting cells), leading to secretion of pro-inflammatory cytokines. Clinical trials have shown that imiquimod is too toxic to be the treatment of choice, as it causes unpleasant but transitory adverse effects: erosion, ulceration, erythema, oedema, flaking/scaling, scabbing and inflammation (Quirk et al., 2006). Imiquimod is not indicated for treating nodular or morpheaform subtypes due to recurrence of these tumour types at the same site after treatment, which may be partly due to inadequate delivery to these deeper BCCs (Chang et al., 2005).

1.3 Sonic Hedgehog (SHH) Signal Transduction Pathway and Mutations in BCC Lesions

1.3.1 Sonic Hedgehog (SHH)

Sonic hedgehog is required for embryonic development of hair follicles (Sato et al., 1999) and postnatally for development beyond the germ stage of hair follicle morphogenesis (Chiang et al., 1999). The anagen phase of hair follicle cycling is induced by SHH (Paladini et al., 2005; Sato et al., 1999) and studies suggest that SHH responsiveness is restricted to the growth phase (anagen) in mouse hair follicles (Oro and Higgins, 2003).

Epidermis derived SHH functions as a paracrine signal regulating development of the mesenchymal component of the hair follicle (Chiang et al., 1999). It has also been suggested that SHH signals the epithelial cells of developing follicles, as it is required for the initial down-growth of epidermal keratinocytes (Chiang et al., 1999; St-Jacques et al., 1998).

Hedgehog (HH) is a protein originally identified in drosophila development and so named because *D. melanogaster* embryos develop as prickly round shapes

18

(resembling a hedgehog) when HH signalling is lost (Nusslein-Volhard and Wieschaus, 1980). Drosophila is a model organism which has been used to identify many developmental genes including Notch and Wnt. It is particularly useful for genetic experiments because it has a short reproductive cycle and is easy to handle in the laboratory (Hausman, 2004). There are three homologues of hedgehog in humans (Ingham and McMahon, 2001): Sonic Hedgehog (SHH), Indian Hedgehog (IHH) and Desert Hedgehog (DHH). Holoprosencephaly is a phenotype which arises from mutations that affect SHH signalling, producing a phenotype of close set eyes with a common scleral rim. Sonic the Hedgehog, a computer game character, also has these characteristics which led to the gene being named after him.

The hedgehog signalling pathway is essential during embryonic development, but is switched off in most adult tissues (Athar et al., 2006). However, SHH maintains stem cell populations and regulates the growth of hair follicles and sebaceous glands in adults (Athar et al., 2006). SHH is needed for down-growth of the epidermis and morphogenesis of the hair follicle (St-Jacques et al., 1998). SHH is also very important for other aspects of embryogenesis, including neural tube patterning, formation of the adjacent ventral somites, development of left-right symmetry, polarising activity in the limbs as well as morphogenesis of the axial skeleton, limbs, lungs, skin, hair and teeth (Athar et al., 2006). In the adult, SHH is also required for hair growth and is expressed in the hair follicle during the anagen (growth) phase (Chiang et al., 1999).

SHH is a 45kDa protein, which induces epidermal hyperplasia and keratinocyte proliferation when it is over-expressed. Importantly, SHH signalling is also activated in many neoplasms. Cells with mutations in PTCH or over-expression of SHH cannot leave the S and G2/M phases of the cell cycle, so proliferation is sustained (Athar et al., 2006).

19

Transport of active hedgehog from the signalling cell to the responding cell occurs in three steps (**Figure 1.9**). First is the formation of a soluble multimeric hedgehog complex, second is the release of the lipid anchored protein from the signalling cell by the enzyme dispatched (Disp) and finally, Tout-velu-dependent synthesis of heparin sulphate proteoglycan enables movement across the plasma membrane of the responding cell (Burke et al., 1999; Zeng et al., 2001). The active hedgehog ligand is double lipid modified with a C-terminal cholesterol moiety and an N-terminal palmitate, which results in activation of the signalling portion, after which the SHH-C terminal portion can diffuse away (Porter et al., 1996).
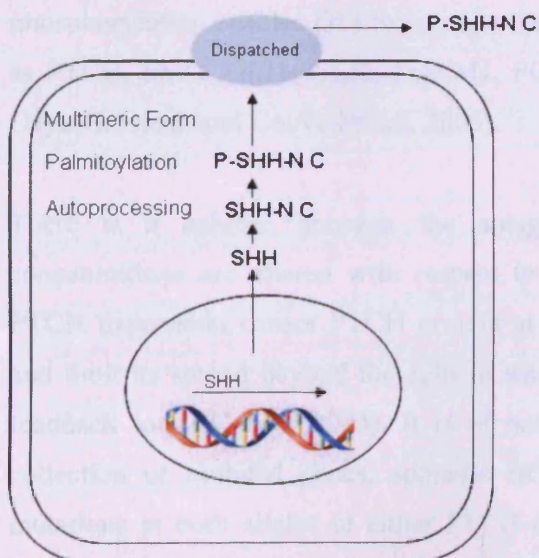
Figure 1.9: Autoprocessing Reaction of Sonic Hedgehog in a Signalling Cell. When SHH is released from the signalling cell by dispatched, it travels along the plasma membrane and interacts with proteins such as PTCH on a responding cell.

In the absence of SHH, patched (PTCH), a 12-pass transmembrane protein located at the cell surface inhibits smoothened (SMO), a 7-pass transmembrane protein located in intracellular endosomes. Once pathway activation occurs, then SMO can move to the cell surface membrane and initiate signalling.

When the SHH ligand binds to its receptor (PTCH), the receptor is internalised and destabilised causing activation of smoothened (SMO). SMO translocates to the plasma membrane and activates GLI zinc finger transcription factors via other signalling proteins such as Suppressor of Fused (SUFU) causing their translocation to the nucleus (**Figures 1.10 and 1.11**).

Mammalian cell culture experiments showed that phosphorylation by Grk2 causes internalisation of SMO and this also involves Arrb2. GLI is maintained in its repressor form by direct binding of SUFU (suppressor of fused), a tumour suppressor (Pearse et al., 1999; Stone et al., 1999). GLI activation by phosphorylation enables GLI to regulate the expression of SHH target genes such as PTCH, SMO, GLI1, GLI2, FOXM1, FOXE1 and HIP (Huangfu et al., 2003; Daya-Grosjean and Couve-Privat, 2005).

There is a balance between the antagonism of SHH and PTCH. Their concentrations are altered with respect to each other because up-regulation of PTCH expression causes PTCH protein at the cell membrane to sequester SHH and limit its spread beyond the cells in which it is produced, creating a negative feedback loop (Cohen, 2003). It is of note that where most cancers require a collection of mutated genes, sporadic BCCs can be induced by homozygous mutations in both alleles of either PTCH or SMO and extremely rarely, SUFU, which is downstream of SMO (Reifenberger et al., 2005).

1.3.2 Hedgehog Signalling Defects in Gorlins (BCN) Syndrome

Aberrant hedgehog signalling was first discovered to be the underlying cause of BCC due to a study of Gorlin's or Basal Cell Nevus (BCN) Syndrome (Hahn et al., 1996; Johnson et al., 1996).
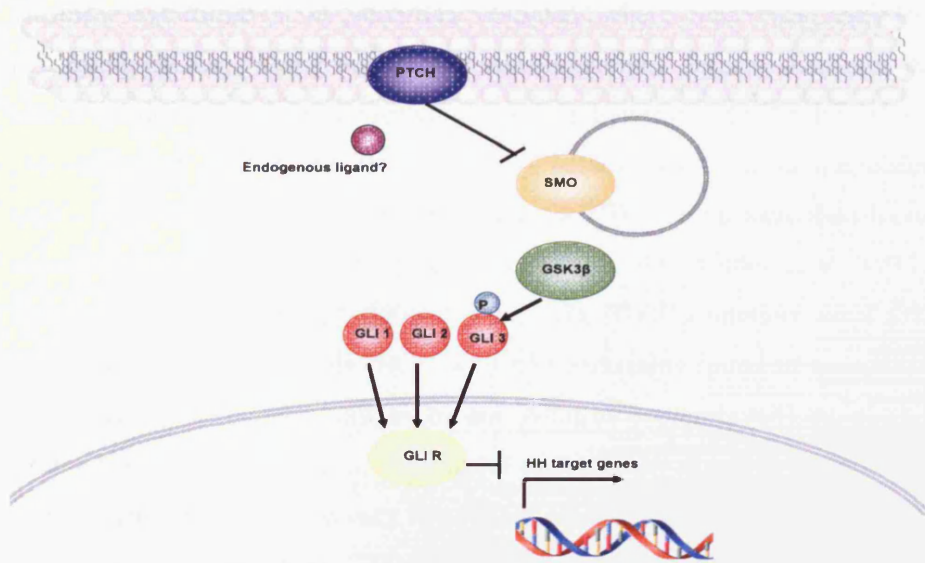
Figure 1.10: Sonic Hedgehog Signalling Pathway in the Absence of Sonic Hedgehog
(GLIR is the repressor form of GLI).
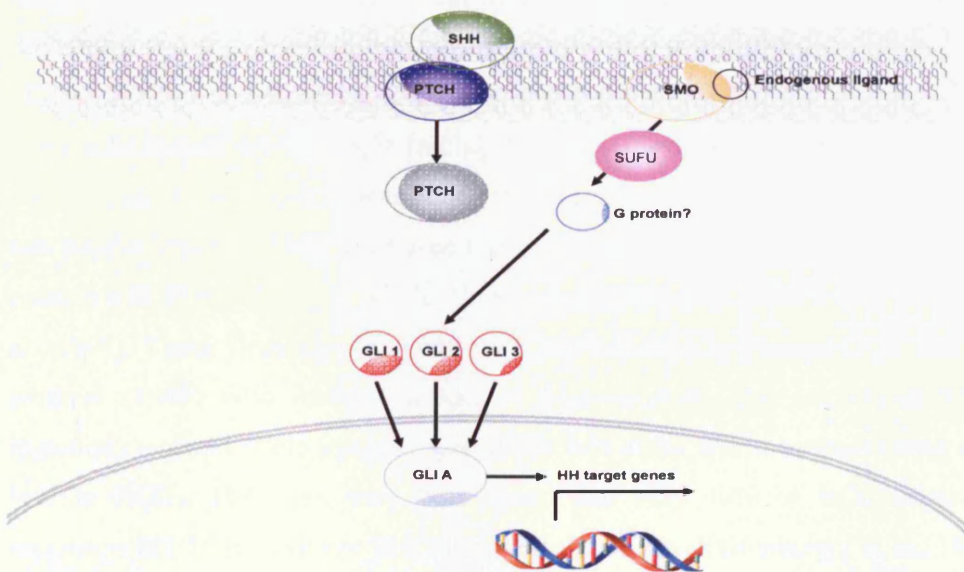
Figure 1.11: Sonic Hedgehog Signalling Pathway in the Presence of Sonic Hedgehog
(GLI A is the active form of GLI).

Gorlin's Syndrome is an inherited disorder, where numerous tumours occur (including BCCs), along with other developmental defects. Linkage mapping narrowed down the gene underlying Gorlin's Syndrome to the PTCH locus on chromosome 9 (9q22) and frequent loss of heterozygosity at 9q was observed in BCCs from Gorlin's patients. Mutations in the PTCH gene were then found to be associated with sporadic BCCs (Gailani and Bale, 1997; Unden et al., 1996; Daya-Grosjean and Couve-Privat, 2005; Lupi, 2007). PTCH mutations were present in both hereditary and sporadic BCC with p53 mutations found in all sporadic and nearly half of hereditary tumours by one group of researchers (Ling et al., 2001). Mutations in p53 are generally correlated with tumour aggressiveness but findings in BCC vary and there are very few recent publications, so the role of p53 is still not clear (Ansarin et al., 2006). Gailani and co-workers (1996) agreed that inactivation of PTCH is probably a necessary step in BCC development. Northern blots and RNA *in situ* hybridization showed that PTCH was expressed at high levels in tumour cells but not in normal skin, suggesting that mutational inactivation of the gene leads to over-expression of a mutant transcript owing to the failure of a negative feedback mechanism (Gailani et al., 1996).

Mutations caused by UV light leading to BCCs may vary within the PTCH or SMO genes. Unden and colleagues (1996) found different types of mutations in one patient's BCCs. They later used fine mapping to identify a region that might contain PTCH mutations to within 1Mb at 9q22.3 (Unden et al., 1996; Unden et al., 1997). These findings were confirmed and extended by Reifenberger and co-workers (1998) who found that loss of heterozygosity due to various SMO mutations (second allele lost, the loss of the first allele was inherited) could also lead to BCCs. However, they later found that only 40% of BCC causative mutations in PTCH, SMO or SUFU had UV signatures (Reifenberger et al., 1998; Reifenberger et al., 2005). Another research group also found various UV signature mutations for PTCH and p53 in BCCs (Soehnge et al., 1997). Allelic loss was frequently found in sporadic BCCs, suggesting that factors other than UVB may be a cause. Only one third of BCCs demonstrating allelic loss also had a

mutation likely to be caused by UVB in the remaining allele, inferring that other factors are probably involved (Gailani and Bale., 1997; Daya-Grosjean and Couve-Privat, 2005).

SHH signalling was shown to be hyper-activated in sporadically occurring BCCs that had high levels of GLI1 and PTCH mRNA in tumour cells (Dahmane et al., 1997; Unden et al., 1997). Sonic hedgehog pathway activation can also cause BCC formation in mouse models and epithelial cell down-growth in organotypic cultures using HaCaT cells (Bigelow et al., 2005; Daya-Grosjean and Couve-Privat, 2005). Over-expression of SHH in normal human keratinocytes was enough to induce BCC-like features in regenerated murine skin transgenic for long terminal repeat-driven SHH on immune-deficient mice (Oro et al., 1997). Furthermore, the lack of collective mutations could explain the lack of aggressiveness, slow growth, and lack of metastases in BCCs (Fan et al., 1999).

GLI accumulation was observed in induced murine BCCs, but GLI destruction signals were also identified and removal of these signals enabled increased tumour formation (Nilsson et al., 2000; Huntzicker et al., 2006). GLI2 over-expression in transgenic mice under the control of a bovine K5 promoter (active in basal layer and hair follicle outer root sheath keratinocytes) led to multiple skin tumours, many resembling BCCs. There was also up-regulation of SHH target genes (Grachtchouk et al., 2000) and together these results showed that the expression of GLI transcription factors due to active SHH signalling was required for BCC tumour formation.

PTCH and SMO mutations have also been shown to cause BCCs in xeroderma pigmentosum patients (Bodak et al., 1999; Couvet-Privat et al., 2002; Daya-Grosjean, 2000). These patients have a high rate of BCCs due to their inability to repair UV-associated DNA damage. Activating mutations in SHH (leading to activation of the SHH signalling pathway) may also cause these BCCs (Couve-Privat, 2004; Daya-Grosjean and Couve-Privat, 2005). However, it has been

shown that activation of SHH occurs very rarely in sporadic tumours, while deactivation of PTCH is extremely common (Teh et al., 2005).

1.3.3 SHH Signalling in the Hair Follicle

The role of SHH pathway signalling is well established in the hair follicle, not just during morphogenesis but also in the adult. Hair follicle induction is independent of SHH, but SHH is essential for down-growth of epidermal cells and consequently for morphogenesis of the hair shaft (Hutchin et al., 2005). In adults, SHH is expressed in the matrix and the developing germ, and cyclopamine (SHH pathway inhibitor) blocks cyclic regeneration of hair (Blanpain and Fuchs, 2006; Silva-Vargas et al., 2005).

In GLI2$^{-/-}$ mice, hair follicle development was arrested, while upon GLI2 activation in transgenic rescue experiments, hair follicles developed, showing that hair follicle down-growth requires GLI2, a SHH pathway effector. GLI2 was shown to be effective only when constitutively expressed in SHH$^{-/-}$ skin, otherwise no hair follicles would develop (Mill et al., 2003). SHH$^{-/-}$ and control embryos showed epidermal placodes and associated dermal condensates but further hair follicle development did not occur. In addition, PTCH and GLI1 expression were also reduced but interestingly late-stage follicle differentiation markers were detected in SHH$^{-/-}$ skin grafts, as well as cultured vibrissa explants treated with cyclopamine which would effectively block SHH signalling (Chiang et al. 1999). Furthermore, anti-hedgehog monoclonal antibody treatment caused a hairless phenotype in mice (Wang et al. 2000).

1.3.4 Origins of BCC

Many researchers believe that BCCs originate from hair follicles. The expression of hair follicle stem cell markers in human BCCs led to the idea that BCCs could be derived from the undifferentiated outer root sheath (ORS) cells of the hair follicle (Reis-Filho et al., 2002). SHH and PTCH mRNA accumulate in follicular, but not in interfollicular skin in normal mice, supporting the argument for BCCs

originating in the hair follicle. Further support for this idea has come from examining SHH expression in hair placodes of embryonic skin and finding that SHH promotes interfollicular basal cell proliferation and hair follicle down-growth (Adolphe et al., 2004; St-Jacques et al., 1998).

It has been suggested that epithelial-mesenchymal interactions are required for the development of epithelial invaginations, as seen in hair follicles and BCCs (Hardy et al., 1992; Schmidt Ullrich and Paus., 2005). Mice conditionally over-expressing GLI2 gave rise to BCCs, but nearly all of these were derived from hair follicles and not interfollicular epidermis as judged by haematoxylin and eosin staining and K17 immunocytochemistry. *In situ* hybridisation for K15 (a marker of undifferentiated follicular epithelium, including stem cells, in adult mice) showed high expression in early tumours located close to a hair follicle but decreased as the tumours grew larger. Once GLI2 expression was removed and tumour cells had regressed, an inductive mesenchyme led to hair follicle formation (Hutchin et al., 2005). This shows a close relationship between SHH signalling in both hair follicles and BCCs. PTCH, SMO, GLI1-3 are all expressed in mesenchymal cells, and interactions involving the SHH pathway between the epithelium and the mesenchyme which are important for down-growth of the hair follicle, may also be necessary for BCC down-growth (Millar, 2002). In mice expressing GLI2, nearly all BCCs arose from hair follicles demonstrating that BCCs are likely to be caused by aberrant follicle organogenesis (Hutchin et al., 2005).

GLI2 also regulates the expression of cyclins D1 and D2 (required for cell cycle progression and interaction with tumour suppressor proteins), which may be involved in tumour progression (Mill, 2003). However, Silva-Vargas and co-workers (2005) showed that interfollicular epidermal cells can acquire characteristics similar to those of bulge stem cells by using β-catenin and SHH expression gradients to induce hair follicle formation (Silva-Vargas et al., 2005).

There are still discrepancies concerning which part of the hair follicle may be the origin of BCCs. Researchers have shown that BCCs may originate from undifferentiated cells of the outer root sheath. Hutchin and colleagues (2005) found that they can arise from follicular ORS epithelium in the proximal hair follicle, leading them to believe that 'BCCs represent an aberrant form of follicle organogenesis'. They found that when conditionally expressing GLI2 in mice, nearly all BCCs arose from hair follicles (Hutchin et al., 2005). A separate group used $GliΔD_N$ (mutant GLI responsive promoter) transgenic mice to show that small BCC-like proliferations developed which appeared to come directly off the hair follicle (Huntzicker et al., 2006). Over-expression of SHH in the skin was found to result in epidermal hyperplasia by antagonising p21 (cyclin-dependent kinase inhibitor 1A) cell cycle arrest. This also resulted in the proliferation of hair follicle like structures into BCC like growths (Fan and Khavari, 1999; Oro et al., 1997). Also, $PTCH^{neo67/+}$ (neo cassette heterozygote) mouse skin irradiated in early anagen (hair follicle down-growth phase), showed a higher rate of BCC induction compared to telogen hair follicles. Immunohistochemistry showed that these BCCs appeared to be derived from the follicular ORS (Mancuso et al., 2006). In a separate study, immunohistochemistry showed similar expression profiles between BCC and the follicular ORS compared to BCC and epidermis (including expression of basal differentiation markers K5 and K14 and no expression of K8, K1 and K10) again hinting that BCCs may be derived from part of the hair follicle (Kruger et al., 1999).

However, there are several publications which are in conflict with the hair follicle origin hypothesis and suggest that BCCs may actually originate in the basal layer of the epidermis. Hedgehog-induced proliferation was found to be restricted to the epidermal basal cell compartment (Adolphe et al., 2004). Also, some immunohistochemistry data has shown that PTCH induced skin tumours originate from the basal cell compartment (Adolphe et al., 2006). In humans and mouse BCC models, 'many tumours arose with no visible connection to the hair follicle', suggesting that ectopic SHH target gene expression in interfollicular cells can

induce hair follicle differentiation (Hu et al., 2003; Oro and Higgins, 2003). It was observed that initiating events in the epidermis can induce BCC features (using SHH expressing keratinocytes to regenerate human skin transgenic for long terminal repeat-driven SHH on immune deficient mice), without any inductive influence from mesenchymal cells and therefore hair follicle structures are not required for BCC development (Fan et al., 1997).

Some believe that BCCs may in fact originate from putative epidermal stem cells, SHH has been shown to have involvement in cell-fate specification and proliferation of stem cells. BCCs also grow slowly and share similarities in gene expression profile to stem cells along with continuous cell renewal (Parisi and Lin, 1998; Tumbar et al., 2004). The action of HH as a stem cell factor in drosophila embryos suggested the importance of SHH in human stem cells as well as in BCCs (Owens and Watt, 2003; Blanpain and Fuchs, 2006). It was also demonstrated that drosophila ovary stem cells cannot proliferate in the absence of HH signalling, inferring that HH is a stem cell factor (Zhang and Kalderon, 2001). Human tumours caused by SHH signalling may have resulted from the expansion of stem cell pools as it had been shown that SHH can regulate human putative epidermal stem cell proliferation. These epidermal stem cells underwent increased proliferation when grown in the presence of SHH (conditioned media from SHH-N expressing cells) and proliferation was decreased in the presence of the SMO inhibitor, cyclopamine (Zhou et al., 2006). BCCs are thought by some to be derived particularly from the interfollicular basal cell layer of the epidermis (Adolphe et al., 2006; Youssef et al., 2010). Tumour cells in the epidermis would be lost by terminal differentiation if they didn't reside in the epidermis long term, so stem cells are a likely point of origin (Owens and Watt, 2003).

BCCs and the lower hair follicle region have similar keratin expression (K5, K6 and K14) as well as $\alpha 2$ and $\beta 1$ integrins. Epidermal cells with high levels of $\beta 1$ integrin can be passaged for a long time, an important "stem cell" property (Fuchs et al., 2008). If BCCs were derived from interfollicular basal stem cells, the

undifferentiated phenotype of BCCs could be explained. It has been shown by expressing SMO selectively using K15, K17 and K19 promoters in subsets of mouse epidermal keratinocytes in different skin compartments, that BCCs did not arise in hair follicle bulge cells, but in the majority (93% in this region) from interfollicular epidermis (Youssef et al., 2010). It may be expected that because stem cell associated keratins (K15 and K19) are expressed in BCCs and in the hair follicle ORS, then the hair follicle may indeed be a likely location for the origin of BCCs. However, BCC formation was not induced by activation of SMO in hair follicle bulge stem cells of mice, but BCCs were found to arise from long-term resident progenitor cells of the interfollicular epidermis and the upper infundibulum by clonal analysis (Youssef et al., 2010).

1.3.5 Mouse Mutations in SHH Pathway

Mouse models have contributed considerably to the understanding of SHH function in the hair follicle and in BCC. Skin of SHH$^{-/-}$ mice showed inhibition of hair follicle morphogenesis, with no dermal papillae, almost no GLI1 present and reduced PTCH expression in primary hair germs (Chiang et al., 1999). This showed that activation of the SHH signalling pathway was essential for hair follicle morphogenesis. A separate research group used SHH$^{-/-}$ mice to show that hair follicle development initiated correctly, but did not proceed normally in the absence of SHH. The follicular structures were abnormal and no hair was formed (St-Jacques et al., 1998). SHH$^{-/-}$ skin grafts on nude mice (lack T-cells) had hairless pigmented skin after 2-3 weeks, further supporting a role for SHH signalling in hair follicle morphogenesis. This group also found that skin grafts from SHH$^{-/-}$ embryos were abnormal and formation of the hair follicle arrested after hair bud formation, supporting the findings of Chiang and co-workers (1999). SHH present in the proximal tip is thought to be involved in down-growth of the hair follicle, and probably involved in epithelial-mesenchymal interactions with the underlying dermis. These publications showed that SHH is not required for placode formation or initiation of down-growth, but is essential for hair follicle formation. Therefore, it is likely that loss of SHH blocks essential epithelial-

mesenchymal interactions which are involved in early hair follicle morphogenesis (St-Jacques et al., 1998).

C57BL/6 mice (postnatal day 19) showed activation of SHH signalling in skin with concomitant increase in expression of SHH, PTCH and GLI1 (Sato et al., 1999). Severe combined immunodeficiency (SCID) mice also showed abnormal BCC-like features when grafted with human keratinocytes expressing SHH (Fan and Khavari, 1999). Furthermore, BCCs were induced in mice over-expressing SHH (Dahmane et al., 1997) and features of basal cell nevus (Gorlin's) syndrome have been observed in mice expressing SHH (Oro et al., 1997). Thus, these reports suggest that expression of SHH in skin leads to activation of the SHH pathway which can then induce the formation of BCCs.

Mice over-expressing wild type GLI2, under the control of a K5 promoter, developed BCCs, whereas mice over-expressing a mutant form, GLI2ΔN2 (GLI2 without N-terminal domain) developed a range of skin tumours, even though the SHH pathway was activated in both types of mice. This showed that the N-terminal domain may have a specific function and an impact on the type of tumour formed, possibly via interactions with Gli1 (Sheng et al., 2002).

Mouse models also had an important role in unearthing the importance of PTCH in embryogenesis and in adult skin. Mice null for the ligand PTCH died during embryogenesis, whilst mice heterozygous for PTCH had developmental defects and some developed medulloblastomas (Bai et al., 2002; Goodrich et al., 1997). To look at the effect of loss of PTCH in adult skin, conditional PTCH knockout mice were created. The inducible activity of Cre recombinase under the control of a keratin 6 (K6) promoter was used to control the expression of PTCH using retinoic acid. Normally, K6 is expressed in the companion layer of the hair follicle and ORS, but with retinoic acid treatment, it is also expressed in interfollicular epidermis. These experiments showed that loss of PTCH function was sufficient for tumour progression, and the tumours formed were reminiscent of BCCs

30

(Adolphe et al., 2006; Aszterbaum et al., 1999). Together these studies confirmed the importance of SHH signalling for tumour development and showed that PTCH deactivation alone enabled SHH pathway activation which resulted in BCC induction.

Transgenic murine skin over-expressing smoothened (SMO), a downstream SHH pathway protein, developed abnormalities similar to BCCs. In these experiments, SMO was under the control of a K5 promoter that directed expression (and therefore downstream SHH signalling) to the basal epidermis and hair follicle ORS (Xie, 1998). As deactivating PTCH mutations and activating SMO mutations cause BCCs, PTCH null and SMO over-expressing mice provide the most accurate models for BCC.

SUFU normally represses activation of GLI transcription factors, so SUFU inactivating mutations cause constitutive SHH pathway activation. $SUFU^{-/-}$ mouse embryos were found to die *in utero* at ~E9.5 with developmental defects, a similar age to $PTCH^{-/-}$ embryos. This was found to be due to potent ligand independent activation of the SHH pathway, which could not be inhibited by the SMO inhibitor cyclopamine or increased by the SMO agonist SAG. $SUFU^{+/-}$ mice developed similar features to Gorlins syndrome including an abnormal basal cell phenotype. This confirmed that SUFU inactivating mutations can lead to disorders caused by SHH pathway signalling. Although we know that SUFU mutations are extremely rare in BCC patients, they may be important in other cancers in which SHH signalling is involved (Svard et al., 2006).

1.3.6 SHH Signalling in Cell Culture Models

There are very few publications describing BCC cell lines, suggesting that these cells do not grow well in culture. Therefore, several keratinocyte cell culture models expressing components of the SHH pathway have been developed for *in vitro* use. For example, an organotypic culture model using immortalised

31

keratinocyte cells over-expressing SHH has been developed. In this model, keratinocytes were grown on a collagen lattice containing fibroblasts at the air-liquid interface (culture medium contacts the cells from the underside). This allows keratinocytes to differentiate and stratify in air as well as invade the collagen gel below. This model was used to view the 'tumour-like' down-growth of SHH over-expressing cells (observed in sections stained with haematoxylin and eosin). Cross-sections of the cultures were cut on a cryostat and dried onto glass slides. Immunocytochemistry with specific antibodies were used to compare the expression of various proteins (e.g. Ki67, a proliferative marker) in SHH expressing cells and normal cells. Treatment with an EGFR activity inhibitor (AG1478) reduced the invasive phenotype and reduced Ki67 staining compared to untreated cells, showing that the EGF signalling pathway may be involved in modulating SHH signalling which could lead to increased invasiveness. In support of this, addition of recombinant EGF increased infiltration of SHH expressing keratinocytes into the collagen lattice containing fibroblasts. Increased MMP-9 (matrix metalloproteinase 9) expression was also observed (Bigelow et al, 2005). MMP-9 breaks down extracellular matrix and is therefore associated with an invasive cell phenotype. This model is simple and lacks many factors such as immune cells and a vascular system but has the key advantage that you can see whether inhibitors to the SHH pathway actually inhibit tumour invasiveness.

Other models include keratinocyte cell lines over-expressing GLI transcription factors. Kasper and colleagues (2006) treated GLI1 over-expressing keratinocytes with recombinant EGF and found that EGF signalling modulated GLI1 target gene expression. This seems to support the finding of Bigelow and co-workers (2005) that SHH pathway activity is modulated by addition of recombinant EGF to SHH over-expressing organotypic cultures (Bigelow et al., 2005). Additionally, a separate publication demonstrated a migratory phenotype in N/TERT1 cells expressing both EGF and GLI1, and showed that GLI1 represses ERK activity even when EGFR is increased (Neill et al., 2008). HaCaT keratinocytes expressing GLI1 and GLI2A under the control of doxycycline showed that c-Jun expression

was elevated (mRNA and protein) in GLI2A expressing cells but to a lesser extent in GLI1 expressing cells. The same was found for N/TERT1 keratinocytes and primary human foreskin keratinocytes expressing GLI2 under retroviral control. This was supported in BCC tissue by immunohistochemistry and qPCR, which showed that c-Jun levels were higher than found in normal skin and located throughout the tumour islands (where SHH pathway components were also found) but not in the stroma. These results showed that c-Jun was a direct target of GLI (Laner-Plamberger et al., 2009).

Another research group found that GLI1 and EGFR co-expression in rat kidney cells (RK3E) induced anchorage-independent growth associated with tumorigenesis, but this was not achieved when GLI1 or EGFR were expressed individually. The tumorigenic capability of these genes when expressed in combination was also demonstrated when HaCaT keratinocytes expressing GLI1 and EGFR under the control of doxycycline were transformed. The importance of the MEK/ERK branch (EGF pathway) was confirmed when inhibition of MEK/ERK activity by adding UO126 reduced anchorage-independent growth. Wortmannin, a PI3K/AKT inhibitor, was also added but had no effect, inferring the PI3K/AKT branch (EGF pathway) was not involved (Schnidar et al., 2009).

The drawback of these cell models is that *in vivo* BCCs have an up-regulated SHH pathway due to deactivation of PTCH or activation of SMO and not due to increased SHH ligand or activation of GLI transcription factors (except for rare cases of SUFU deactivating mutations, where GLI cannot be repressed). This model therefore bypasses the protein interactions between SHH and GLI which may be important for BCC development.

1.3.7 SHH Signalling Pathway Mutations in Other Disorders

SHH signalling pathway mutations in SHH, PTCH, GLI2, GLI3 and SMO have been reported in a variety of other genetic disorders (Table 1.1) and there is evidence that SHH may be influenced by other signalling pathways.

Table 1.1: Genetic Disorders Caused by Defective SHH Signalling.

Disorder	Clinical Presentation	Publication
Holopros-encephaly	Failure of the front lobes of the brain to separate	*Ming et al., 2002*
Greig cephalo-poly-syndactyly	Rare autosomal disorder characterised by physical abnormalities of the head, face, fingers and toes	*Vortkamp, 1991*
Pallister-Hall syndrome	Abnormal development of many parts of the body	*Biesecker, 1997*
Medulloblastoma	Most common brain tumour in children	*Erez et al., 2002; Xie et al., 1997; Smyth et al., 1999*
Meningioma	Common benign brain tumour	*Xie et al., 1997*
Squamous Cell Carcinoma	Carcinoma of skin, lips, mouth, oesophagus etc.	*Ping et al., 2001; Ahmadian et al., 1998*
Tricho-epithelioma	Small benign nodules of the skin (derived from hair follicle)	*Vorechovsky et al., 1997*
Oesophageal carcinoma	Malignancy of the oesophagus	*Maesawa et al., 1998*
Foetal rhabdomyoma	Derived from striated muscle	*DiSanto et al., 1992; Klijanienko et al., 1988*
Rhabdomyo-sarcoma	Malignant tumour derived from striated muscle	*Beddis et al., 1983*
Small cell lung cancer	Carcinoma of larger airways, often metastatic	*Watkins et al., 2003*
Prostate cancer	Cancer that develops in the prostate epithelium	*Karhadkar et al., 2004*
Breast cancer	Cancer that develops in the breast, various types	*Xie et al., 1997*

34

1.4 Epidermal Growth Factor (EGF)

Epidermal growth factor (EGF) is an important molecule that stimulates cell proliferation in embryonic development and in the adult, but it is also involved in the growth of tumours during invasion (Bigelow et al., 2005; Hausman, 2004).

1.4.1 EGF Signalling Pathway

EGF is a 53 amino acid polypeptide that binds to a specific transmembrane tyrosine kinase receptor (EGFR). These enzymes modify proteins by adding phosphate groups to either tyrosine, or in some cases serine/threonine residues (Normanno et al., 2005; Cooper and Hausman, 1998). EGFR is expressed in the basal layer and to a lesser extent in suprabasal cells of the epidermis (Bigelow et al., 2005; Hausman, 2004) and when EGFR is blocked, cells undergo apoptosis (Bigelow et al., 2005).

EGFR (also known as ErbB1) belongs to the ErbB1-4 family of receptors and the other family members (ErbB2-4), also known as HER2-4 in humans, have different ligands. EGFR is inactive as a monomeric transmembrane protein but binding of EGF ligand to the receptor (EGFR) on the cell surface induces conformational changes that promote protein-protein interactions leading to receptor dimerisation and activation (**Figure 1.12**). A large number of phosphorylation events are involved in the EGF signalling cascade, leading to functional changes in target proteins. These include increasing enzyme activity, cellular location or association with other proteins in the signalling cascade. Once dimerised, EGFR polypeptide chains cross-phosphorylate one another at tyrosine residues within the catalytic domain to further increase protein kinase activity.

In addition, further phosphorylation of tyrosine residues outside of the catalytic domain, creates binding sites for additional proteins that then transmit intracellular signals downstream of the activated receptor. These proteins bind to the receptor phosphotyrosine residues via src homology 2 (SH2) domains (**Figure 1.12**) leading to activation of various signalling cascades including PIP2/IP3, MEK/ERK

and P13K/AKT (Bigelow et al., 2005). The SH2 domain was originally identified as a conserved domain in the oncogene src but was subsequently found in many other signalling proteins with phosphotyrosine containing target domains (Filippakopoulos et al., 2009).

An important part of the EGF pathway involves phosphatidylinositol 4, 5-biphosphate (PIP2), inositol 1, 4, 5-triphosphate 3 (IP3) and diacylglycerol (DAG). PIP2 is bound to the inner plasma membrane and close to phospholipase C (PLC). When cells are stimulated by EGF, the G-protein linked receptor activates PLC which cleaves PIP2 into IP3 and DAG at the plasma membrane (**Figure 1.12**). DAG remains at the membrane and is a physiological activator of protein kinase C (PKC) while IP3 diffuses to the endoplasmic reticulum and opens Ca^{2+} channels to release Ca^{2+} from storage, which then goes to the plasma membrane to co-activate PKC. In addition, PIP2 can also be further phosphorylated at position 3 by PI3 kinase (PI3K) to make PIP3. The pleckstrin homology domain of AKT binds to PIP3, recruiting AKT to the inner plasma membrane for phosphorylation and activation by another protein kinase, PDK1 (Cooper and Hausman, 1998; Henson et al., 2007). AKT then regulates the function of many downstream targets by phosphorylation on serine/threonine residues to promote cellular survival (Cooper and Hausman, 1998).

Another important arm of the EGFR pathway is the MEK/ERK cascade involving a family of serine/threonine protein kinases. Ras activates Raf which then activates MEK (MAP Kinase/ERK Kinase). MEK then activates members of the ERK family by phosphorylation at both threonine and tyrosine residues (has dual specificity). ERK then phosphorylates and activates various target protein kinases and transcription factors. Activation of the ERK signalling pathway is known to lead to cell proliferation, survival and differentiation (Cooper and Hausman, 1998; Henson et al., 2005).

Fos, part of the AP-1 transcription complex is activated by phosphorylation of Elk-1 by ERK (Schnidar et al., 2009; Laner-Plamberger et al., 2009). c-Jun represents the other part of the AP-1 complex and this is normally activated by JNK, on a separate branch of the RAS pathway (**Figure 1.12**). It has been shown that MEK/ERK somehow interacts with c-Jun/AP-1 and that UO126 (MEK inhibitor) can abolish c-Jun phosphorylation.
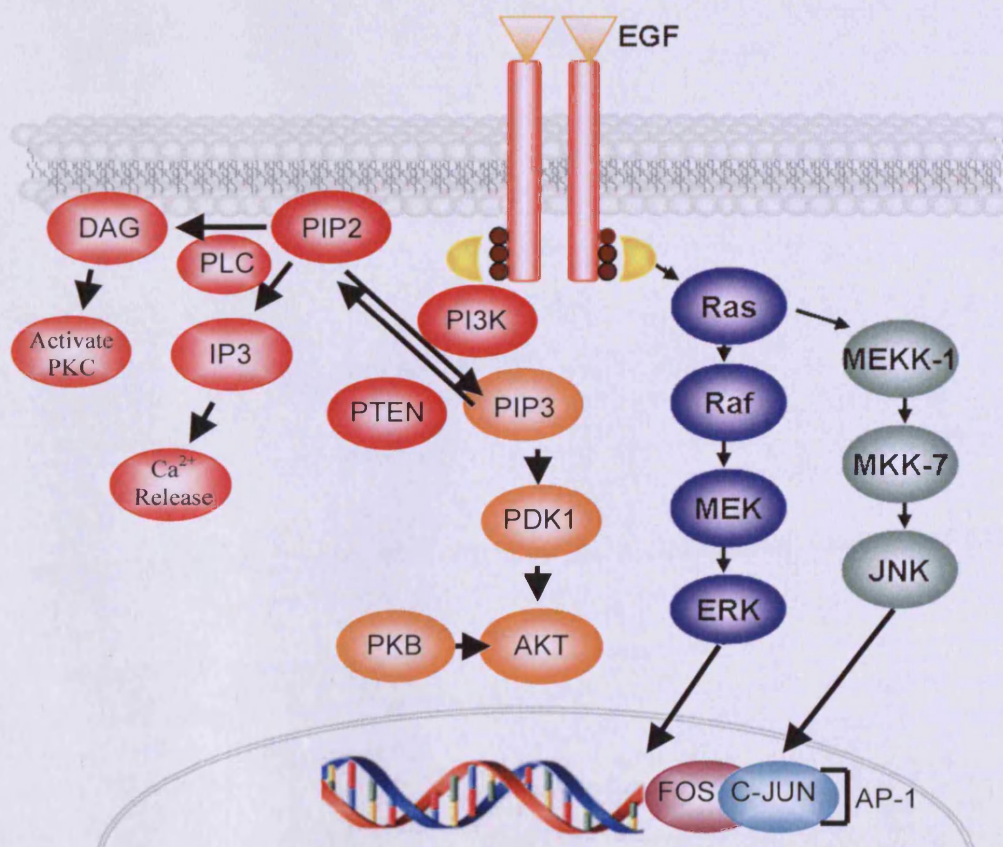
Figure 1.12: EGF Signalling Pathway. *Phosphorylation of the EGF receptor leads to downstream signalling through PI3K/AKT and MEK/ERK pathways.*

1.4.2 EGF and Cancer

The EGF pathway has previously been shown to function in cancers other than BCC, including epithelial cancers of the prostate and breast. Activation of the EGF pathway is thought to make tumours more aggressive and more likely to metastasize, a function linked to a role in epithelial mesenchymal transition [EMT] (Hardy, 2010).

EMT occurs when epithelial cells lose their epithelial characteristics and express mesenchymal markers (keratinocytes become fibroblast-like). Indeed, in BCCs and SCCs, ErbB1 (EGFR) ligands were found to increase in the adjacent "normal" epidermis (qPCR and immunohistochemistry data). However, downstream ERK1/2 and AKT were found to be activated in normal epidermis adjacent to SCCs, but importantly this was not observed for BCCs (Rittie et al., 2007). This suggests a lack of activation of either the PI3K/AKT or MEK/ERK branches of the EGF pathway in BCCs. Significant elevation of EGFR ligands in papillomas and SCCs has also been supported (Kiguchi et al., 1998). Additionally, EGFR was found in proliferating layers of skin cancers (both BCCs and SCCs) and one research group found expression in all cells of BCCs by immunohistochemistry (IHC) on frozen sections (Kikuchi et al., 1990; Lavrijsen et al., 1989). EGF pathway transcription complex (AP-1) components c-Jun and c-Fos were also shown to be increased in BCCs, suggesting that at least part of the EGF pathway is activated. Together, these results do not clearly show that the EGF pathway is activated in BCCs. As the EGF pathway is generally thought to be involved in cell survival and proliferation, the low levels of p-ERK and p-AKT found previously are consistent with the fact that BCCs are slow growing tumours that rarely metastasize.

However, there is evidence for an interaction between SHH and EGF signalling (particularly via MEK/ERK) at the level of GLI transcription factors, causing an infiltrative BCC phenotype. HaCaT cells in organotypic culture that expressed SHH showed increased EGFR phosphorylation compared to cells that did not.

Furthermore, cells expressing SHH also showed an ability to invade a collagen matrix and this invasion was prevented when EGFR signalling was inhibited (Bigelow et al., 2005). Gene expression profiling (qPCR) of N/TERT1 keratinocytes over-expressing GLI1 and stimulated with EGF, identified a subset of GLI1 target genes modulated via MEK/ERK signalling. The same research group showed that GLI and EGF are both required for induction of cell cycle progression and that EGF signalling inhibited GLI1 controlled stem cell marker expression (Kasper et al., 2006). Another research group found p-ERK in the tumour margin of one BCC sample by immunohistochemistry, suggesting that EGF signalling may cause invasive characteristics in some tumour cells (Neill et al., 2008). Interestingly, increased levels of the transcription factor c-Jun were found in BCCs *in vivo* and in SHH over-expressing organotypic cultures. However, c-Jun expression can be controlled by GLI1 and GLI2, as well as by EGF signalling, so c-Jun may be important for transcription of augmented downstream genes (Laner-Plamberger et al., 2009; Bigelow et al., 2005; Schnidar et al., 2009).

If there are interactions between the EGF and SHH signalling pathways, inhibitors of the EGF pathway might provide an effective treatment for BCC. Research has been carried out with topical formulations that inhibit MAPK and PI3K/AKT signal transduction pathways and these successfully limited cell proliferation in breast cancer (Davison et al., 2008a) so it may be worth trying this approach for BCCs.

c-Jun is thought to be up-regulated in BCCs, and constitutive activation of the AP-1 complex can lead to cell proliferation (**Figure 1.13**). It is not known how c-Jun might be activated in BCCs but crosstalk between the MEK/ERK arm of the EGF pathway (which is possibly activated) and the MEKK1/JNK arm (activated by inflammatory cytokines and cell stress leading to apoptosis), may play a role. Reducing c-Jun levels with RNAi (interference RNA; inhibit gene expression by

inactivating specific mRNAs) in cells with active GLI and EGFR signalling reduced transformation inferring a role for c-Jun (Schnidar et al., 2009).
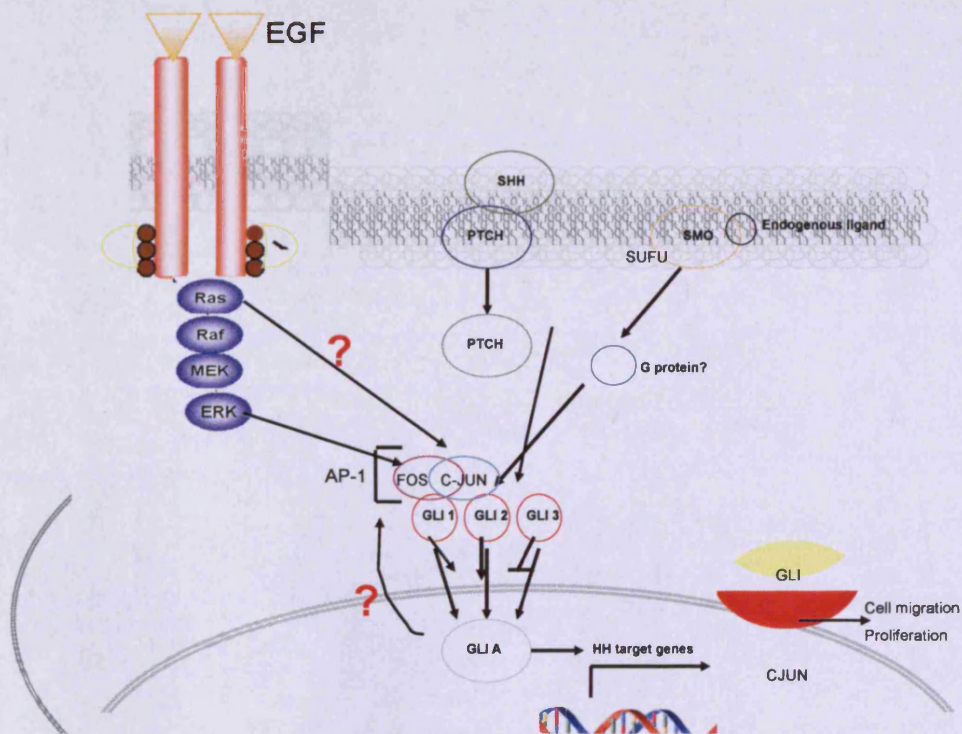
Figure 1.13: Possible Interactions between SHH and EGF Signalling Pathways.
Interactions between the MEK/ERK arm of the EGF pathway at the level of GLI transcription factors (possibly via AP-1 complex) could lead to modulation of SHH pathway target genes by a physical interaction between c-Jun and GLI2 (and to a lesser extent with GLI1). This would lead to a positive feedback loop with activated GLI up-regulating c-Jun. Combining c-Jun and GLI may lead to up-regulation of EGFR and SHH target genes, which would increase cell migration and proliferation.

GLI target genes (S100A7 and IL-1R2) have their transcription modulated by a physical interaction between GLI2 and c-Jun (c-Jun promoter has a functional GLI binding site) (Laner-Plamberger et al., 2009). When c-Jun is knocked out with shRNA (small hairpin RNA, used to silence gene expression), expression of these genes decrease, and primary c-Jun^{-/-} keratinocytes show reduced proliferation

(Laner-Plamberger et al., 2009; Zenz et al., 2003). Both c-Fos and c-Jun are part of the AP-1 transcription complex, so transcription may be inhibited by the MEK inhibitor PD98059 (also inhibits c-Fos). In addition, c-Jun is also thought to be a target of MEKK1/JNK (Franklin et al., 1992).

1.5 Development Rationale for Novel Topical Treatments

There is a clinical need for a formulation which can be used to treat more invasive BCC subtypes in order to reduce health service costs in the western world.

The general strategy is to look at expression of EGF proteins in BCC biopsies to decide whether there is a need to target the EGF pathway in addition to using a SMO inhibitor such as cyclopamine. In addition to this, a cell culture model of BCC will be developed which can be used to test inhibitor efficacy prior to the development of a suitable formulation.

Many possible treatments are toxic and can cause severe side effects because the drugs are non-specific (act on more than one part of a signal transduction pathway). If formulations targeting EGF were given orally, they would have high toxicity due to this lack of specificity. BCCs are not metastatic, so a systemic drug reaching organs other than the skin is not necessary and so this toxicity can be decreased by topical administration. This reduces first pass metabolism (when the drug is metabolised by the liver, reducing the amount that reaches the systemic circulation), so less of the drug is needed for topical delivery thus reducing toxicity (Rang, 2003). This means that the drug can be administered at home rather than in hospital, saving health care costs.

1.5.1. EGF Signalling Pathway Inhibitors

There are two main types of EGF pathway inhibitor: monoclonal antibodies and protein kinase inhibitors (Henson and Gibson, 2006). Suramin and Trastuzumab (Herceptin) are monoclonal antibodies which inhibit the whole EGF pathway and they have been used to treat prostate cancer and breast cancer respectively (Boylan

et al., 1998; Harries and Smith, 2002; Kalli et al., 2004). Small molecule inhibitors are more specific and include PX-866 (a PI3K inhibitor which has been effective on lung cancer cell lines; Henson and Gibson, 2006), PD98059 (MAPK phosphorylation inhibitor) and LY249002 (another PI3K inhibitor), which have been used in combination with tamoxifen to limit breast cancer cell growth (Davison et al., 2008a; Ellis, 2004).

1.5.2 EGF Antagonists (PD98059 and LY294002)

PD98059 and LY294002 are EGF antagonists which may be suitable for use in a topical formulation (**Figure 1.14**). Both inhibitors have previously been used in the treatment of other carcinomas in which EGF signalling is active. LY294002 is a derivative of the naturally occurring bioflavanoid quercetin, a PI3K inhibitor. It acts by competitively inhibiting the ATP binding site of PI3K, thus preventing the transfer of the terminal phosphate of ATP to phosphoinositol. This then inhibits the formation of PIPs and activation of AKT. PI3K affects oncogenes such as v-src and v-abl so its inhibition is likely to be useful for reduction of tumorigenesis (Vlahos et al., 1994). Wortmannin is a more potent inhibitor of PI3K but acts irreversibly, whereas the action of LY294002 is reversible.

PD98059 is a flavonoid that acts as a potent and selective inhibitor of MEK phosphorylation by cRAF or MEK kinase. This leads to inhibition of MAPK phosphorylation, directly downstream of MEK (Alessi et al., 1995; Dudley et al., 1995).
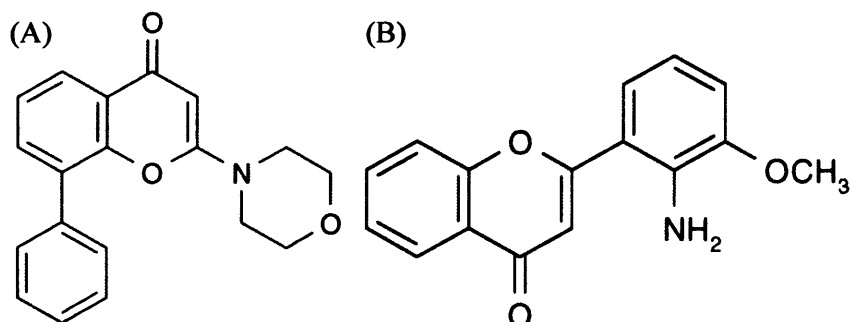
Figure 1.14: Chemical Structures of LY294002 (A) and PD98059 (B).

1.5.3 Cyclopamine

Cyclopamine (**Figure 1.15**) is a teratogenic steroidal alkaloid derived from plants (*Veratrum* genus), which induces a cephalic defect (cyclopia) in vertebrate embryos by preventing the division of the foetal brain into two lobes (holoprosencephaly), giving rise to its name based on Homer's Cyclops from Greek Mythology (Taipale et al., 2000).
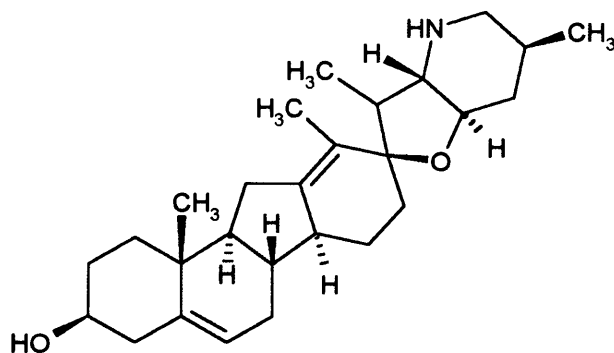
Figure 1.15: Chemical Structure of Cyclopamine.

Its action was first discovered when sheep grazing on *Veratrum californicum* gave birth to lambs, suffering from cyclopia, on the 14th day of gestation. Similarities noticed between *Veratrum*-induced cephalic defects in lambs (including cyclopia) and holoprosencephaly-like abnormalities (**Figure 1.16**). These are associated with the loss of SHH pathway signalling which eventually led to the discovery that

cyclopamine binds directly to the SMO heptahelical protein bundle. Cyclopamine inhibits SMO by influencing its protein conformation and thus blocking activation of downstream genes in the sonic hedgehog pathway. This antagonistic action on SHH signalling has been shown to be SHH and PTCH independent (Chen et al., 2002a; Chen et al., 2002b; Taipale et al., 2000).

Figure 1.16: **Veratrum Californicum,** *Sonic Hedgehog Game Character and an example of Cyclopia in Sheep.*

Cyclopamine and related steroidal alkaloids have similar structures to cholesterol. However, steroidal alkaloids with a structure similar to cyclopamine are not all potent inhibitors of SMO. There appear to be similarities between the functions of cholesterol and cyclopamine, which may use a common vesicular pathway for their actions. This is thought to be the case because PTCH and the Niemann-Pick CI protein (a transmembrane molecular pump involved in cholesterol homeostasis), are structurally similar (Davies et al., 2000). In addition, compounds that block cholesterol transport by affecting the vesicular trafficking of the Niemann-Pick C1 protein, are also weak SHH antagonists. Furthermore, co-localisation of PTCH and Niemann-Pick C1 protein was confirmed in vesicular compartments of cells.

44

1.5.4 Small Molecule SHH Pathway Inhibitors

There are a number of small molecule inhibitors to components of the SHH pathway, which may be useful for the treatment of BCC or other cancers dependent on SHH signalling. Many have progressed to clinical trial (**Table 1.2**), but not all were available at the start of, or during, this study. The targets of some of these inhibitors are shown in **Figure 1.17**.
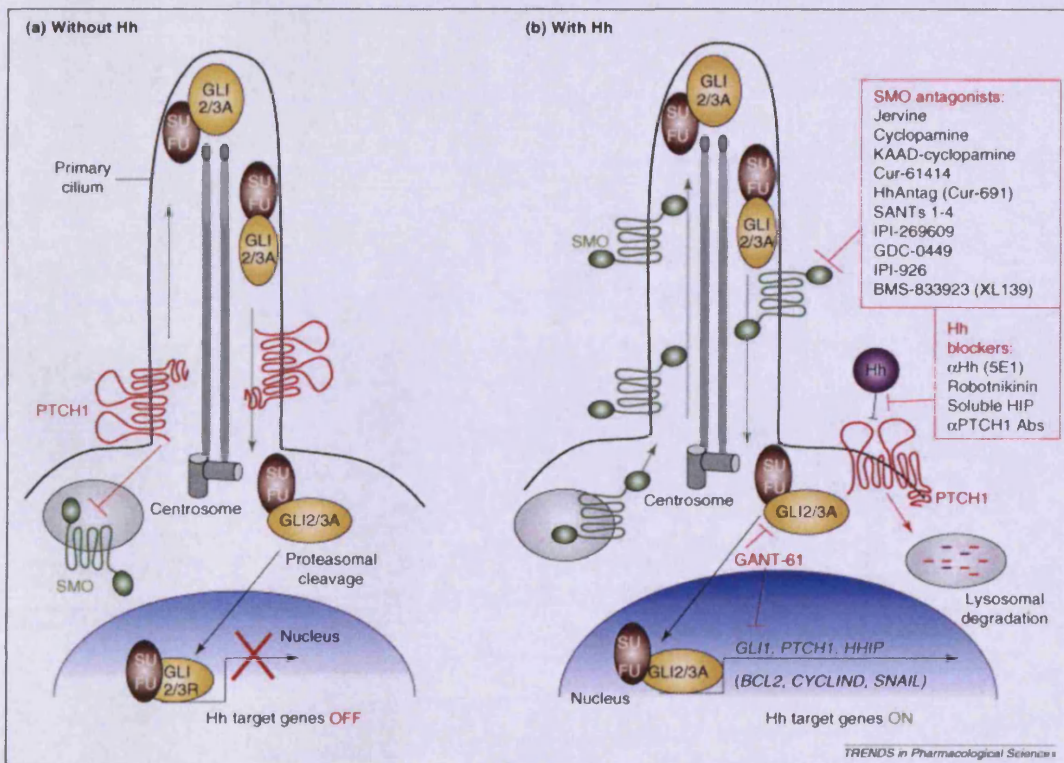
Figure 1.17: Inhibitors of the Basic Components in the Sonic Hedgehog Pathway. SHH pathway (a) in the absence of SHH and (b) in the presence of SHH, and where the pathway would be de-activated by inhibitors (adapted from Scales and Sauvage, 2009).

Normally, in sporadic cases of BCC, SHH inhibitors would not be useful since the pathway is constitutively activated in the absence of SHH. However, in xeroderma pigmentosum patients, where BCCs can be caused by SHH mutations, they may be applicable. Most inhibitors to the SHH signalling pathway target SMO, but some also inhibit GLI transcription factors (**Table 1.2**). Inhibition of GLI still leaves the

pathway upstream active which has lead to the discovery of transcriptional modulation by non-canonical pathways (Jenkins, 2009).

Table 1.2: Small Molecule SHH Pathway Inhibitors in Development *(adapted from Toftgard and Tegund, 2010).*

Compound	Target	Developmental Phase
Robotnikinin	SHH	Preclinical
Cyclopamine	SMO	Preclinical
KAAD-Cyclopamine	SMO	Preclinical
Jervine	SMO	Preclinical
IPI-609	SMO	Preclinical
IPI-926	SMO	Clinical phase I (advanced and/or metastatic solid tumours)
SANT1, 2, 3, and 4	SMO	Preclinical
CUR-61414	SMO	Clinical phase I (BCC), halted
HhAntag691/HhAntag	SMO	Preclinical
GDC-0449	SMO	Clinical phase I (advanced and/or metastatic solid tumours, medulloblastoma, pancreatic cancer) Clinical phase II (advanced BCC, metastatic colorectal cancer, ovarian carcinoma)
BMS-833923/XL139		Clinical phase I (advanced or metastatic cancer)
GANT61	GLI	Preclinical
HPI-1, 2, 3, and 4	GLI-A function	Preclinical

1.6 Hypothesis

Inhibition of EGF signalling in combination with blocking SHH signalling restricts BCC growth.

1.6.1 Research Aims:

- To develop an *in vitro* cell model to test drug formulations.
- To probe EGF signalling in BCC in order to confirm the *in vivo* relevance of a formulation containing EGF inhibitors on all sub-types of BCC.
- Determine a suitable vehicle for drug delivery.

Chapter 2

Sonic Hedgehog and Epidermal Growth Factor Signalling in Monolayer Cultures

2.1 Introduction

In recent years, several research groups have been in agreement that epidermal growth factor (EGF) signalling cascades somehow modulate the Sonic Hedgehog (SHH) pathway, leading to augmented expression of a subset of target genes. It has been shown that the combined expression of EGF and SHH causes neural stem cell proliferation (Palma et al., 2005), which may be important in prostate carcinoma. More recently, however, publications have suggested that it is particularly the MEK/ERK portion of the EGF pathway which is augmenting SHH signalling at the level of GLI transcription factors (Schnidar et al., 2009).

Experiments using Gli1-overexpressing N/TERT1 keratinocytes and qRT-PCR have shown that recombinant EGF augments the expression of a subset of Gli-induced genes. Furthermore, five of these genes (ARC, S100A7, IL1-R2, EGR-3 and JAG-2) demonstrated large increases in the presence of recombinant EGF. In fact, S100A7 levels increased 2.3 fold with EGF alone, 9.8 fold with GLI1 alone and up to 1,300 fold with both GLI1 and EGF compared to untreated controls (Kasper et al., 2006). In order to confirm which parts of the EGF pathway are involved in the change of GLI1 target gene expression, HaCaT keratinocytes expressing a doxycycline-regulated conditional allele of GLI1 supplemented with recombinant EGF, were treated with a PI3K inhibitor (LY294002) or a MEK1/2 inhibitor (U0126). Data from qRT-PCR experiments showed that the MEK/ERK arm of the EGF pathway but not PI3K/AKT arm is involved in augmenting the SHH pathway (Kasper et al., 2006).

In SHH-overexpressing HaCaT keratinocytes, it has been shown that the addition of recombinant EGF allowed tumour invasion in organotypic cultures. The importance of the EGF pathway for invasion was also confirmed by showing that an EGFR inhibitor (AG1478) reduced matrix infiltration. Higher levels of phosphorylation of both the EGFR and RAF (MEK/ERK cascade of EGF pathway) were also observed in SHH expressing organotypic cultures. This is

additional confirmation of the importance of not only the EGF pathway but specifically the MEK/ERK arm (Bigelow et al., 2005).

EGF has also been shown to repress Gli1-induced expression of stem cell characteristics (colony formation) and markers (such as EMT marker vimentin) in N/TERT1 cells. Cell-to-cell adhesion was increased in the presence of GLI1 and E-cadherin localisation also changed from perinuclear to the plasma membrane in GLI1 expressing cells. In contrast to other published research, Neill and colleagues (2008) also found a decrease in EGFR and ERK activity associated with colony formation in GLI1 expressing cells. Furthermore, ERK was not increased in GLI1 expressing cells even in the presence of exogenously increased EGFR (Neill et al., 2008), which suggested a negative feedback loop between GLI1 and ERK. In agreement with other publications, they found no change in AKT activity.

Schnidar and co-workers (2009) showed that UO126 (MEK1/2 inhibitor) reduced anchorage independent growth and c-Jun/AP-1 induced gene expression while wortmannin (PI3K inhibitor) did not. They used HaCaT keratinocytes where GLI1 expression was under the control of doxycycline and this data supports a role for the MEK/ERK arm of the EGF pathway (combined with GLI activation) in oncogenic transformation (Schnidar et al., 2009).

The same group also suggested a mechanism involving an AP-1 transcription factor (c-Jun) in this oncogenic transformation. The AP-1 complex can be activated by MEK/ERK which then augments the SHH pathway at the level of GLIA (also termed GLIact) to induce GLI/EGF target gene expression and oncogenic transformation. This has been shown by *in silico* promoter analysis where GLI and AP-1 binding sites were both present in GLI/EGF target genes and this was not found in EGF-independent GLI target genes. Stimulation of EGFR signalling activates c-Jun/AP-1 via MEK/ERK, with c-Jun binding to the promoters of GLI/EGF target genes. In confirmation of this, inhibition of

MEK/ERK prevents activation of c-Jun, reduces GLI/EGF target gene expression and also reduces transformation (Schnidar et al., 2009).

GLI1 and GLI2A-expressing HaCaT and N/TERT1 keratinocyte cell lines have been used to show that GLI1 and GLI2A can regulate transcription of c-Jun. The proliferative potential of GLI was found to be reduced in the absence of c-Jun (Laner-Plamberger et al., 2009) and c-Jun has also been found in the nuclei of BCC cells, suggesting that it is important for BCC development.

The publications described above showed some discrepancies, such as whether ERK is increased in BCC and whether c-Jun is a transcription factor downstream of MEK/ERK. The use of different cell lines (HaCaT and/or N/TERT1) that over-express different parts of the SHH pathway could explain the variable results obtained in some of these studies. However, they all seem to agree that MEK/ERK is involved in BCC development but the detailed mechanisms are still to be fully elucidated.

The main objective in our current research is to confirm the activity of both SHH and EGF pathways after addition of recombinant SHH and/or EGF to N/TERT1 keratinocytes and to show pathway activation by measuring expression of a subset of target genes (EGR-3, IL1R2, S100A7 and PTCH).

The ERK arm of the EGF pathway has been shown to augment SHH signalling and has been considered to be a good target for treating BCC alongside inhibitors of the SHH pathway. Monolayer keratinocyte cultures activated by the presence of recombinant SHH and/or EGF were therefore considered a good starting point for testing these inhibitors.

2.1.2 Aims

- To determine whether SHH and EGF signalling could be activated in N/TERT1 cells so that an *in vitro* model for BCC could be developed.
- To compare levels of SHH target genes when SHH and EGF were both present to determine whether EGF has an effect on SHH signalling.

2.2 Methods

2.2.1 Cell Lines

Normal human somatic cells have a limited capacity to replicate in culture, and quickly become senescent. In general, this is due to short telomere length or DNA damage, which reduces the lifespan of the cell. However, in principal, immortalisation allows cells to replicate for an unlimited number of passages. Two keratinocyte cell lines have been utilised for this project, N/TERT1 (from Dr James Rheinwald, Brigham and Women's Hospital, Harvard Institute of Medicine, Boston, MA, USA) and HaCaT (from Prof. Petra Boukamp, German Cancer Research Center [DKFZ], Heidelberg, Germany).

Normal human epidermal keratinocytes were immortalised by stable hTERT expression and loss of $P16^{INK4a}$ to produce the N/TERT1 cell line. hTERT is the activity-limiting component of telomerase, a holoenzyme with a template for telomere synthesis and a catalytic protein subunit with reverse transcriptase activity which prevents the loss of telomeres in cells. $P16^{INK4a}$ is involved in cell cycle control and would normally limit the lifespan of cells and loss of $P16^{INK4a}$ prevents the change from G1 to S growth phase. However, N/TERT1 cells retain responsiveness to growth control and differentiation signals and histologically appear similar to normal human keratinocytes in organotypic cultures or when grafted onto mice. Their survival in the absence of exogenous growth stimuli is enhanced compared to primary keratinocytes. Therefore, they provide a useful

model to study gene expression changes in response to well-defined stimuli (Dickson et al., 2000).

HaCaT cells represent a spontaneously immortalised human keratinocyte cell line. The cells were originally obtained in 1988 from histologically normal skin distal to an excised melanoma. This cell line was named HaCaT because of the human adult skin keratinocyte origin and because cells were propagated in low Ca^{2+} medium and at an elevated temperature (Boukamp et al., 1988). Spontaneous immortalisation of human cells is quite rare, probably because the genome is more stable than for other animal cells, such as rodents. Early in the immortalisation process, HaCaT cells differentiated and stratified in high calcium conditions, but grew as a monolayer in low calcium. Further passages reduced the effects of low calcium levels and cells that survived increased temperature were able to grow autonomously in culture. Marker chromosomes resulted which were able to show that the cell line was monoclonal by karyotyping. This also showed that HaCaT cells were aneuploid but many cells in late passages were polyploid. It has been suggested that polyploidy may be the cause of autonomous growth in culture.

HaCaT cells have been shown to be non-tumorigenic and non-invasive. Like normal keratinocytes, they grow into a well-structured epidermis when transplanted onto mice, having the same keratin expression profile, exhibiting normal differentiation and retaining all these properties at higher passages. Cells immortalised by virus infection (e.g. Simian Virus-40), a commonly used technique, tend to have altered growth properties, distorted keratinisation and deficient differentiation (Boukamp et al., 1988).

2.2.1.1 Maintaining Cell Lines (N/TERT1 and HaCaT)

N/TERT1 cells were thawed at 37°C in a water bath, transferred to a 20ml Universal tube and 9 volumes of DMEM (calcium-free, glutamine-free) /Ham's F12 (1:1, v/v) (Gibco, Invitrogen, Paisley, UK) containing 10% FBS (Lonza, Slough, UK) were slowly added. After careful mixing by pipette, the cells were

pelleted by centrifuging at 1,200 rpm for 5 minutes at room temperature (RT) and the supernatant was discarded. The N/TERT1 cell pellet was resuspended in 20ml keratinocyte serum-free medium (K-SFM) containing bovine pituitary extract (25µg/ml), EGF (0.2ng/ml) and 0.3mM $CaCl_2$ (Gibco, Invitrogen, Paisley, UK). The cells were carefully mixed and incubated at 37°C (5% CO_2) in a T75 culture flask (Corning, Fisher Scientific, Loughborough, UK). The medium was changed every 2-3 days but as N/TERT1 cells did not grow that well in this medium, there were sub-cultured at low density (30% confluency).

To subculture N/TERT1 cells, the medium was aspirated and the cells were washed once with dPBS. Trypsin-EDTA (Gibco, Invitrogen, Paisley, UK) was added (5ml) and the cells incubated at 37°C (in 5% CO_2) for approximately 10 minutes or until the cells were no longer adherent. An equal volume (5ml) of serum containing medium (DMEM/Ham's F12 [1:1, v/v] containing 10% FBS) was added to the cells to inhibit the trypsin. The cell suspension was carefully mixed, transferred to a 50ml falcon tube and centrifuged at 1,200 rpm for 5 minutes at RT. The supernatant was discarded, the cell pellet resuspended in 2-10ml K-SFM and cell number counted using a haemocytometer. Cells were then placed into new flasks (at approximately $1x10^5$ cells per T75) and K-SFM was added to make a total of 20ml.

HaCaT cells were thawed at 37°C in a waterbath and 20ml DMEM (Lonza, Slough, UK) containing 2 mM L-glutamine and 10% FBS was slowly added and mixed by pipetting. The cells were then incubated at 37°C (5% CO_2) in a T75 culture flask and the medium changed every 2-3 days. HaCaT cells were subcultured at higher density (~80% confluency). Medium was aspirated and the cells washed once with PBS before adding 5ml trypsin-EDTA. The cells were then incubated at 37°C (5% CO_2) for approximately 10 minutes or until cells were no longer adherent. DMEM with 10% FBS (5ml) was added to inhibit trypsin activity and after careful mixing, the cell suspension was transferred to a 50ml falcon tube. The cells were centrifuged at 1,200 rpm for 5 minutes at RT and the supernatant

discarded. The pellet was resuspended in 2-10ml DMEM with 10% FBS and the cell number counted using a haemocytometer. Cells were placed into new flasks (at approximately 1×10^5 cells per T75) and DMEM containing 10% FBS was added to a total of 20ml. Cells were then incubated at 37°C (5% CO_2) until confluent (5-7 days).

2.2.1.2 Growing N/TERT1 Keratinocytes to High Confluency

In order to grow N/TERT1 keratinocytes to a level above 30% confluency, a different medium was required. In this case, cells were cultured in a mixture of K-SFM and DF-K media (1:1, v/v). DF-K is calcium-free, glutamine-free DMEM/Ham's F12 mixture (1:1, v/v) containing 0.2ng/ml EGF, 25μg/ml bovine pituitary extract and 1.5mM L-glutamine (Gibco, Invitrogen, Paisley, UK). This medium was replaced every 2 days and N/TERT1 cells become fully confluent 5-7 days after subculture.

2.2.1.3 Cryopreserving Keratinocytes for Storage

In order to keep cells over a long period of time in liquid nitrogen, a specialised freezing mixture is required. N/TERT1 cells were stored in a mixture of DMEM and F12 (1:1, v/v) with 16% FBS and 20% DMSO which was premade and stored at -80°C. The components were thoroughly mixed, allowed to stand at 4°C for 2 hours, filter-sterilised (at 0.2μm), 1ml aliquots placed into 2ml cryovials and stored at -80°C.

The N/TERT1 cells were prepared by aspirating the medium and washing the cells with dPBS (sterile phosphate buffered saline). Trypsin-EDTA (5ml) was added and the cells incubated at 37°C (5% CO_2) for 5-12 minutes. An equal volume (5ml) of DMEM-F12 [1:1, v/v] containing 10% FBS was then added and carefully mixed to inhibit the trypsin activity. The cells were pelleted by spinning at 1,200 rpm for 5 minutes at RT and the medium was aspirated. Cells were then re-suspended in 3-4ml K-SFM and counted using a haemocytometer.

N/TERT1 cells were frozen at the recommended cell concentration (5×10^4 to 2×10^5 cells per ampule) by adding 1ml of the cells in K-SFM to a 1ml freezing mixture aliqout (1:1, v/v). The vials were wrapped in tissue, placed in a polystyrene tube box and frozen at -80°C. After 24 hours, the vials were transferred to liquid nitrogen for long term storage.

HaCaT cells were frozen by adding culture medium containing cells directly to filter-sterilised (at 0.2µm) FBS containing 10% DMSO. Again, this freezing mixture was premade and stored in 1ml aliquots at -80°C.

HaCaT cell cultures were prepared for freezing by aspirating the medium, washing the cells in dPBS and then adding 5ml trypsin-EDTA. The cells were incubated at 37°C (5% CO_2) for 5-12 minutes and then an equal volume (5ml) of DMEM containing 2mM L-glutamine and 10% FBS was added to inhibit the trypsin activity. The cells were pelleted by spinning at 1,200 rpm for 5 minutes at RT and the supernatant aspirated. The cells were resuspended in 3-4ml DMEM containing 10% FBS, counted and adjusted to a concentration of 3×10^6 cells per ml of medium. The cells in medium (1ml) were then added to a cryovial containing 1ml of freezing mixture. The vials were wrapped in tissue, placed in a polystyrene tube box and frozen at -80°C. After 24 hours, the vials were transferred to liquid nitrogen for long term storage.

2.2.1.4 Confirming EGF Pathway Activation

In order to carry out further experiments using recombinant EGF, it was important to confirm that the EGF pathway could be activated in N/TERT1 and HaCaT keratinocytes.

N/TERT1 cells were plated at approximately 6×10^5 cells/dish in four 10cm dishes with 10ml K-SFM containing growth supplements (bovine pituitary extract [25µg/ml], EGF [0.2ng/ml] and 0.3mM $CaCl_2$ per dish). The cells were incubated at 37°C (5% CO_2) for 36 hours, the K-SFM aspirated, the cells washed three times

55

with dPBS and 10ml K-SFM without EGF or bovine pituitary extract was added to each dish. The cells were incubated at 37°C (5% CO_2) for 24 hours and then exposed to 10ng/ml EGF (Gibco, Invitrogen, Paisley, UK) for 5, 10 or 20 minutes (3 separate dishes). Extraction buffer (0.8ml) was applied to each dish and the cells were scraped into 1.5ml eppendorf tubes, then boiled for 5mins and stored at -20°C for western blot analysis. The extraction buffer contained 1ml 0.5M Tris (Fisher Scientific, Loughborough, UK), 0.8ml glycerol (Sigma-Aldrich Company Ltd, Gillingham, UK), 1.6ml 10% SDS (Fisher Scientific, Loughborough, UK), 0.08ml 1M dithiothreitol (Sigma-Aldrich Company Ltd, Gillingham, UK) and 0.2ml bromophenol blue (Sigma-Aldrich Company Ltd, Gillingham, UK).

HaCaT cells were also plated (at approximately $6x10^5$cells/dish) in four 10cm dishes with 10ml DMEM containing 10% FBS and incubated at 37°C (5% CO_2) for 36 hours. The medium was aspirated, cells washed three times with dPBS and then 10ml DMEM (no FBS) was added to each dish. The cells were incubated at 37°C (5% CO_2) for 24 hours and then exposed to 10ng/ml EGF (Gibco, Invitrogen, Paisley, UK) for 5, 10 or 20 minutes (3 separate dishes). Extraction buffer (0.8ml) was applied to each dish and the cells were scraped into 1.5ml eppendorf tubes, then boiled for 5 minutes and stored at -20°C for western blot analysis.

2.2.1.5 EGF and SHH Pathway Induction in N/TERT1 Cell Line

N/TERT1 cells were plated at approximately $6x10^5$ cells per 10cm dish in 10ml K-SFM plus growth supplements: bovine pituitary extract (25µg/ml), EGF (0.2ng/ml) and 0.3mM $CaCl_2$. The cells were incubated at 37°C (5% CO_2) for 36 hours and then the K-SFM was aspirated, the cells were washed three times with dPBS and 10ml K-SFM without EGF or bovine pituitary extract was added to each dish. The cells were incubated at 37°C (5% CO_2) for 24 hours and then exposed to EGF (10ng/ml) and/or SHH (10ng/ml), (mouse recombinant proteins from E. Coli: Sigma-Aldrich Company Ltd, Gillingham, UK) in the presence or absence of the agonists, LY294002 (20µM) and/or PD98059 (20µM), for 24 hours. SDS sample

buffer (0.8ml) was applied to each dish and the cells were scraped into 1.5ml eppendorf tubes, then boiled for 5 minutes and stored at -20°C for western blot analysis. Alternatively, 0.9ml Trizol was applied to each dish and the cells were scraped into 1.5ml eppendorf tubes and stored at -80°C for RNA extraction.

2.2.1.6 Cell Viability Assay

This assay records luminescence signals from viable cells based on the quantity of ATP present, thus showing if there is an increase or decrease in cell viability when N/TERT1 keratinocytes were treated with inhibitors to the EGF pathway. N/TERT1 keratinocytes were plated in a 96 well plate at a density of approx 440 cells/well in 100μl K-SFM containing growth supplements. The cells were incubated at 37°C (5% CO_2) for 24 hours to approximately 30% confluent. The K-SFM was then aspirated and replaced with 100μl K-SFM per well plus the treatments shown in **Table 2.1** (4 replicates per treatment).

Table 2.1: Treatments used for N/TERT1 Keratinocyte Cell Viability Assay.

Treatment	Quantities
Control	20μl K-SFM
Inhibitor diluent	15μl DMSO + 5μl K-SFM
PI3K inhibitor	20μM LY294002 in 15μl DMSO + 5μl K-SFM
MEK inhibitor	20μM PD98059 in 15μl DMSO + 5μl K-SFM
PI3K + MEK inhibitors	20μM LY294002+20μM PD98059 in 15μl DMSO + 5μl K-SFM

After 24 hours, an aliquot of fresh Cell Titer-Glo (CTG) reagent (Promega UK Ltd, Southampton, UK) was made by mixing 10ml substrate and 10ml buffer from the kit. The medium was removed from the 96 well plate, cells were washed three times in dPBS and then 100μl K-SFM was added to each well. The plate was allowed to equilibrate for 30 minutes at RT before the addition of 100μl CTG reagent, to each well. The plate contents were mixed on an orbital shaker to induce cell lysis and then the plate was allowed to incubate at RT for 10 minutes to stabilise the signal. Luminescence was measured on a Tropix TR717 microplate luminometer using an integration time of 0.5 seconds.

2.2.2. Molecular Biology

2.2.2.1 RNA Extraction

Total RNA was extracted from skin or cultured cells using Trizol reagent (Gibco, Invitrogen, Paisley, UK). Briefly, 0.9ml trizol was added to cryostat cut (0.7μm) slices of normal human skin or to a 10cm plate of confluent cells and the contents were scraped into a 1.5ml eppendorf tube and vortexed for 5 minutes. An aliquot (0.25ml) of chloroform (Fisher Scientific, Loughborough, UK) was added, the solution was shaken for 15 seconds and then left to stand for 2-15 minutes. This was centrifuged at 12,000 rpm for 10 minutes at 4°C. The top aqueous layer was removed and transferred to a clean 1.5ml tube and 0.6ml isopropanol added, mixed and left to stand for 10 minutes. The mixture was centrifuged at 12,000 rpm for 4 minutes at 4°C and the supernatant discarded. The pellet was washed with 1ml 75% ethanol (Fisher Scientific, Loughborough, UK) and centrifuged at 7,500 rpm for 5 minutes at 4°C. The ethanol was discarded and the pellet air dried until it became translucent. The pellet was resuspended in 15-30μl nuclease-free water (Sigma-Aldrich Company Ltd, Gillingham, UK), and an aliquot (3-4μl) removed to measure the RNA concentration by spectrophotometry (absorbance at 260 nm).

2.2.2.2 Reverse Transcription-Polymerase Chain Reaction (RT-PCR)

Reverse transcription was carried out to make cDNA from total RNA previously extracted from cells. RNA (1μg), Oligo dT (n=15) primer (1μl at 500μg/ml) (Promega Uk Ltd, Southampton, UK) and enough dH$_2$O to make up to 6μl were mixed in a 0.2ml eppendorf tube and placed in thermal cycler (PTC-200 Peltier Thermal Cycler, GRI) for 10 minutes at 70°C. Reverse transcriptase (1μl at 10U/μl from Promega UK Ltd, Southampton, UK), RNAse inhibitor (1μl at 40U/μl from Promega UK Ltd, Southampton, UK) and 12μl reaction master mix were added and the tube returned to the cycler for 30 min at 42°C, followed by 70°C for 10 minutes. The reaction master mix contained 4μl 5x RT buffer (Promega UK Ltd, Southampton, UK), 4μl dNTP mix (10nM each from Roche Applied Science, Mannheim, Germany) and 4μl dH$_2$O.

PCR primers were designed to include intron/exon boundaries where possible (size increase indicates genomic DNA contamination), to have 50-60% guanine (G) and cytosine (C) content, preferably end on a G or C and be approximately 21 base pairs in length. Also, both primers should have an annealing temperature within 5°C of each other according to the equation: 4(G+C)+2(A+T)-5°C (where A and T are Adenine and Thymine and G and C are Guanine and Cytosine respectfully). Finally, primers were located on the cDNA 200bp to 1.5 Kb apart so the amplicon produced by PCR was clearly visible on an agarose gel.

Primers were prepared at a concentration of 0.1μg/μl and the master mix was prepared using Qiagen HotStarTaq Plus kit reagents: 2.5μl 10x CL buffer (Coral Load buffer, pH 8.7 containing 15mM $MgCl_2$, KCl and $(NH_4)_2SO_4$, gel loading reagent, red dye and orange dye), 0.5μl 10mM dNTPs, 1μl cDNA (1μg/μl), 18.72μl dH_2O and finally 0.25μl 5U/μl Taq polymerase (Promega UK Ltd, Southampton, UK). The appropriate forward and reverse primers (1μg of each in 1μl, see **Table 2.2**) were added to each tube, making a total reaction volume of 25μl. All tubes (including a water control) were put in the thermal cycler for 5 minutes at 95 °C (enzyme activation step) and then left for 35-40 cycles (94°C denaturing, 59°C annealing and 72°C synthesis). Finally, the reaction was incubated at 72°C for 10 minutes to extend all remaining products to full length. PCRs were optimised by varying the annealing temperature by 1-2 degrees, and by varying the $MgCl_2$ concentration (1.5mM to 5mM) per reaction. The conditions which gave the strongest amplicon of the correct size with least non-specific bands were chosen.

Table 2.2: PCR Custom Primers (from Sigma-Aldrich Ltd, Gillingham, UK).

Gene	NCBI Accession #	Type	Primer Sequence (5' to 3')	Size (bp)
SMO	NM 005631	F	TGC TGT GTG CCG TAT ACA TGC	1045
SMO	NM 005631	R	AAG TCG TAG AAG TGG CAG CTG	
PTCH	NM 000264	F	TTA CTC ATG CTC GCC TAT GCC	998
PTCH	NM 000264	R	CTG GTT TCC CGA GGT ACA ATG	
SHH	NM 000193	F	AGA TGT CTG CTG CTA GTC CTC	1043
SHH	NM 000193	R	AGC ACC CGG TTG ATG AGA ATG	
GLI1	NM 005269	F	TCA ACT CGC GAT GCA CAT CTC	1333
GLI1	NM 005269	R	GTA TAG GCA GAG CTG ATG CTG	
APRT	NM 000485	F	GCT GCG TGC TCA TCC GAA AG	277
APRT	NM 000485	R	CCT TAA GCG AGG TCA GCT CC	

2.2.2.3 Quantitative PCR (qPCR)

This is a quantitative method of PCR, which enabled comparison of fold-change in gene expression between cells cultured under different conditions (e.g. in the presence or absence of recombinant EGF and/or SHH). Primers were designed as for conventional PCR except that the amplicons were smaller (ideally 100-250bp in size) to increase amplification efficiency (see **Table 2.3** for qPCR primer sequences and amplicon sizes).

Reactions were run in a 96 well plate containing 6μl dH$_2$O, 12.5μl Brilliant SYBR Green qPCR Mastermix (Agilent Technologies, West Lothian, UK), 1.25μl forward primer (F), 1.25μl reverse primer (R) and finally 4μl (0.5, 1, or 1.5μg) cDNA per sample well. The primers (Custom Oligos, Sigma-Aldrich Company Ltd, Gillingham, UK) were made up to correct concentration (μg/μl) as per the optimisation procedure results. Reactions were run at 58°C using the ΔCt method on an MXP3000 thermal cycler with MX Pro software. Although the ideal annealing temperatures varied between primer pairs, a compromise had to be made to allow the house-keeping gene to be run at the same time. Since all annealing temperatures were within 5°C, it was possible to optimise all PCR reactions at 58°C.

Table 2.3: QPCR Custom Primers (from Sigma-Aldrich Ltd, Gillingham, UK).

Gene	NCBI Accession #	Type	Sequence (5' to 3')	Size (bp)
PTCH	NM 000264	F	GAT GCA GAA TTC TGA AGT CGA C	114
PTCH	NM 000264	R	GAG AAA GTT CTA CAC CAT GCA G	
EGR-3	NM 004430	F	CAG GAT TAC CAC TCG GCC AAG	183
EGR-3	NM 004430	R	GAA TGC CTT GAT GGT CTC CAG	
IL1R2	NM 173343	F	CAA GAG AGG ATT TGC ACA TGG	172
IL1R2	NM 173343	R	CAC CGT CTG TGC ATC CAT ATT	
S100A7	NM 002963	F	CTG CTG ACG ATG ATG AAG GAG	177
S100A7	NM 002963	R	GCT CTG CTT GTG GTA GTC TGT	
ACTB	NM 001101	F	AGA AAA TCT GGC ACC ACA CCT	174
ACTB	NM 001101	R	ATA GCA CAG CCT GGA TAG CAA	
TF2H	NM 022011	F	AAG TTC GAC TTG GAA TGA TGC G	97
TF2H	NM 022011	R	ATG ACA CGT CAG TCT ATT AGG CTT	
ARP	NM 001003	F	AGC CGG TGT AAA TGT TGA GC	81
ARP	NM 001003	R	CAG ATG AGG CTC CCA ATG TT	
APRT	NM 009698	F	GCT GCG TGC TCA TCC GAA AG	247
APRT	NM 009698	R	CCT TAA GCG AGG TCA GCT CC	

Various cDNA and primer concentrations for each gene were run as a series of different combinations to find the optimal concentration for the reaction (**Table 2.4**). Further optimisation was carried out as necessary. Low Ct (threshold cycle) values were preferable. The Ct is the earliest detectable point above background levels and was calculated by the MX Pro software. A Ct at a low cycle number is only achievable with high levels of cDNA and if there is a large amount of the

gene of interest in the cells. Thus, lower Ct values were more easily achievable for housekeeping genes such as ACTB than for EGR-3, IL1-R2, S100A7 or PTCH.

Once the cDNA and primer concentrations required to achieve the lowest Ct value for each gene were determined, another qPCR reaction was run using a cDNA dilution series (neat (0.5, 1 or 1.5μg), 1:10, 1:100 and 1:1000) and the cycle number for each dilution was plotted against the fluorescence to create an amplification curve. Amplification curves for this dilution series should give four equally spaced plots (one for each dilution). The Ct values (determined by the MX Pro software) on this graph were taken for each curve and plotted again against the dilution (Ct against the log quantity of the sample) to give a standard curve. From this R^2, slope and efficiency values were derived by the MX Pro software. For good optimisation, the R^2 value should be as close to 1 as possible, the slope should be between -3.2 and -3.5 and the efficiency should be between 90 and 110%.

Table 2.4: cDNA and Primer Concentrations for QPCR Optimisation.

cDNA (μg)	Primers (μg/μl.)
1.5	0.15
1.5	0.1
1.5	0.05
1	0.15
1	0.1
1	0.05
0.5	0.15
0.5	0.1
0.5	0.05

At the end of the qPCR, a melting or dissociation curve was made by heating the reaction to denature the dsDNA (double stranded DNA), SYBR green fluorescence is strong when bound to dsDNA but is very low when unbound, so melting the dsDNA should result in one smooth curve for all replicates

(fluorescence plotted against temperature) if only one product was formed in the reaction (no contamination and no primer dimers).

After optimisation the qPCR reactions were carried out under the optimised conditions for each set of primers to find fold changes in gene expression when N/TERT1 cells were grown in the presence or absence of SHH and/or EGF and also presence or absence of inhibitors (LY294002 or PD98059). The fold change with each treatment was plotted as bar charts by the MX Pro software for analysis.

2.2.2.4 Statistical Analysis.

Statistical analysis was done using INSTAT by Ordinary ANOVA, Parametric, Tukey test. This statistical test was used because it is a single step comparison of whether or not the means of all possible pairs in unrelated groups are significantly different from one another.

2.2.2.5 Gel Electrophoresis

PCR reactions (10μl) containing coral load buffer (see section 2.2.2.2) were run on a 1% agarose gel to compare the expression of genes qualitatively. A 100bp ladder (5μl; New England Biolabs, Hitchin, UK) was also run alongside to estimate the correct amplicon size.

Agarose gels (1%) were prepared in a VWR AGT-1 horizontal gel tank with a UV transparent base. Briefly, 0.5g agarose (Sigma-Aldrich Company Ltd, Gillingham, UK) was dissolved in 50ml 2x TAE buffer containing 0.01% v/v ethidium bromide (5μl stock added). The stock TAE buffer (50x) contained 242g Tris (Fisher Scientific, Loughborough, UK), 57.1ml acetic acid (Fisher Scientific, Loughborough, UK) and 100ml 0.5M EDTA, adjusted to pH8 (Sigma-Aldrich Company Ltd, Gillingham, UK). Gels were made from 50ml of agarose in TAE and generally contained 20 wells. The gel was immersed in approximately 50ml of 2x TAE electrophoresis buffer and run at 50V for approximately 1 hour. The gel

tank (UV transparent) was placed on a 365nm transilluminator and digital images acquired using AlphaImager HP digital camera and software.

2.2.2.6 DNA Purification using Qiagen PCR Purification Kit

DNA amplified by PCR was purified prior to sequencing using a purification kit (Qiagen, Crawley, UK). Five volumes of buffer PB were added to one volume of PCR sample and mixed. A spin column was placed into a 2ml collection tube and the sample was applied to the column and centrifuged at 13,000 rpm for 60 seconds at RT. The flow-through in the collection tube was discarded and the column placed back in the tube. Buffer PE (0.75ml) was added to column and centrifuged at 13,000 rpm for 60 seconds at RT to wash the DNA. Again, the flow-through was discarded, the column put back in the tube and centrifuged at 13,000 rpm for 1 minute at RT. The column was then placed in a clean 1.5ml tube and 50μl buffer EB added to the centre of the membrane to elute the DNA. This was centrifuged at 13,000 rpm for 1 minute at RT.

2.2.2.7 DNA Sequencing

Sequencing was carried out to confirm that the PCR had amplified the correct products and the insert had been cloned in the correct orientation. The reaction mix contained 2μl DNA, 1μl forward primer (F) (see **Table 2.1**), 2μl 5x sequencing buffer (Amersham Biosciences, GE Healthcare Life Sciences, Little Chalfont, UK), 2μl big dye reagent mix (Applied Biosystems, Foster City, CA, USA) and 3μl dH$_2$O. Reactions were placed in a thermal cycler for one cycle (96°C 1 min, 96°C 10s, 50°C 5s, 60°C 4 min) and then 25 cycles without the initial step (96°C 10s, 50°C 5s, 60°C 4 min). After cycling, 25μl ice cold 95% ethanol (Fisher Scientific, Loughborough, UK) and 1μl 3M sodium acetate (Sigma-Aldrich Company Ltd, Gillingham, UK) were added to the reaction mix. This was kept on dry ice for 10 minutes and then the tube was centrifuged at 15,000 rpm for 25-30 minutes at 4°C and the supernatant removed. An aliquot (180μl) of 75% ethanol was added, the tube centrifuged at 4°C for 2 minutes and the ethanol removed.

64

This procedure was repeated with another 180μl aliquot of 75% ethanol and the tube centrifuged for 2 minutes at 4°C and the supernatant removed. The pellet was air dried for 10-15 minutes and stored at -20°C until ready for automated sequencing. This was provided by Central Biotechnology Services (CBS) in the School of Medicine (Andrew Francis and Keith Hart in, Henry Wellcome Building, School of Medicine, Cardiff University). Fluorograms and sequencing data (text) was sent by e-mail and viewed using free software (FinchTV v1.4.0 from Geospiza Inc).

2.2.3 Cloning

2.2.3.1 PCR Amplification of SHH cDNA

Primer sequences for the two separate portions of SHH cDNA (named SHH 5' and SHH 3') are shown in **Table 2.5**. RNA was extracted from normal skin (see section 2.2.2.1) and RT-PCR was carried out using various primer combinations and an annealing temperature of 59°C. PCR reactions were run on 1% agarose gels (2.2.2.4) and viewed on a UV light box (stained with ethidium bromide).

Table 2.5: PCR Custom Primers (from Sigma-Aldrich Company Ltd, Gillingham, UK)

Gene	NCBI Accession #	Type	Sequence (5' to 3')	Size (bp)
SHH 5'	NM 000193	F	GATGCTGCTGCTGGCGAGAT	830
SHH 5'	NM 000193	R	TTGTGCGGCGCCACAAAGAG	
SHH 3'	NM 000193	F	CTCACTTTCCTGGACCGCGA	655
SHH 3'	NM 000193	R	CTTCAGGTGGACTTGACCGC	

2.2.3.2 Ligation into Cloning Vector:

PCR products from the 5' and 3' ends of SHH were ligated separately into a cloning vector using a pGEM-T easy kit (Promega UK Ltd, Southampton, UK). An aliquot (5μl) of each PCR reaction product was mixed with 1μl vector (50ng/μl), 1μl T4 ligase (3U/μl) and 5μl 2x rapid ligation buffer (pGEM-T easy kit) and then incubated at 4°C overnight.

2.2.3.3 Transformation:

The vials containing the ligation reaction were centrifuged briefly and placed on ice. An aliquot (50µl) of chemically competent bacteria (One Shot Top10 from Invitrogen, Paisley, UK) were thawed on ice. Two 3µl aliquots of each ligation reaction were pipetted into separate sterile tubes and 25µl of the competent cell mix was added to each, mixed and incubated on ice for 30 minutes. The bacteria were then transformed by heat shock at 42°C for 30 seconds and then put back on ice. An aliquot (250µl) of pre-warmed S.O.C medium (Invitrogen, Paisley, UK) was added to each and the vials were place in a shaking incubator at 37°C for 1 hour (shake at 300 rpm) to allow time for expression of the ampicillin resistance gene before plating. An aliquot (100µl) of each transformation mix was spread on a separate LB agar plate containing ampicillin (1:1000 50mg/ml stock), IPTG (4µl 0.2% IPTG (Isopropyl β-D-1-thiogalactopyranoside) and 40µl X-Gal (dissolved in dimethylformamide at 20mg/ml) for blue/white selection (Fluka Analytical, Sigma-Aldrich Company Ltd, Gillingham, UK). The plates were inverted and incubated at 37°C overnight. A white colony was removed from each plate and spread down half a new LB agar plate containing ampicillin (1:1000 of 50mg/ml stock) and a second colony was spread on the other half of the plate. The plates were incubated at 37°C overnight. A single colony was removed from each half plate and placed in separate tubes containing 5ml liquid broth with 5µl 50mg/ml ampicillin. The tubes were incubated overnight at 37°C while shaking at 300 rpm.

2.2.3.4 Bacterial DNA Isolation by Miniprep:

A 1.5ml aliquot of each bacterial culture was centrifuged at 8,000rpm for 2 minutes at RT and the supernatant was discarded. Three buffers were used from a Qiagen Miniprep Kit (Qiagen, Crawley, UK). P1 buffer (100µl) was added and mixed, then P2 buffer (100µl) and finally P3 buffer (100µl). The solution was then centrifuged at 13,000 rpm for 15 minutes at RT. The supernatant was transferred to a fresh tube and 900µl 100% ethanol (Fisher Scientific, Loughborough, UK) was added and mixed. The tubes were spun at 13,000 rpm for 15 minutes at RT, the supernatant discarded and the DNA pellet was washed with 70% ethanol

(500μl). The tubes were centrifuged again at 13,000 rpm for 2 minutes at RT and the supernatant removed. The DNA pellet was air dried and resuspended in 50μl TE buffer.

2.2.3.5 Restriction Digests:

Each DNA sample (1μl) was digested with 0.5-1μl of an appropriate restriction endonuclease (20,000/ml) (New England Biolabs, Hitchin, UK) in 2.5μl buffer (as appropriate) and enough dH_2O to make up to a total reaction mix of 25μl. Where appropriate (depending on the restriction endonuclease used), 0.5μl BSA (10 mg/ml, from New England Biolabs, Hitchin, UK) was added. This mixture was incubated for 1.5 hrs at 37°C and the digestion products run on a 1% agarose gel.

Double restriction digests required addition of 0.5-1μl of a second restriction endonuclease (New England Biolabs, Hitchin, UK), a buffer appropriate for both enzymes and an appropriate reduction in dH_2O. If the double digest failed, then each cut must be done separately with a clean up and DNA precipitation between the two reactions.

2.2.3.6 Gel Extraction of Restriction Fragments using Qiagen Gel Extraction Kit.

DNA fragments were excised from an agarose gel with a clean scalpel and the gel slice weighed in a 1.5ml eppendorf tube. Three volumes of QG buffer were added to each gel slice (300μl per 100μg). The gel slice was incubated at 50°C for 10 minutes and then one volume of isopropanol was added and the sample mixed. This mixture was applied to a spin column in a 2ml tube and centrifuged at 13,000 rpm for 1 minute at RT. The initial flow-through was discarded, and a further 0.5ml of QG buffer was added to the spin column which was then centrifuged at 13,000 rpm for 1 minute at RT. Then, 0.75ml of PE buffer was added to the spin column to wash off the QG buffer and the tubes centrifuged again at 13,000 rpm for 1 minute at RT. The flow-through was discarded and the tube was centrifuged at 13,000 rpm for another minute at RT. The spin column was then placed into a

clean 1.5ml tube and the DNA eluted by adding 30μl dH$_2$O to the column membrane and centrifuging at 13,000 rpm for 1 minute at RT.

The two portions (5' and 3') of SHH cDNA were then ligated together to create a full length version. At the start of this project SHH cDNA was not commercially available.

2.2.3.7 Subcloning:

The SHH cDNA was ligated into a pcDNA3 expression vector (Invitrogen, Paisley, UK), which has a neomycin resistance gene for the selection of successfully transfected cells. G418 (Geneticin from Invitrogen, Paisley, UK), an aminoglycoside antibiotic blocks polypeptide synthesis in all cells by inhibiting 80S ribosomal function so the cells do not survive. The neomycin resistance gene in cells that were successfully transfected with pcDNA3, deactivates G418 by phosphorylation, enabling these cells to survive. Thus, a cell line that is stably transfected can be selected.

pcDNA3 vector (1μl) was linearised by digestion (see section 2.2.3.5) with EcoRI (1μl, 20,000U/ml) in enzyme buffer (2.5μl) and dH$_2$O (21.5μl). This was incubated for 1.5 hours at 37°C after which 1μl CIP (10,000U/ml) (calf intestinal alkaline phosphatase from New England BioLabs, Hitchin, UK) was added to remove phosphate groups from the cleaved ends of plasmid. The tube was incubated at 37°C for a further hour. The linearised pcDNA3 vector was then gel purified (see section 2.2.3.6) to remove any uncut vector. The two sections of SHH cDNA which were previously cloned in pGEM-T vectors (1.5μl of each) were linearised with EcoRI and XmnI restriction enzymes (see 2.2.3.5) and ligated into the linearised pcDNA3 expression vector (1μl) by incubating at 4°C overnight (see section 2.2.3.2) with 1μl T4 ligase (3U/μl) and 5μl 2x rapid ligation buffer (pGEM T-easy kit). To ensure they were in a 5' to 3' orientation, EcoRI digests were carried out (see 2.2.3.5) followed by sequencing.

2.2.3.8 Endofree Plasmid Maxi Kit

An Endofree Plasmid Maxi Kit (Qiagen, Crawley, UK) was used to purify endotoxin-free plasmid DNA. A single colony picked from a freshly streaked plate was used to make a starter culture by inoculating 3ml LB (Luria Bertani) medium containing 6μl ampicillin (50mg/ml) and shaking (300 rpm) in an orbital incubator at 37°C for 12 hours. The 250μl starter culture was placed in a 500ml conical flask containing 250ml LB medium and incubated in an orbital incubator at 37°C overnight at 300 rpm. The bacterial cells were harvested by centrifugation at 7,000 rpm for 15 minutes at 4°C and then purified using a modified alkaline lysis procedure. The plasmid DNA was added to Qiagen anion-exchange resin and a medium-salt wash was performed to remove impurities. The plasmid DNA was eluted with a high salt buffer, the DNA concentrated by isopropanol precipitation and washed in 70% ethanol (made with endotoxin free water). The pellet was then resuspended in 300μl endotoxin free TE and the DNA concentration measured by spectrophotometry (absorbance at 260nm) before making an appropriate stock dilution for transfection (1μg/μl). The construct was checked by re-digestion with EcoRI restriction endonuclease (see 2.2.3.5) followed by sequencing.

5'end SHH | pGEM T-easy (cloning vector) | 3' end SHH

LIGATION

EcoRI XmnI EcoRI
5' end SHH
XmnI

EcoRI XmnI EcoRI
3' end SHH
XmnI

TRANSFORMATION

MINIPREP

RESTRICTION ENDONUCLEASE (XmnI)

XmnI _____ XmnI

XmnI _____ XmnI

RESTRICTION ENDONUCLEASE (XmnI and EcoRI)

EcoRI _____ XmnI

XmnI _____ EcoR1

LIGATION WITH PLASMID

EcoRI XmnI XmnI EcoRI

pcDNA3 (expression vector)
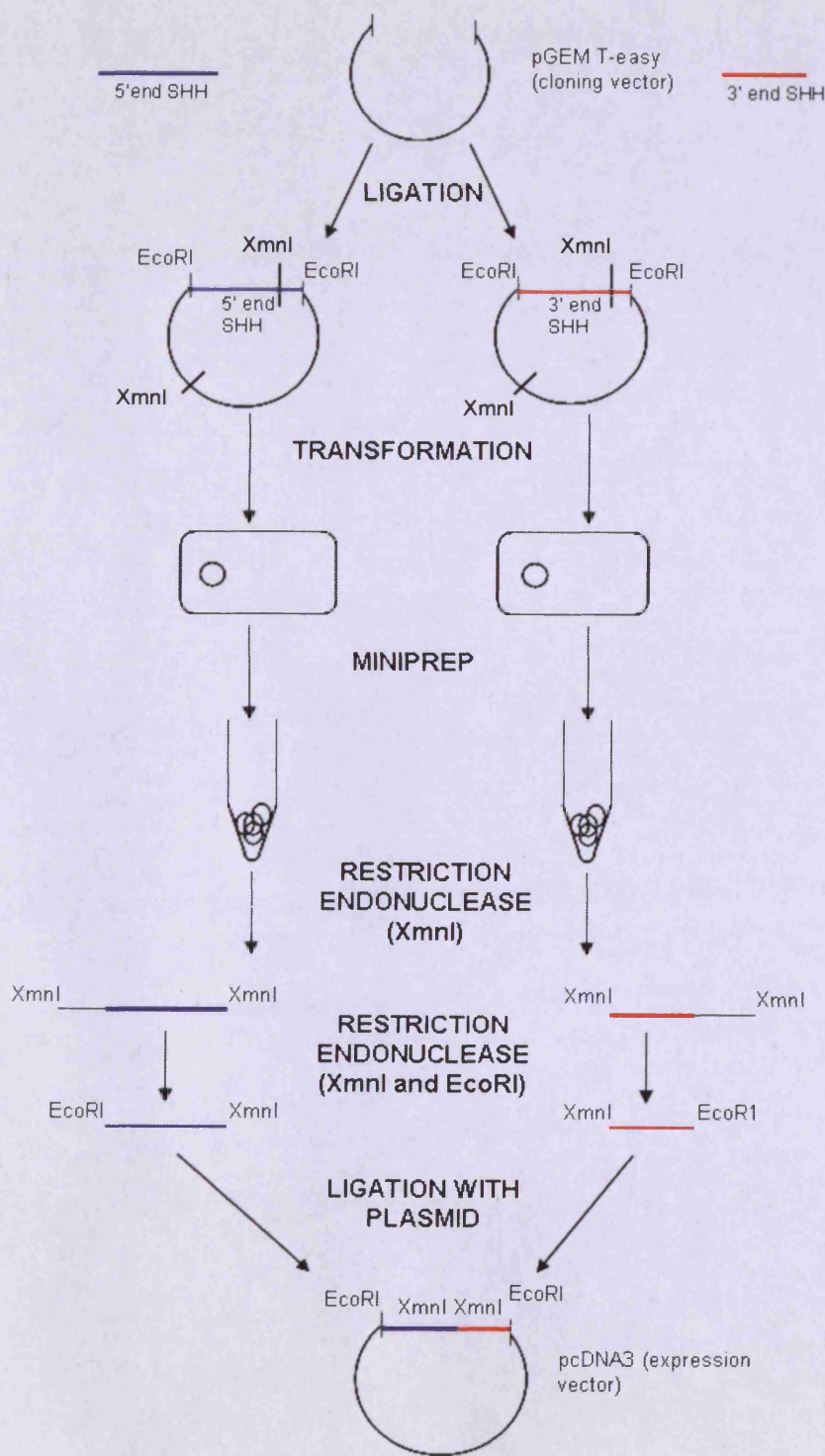
Figure 2.1. A simple diagram to show cloning.

70

2.2.3.9 Electroporation (Amaxa Kit)

Culture medium was aspirated from a T75 flask of N/TERT1 cells grown to 80% confluency (see section 2.2.1.2). The cells were washed once with dPBS and then harvested with trypsin-EDTA. Trypsinization was stopped by adding an equal volume of DMEM-F12 medium containing 10% FBS. Cells were counted using a haemocytometer and medium containing 2.5×10^6 cells was centrifuged at 1,200 rpm for 10 minutes at RT. The supernatant was aspirated completely and the pellet resuspended in 100μl nucleofector solution from the electroporation kit (Amaxa V from Lonza, Slough, UK) which contained 5μg of Tet-on advanced plasmid DNA (Takara Bio Europe/Clontech, Saint-Germain-en-Laye, France). The sample was transferred into a cuvette which was placed into the Nucleofector II (Lonza, Slough, UK). The U-20 program was run, which had been optimised for HaCaT keratinocytes (this programme was selected as both HaCaT and N/TERT1 are keratinocyte cell lines and time constraints did not allow separate optimisation for N/TERT1 cells). After electroporation, warm K-SFM medium containing supplements (500μl) was added to each cuvette and carefully mixed. This mixture was then added to two 10cm plates containing 10ml pre-warmed K-SFM medium (including supplements) and carefully mixed to allow even distribution of cells.

The medium was changed after 24 hours to K-SFM plus 400μg/ml G418 per plate to kill all non-stable transfected cells. Medium containing G418 was then changed every 4 days until colonies of stable transfected cells emerged.

2.2.3.10 N/TERT1 Transfection with MIRUS TransIT®-LT1 Reagent

Cells were plated at a density of 2×10^5 cells per well 24 hours prior to transfection in a 6 well plate containing 2ml K-SFM per well. Immediately prior to transfection, the serum free medium was removed and replaced with 2ml warm DMEM-F12 plus 10% FBS 0.2ng/ml EGF, 25μg/ml bovine pituitary extract and 1.5mM L-glutamine. TransIT®-LT1 transfection reagent (72μl) was added to 1500μl pre-warmed serum free medium in a sterile 5ml tube and mixed by gentle pipetting. After incubating at RT for 20 minutes, 14.16μl of Tet-On advanced

vector DNA (0.5µg/µl) (Takara Bio Ltd/Clontech, Saint-Germain-en-Laye, France) containing SHH DNA was added and mixed by gentle pipetting. This was then incubated at RT for 15-30 minutes. The TransIT®-LT1 reagent/DNA complex mixture was added dropwise to each well (264.4µl/well) of the 6 well plate and again mixed by gentle pipetting. Cells were then incubated for 24 hours at 37°C in 5% CO_2. The success rate of transfection was monitored by repeating the transfection using a control pmaxGFP vector (Amaxa, Lonza, Slough, UK) which contains green fluorescent protein from the Planktonic copepod *Pontellina plumata*. An aliquot (19.2µl at 0.5µg/µl) was added in the place of Tet-On advanced vector containing SHH. This pmaxGFP vector makes successfully transfected cells fluoresce green when exposed to blue light and cells were counted under an inverted microscope using a GFP filter to assess the percentage of cells that had been successfully transfected.

2.2.4. Polyacrylamide Gel Electrophoresis and Western Blotting

2.2.4.1 Sodium Dodecyl Sulphate Polyacrylamide Gel Electrophoresis (SDS-PAGE)

SDS-PAGE was carried out using the XCell Surelock mini-cell (Invitrogen, Paisley, UK). Proteins were separated on an SDS gel by electrophoresis and transferred to a membrane for western blotting using the XCell II Blot module. Immunochemistry was performed to detect the presence of proteins and to compare expression and phosphorylation levels in cells under different culture conditions.

Cells from each well of a 6-well plate (2.2.1.4) were suspended in 0.9ml SDS sample buffer containing 4.12ml H_2O, 1ml 0.5M Tris, 0.8ml glycerol, 1.6ml 10% SDS, 0.08ml 1M DTT and 0.2ml bromophenol blue and boiled for 5 minutes. Enough mixture for two 10% separating gels was made (containing 0.1ml 10% SDS, 2.5ml 1.5M Tris, 3.3ml 30% acrylamide gel solution (Sigma-Aldrich Company Ltd, Gillingham, UK), 75µl APS (ammonium persulphate from Fisher Scientific, Loughborough, UK) and 7.5µl N,N,N',N'-tetramethylethylenediamine (TEMED from Sigma-Aldrich Company Ltd,

Gillingham, UK) and 4.1ml H_2O. This was pipetted into cassettes and overlaid with water. Once set, the water was removed and a 4% stacking gel (50µl 10% SDS, 1.25ml 0.5M Tris, 0.65ml 30% acrylamide gel solution, 3.05ml H_2O, 50µl 10% APS and 10µl TEMED) was added above the separating gel. A 12 prong comb was placed into the top of the cassette and after the gel had set (about 5 minutes), the comb was carefully removed and the wells washed with dH_2O. The cassettes were placed into the apparatus and 1x running buffer (30g Tris, 144g glycine (Sigma-Aldrich Company Ltd, Gillingham, UK), 10g SDS per litre of H_2O) was poured into the apparatus, ensuring that the wells were full of buffer. The protein extracts (10µl) were loaded into the wells (volumes should give equal quantities of protein in each well for comparison) and molecular weight standards loaded on the gel (usually the end lanes). Three markers were used in combination: 10µl Precision Plus protein marker (Bio-rad, Hemel Hempstead, UK) or 5µl low molecular weight marker (Promega UK Ltd, Southampton, UK) together with 2µl Magicmark (Invitrogen, Paisley, UK). The outer and inner chambers were filled with running buffer and 125V at a starting current of 25mA per gel applied until the tracker dye reached the bottom of the separating gel. Cassettes were opened and the gel was stained with 0.25% Coomassie brilliant blue R250 (Sigma-Aldrich Company Ltd, Gillingham, UK) in 40% methanol (Fisher Scientific, Loughborough, UK) and 10% acetic acid (Fisher Scientific, Loughborough, UK) for one hour. The gel was then destained for 30 minutes in 40% methanol and 10% acetic acid. Duplicate gels were important as one was used for staining of the protein to check for even loading while the other gel remained unfixed and was used for western blotting.

2.2.4.2 Western Blotting

Immobilon membrane (PDVF Millipore) was immersed in methanol and then vigorously shaken in water to hydrate. Whatman paper and pads were soaked in western blot buffer (14.4g glycine, 3g Tris and 100ml methanol per litre dH_2O). Two pads were placed in the bottom of the western blot module, then a gel/membrane sandwich was assembled (Whatman paper, gel, Immobilon

membrane, Whatman paper) and placed on top of the pads. The module was then filled with further pads and the top locked. Buffer was added to the blotting module and the tank filled with dH_2O to keep the gel cool during transfer. Transfer continued for 1-2 hours at 25v with a starting current of approximately 100mA.

2.2.4.3 Protein Detection by Immunochemistry

Western blots on Immobilon membrane were rehydrated with methanol and washed in water, then placed in 5% skimmed milk (Marvel, Tesco, UK) in Tris-buffered saline with 0.1% Tween 20 (TBST from Sigma-Aldrich Company Ltd, Gillingham, UK) for 1 hour to block antigenic sites. Marvel was replaced with 10ml 5% marvel containing primary antibody (see **Table 2.6** for dilutions of antibodies used) for 1 hour, then washed for five times for 5 minutes in TBST. Another 10ml Marvel containing the secondary antibody (see **Table 2.6** for details) was added, left to incubate for 1 hour and then the membrane was washed in TBST (again five times 5 minutes).

The membrane was laid on Saran wrap in the dark room and covered with ECL reagent for 5 minutes. The reagent was made by combining 1ml solution 1 (1ml 250mM stock luminol (Sigma-Aldrich Company Ltd, Gillingham, UK) in DMSO, 0.44ml 90mM coumaric acid stock (Sigma-Aldrich Company Ltd, Gillingham, UK) in DMSO, 10ml Tris, pH 8.5 plus dH_2O to a total of 100ml) and 1ml solution 2 (64μl 30% H_2O_2 and 10ml Tris, pH8.5 plus dH_2O to a total of 100ml). The reagent was poured off, the membrane wrapped in Saran film and placed in a cassette together with sensitive X-ray film (Amersham Biosciences, GE Healthcare Life Sciences, Little Chalfont, UK). This was left for 2 to 10 minutes (longest incubation carried out first) and then the X-ray film was placed in Kodak D-19 developer, water and finally Kodak Processing Chemical Fixer (Sigma-Aldrich Ltd, Gillingham, UK).

Table 2.6: Primary and Secondary Antibodies for Western Blotting.

Antigen	Cat #	Company	Species	WB Dilution	Storage
ERK	9102	Cell Signalling Technology Inc, Danvers, MA, USA	Rabbit	1:1000	-20°C
P-ERK	9106S	Cell Signalling Technology Inc, Danvers, MA, USA	Mouse	1:1000	-20°C
Keratin 14	LL002	Gift from Prof E.B. Lane	Mouse	1:100	4°C
PTCH	Sc1194	Santa Cruz Biotechnology Inc, Santa Cruz, CA, USA	Goat	1:100-1:1000	4°C
SMO	Sc6152	Santa Cruz Biotechnology Inc, Santa Cruz, CA, USA	Rabbit	1:100-1:1000	4°C
Gli1	Sc13943	Santa Cruz Biotechnology Inc, Santa Cruz, CA, USA	Goat	1:100-1:1000	4°C
SHH	Sc6149	Santa Cruz Biotechnology Inc, Santa Cruz, CA, USA	Goat	1:100-1:1000	4°C
Anti-Mouse IgG-HRP	P0161	Dako UK Ltd, Ely, UK	Rabbit	1:500	4°C
Anti-Rabbit IgG - HRP	P0127	Dako UK Ltd, Ely, UK	Swine	1:500	4°C
Anti-Goat IgGs - HRP	A5420	Sigma-Aldrich Company Ltd, Gillingham, UK	Rabbit	1:40000	4°C

2.3 Results

2.3.1 SHH Signalling and Activation of the EGF Pathway.

Initially, we had to confirm that the key components of the SHH pathway were present in N/TERT1 and HaCaT keratinocyte cell lines. RT-PCR showed that SMO and PTCH were expressed in both N/TERT1 and HaCaT cells, although in HaCaT, there were miscellaneous bands in addition to a strong band of the correct size for PTCH (**Figure 2.2**). The product size was incorrect for SHH so it was concluded that this result was spurious and that no SHH was present in either cell line (HaCaT nor N/TERT1). Finally, GLI1 was expressed in HaCaT cells but not in N/TERT1 cells. GLI1 expression was relatively low suggesting there is little or no signalling before the addition of commercial recombinant SHH. The absence of SHH and GLI1 in N/TERT was unexpected but proved useful as PCR could be used to detect expression of SHH pathway target genes when N/TERT1 cells were grown in the presence of recombinant SHH (see **Table 2.7** for list of target genes examined). This subset of target genes have been specifically chosen due to the known increased expression in N/TERT1 keratinocytes treated with recombinant EGF where GLI1 levels can be high (Kasper et al., 2006).

Ideally, western blot analysis should have been used to confirm the expression of SHH pathway components. However, antibodies to these proteins (SHH, PTCH, SMO and GLI1) were not reliable (see **Table 2.6**) and could not be optimised.

In order to confirm that the EGF pathway was active after treatment of N/TERT1 keratinocytes with recombinant EGF, total protein was extracted from the treated cells at three time-points after treatment: 5, 10 and 20 minutes and cells with no EGF were used as a control. The protein extracts were separated by SDS-PAGE and western blots performed.

Figure 2.2: SHH Pathway Components in N/TERT1 and HaCaT Keratinocytes.
Ethidium bromide gel showing expression of SHH signalling pathway components: SMO,
PTCH, SHH and GLI1 in N/TERT1(yellow) and HaCaT (blue) keratinocyte cells, with
APRT control and 100bp molecular weight marker. 10μl of each PCR product in coral
load buffer was applied to each well.

Table 2.7: Change (fold mRNA induction) in SHH Target Genes (EGR-3, S100A7, IL-1R2
and PTCH) in N/TERT1 cells expressing GLI1 and/or EGF compared to Untreated
Controls (data from Kasper et al., 2006).

	EGF	GLI1	EGF/GLI1
EGR-3	7.7	1.2	652.6
S100A7	2.3	9.8	1351.1
IL1-R2	2.4	9.9	999.5
PTCH	-2.1	29.9	19.7

K14 is the same at all time points, which shows equal loading of the wells because
K14 levels should always be the same in cells of the same type. There was little
change in ERK1, except for a slight increase in N/TERT1 cells. ERK2 in
N/TERT1 cells appeared to increase over time, with slightly lower ERK1/2 bands
at the zero time point. ERK1/2 phosphorylated (N/TERT1) was very low in
absence of EGF but dramatically increased in the presence of EGF and remained

the same for those time points. ERK1/2 in HaCaT cells remained the same at all time points. ERK1/2 phosphorylated in HaCaT cells was absent at the zero time point where EGF is absent. However, it was increased in the presence of EGF at all time points. The p-ERK1 band was missing at 10 and 20 minutes (**Figure 2.3**).

(a)   (b)
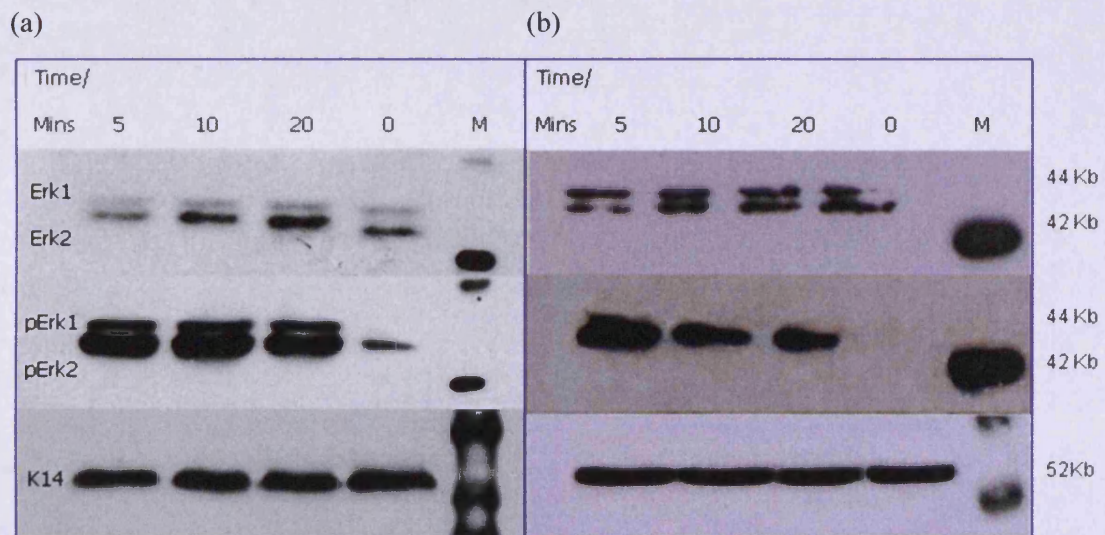
Figure 2.3: EGF Signalling Pathway Components in N/TERT1 and HaCaT Keratinocytes. Western blots of ERK1/2 expression and phosphorylation in N/TERT1 (a) and HaCaT cells (b) at different time points after the addition of EGF to the culture medium with a Magicmark protein marker. K14 control indicated equal protein sample loading (10µl per well).

2.3.2. Cell Viability Tests

Baseline luminescence was extremely small in the absence of N/TERT1 cells indicating that the values achieved in the presence of cells were a genuine measure of viability (**Table 2.8**). The luminescence in the absence of diluents and inhibitors represents the control. DMSO reduced the luminescence by about 5% but there was no additional effect in the presence of LY294002, this was similar to when DMSO was applied alone. PD98059 had a much greater effect, causing a 23% reduction in luminescence. The effect of PD98059 on luminescence was increased in the presence of LY294002.

78

Table 2.8: N/TERT1 Cell Viability in the Presence of EGF Pathway Inhibitors LY294002 and/or PD98059. Cell viability decreased slightly in the presence of DMSO diluents or LY294002. However, there was a larger decrease in cell viability (23% reduction in luminescence) in the presence of PD98059. Data expressed as the mean of 4 cell culture well replicates for each treatment. RLU = Relative Light Unit

	Control (no DMSO, no inhibitors)	DMSO (no inhibitor control)	20μM LY294002	20μM PD98059	20μM LY294002 + 20μM PD98059
Luminescence (RLU)	489542	464784	473072	377220	314754
% Reduction Luminescence	0	5.06	3.36	22.94	35.70
Reduction		-24,758	-16,470	-112,322	-174,788

2.3.3 N/TERT1 Cells treated with Recombinant SHH, EGF and EGF Pathway Inhibitors (PD98059 and LY294002).

Although the key components (PTCH and SMO) of the SHH pathway were present in N/TERT1 and HaCaT cell lines, it was important to confirm that the pathway could be activated.

The N/TERT1 cells were grown and treated with recombinant SHH and/or EGF and then treated with LY294002 and/or PD98059 as described in the methods. Expression of K14 (control), EGR-3, PTCH and S100A7 was examined by RT-PCR (**Figure 2.3**). The data shown in **Figure 2.3** was also analysed using Image J density gradient software (http://rsbweb.nih.gov/ij/) and the results were normalised against the K14 control data. This software was also used to compare reproducibility in the duplicate experiments shown. This programme measured the density over the area of bands on a DNA gel, which were then used to calculate

the relative band density compared to the control (K14) and the data was then displayed in graphic form using Microsoft Excel (see **Figures 2.4 to 2.6**).

K14 levels are equal in all circumstances (**Figure 2.3 and 2.4**). PTCH was increased with SHH but this increase was blocked by EGF. PTCH was also increased with LY294002, but this increase was blocked by SHH and reduced by EGF. However, PTCH levels in the presence of PD98059 with LY294002 were similar to the control, with both arms of the EGF pathway inhibited.

EGR-3 was slightly increased in the presence of SHH but there was a greater increase in the presence of EGF. LY294002 completely blocked EGR-3 expression, whereas PD98059 had no effect on the control but blocked EGR-3 in the presence of SHH or EGF. LY294002 and PD98059 combined completely blocked EGR-3 except when both SHH and EGF were present.

S100A7 was low in the control but increased in the presence of SHH or EGF. LY294002 caused the S100A7 control to increase. SHH or EGF increased S100A7 further but the level was reduced when both were present. PD98059 had little effect on S100A7 and knocked down the effect of LY294002 when both were applied. These change differed slightly between the two samples for each gene.
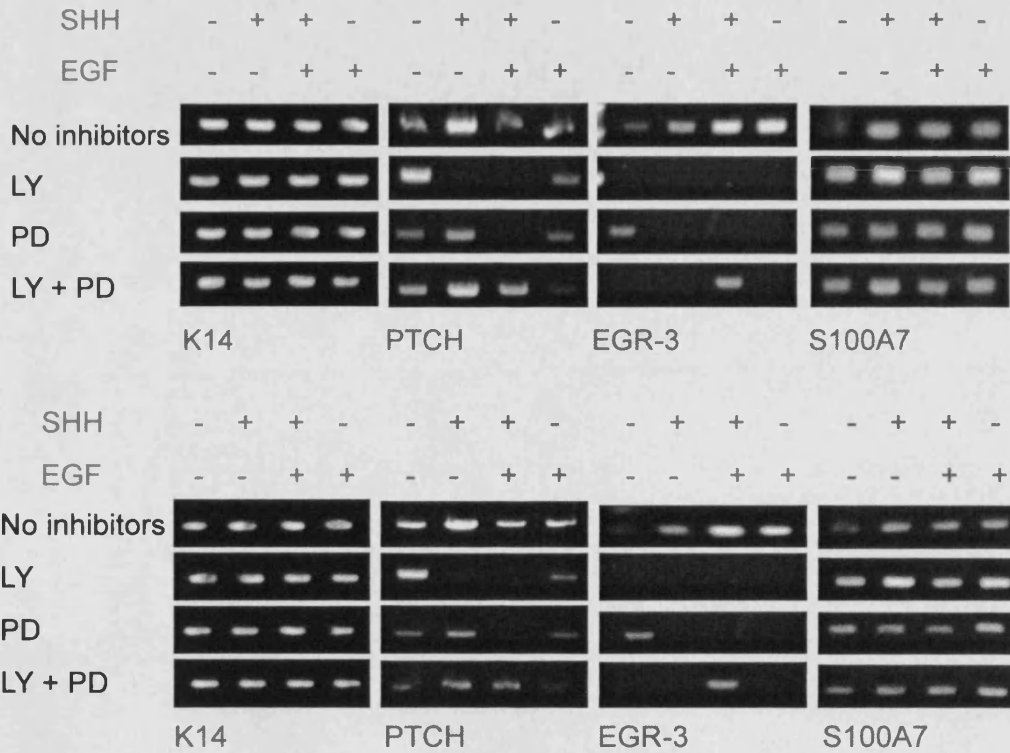
Figure 2.4: RT-PCR of SHH Target Genes (PTCH, EGR-3 and S100A7) and K14 Control in N/TERT1 Cells. Stimulation with EGF and/or SHH for 24 hours in the presence and absence of EGF signalling inhibitors (LY294002 and/or PD98059). Duplicate experiments are shown.

There is variation between the two experiments (yellow is the first and blue is the second experiment). PTCH was increased with SHH, whereas EGF alone had no effect. However, EGF blocked the increase in PTCH caused by SHH (**Figure 2.4a**). LY294002 blocked PTCH expression in the presence of SHH and/or EGF, but PTCH was increased in the control cells (**Figure 2.4b**). PD98059 reduced PTCH expression slightly, blocked the SHH induced increase in PTCH, but had little effect on EGF modulation of PTCH (**Figure 2.4c**). PD98059 and LY294002 interfere with one another so PTCH levels in the presence of SHH were higher and almost returned to the levels seen in the absence of inhibitors (**Figure 2.4d**).

81
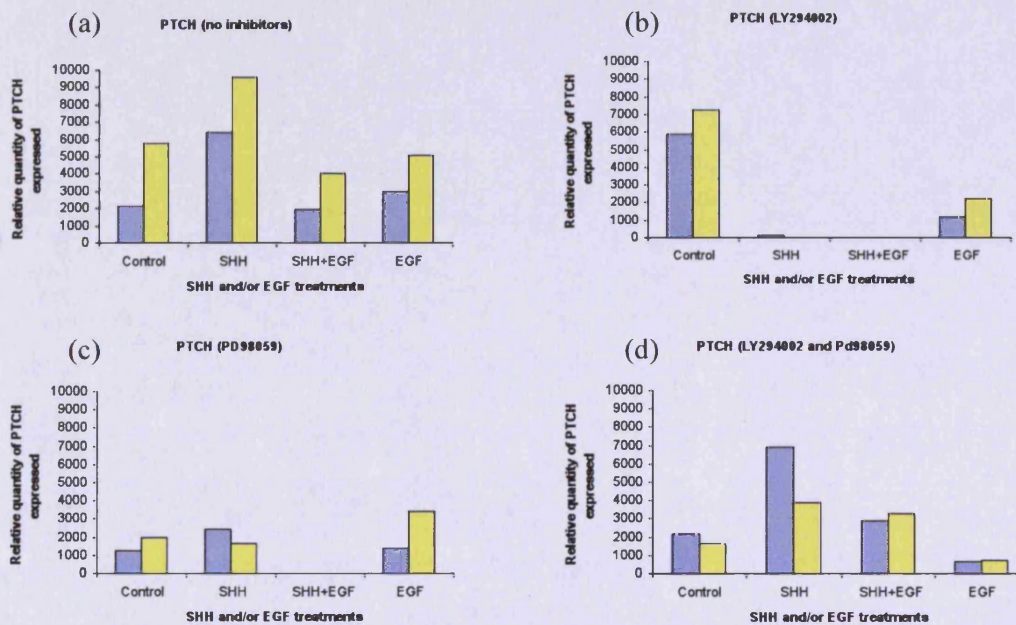
Figure 2.5: Relative expression of PTCH in N/TERT1 Keratinocytes treated with Recombinant SHH and/or EGF in the Presence or Absence of Inhibitors (LY294002 and/or PD98059). Graphs show PTCH expression in two PCR experiments: blue bars represent one experiment (top part of Figure 2.3) while the yellow bars represent the other (bottom part of Figure 2.3).

EGR-3 was increased in the presence of SHH or EGF, but this effect was neither additive nor synergistic (**Figure 2.5a**). LY294002 totally blocked EGR-3 expression and inhibited the effect of SHH or EGF (**Figure 2.5b**). However, PD98059 had little effect in the absence of SHH or EGF but totally blocked EGR-3 expression in their presence (**Figure 2.5c**). This block was relieved in the presence of SHH and EGF together when both inhibitors were used (**Figure 2.5d**).

These results suggest that there may be some SHH pathway activity and the small increase in expression in the presence of both SHH and EGF may be evidence of a mild synergistic effect but nowhere near as large as described by Kasper et al (2006).
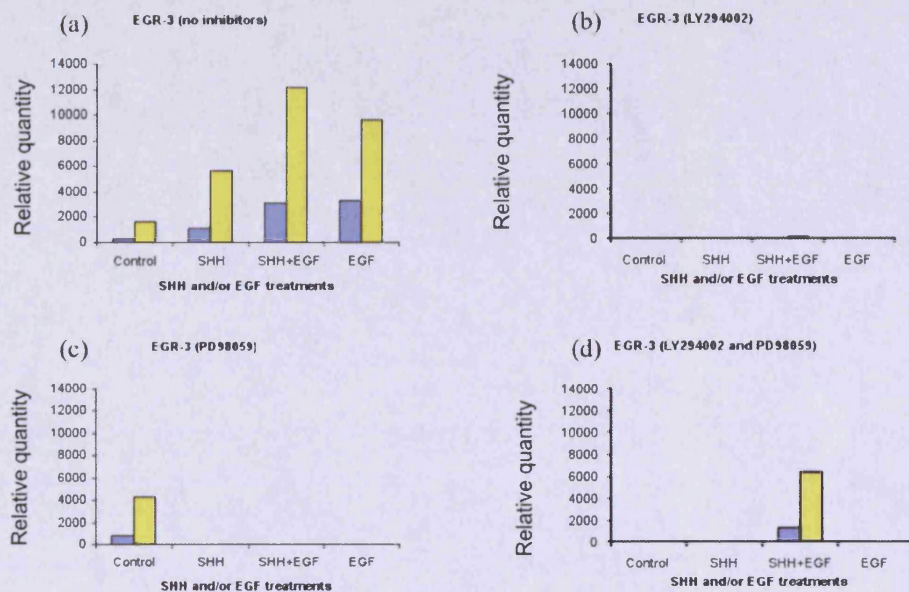
Figure 2.6: Relative Expression of EGR-3 in N/TERT1 Keratinocytes treated with Recombinant SHH and/or EGF in the Presence or Absence of Inhibitors (LY294002 and/or PD98059). Graphs show EGF-3 expression in two PCR experiments: blue bars represent one experiment (top part of **Figure 2.3**) while the yellow bars represent the other (bottom part of **Figure 2.3**).

S100A7 was increased by SHH or EGF, but together they only caused a small increase in S100A7 which was not additive (**Figure 2.6a**). LY294002 increased S100A7 expression slightly in the absence and to a greater extent in the presence of SHH or EGF but there was little effect when both SHH and EGF were present (**Figure 2.6b**). PD98059 increased S100A7 but SHH had no additional effect, whereas EGF did increase S100A7 slightly, but this was lost when both were applied together (**Figure 2.6c**). The positive effect of LY294002 was lost in the presence of PD98059 (**Figure 2.6d**).
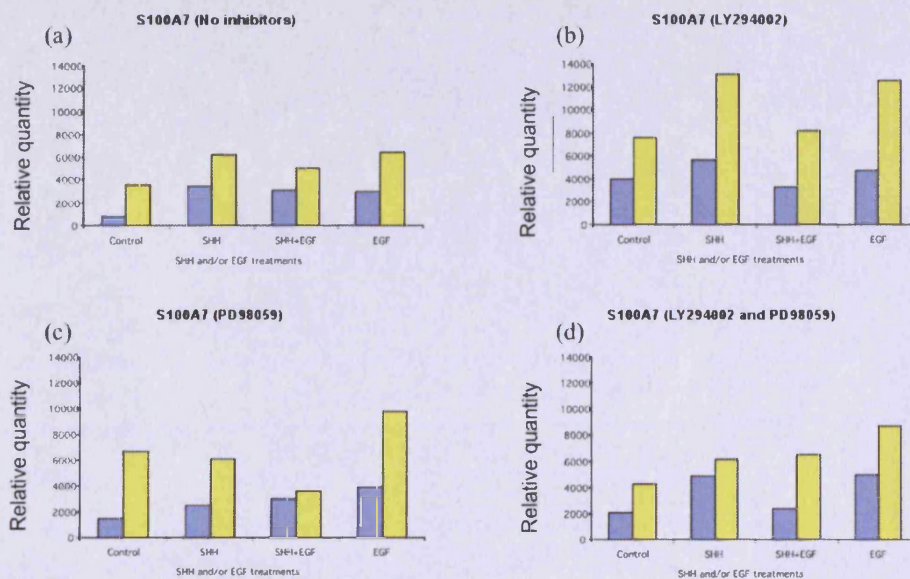
Figure 2.7: Relative Expression of S100A7 in N/TERT1 Keratinocytes treated with Recombinant SHH and/or EGF in the Presence or Absence of Inhibitors (LY294002 and/or PD98059). Graphs show S100A7 expression in two PCR experiments: blue bars represent one experiment (top part of **Figure 2.3**) while the yellow bars represent the other (bottom part of **Figure 2.3**).

2.3.3.1 Quantitative PCR (qPCR)

Conventional PCR did not identify the large changes in expression of GLI1 and EGF target genes observed by Kasper et al. (2006) but some small differences were apparent. These would be difficult to evaluate by conventional RT-PCR, so quantitative analysis was performed by qPCR to measure the fold change in gene expression.

The expression of three GLI/EGF target genes (EGR-3, IL-1R2 and S100A7) and (one SHH target gene PTCH) was assessed in N/TERT1 cultures by qPCR following primer optimisation. Cells were stimulated with recombinant SHH and/or EGF and then treated with either a PI3K inhibitor (LY294002) or a MEK inhibitor (PD98059). Each experiment was done in the presence and absence of

84

inducers (SHH or EGF) and in the presence and absence of inhibitors (LY294002 or PD98059) together with control data. In this way, any effect of the inhibitors on gene expression could be assessed.

2.3.3.1.1 Selection of a Suitable Housekeeping Gene

Three housekeeping genes were selected and primer pairs were optimised for qPCR: transcription factor IIH (TF2H), actin related protein (ARP) and adenine phosphoribosyl transferase (APRT). Expression of these three genes was then measured during stimulation of N/TERT1 cells by SHH and/or EGF and any effect of the inhibitors (LY294002 and PD98059) assessed.

In all three cases, the housekeeping genes showed a major reduction in expression (up to 10,000 fold) when cells were treated with both inhibitors together (**Figure 2.7**). Based on these results, it became clear that by inhibiting both sides of the EGF pathway, expression of many genes in the N/TERT1 cell line are affected. This is a consideration with regards to the potential toxicity of the proposed formulation. The combined LY294002/PD98059 treatment was therefore not continued in further experiments.

Table 2.9 shows the combinations of recombinant SHH and/or EGF or no recombinant proteins applied to N/TERT1 keratinocytes. There are four replicates for these combinations where N/TERT1 cells were grown in the absence of inhibitors or the presence of PI3K inhibitor LY294002 and/or MEK inhibitor PD98059 in addition to the SHH and/or EGF recombinant proteins. Due to the complexity of qPCR amplification plots for these experiments, a key is included in this table to make it clearer what each plot represents.

Table 2.9: Combinations of recombinant SHH, EGF and signal transduction pathway inhibitors used to treat keratinocytes.

Inhibitors	Plate no.	SHH	EGF	Key to amplification plots
No Inhibitors	1	-	-	Brown square (solid)
	2	+	-	Blue circle (solid)
	3	+	+	Brown triangle (open)
	4	-	+	Turquoise diamond (open)
LY294002	5	-	-	Orange triangle inverted (solid)
	6	+	-	Grey diamond (solid)
	7	+	+	Yellow star
	8	-	+	Purple square (open)
PD98059	9	-	-	Green inverted triangle (open)
	10	+	-	Green triangle (solid)
	11	+	+	Orange star
	12	-	+	Grey circle (solid)
LY294002+PD98059	13	-	-	Purple diamond (solid)
	14	+	-	Olive square (solid)
	15	+	+	Blue-green triangle (solid)
	16	-	+	Orange star
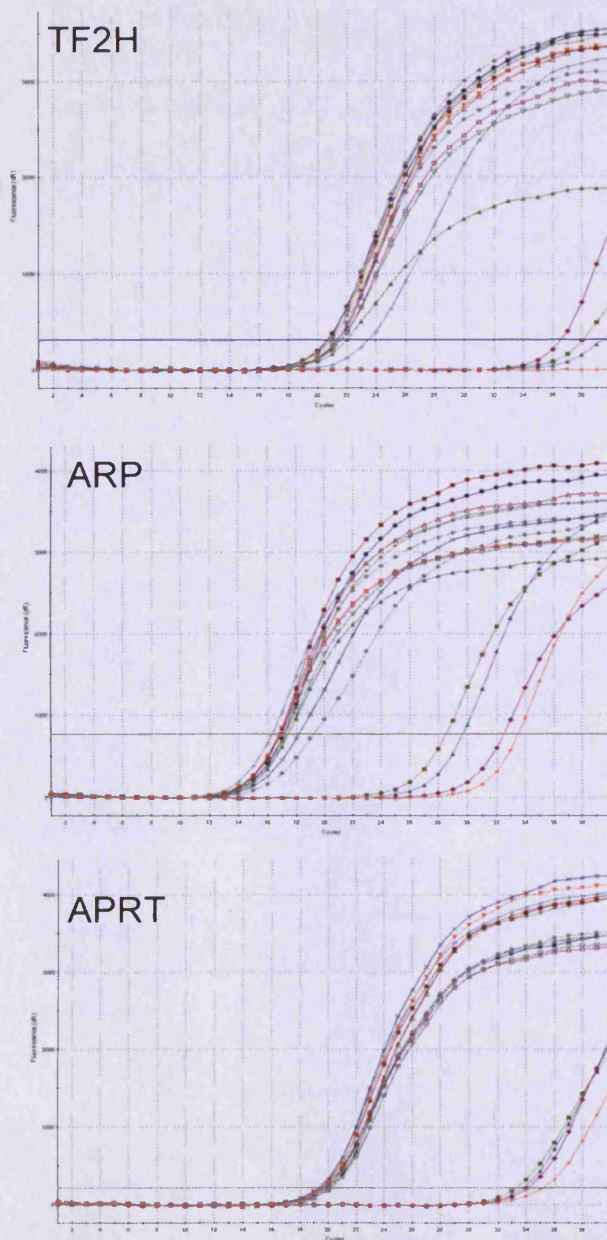
Figure 2.8: QPCR Data for Housekeeping Gene Expression in N/TERT1 Keratinocytes.
Amplification plots for TF2H, ARP and APRT showing expression in cultured cells in the
presence of LY294002 and/or PD98059. In all three cases, expression was dramatically
decreased in the presence of both inhibitors (LY294002 and PD98059, shown in purple,
*olive green, cyan and orange, see **Table 2.9** for key).*

Optimisation of ACTB (β-actin) primers also showed outlying curves in the amplification plots when LY294002 and PD98059 were both present. However, when these treatments were not included all the Ct (cycle threshold) values were clustered together and the β-actin gene maintained stable expression (**Figure 2.8**). The alternative housekeeping genes would have also been useful where experiments using both inhibitors in combination were not included, however ACTB was chosen because the amplification plots were close together giving very similar Ct values at a low number of cycles.
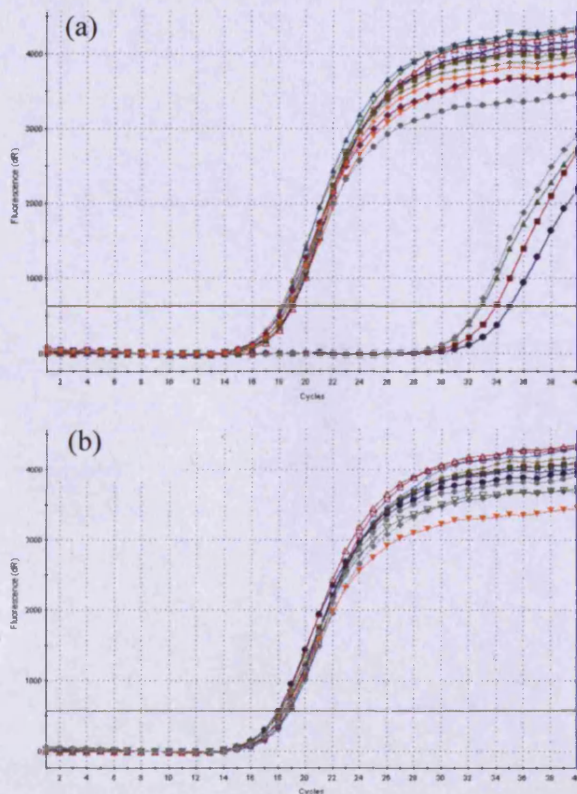
Figure 2.9: QPCR Data for ACTB (Housekeeping Gene) Expression in N/TERT1 Keratinocytes. *Amplification plots after optimisation of cDNA from SHH and/or EGF stimulated N/TERT1 keratinocytes treated with inhibitors (LY294002 or PD98059). ACTB expression remained stable in N/TERT1 keratinocytes under these treatment regimes.*

2.3.3.1.2. ACTB (β-actin) Optimisation

QPCR is used to measure DNA amplification because it can give more accurate results than end point PCR, which may continue and give results which are past the exponential phase of the reaction. In qPCR, the fluorescence caused by binding of Sybr Green is measured throughout the reaction. Fluorescence increases by 1000 fold When Sybr Green binds double stranded DNA. Measurements are used at the threshold cycle (Ct), which is the cycle at which fluorescence is determined to be statistically significant above the background. It is more accurate to measure the Ct value because this is the exponential phase of the qPCR rather than the endpoint of a PCR cycle and endpoint values can be influenced by limiting reagents, cycling parameter differences or reaction components. Lower Ct values are preferable because primer dimers are more likely to occur at later timepoints, but high Ct values can be caused by low levels of DNA. QPCR optimisation means that it is possible to check for primer dimers, chose the conditions required for a low Ct value and make sure the experiment will be as accurate as possible using a housekeeping gene which maintains the same Ct value under all conditions.

The lowest Ct value for ACTB primers was obtained with 1μg cDNA and 1.5 μg ACTB primers, therefore, further optimisation around these values was continued. The dissociation or melting curve for the ACTB primers (**Figure 2.9a**) shows that when the amplification products of QPCR were heated, there was only one melting point. This means that there was one product and therefore no primer dimers interfering with the results. The amplification plot for ACTB shows that at serial cDNA dilutions of 1, 1:10, 1:100 and 1:1000μg/μl, the plots were evenly spaced (**Figure 2.9b**). The Ct values taken from the amplification plots with the serial dilutions were then plotted against the cDNA concentrations used to make the standard curve, which should have an efficiency as close to 100% as possible and an R^2 value as close to 1 as possible for the most accurate qPCR experiments. The standard curve for ACTB was very good, staying within the recommended range

and thus qPCR carried out under the optimised conditions should give very accurate results (**Figure 2.9c**).

The levels of each gene (EGR-3, IL1-R2, PTCH1 and S100A7, see **Table 2.2** for primer sequences) when N/TERT1 cells had been treated with SHH, EGF and inhibitors (**Table 2.9**) were normalised to the levels of housekeeping gene ACTB, which always remains constant. The effect of SHH, EGF, LY294002 and PD98059 treatments could then be compared graphically.

(a) Dissociation Curve   (b) Amplification Plot

(c) Standard Curve

$R^2 = 0.995$
Slope = -3.3
Eff = 96.6%
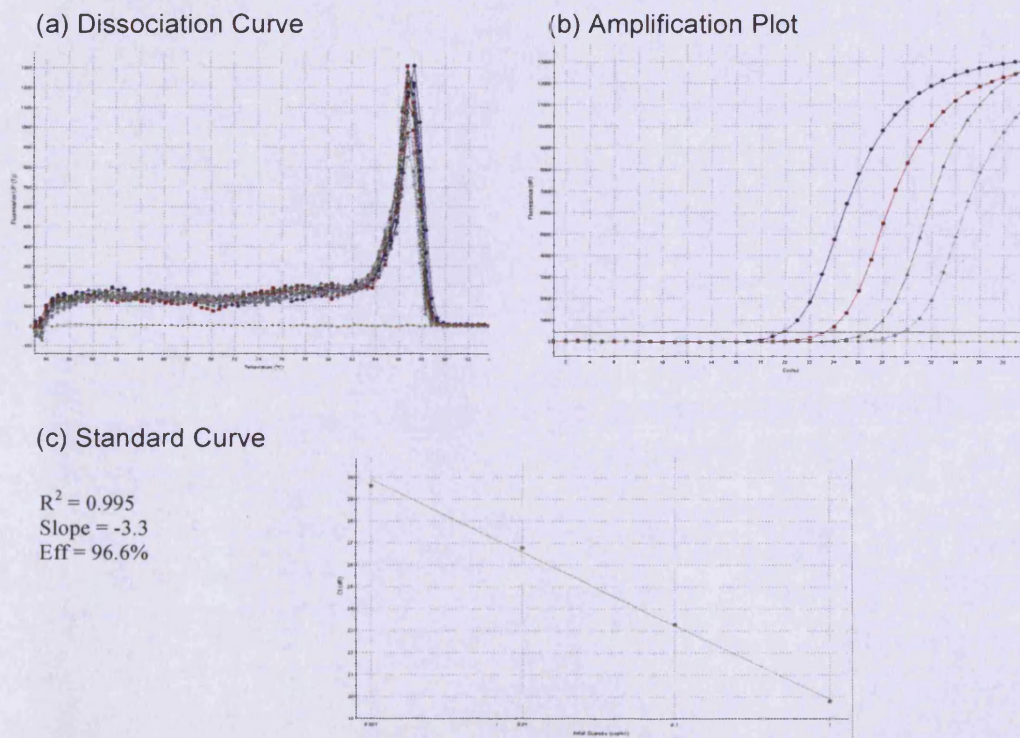
Figure 2.10: Optimisation of ACTB primers with cDNA from N/TERT1 keratinocytes. (A) dissociation curve for ACTB primers with N/TERT1 cDNA; (B) Dilution series of N/TERT1 cDNA neat (1.5µg) cDNA (blue), 1:10 dilution cDNA (red), 1:100 dilution cDNA (green) and 1:1000 dilution cDNA (grey) with ACTB primers (C) Standard curve for N/TERT1 cDNA dilution series with ACTB primers.

β-actin is abundant in keratinocytes because it is a cytoskeletal protein and so a relatively low Ct value can be obtained by optimisation of the qPCR reaction. However, EGR-3, IL1-R2, S100A7 and PTCH are present in much lower amounts and so this makes it much harder to optimise those primers for qPCR because very large amounts of cDNA would be required.

2.3.3.1.3 EGR-3 optimisation for N/TERT1 keratinocytes.

2μg cDNA and 1μg EGR-3 primers gave the lowest Ct value so these concentrations were used for further qPCR of this gene. The dissociation curve showed a small extra curve (blue line), which may be caused by some contamination or primer dimerisation, but the rest of the lines follow one curve so have no contamination or primer dimers (**Figure 2.10a**). The amplification plots show that the dilutions did not have equal spacing between them (**Figure 2.10b**) and although the R^2 value was 0.995, the slope and efficiency could not be optimised to within the suggested limits of between -3.2 and -3.5 slope and between 90-110% efficiency, although optimisation was repeated several times (**Figure 2.10c**). This may lead to reduced accuracy in the results for expression of this gene.

(a) Dissociation Curve

(b) Amplification Plot

(c) Standard Curve

$R^2 = 1$
Slope = -2.66
Eff = 137%
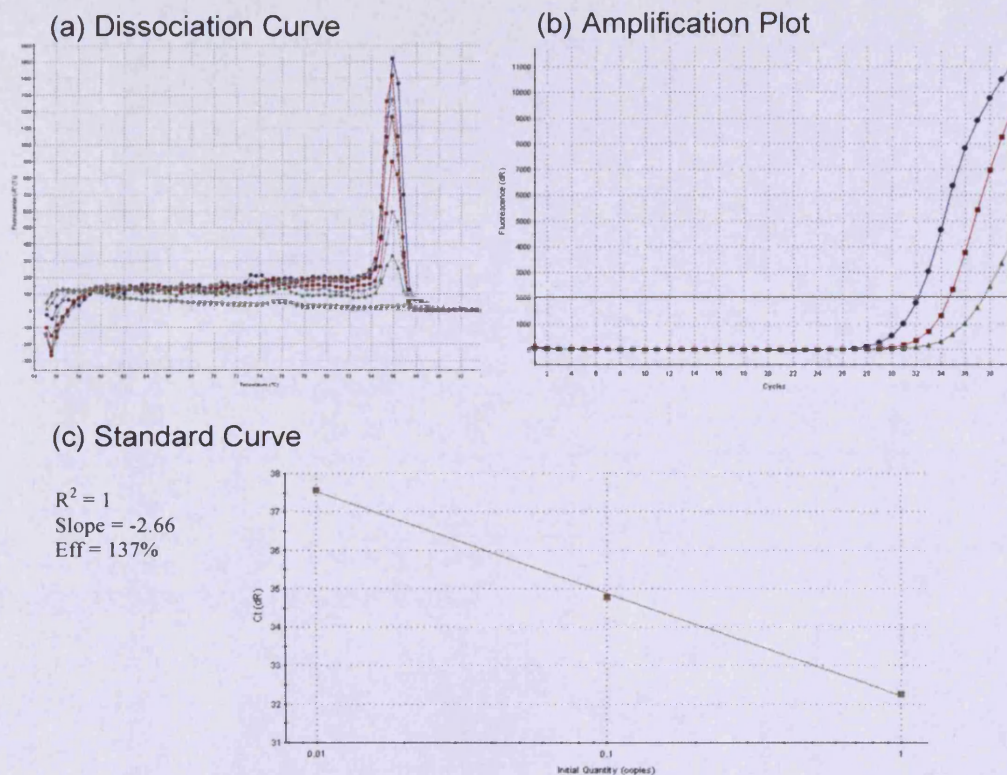
Figure 2.11: Optimisation of EGR-3 Primers and N/TERT1 Keratinocyte cDNA. (a) Dissociation curve for N/TERT1 cDNA with EGR-3 primers. (b) Amplification plot of dilution series of N/TERT1 cDNA neat (1.5μg) cDNA (blue), 1:10 dilution cDNA (red), 1:100 dilution cDNA (green) and 1:1000 dilution cDNA (grey) and EGR-3 primers. (c) Standard curve for N/TERT1 cDNA dilution with EGR-3 primers.

2.3.3.1.4 Effect of SHH/EGF on EGR-3 expression in N/TERT1 keratinocytes.

Having optimised the EGR-3 and ACTB housekeeping gene primers, qPCR was run with the N/TERT1 cDNA to compare EGR-3 expression under different conditions (for treatments with SHH/EGF and/or inhibitors see **Table 2.9**). There were two control conditions used, the first was from untreated N/TERT1 cells and the second was not treated with SHH or EGF but was one or both inhibitors were applied (**Figure 2.11b and c**)

92

EGR-3 levels did not significantly change in the presence of SHH and/or EGF when no inhibitors were present (**Figure 2.11a**). The PI3K inhibitor (LY294002) increased EGR-3 levels in response to SHH (~2 fold, p=0.05) or EGF (~1.5 fold, NS) compared to both controls. However, in combination SHH and EGF action was blocked (EGR-3 levels in the presence of SHH were significantly greater than SHH and EGF in combination, p=<0.001). The control in the presence of LY294002 (PI3K inhibitor) caused reduced expression (0.5 fold EGR-3 expression) compared to the control where no inhibitors were present (1 fold EGR-3 expression) but this was not significant. MEK inhibitor PD98059, reduced EGR-3 expression in the control and in the presence of SHH and/or EGF (p=<0.001 for all) compared to the control where no inhibitors were present (**Figure 2.11**).

The large-fold increase in EGR-3 seen by Kasper et al. (2006) when cells are treated with both GLI1 and EGF is not reproduced in the current work with presence of both recombinant SHH and recombinant EGF in N/TERT1 medium. The 7.7 fold increase in EGR-3 expression in the presence of EGF alone which was shown by Kasper et al. (2006) was also not shown in the qPCR results of the current work (**Figure. 2.11A**).
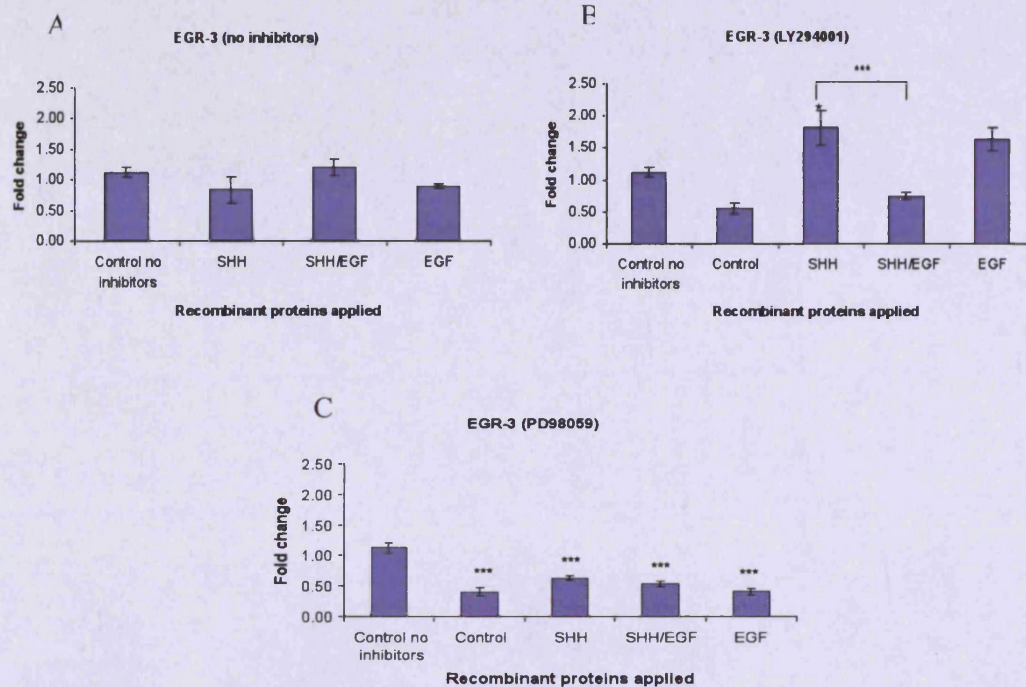
Figure 2.12: Relative Fold Change (qPCR) in EGR-3 Levels in N/TERT1 Cells treated with SHH and/or EGF in the Presence or Absence of Inhibitors (PD98059 or LY294002). Relative fold change in EGR-3 levels determined by qPCR in the absence (a) and presence of two inhibitors, LY294002 (b) and PD98059 (c). Each bar represents data in the absence of SHH and EGF (control), presence of either SHH or EGF or both. Statistical analysis was done by Ordinary ANOVA, Tukey test. * P=<0.05, ** P=<0.005, *** P=<0.001. Data expressed as a mean +/- SD for n=3 experiments with 3 replicates for each experiment.

2.3.3.1.5 IL1R2 optimisation.

2µg cDNA and 0.5µg IL1R2 primers gave the lowest Ct value for qPCR so these concentrations were used for further qPCR of this gene. Optimisation provided a dissociation curve which showed a small peak in front of the large clean peak for the melting of the amplification products, which means there may have been a primer dimer or contamination in the qPCR reaction (**Figure 2.12a**). The dilution series reactions showed that the final curve (1:1000 dilution) had a very late Ct value which meant it didn't even fit on the graph (**Figure 2.12b**). However, the first three Ct values for the dilution series were plotted against the dilution the slope and efficiency fell within the suggested guidelines (**Figure 2.12c**), which would mean that the accuracy of qPCR experiments for this gene was high.

(a) Dissociation Curve

(b) Amplification Plot

(c) Standard Curve

$R^2 = 0.998$
Slope = -3.37
Eff = 98%
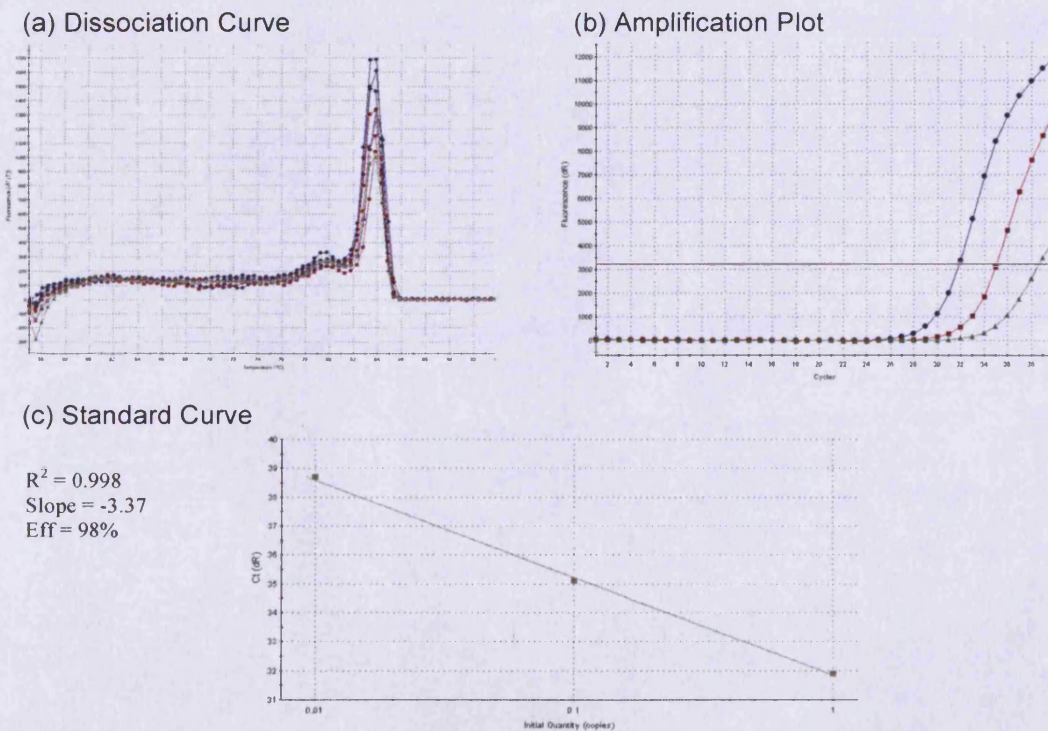
Figure 2.13: Optimisation of IL-1R2 Primers and N/TERT1 Keratinocyte cDNA. (A) Dissociation curve for N/TERT1 cDNA with IL-1R2 primers (B) Dilution series of N/TERT1 cDNA: neat (1.5µg) cDNA (blue), 1:10 dilution cDNA (red), 1:100 dilution cDNA (green) and 1:1000 dilution cDNA (grey) with IL-1R2 primers (C) Standard curve for N/TERT1 cDNA dilution series with IL-1R2 primers.

2.3.3.1.6 Effect of SHH/EGF on IL1R2 expression

SHH caused no significant increase in IL1R2 levels. EGF caused a 5 fold increase ($p=<0.001$), but the effect of EGF on IL1R2 was inhibited slightly by SHH ($p=<0.001$ when compared to the control) (Figure **2.13a**).

PI3K inhibitor LY294002 led to no change in IL1R2 levels for the control or in the presence of SHH compared to the control where no inhibitors were present. EGF caused a 2 fold increase ($p=<0.005$) and there was an additive increase (~3 fold) when both SHH and EGF in were applied ($p=<0.001$). IL1R2 levels in the presence of SHH and EGF are significantly greater than in the presence of SHH ($p=<0.001$) or EGF ($p=<0.005$) individually (**Figure 2.12b**).

MEK inhibitor PD98059 did not effect the IL1R2 levels in the controls. SHH did not effect IL1R2 either. EGF increased IL1R2 3 fold ($p=<0.005$) which was maintained in the presence of SHH ($p=<0.005$). This was also significantly increased compared to in the presence of SHH ($p=<0.001$) (**Figure 2.13c**).

As with EGR-3, IL1R2 expression did not show the large fold increase seen by Kasper et al. (2006) when SHH and EGF in combination was used to treat the cells.
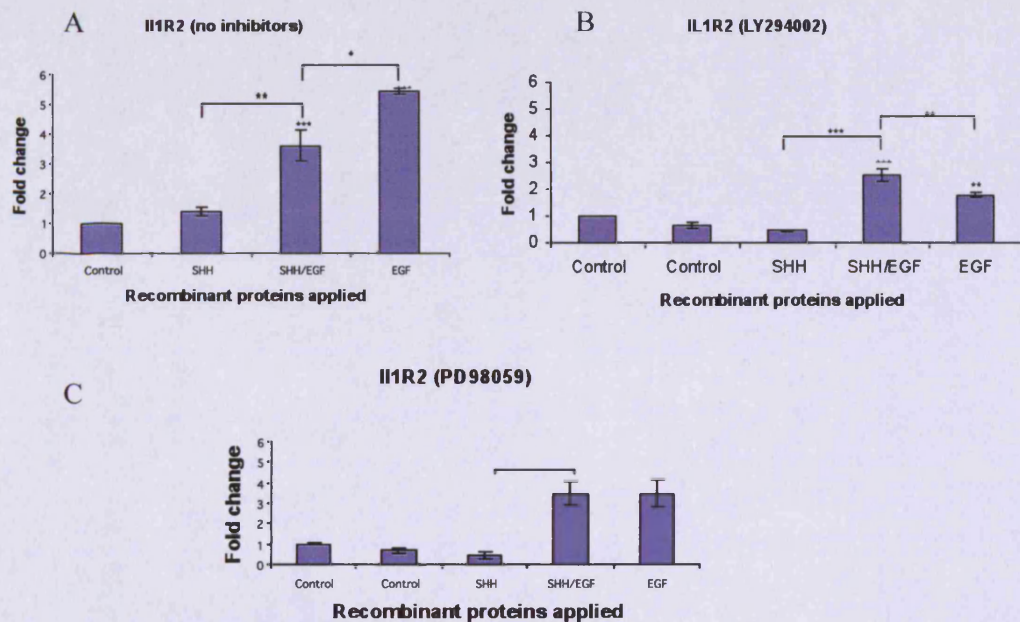
Figure 2.14: Relative Fold Change (qPCR) in IL-1R2 Levels in N/TERT1 Cells treated with SHH and/or EGF in the Presence or Absence of Inhibitors (PD98059 or LY294002). Relative fold change in IL1-R2 levels determined by qPCR in the absence (a) and presence of two inhibitors, LY294002 (b) and PD98059 (c). Each bar represents data in the absence of SHH and EGF (control), presence of either SHH or EGF or both. Statistical analysis was done by Ordinary ANOVA, Tukey test. * P=<0.05, ** P=<0.005, *** P=<0.001. Data expressed as a mean +/- SD for n=3 experiments with 3 replicates for each experiment.

2.3.3.1.7 S100A7 optimisation.

2µg cDNA and 1.5µg S100A7 primers gave the earliest Ct values so these concentrations were used for further qPCR of this gene (**Figure 2.15b**). Optimisation provided a clean dissociation curve which shows no primer dimers or contamination in the qPCR reaction (**Figure 2.15a**). However, the qPCR with a dilution series did not give curves at equal intervals reactions and the Ct values were still not early enough for a very efficient qPCR, probably due to the low levels of S100A7 in these cells (**Figure 2.15b**). Optimisation did not enable slope

97

and efficiency to fall within the suggested guidelines even after repeating optimisation several times (**Figure 2.15c**), which may reduce accuracy of QPCR experiments for this gene, again poor qPCR may be due to the low levels of S100A7 present.

(a) Dissociation Curve

(b) Amplification Plot

(c) Standard Curve

$R^2 = 1$
Slope = -2.61
Eff = 141.8%
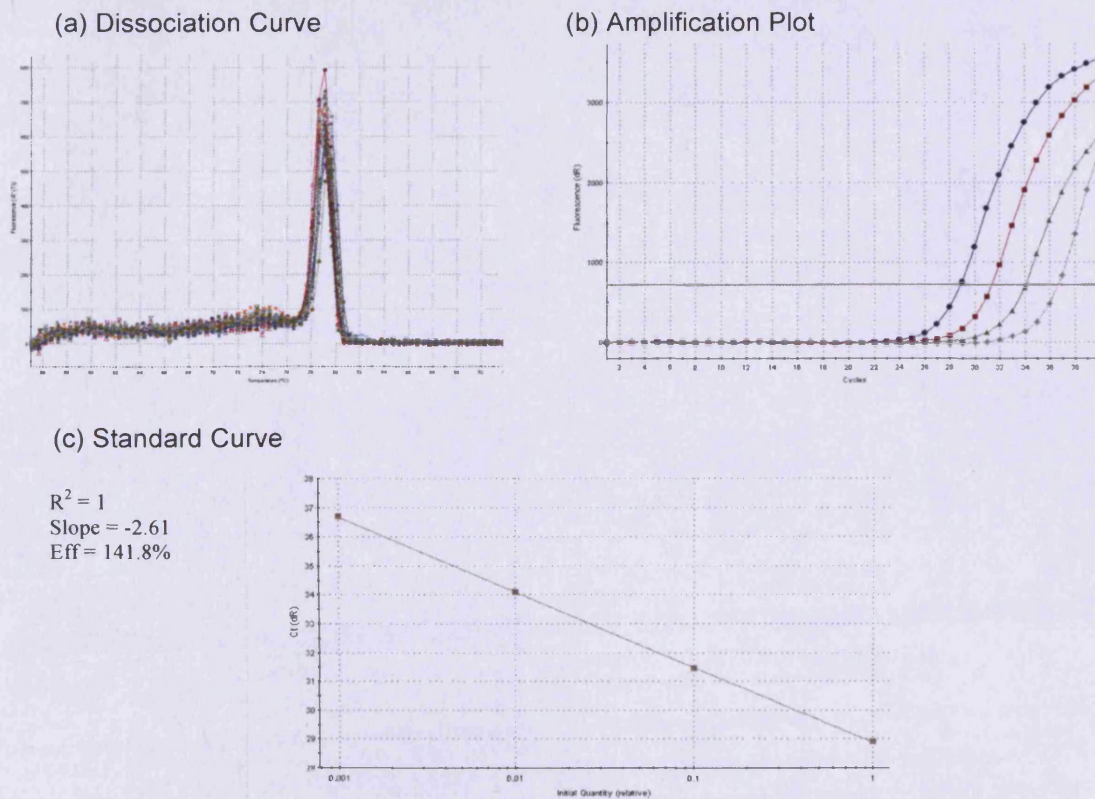
Figure 2.15: Optimisation of S100A7 Primers and N/TERT1 Keratinocyte cDNA. (A) Dissociation curve for N/TERT1 cDNA with S100A7 primers. (B) Dilution series of N/TERT1 cDNA using 1.5µg cDNA (blue), 1:10 dilution (red), 1:100 dilution(green) and 1:1000 dilution (grey) with S100A7 primers. (C) Standard curve for N/TERT1 cDNA dilution series and S100A7 primers.

2.3.3.1.8 Effect of SHH/EGF on S100A7 expression in N/TERT1 keratinocytes.

SHH increased S100A7 expression 4 fold (NS) and EGF increased S100A7 12 fold when compared to the control (p=<0.001). However, SHH blocked the effect of EGF (**Figure 2.15A**).

LY294002 (PI3K inhibitor) increased S100A7 1 fold (p=0.05). SHH had little effect, but EGF slightly increased S100A7 (p=0.05) and in combination with SHH there was an additive increase in S100A7 (p=0.001), which was also significantly larger than in the presence of either SHH (p=0.001) or EGF (p=0.005) (**Figure 2.15B**).

PD98059 (MEK inhibitor) increased S100A7 4 fold (p=0.001). The addition of SHH had little effect, EGF increased S100A7 4 fold and with SHH and EGF in combination the increase was 5 fold (NS; **Figure 2.15C**).

2.3.3.1.9 PTCH Optimisation

The 2μg cDNA and 1μg PTCH primers gave the earliest Ct value so these concentrations were used for further qPCR optimisation for this gene. PTCH primer optimisation gave dissociation curves with a small peak ahead of the main large clean melting curve for each of the treatments (SHH and/or EGF and/or inhibitors) which means there may have been primer dimers or contamination in the qPCR reaction (**Figure 2.16a**). The amplification plots gave equally spaced Ct values and therefore good slope and efficiency levels were derived from the standard curve (**Figures 2.16b and c**). These should give accurate results PTCH levels by qPCR.
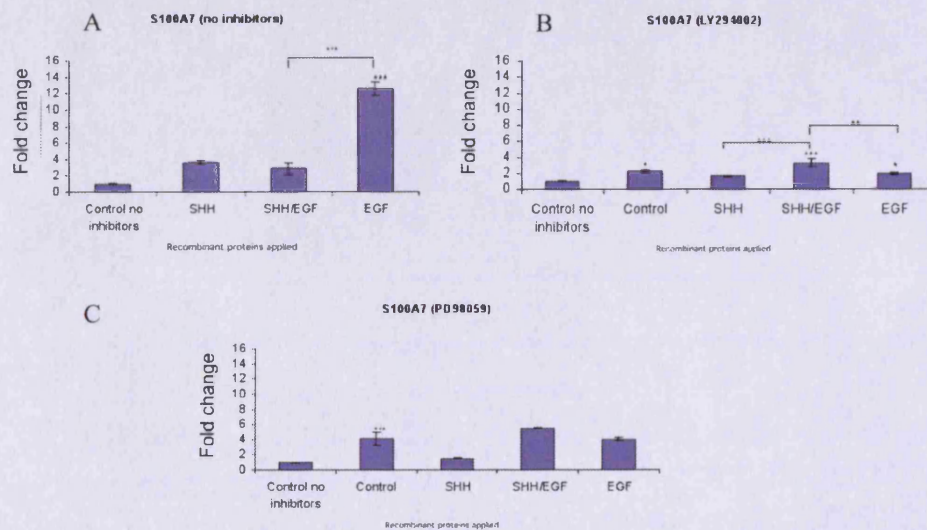
*Figure 2.16: Relative Fold Change (qPCR) in S100A7 Levels in N/TERT1 Cells treated with SHH and/or EGF in the Presence or Absence of Inhibitors (PD98059 or LY294002). Relative fold change in S100A7 levels determined by qPCR in the absence (a) and presence of two inhibitors, LY294002 (b) and PD98059 (c). Each bar represents data in the absence of SHH and EGF (control), presence of either SHH or EGF or both. Statistical analysis was done by Ordinary ANOVA, Tukey test. * P=<0.05, ** P=<0.005, *** P=<0.001. Data expressed as a mean +/- SD for n=3 experiments with 3 replicates for each experiment.*

(a) Dissociation Curve

(b) Amplification Plot

(c) Standard Curve

$R^2 = 0.969$
Slope = -3.0
Eff = 113%
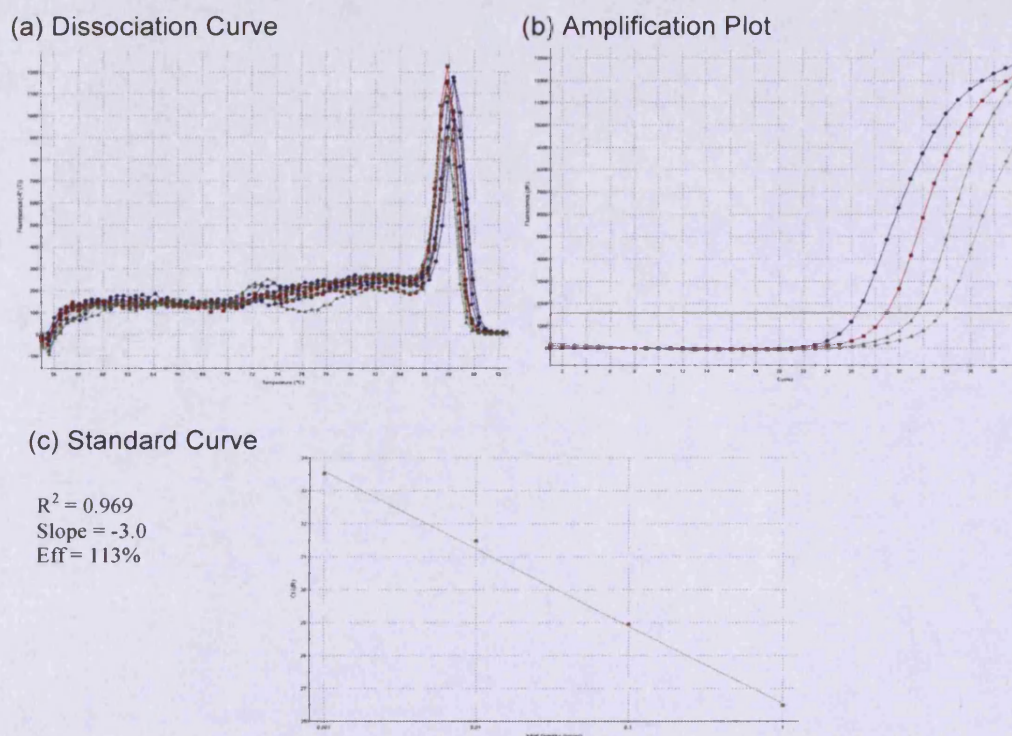
Figure 2.17: Optimisation of PTCH primers on N/TERT1 keratinocytes. (A)
Dissociation curve for N/TERT1 cDNA with PTCH primers. (B) Dilution series of
N/TERT1 cDNA using 1.5µg cDNA (blue), 1:10 dilution (red), 1:100 dilution(green) and
1:1000 dilution (grey) with PTCH primers. (C) Standard curve for N/TERT1 cDNA
dilution series and PTCH primers.

2.3.3.1.10 Effect of SHH/EGF on expression of PTCH in N/TERT1 keratinocytes.

SHH and/or EGF caused little change in PTCH levels (NS). However, PI3K
inhibitor LY294002 decreased PTCH 0.2 fold, SHH had little effect and EGF
decreased PTCH 0.4 fold, this effect was additive when both were present in
combination with a 0.2 fold decrease in PTCH (NS). MEK inhibitor PD98059
caused a 0.4 fold increase in PTCH, SHH and EGF had little effect but when
present in combination there was a 0.2 fold decrease in PTCH levels.
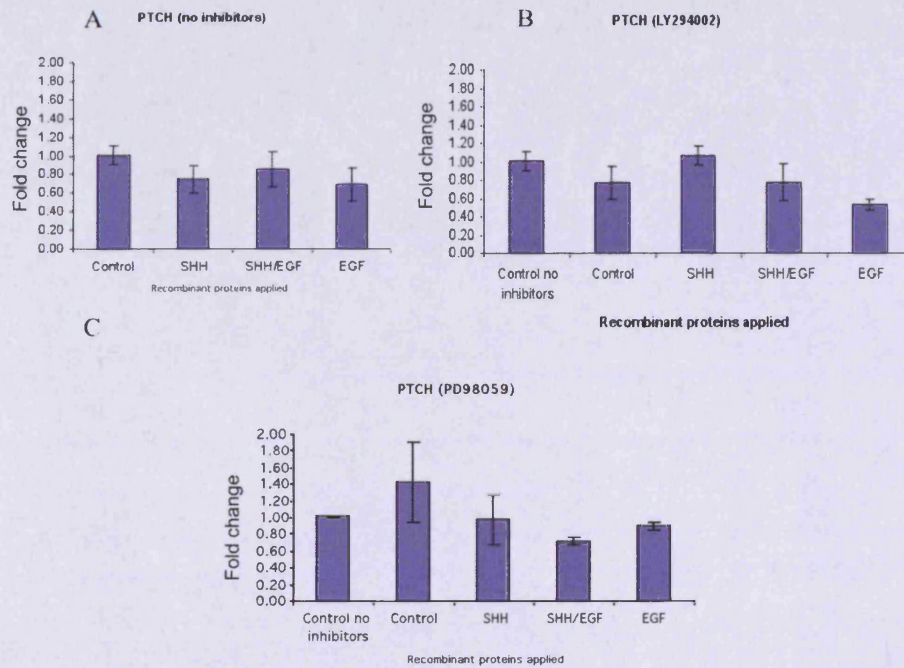
Figure 2.18: Relative Fold Change (qPCR) in PTCH Levels in N/TERT1 Cells treated with SHH and/or EGF in the Presence or Absence of Inhibitors (PD98059 or LY294002). Relative fold change in PTCH levels determined by qPCR in the absence (a) and presence of two inhibitors, LY294002 (b) and PD98059 (c). Each bar represents data in the absence of SHH and EGF (control), presence of either SHH or EGF or both. Statistical analysis was done by Ordinary ANOVA, Tukey test. * P=<0.05, ** P=<0.005, *** P=<0.001. Data expressed as a mean +/- SD for n=3 experiments with 3 replicates for each experiment.

Figure 2.17A shows no increase in gene expression in the presence of SHH comparable to GLI overexpression (see **Table 2.5**) (Kasper et al. 2006). This seems to suggest a lack of activation of the SHH pathway by addition of recombinant SHH to N/TERT1 cells, as PTCH is a target gene upregulated in the event of SHH pathway activation that is important in negative feedback of the pathway.

102

There was also no significant inhibition of PTCH by EGF observed in GLI over-expressing cells. Consistent with this LY294002 or PD98059 also have little effect on PTCH expression (**Figure 2.17 B, C**). Thus not confirming the conventional PCR data (see **Figures 2.4, 2.5**).

The results for QPCR were not as expected. Not one of the genes shows the large fold increases in gene expression for cells treated with both recombinant SHH and EGF in combination compared to SHH or EGF treatments individually, which was reported with GLI1 and EGF by Kasper et al. (2006). The unexpected results obtained by conventional PCR when N/TERT1 cells were treated with EGF pathway inhibitors, LY294002 and PD98059 including a decrease in PTCH and EGR-3 in the presence of PD98059 or LY294002 were not confirmed by QPCR analysis.

2.3.4 Cloning

As the SHH gene is GC rich, it proved difficult to amplify a full length copy so the cDNA was amplified in two overlapping sections. The 5' section was 830bp in length and the 3' section was 655bp. They were cloned separately in the pGEM-T easy cloning vector. The overlapping region contained an XmnI site that cuts SHH only once and allows the two sections to be ligated together to create the full length cDNA (**Figure 2.1 in methods**).

The two separate pieces of the SHH cDNA were released from the pGEM-T easy vector with a double digest (XmnI and EcoRI). However, since there is an XmnI site in the pGem-T easy vector, this digest resulted in three bands (**Figure 2.19**). Ideally the pGEM-T easy vector would have been cut on its own to prove that it has an XmnI site and therefore is cut into two pieces. After this digest pGEM-T easy should also have been run on the same gel as the two SHH sections to show that the two upper bands in the first and second lanes are definitely pGEM-T easy vector. The products were sequenced to check that there were no polymorphisms

and XmnI sites at the beginning and end of the SHH sections can be seen in Figures 2.20 and 2.21.
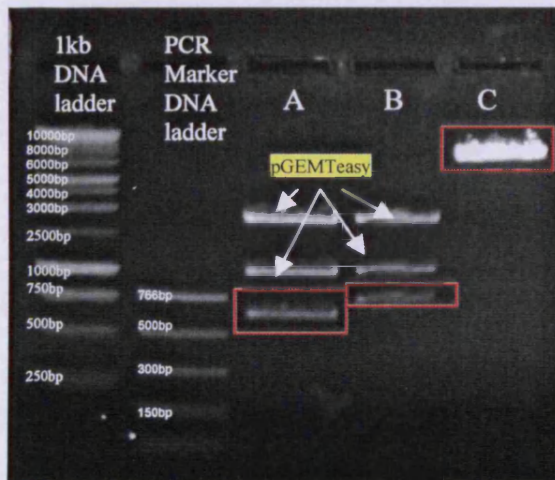
Figure 2.19: XmnI/EcoRI Double Digests for Sub-cloning into pcDNA3. XmnI/EcoRI restriction digest of pGEM-T Easy DNA clones of the 3' section of SHH (A) and the 5' section of the SHH cDNA (B) and EcoRI linearised pcDNA3 (C). The required SHH cDNA sections of 655bp and 830bp are highlighted by the red boxes.
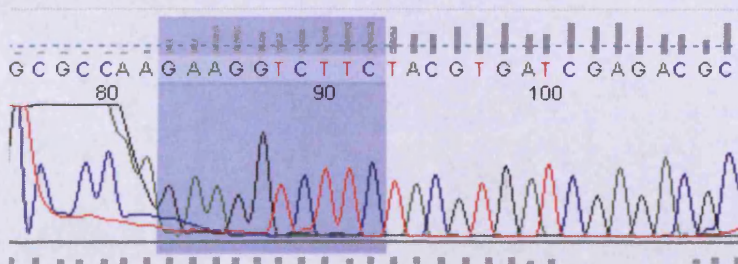
Figure 2.20: XmnI site present near the beginning of sequence for the bottom half of SHH sequenced with T7 primer. XmnI site is highlighted in blue.

104
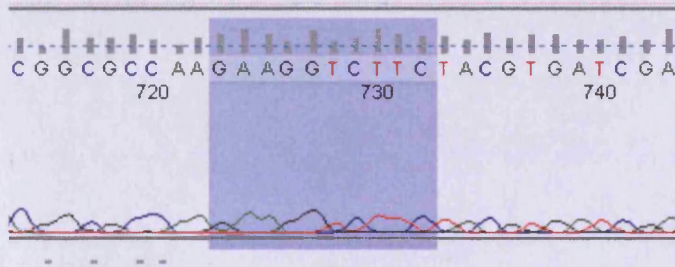
Figure 2.21: XmnI site was present near the end of the bottom section of SHH sequence with a SHH2F primer. XmnI site is highlighted in blue, however, the DNA levels appear low.

The two sections were then ligated together and then ligated into the EcoRI site (within multiple cloning site) of the pcDNA3 eukaryotic expression vector. Restriction digestion was also used to confirm the successful ligation of the full length SHH cDNA in to the expression vector (**Figure 2.22**). Sequencing confirmed which clones were successful in achieving the top section of SHH ligated to the bottom section at the XmnI site rather than two top sections or two bottom sections ligated together (correct orientation) (**Figure 2.23**). The sequencing was also used to confirm that no polymorphisms had been introduced into the sequence during transformation. A portion of SHH sequence and pcDNA3 sequence are shown in Figure 2.24.
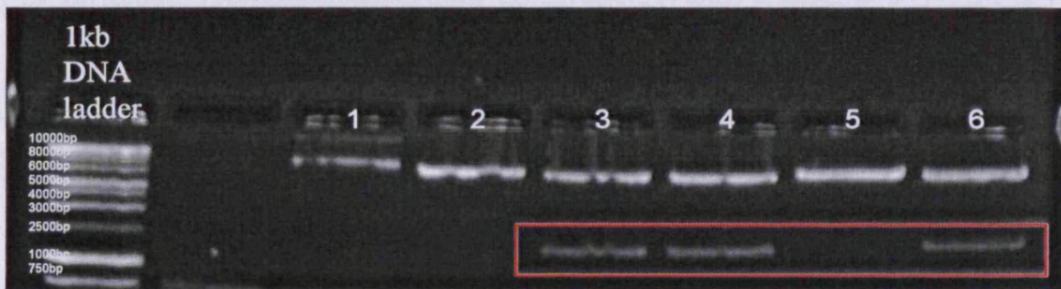
Figure 2.22: Full Length SHH cDNA Cloned into the pcDNA3 Plasmid. DNA was isolated from each of the six clones (1-6) and cut with EcoRI. The pcDNA3 vector (5446bp) is present in all lanes but ligated SHH DNA (1485bp) is only present in samples 3, 4 and 6 (highlighted by red box).
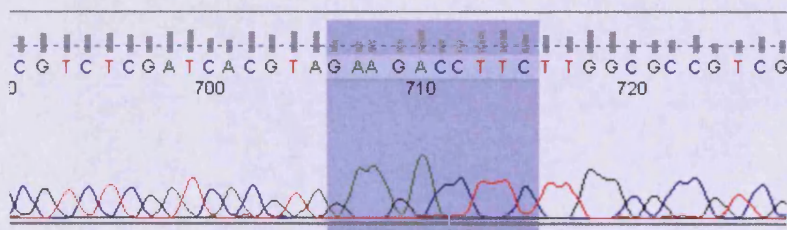
Figure 2.23: Top and bottom sections ligated in the correct orientation as shown by sequencing data. XmnI sites successfully ligated together (highlighted in blue) The top section of SHH is on the right of the XmnI site, the bottom section on the left. The quality of the trace is poor possibly due to low DNA levels.
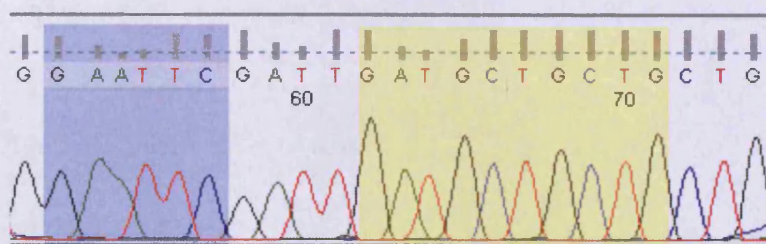
Figure 2.24: EcoRI and SHH sequences.
Good quality sequence data.

106
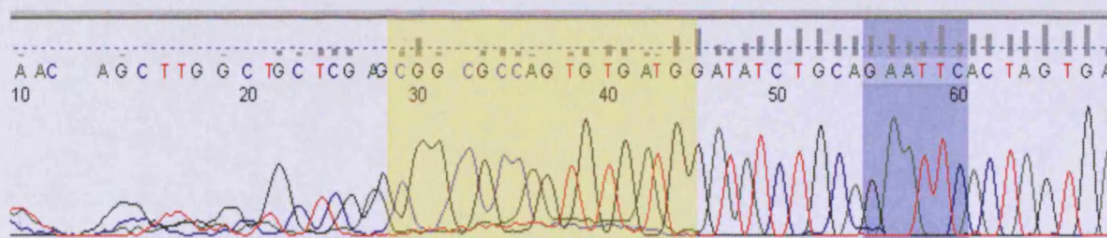
Figure 2.25: EcoRI sequence leads onto SHH sequence (2F primer). *Full length SHH successfully transfected into pcDNA3 expression vector (sequence highlighted yellow) at EcoRI site (sequence highlighted blue).*

Although SHH was cloned successfully, attempts to transfect N/TERT1 cells were unsuccessful due to time limitations and cell culture infections. Two methods of transfection were tried during the course of this study using a Tet-on vector including electroporation and Mirus transfection reagent. A GFP control vector was used to assess transfection efficiency. The electroporation conditions used were those recommended for the HaCaT cell line (not optimised to N/TERT1 because both are keratinocytes and also due to time constraints) and therefore not necessarily ideal. After G418 selection no cells survived to form colonies. Therefore the Mirus method was attempted since this had been used successfully by others using N/TERT-1. Low levels of GFP (Figure 2.26) were observed but on subculturing, changes in cell morphology occurred suggested the cells had been stressed so selection was not continued.

Due to the problems encountered and the time-consuming double selection required for the creating a Tet-on stable cell line SHH was cloned as described into pcDNA3. However, before creating an over-expressing cell line, further optimisation of transfection of N/TERT-1 with different reagents or electroporation conditions would be required.

107
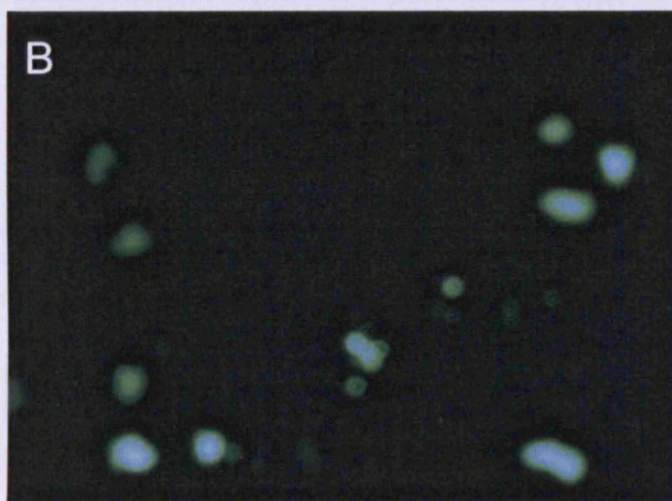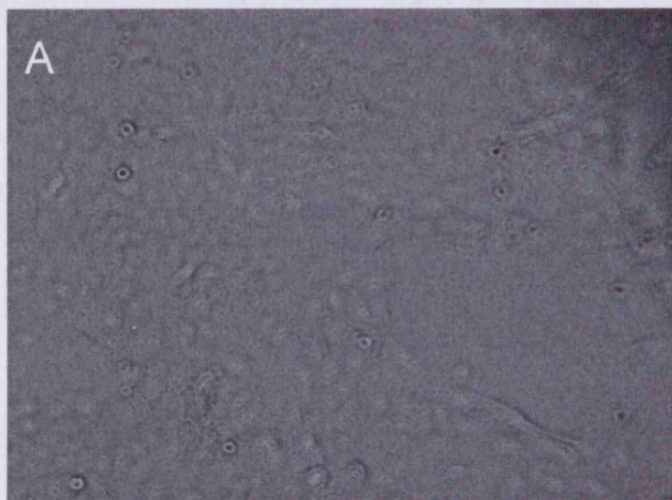
Figure 2.26: N/TERT1 cells Transfected with GFP Vector using Mirus Agent. (A) N/TERT1 cells showed normal morphology at ~70-80% confluency [10x magnification] (B) Low number of N/TERT1 cells expressing GFP indicates poor transfection efficiency [10x magnification with green filter].

2.4 Discussion

Kasper et al. (2006) found particularly large increases in the expression of a subset of SHH target genes (EGR-3, S100A7, IL1-R2) in N/TERT1 keratinocytes with doxycycline-induced overexpression of GLI1, and the addition of recombinant EGF (see **Table 2.7**). PTCH transcription was also up-regulated by GLI1 so up-regulation by SHH pathway activation alone would be expected (Daya-Grosjean and Couve-Privat, 2005). These genes were therefore used as markers for SHH/EGF pathway activation. If recombinant SHH and EGF applied to the N/TERT1 cells in combination showed a large increase in these target genes then inhibitors to SHH and EGF signalling may be useful for treating BCC.

Decreased cell viability in the presence of PD98059 may have caused altered gene expression as death signalling pathways, which include parts of the EGF signalling pathway would have been activated in the cells (Jin and El-Deiry., 2005). However, cDNA quantities were carefully measured and equalised prior to PCR, so reduced cell numbers would not have affected the quantity of DNA actually used in the study. It would also have been a good idea to carry out these cell viability tests in the presence of the recombinant SHH and EGF which were added to the cells.

Activity of the EGF pathway was confirmed only for the MEK/ERK branch, but it would also have been useful to confirm activity of the PI3K/AKT by looking at AKT phosphorylation after EGF addition by western blotting prior to use of the PI3K inhibitor LY294002 in this study.

The response to PD98059 and LY294002 in the conventional PCR experiments showed complete inhibition of PTCH and EGR-3 in the presence of SHH, this appears to be unrelated to EGF signalling. Since these are not confirmed by qPCR they should be interpreted with caution. These PCRs had to be carried out at 35-40 cycles to be visable, a point at which PCRs are not quantitative. In addition it is

impossible to know, using conventional methods, whether these reactions are efficient at all concentrations of the target gene as can be observed from the amplification plots obtained in QPCR. For example in **Figure 2.8** an amplification plot for one sample for TF2H started off at the same CT but then failed to reach a similar end point.

Using Image J analysis of the band density of the PCR gels, similar data for target gene expression (PTCH, EGR-3 and S100A7) was obtained in the duplicate experiments (see **Figures 2.4, 2.5 and 2.6**). In all cases, the second experiment gave higher levels of expression, although the same amount of DNA was used. However, these results did not give the large fold increases in target gene expression (EGR-3 and S100A7) observed by Kasper et al (2006). This may be due to the fact that they used N/TERT1 cells expressing GLI1 and then treated with EGF, rather than trying to induce GLI1 with recombinant SHH as done in the current experiments. Thus, the results are not likely to be anomalous.

Although conventional PCR suggested some activity in response to SHH due to increased PTCH, EGR-3 and S100A7, the more accurate real time method (which enables you to avoid reaching a plateau when amplifying genes so a comparison between different treatments is more reliable) showed no significant increase in expression of any of these genes. The augmentation of GLI target gene expression by EGF observed by Kasper et al (2006) were not observed in N/TERT1 cells treated with recombinant SHH and EGF in combination.

As expected, PTCH had the highest expression in the presence of SHH, but was reduced in the presence of EGF. However, this was not entirely inconsistent with Kasper et al (2006) where EGF inhibited PTCH expression (see **Table 2.7**).

There is some evidence for stimulation of EGR-3 in the presence of both SHH and EGF (**Figures 2.3 and 2.5**). S100A7 showed increased expression in the presence of SHH and EGF either alone or together (**Figures 2.3 and 2.6**). However, these

results do not show the same large fold increases in expression for these genes that were described by Kasper et al (2006) in the presence of EGF and up-regulated GLI1 (see **Table 2.5**). The results for PTCH, EGR-3 and S100A7 in the presence of inhibitors are also hard to rationalise because PTCH expression appeared to decrease in the presence of either PD98059 or LY294002 (**Figure 2.4 and 2.5**), but showed no change when cells were treated with both LY294002 and PD98059 in combination. This work was repeated twice with the same result (**Figures 2.4 to 2.6**).

The lack of SHH signalling found in N/TERT1 cells lines could be explained because SHH signalling does not occur in adult epidermal cells except for during the anagen (down-growth) phase of the hair follicle. This means that the lack of GLI1, a SHH pathway transcription factor also comes as no surprise. However, addition of recombinant SHH to these cell lines would be expected to activate the pathway and testing GLI1 levels after SHH addition by RT-PCR or western blotting would have been useful to confirm successful activation. A lack of availability of useful GLI1 antibodies meant this could not be carried out successfully for this study. Western blotting for the SHH, PTCH, SMO and GLI1 proteins would also have been useful to confirm the RT-PCR results, but the same problems with antibodies prevented this being a useful option.

RT-PCR results seemed to show some activation of SHH signalling, with up-regulation of PTCH upon SHH addition to the cell medium. The reduction in PTCH levels by EGF inhibitors PD98059 (MEK inhibitor) and LY294002 (PI3K inhibitor) when applied individually may show that EGF does increase SHH target gene expression. Addition of both inhibitors simultaneously to the cell medium seemed to cancel out any effect each had individually. This probably means that another part of the EGF pathway was instead activated in the absence of MEK/ERK and PI3K/AKT or that the inhibitors actually lost their efficacy in combination. If this is the case it could be problematic for a topical formulation containing both inhibitors.

111

Further evidence of SHH pathway activation was shown using RT-PCR by the small increases in EGR-3 and S100A7 in the presence of recombinant SHH or EGF. However, there was not the additive effect in expression when both SHH and EGF were added to the medium which was found by Kasper and colleagues when they added recombinant EGF to GLI1 expressing cells (Kasper et al. 2006).

The effect of PD98059 and LY294002 were unexpected because if the EGF pathway really does modulate SHH signalling by increasing target gene expression, a decrease in S100A7 (one such target gene) would be expected when inhibitors to the EGF pathway are present. This would particularly be expected in the presence of PD98059 because it has been suggested in publications that the MEK/ERK branch of the EGF pathway is involved in augmenting SHH target genes (Schnidar et al., 2009). It is interesting that the presence of LY294002, a PI3K inhibitor has seemingly increased S100A7 expression. This seems to show that in this case LY294002 is not inhibiting a signalling pathway which increases S100A7 expression, but may in fact be inhibiting a separate signalling pathway which would otherwise inhibit S100A7.

In the case of the S100A7, expression increased in response to EGF and was inhibited by both PD98059 and LY294002. However, what is surprising is the inhibition of the EGF response by SHH. There was no significant inhibition of PTCH by EGF as seen previously which was consistent with no significant changes in PTCH levels in response to the inhibitors. The general decrease in EGR-3 expression in the presence of PD98059 in comparison to no inhibitors present agrees with the conventional method of PCR which showed very little if any expression in the presence of LY294002 and PD98059 (**Figure 2.5**).

There are a number of possible explanations why there is a little response to SHH. Firstly, SHH and GLI1 components of the SHH pathway were absent from N/TERT1 and HaCaT keratinocytes. Other components whose presence was not

112

confirmed by PCR, such as SUFU, may have also been deficient. Western analysis was not helpful in confirming the expression of proteins in the SHH pathway due to poor antibodies. Other SHH signalling genes such as SUFU may have been interesting to look at in order to confirm that the pathway could be activated. The absence of GLI1 in N/TERT1 and HaCaT keratinocytes may mean that target genes could not be transcribed. However, one might expect an increase in GLI1 in the event of pathway activation.

Secondly, it may have been due to the recombinant SHH (20kDa N-terminal domain) which was added to cell culture medium because this was made in *E.coli* and therefore does not have the post translational modifications necessary for increased activity (palmitoylation and cholesterol attachment) (Incardona and Eaton, 2000; Pepinsky et al., 1998). In order to overcome this SHH was cloned to make recombinant SHH in cell culture medium (conditioned medium) or for making an N/TERT1 overexpressing cell line for comparison with the SHH expressing HaCaT cell line used previously (Bigelow et al., 2005). Due to time constraints it has not been possible to determine if this was the reason for the lack of response. However, the recombinant SHH used had been batch tested for activity in C3H10Y1/2 fibroblast cells by the supplier (Sigma Aldrich Company Ltd, Gillingham, UK). Ideally these C3H10Y1/2 cells should have been used in this study as a positive control, for SHH activity and stability over the time course of the experiment, however due to financial constraints this was not possible. In addition a dose response curve should have been carried out for expression of a GLI-responsive gene to determine the ED50 (effective dose or the amount of drug that produces a therapeutic response in 50% of the subjects taking it) for N/TERT1 cells which may be different to C3H10Y1/2 cells. Another useful experiment would have been to use immunocytochemistry to view the localisation of GLI in the nucleus on treatment of cells with the recombinant SHH. However, commercially available antibodies to GLI1 are rarely effective. This may be useful to carry out in the future as new GLI1 antibodies are becoming commercially available.

Thirdly, it could also be explained by a negative feedback loop, not relevant in GLI1 over-expressing cells. Normally SHH signalling up-regulates PTCH, thus inhibiting SMO, leading to a requirement for higher levels of SHH to keep the pathway activated. But no increase in PTCH expression was seen so this suggests a lack of activation of the SHH pathway signalling by SHH. Another possibility is that GLI3 inhibits GLI1 and GLI2 transcription.

Also, a paracrine effect may be important for SHH activation, where fibroblasts need to be present in order for the pathway to be activated effectively in keratinocytes. Using organotypic culture models Bigelow et al. (2005) successfully achieved tumour down-growth into the model dermis in response to SHH (Bigelow et al., 2005). This suggests that it is possible that a paracrine effect is needed for the formation of BCC/SHH signalling.

The primary cilium, an antenna-like structure in the cell membrane, may also be required. It is currently thought that the primary cilium acts as a site where all the major components of the SHH pathway can be gathered together to allow interaction to occur. PTCH is present in the cilia in the absence of SHH and on SHH addition is deactivated and moves out of the cilium into the cell. Smoothened then enters the cilium enabling downstream pathway activation. It is not known whether the primary cilium is present in N/TERT1 keratinocytes, this should be explored further based on recent publications suggesting their requirement for SHH signalling.

The timings used may not have been the most appropriate for maximal gene expression. RNA extraction was carried out 24 hours after addition of recombinant SHH and EGF because Kasper et al. added recombinant EGF to their cells (NTERT1s expressing GLI1 under the control of doxycycline) 24 hours prior to RNA extraction (Kasper et al., 2006). It seemed most appropriate to conduct a comparable experiment with recombinant SHH rather than expressing GLI1.

114

However, although Kasper et al. did successfully find augmentation with recombinant EGF after 24 hours, GLI1 was constitutively active. Here the negative feedback loop might have produced enough PTCH to inhibit SHH signalling in 24 hours thus bringing levels of Gli responsive genes to unstimulated levels (including PTCH). Another option would have been to show activation of the SHH pathway using western blotting to show increased protein expression of PTCH. Unfortunately, as explained above, the PTCH antibodies available are not reliable and do not give clear results.

A possible problem with the attempted activation of SHH signalling at the level of the SHH ligand in a BCC model is that the signalling pathway is activated by PTCH or SMO mutations in BCCs.

Another potential problem is that EGFR is internalised rapidly on ligand binding, so it may be that EGF signalling activates transcription factors at a greater speed than SHH signalling. Laner-Planberger and co-workers showed that c-Jun interacted more strongly with GLI2 so Gli2 may need to accumulate (GLI2 upregulates GLI1) before EGF addition, which would eventually lead to the activation of c-Jun. Using constitutive activation of SHH signalling would have solved this problem because EGF could be added at any time and there would already be plenty of GLI transcription factors present. Alternatively if SHH had been added to the medium prior to EGF a synergistic effect between these pathways may have been observed. Various time points could be tested to find the time point for optimal GLI1/2 signalling, where target gene expression could be used as a marker for activation. Care would need to be taken to select an appropriate gene, as there are early and late response genes (Dessaud et al. 2007). Ideally further time would be spent creating the constitutively expressing SHH N/TERT1 keratinocyte cell line as sustained SHH pathway signalling is required to form BCCs.

Cloning of SHH was time consuming and although eventually successful there was not time to successfully transfect N/TERT1 cells with the SHH containing vector. In order to repeat the QPCR experiments on SHH expressing N/TERT1 keratinocytes the Mirus transfection method could be continued in future and cell selection completed. Alternatively, a transient transfection could be carried out on the N/TERT1 cell line. However, recombinant SHH addition to the culture medium may after all have the same effect as SHH expressing cells because SHH protein is released from the SHH expressing cell and then acts as a ligand to activate the signalling pathway in adjacent cells.

Chapter 3

Sonic Hedgehog and Epidermal Growth Factor Signalling in Co-cultures of Keratinocytes and Fibroblasts

117

3.1. Introduction

Recent publications have implicated that paracrine signalling and the requirement for the presence of a primary cilium is required to achieve SHH pathway activation (Walter *et al.*, 2010; Eggenschwiler and Anderson., 2007; Haycraft *et al.*, 2005; Clement *et al.*, 2009; Wong *et al.*, 2009). These extra requirements may explain the low level of SHH signalling activity observed in monolayer cultures (see Chapter 2) and perhaps the influence of other factors on SHH signalling requires further consideration.

For example, it is thought that SHH is involved in pancreatic tumour development and progression (Walter *et al.*, 2010; Bailey *et al.*, 2009; Liu *et al.*, 2007). Over-expression of SHH ligand occurs in 70% of primary pancreatic adenocarcinomas, while the PTCH and SMO mutations seen in BCC, have not been observed (Thayer *et al.*, 2003; Liu *et al.*, 2007, Tian *et al.*, 2009). SHH is not expressed in the normal adult pancreas, but primary and metastatic pancreatic cancer cell lines were found to express components of the SHH pathway (expression of SHH, PTCH and SMO has been reported in up to 70% of pancreatic ductal carcinomas). Implanting either SHH expressing primary cells or a pancreatic cancer cell line expressing SHH into mice results in increased tumour size and number of metastases compared to cells that do not express SHH (Bailey *et al.*, 2009). This shows that the more aggressive pancreatic tumours have a requirement for SHH expression.

Work with an epithelial pancreatic cell line (T-HPNE) reinforced this finding. These cells were transformed with retro-viral vectors that provide oncogenic insults to mimic the progression model of pancreatic cancer. In this model, inhibition of SHH signalling reduced tumour growth, lymphangiogenesis and metastasis (Bailey *et al.*, 2009) confirming that active SHH supported tumour growth. The importance of SHH was confirmed by global gene expression analysis using an Affymetrix exon microarray of primary pancreatic carcinoma cells versus non-neoplastic pancreatic cells which indicated SMO over-expression in

pancreatic cancer cells. Immunohistochemistry on primary human pancreatic cancer tissue not only further substantiated this finding but also suggested a paracrine effect by demonstrating SMO expression in human pancreatic adenocarcinoma stromal fibroblasts.

3.1.1 Paracrine signalling

Paracrine signalling is essential for mediating SHH pathway activity in development, and such epithelial-mesenchymal interactions are essential for skin development. SHH signalling is also heavily involved during hair follicle development being necessary for the cross-talk between the dermal papilla and epithelial components (Lacina *et al.*, 2007; Yauch *et al.*, 2008).

Paracrine signalling via the SHH pathway has also been identified in various epithelial cancers. It has been suggested that stromal cells may be stimulated by SHH expressing tumour cells (Walter *et al.*, 2010; Feldman *et al.*, 2007). Additionally, cancer-associated fibroblasts were shown to stimulate pancreatic tumour cells and SHH over-expression in mice during development resulted in pancreatic cancer precursor lesions (Thayer *et al.*, 2003; Morton *et al.*, 2007).

Xenografts (grafts from one species to another) of human tumours highly expressing SHH were implanted onto mice and it was found that the stromal cells next to the tumour had increased GLI1, indicating the SHH pathway had been activated in a paracrine manner. It was also demonstrated that SHH activity in the stromal microenvironment can provide a growth advantage to tumour cells. It was found that BCC fibroblasts influence the growth and differentiation pattern of normal keratinocytes, pushing them towards a malignant phenotype (Lacina *et al.*, 2007). These interactions may be due to the influence of soluble growth factors or the collagen extracellular matrix on keratinocytes. Other xenograft mouse models that have been used for pancreatic cancer also showed a paracrine requirement for the SHH pathway, as tumour cells produced SHH ligand that activated the SHH pathway in the stroma (Tian *et al.*, 2008). These authors also confirmed that

paracrine but not autocrine SHH signalling occurs in pancreatic carcinomas. This was demonstrated by expressing the SMOM2 allele of SMO and a PTCH-LacZ reporter allele in the pancreas to activate canonical SHH signalling in a cell-autonomous manner. The results showed that canonical SHH signalling did not occur in pancreatic epithelium in an autocrine manner. Furthermore, qRT-PCR experiments on laser capture micro-dissected human and mouse tumour samples confirmed the presence of SHH signalling in tumour stroma (Tian et al., 2009).

Another publication co-culture of a pancreatic cancer cell line with 10T1/2 cells (multipotent mouse embryo cell line stably transfected with a GLI reporter construct) resulted in the induction of GLI reporter activity and this correlated with the level of ligand produced by the tumour cells. This demonstrated that SHH produced by tumour cells could act on the stromal compartment again suggesting paracrine signalling (Yauch et al., 2008).

The same researchers examined signalling in vivo by xenografting pancreatic cells expressing SHH onto PTCH1-LacZ-Rag2$^{-/-}$ mice and found anti-β-galactosidase stained stromal cells adjacent to tumour cells indicating paracrine signalling (Yauch et al., 2008). The same group also showed that xenografting human tumour biopsies onto nude mice led to the replacement of human-derived stroma by mouse stroma.

However, the situation in prostate cancer cell lines is still unclear and it is uncertain if SHH signalling is autocrine and/or paracrine. Work with three cell lines (LNCaP, PC3 and 22RV1) transfected with activated GLI2 showed SHH target gene activation, but this did not occur when the same cells were transfected with activated SMO. Also, cyclopamine (SMO inhibitor) did not affect the expression of target genes, but did limit cell proliferation. Therefore, autocrine SHH signalling does not seem to regulate tumour growth in these cells (Zhang., 2007). However, analysis of gene expression in benign and malignant prostate tissue did show that SHH signalling molecules in the stroma surrounding a

prostate tumour did accelerate growth, mimicking SHH signalling in the mesenchyme during prostate development (Shaw *et al.*, 2009).

3.1.2 Primary Cilia

There are two types of mammalian cilia, motile and non-motile. Motile cilia can be found lining the trachea where they beat to clear dirt and mucus from the airway. Non-motile (primary) cilia generally function as sensory organelles. They protrude from cells into the extracellular space and many can have specialised functions (e.g. in the outer segments of photoreceptors) but some do remain unspecialised.

Cilia have a basal body which is formed by transitional fibres, a terminal plate (these physically prevent entrance of proteins into the cilia) and triplet microtubules which become the doublet microtubules (9+0 arrangement in primary cilia but 9+2 in motile cilia) in the long microtubular axenome (**Figure 3.1**). Generally, the cilia membrane is continuous with the plasma membrane (Singla and Reiter, 2006).
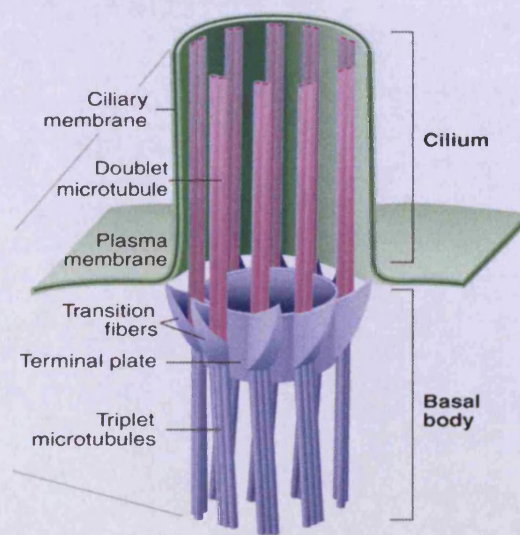
Figure 3.1: Structure of a Primary Cilium. The membrane is continuous with the plasma membrane and contains an array of microtubules (Singla and Reiter, 2006).

121

Cilia are formed when cells enter growth arrest and are then shed just before cells enter mitosis. There are three main stages of primary cilia development (**Figure 3.2**). First a golgi vesicle attaches to the mother centriole, enabling the centriole to extend and become the basal body forming the axoneme. Secondly, nearby vesicles join to form the cilia membrane which surrounds the axoneme. Thirdly, the axoneme covered in membrane reaches the cell surface, where the cilia and plasma membranes fuse to become continuous allowing the cilium to elongate further (Pedersen *et al.*, 2008).
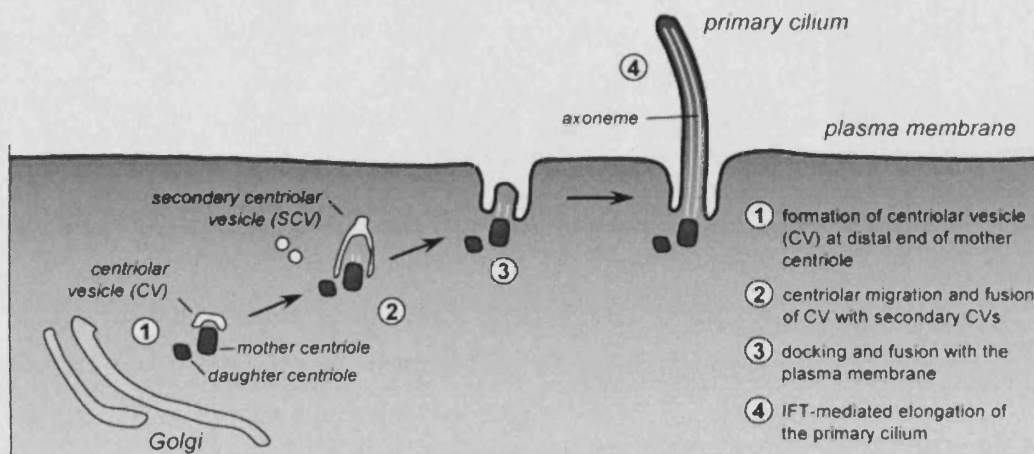
Figure 3.2: Development of the Primary Cilium (adapted from Pedersen et al., 2008).

Primary cilia defects lead to a variety of disorders or 'ciliopathies' usually caused by an inability of the centrioles to form the primary cilia or to migrate prior to ciliogenesis. Polycystic kidney disease is an example of a ciliopathy and this is caused by unregulated cilia function due to loss of cilia length control. This leads to a misalignment of hepatic bile duct and renal tubule cells resulting in cyst growth that can lead to loss of kidney function (Bonnet *et al.*, 2009).

Recently, it has been shown that the primary cilium must be present on cells for SHH signalling to occur. In the absence of SHH, PTCH remains at the base of the cilium and SMO is inhibited. GLI2 and GLI3 are moved up and down the cilia via intraflagellar transport (IFT), and they are cleaved into repressor forms by the

122

centrosome-proximal proteasome so they cannot activate gene transcription. When present, SHH binds to PTCH and this translocates PTCH out of the cilium and SMO is no longer inhibited. SMO then moves into the cilium tip and interacts with SUFU, GLI and other proteins localised here to activate the SHH signalling pathway. These interactions prevent cleavage of GLI2 and GLI3, which are translocated to the cilium base and on to the nucleus by IFT proteins (see **Figure 3.3**). GLI is then able to stimulate target gene transcription in the nucleus by binding to GLI-promoters in various target genes (Eggenschwiler and Anderson., 2007).

IFT proteins, which move up and down the cilium continuously are required for GLI activity and in their absence, modulation of SHH/GLI target genes are blocked (Haycraft *et al.*, 2005; Clement *et al.*, 2009; Wong *et al.*, 2009). In support of this, mice homozygous for IFT88 (an intraflagella transport protein) survived until after birth, but a targeted null allele of mouse IFT88/polaris (intraflagellar transport component) caused lethality at mid-gestation and mutant embryos displayed randomised left-right symmetry (under the control of the SHH pathway in mammalian development) associated with loss of cilia (Murcia *et al.*, 2000).
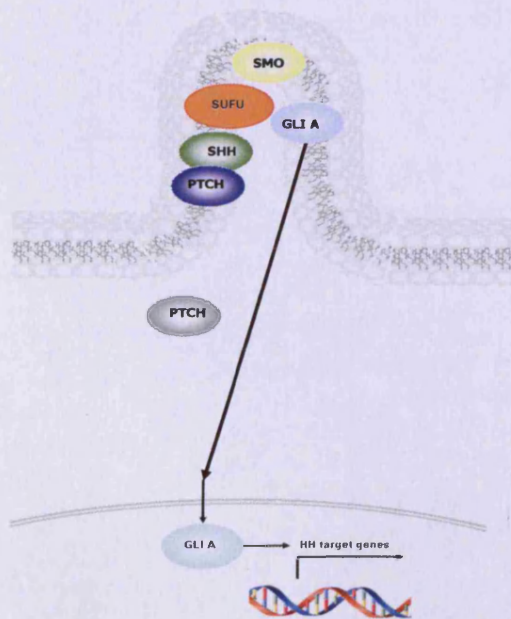
Figure 3.3: SHH Pathway Signalling in the Primary Cilium. In the presence of SHH (ligand), PTCH translocates out of the cilium, releasing SMO from inhibition, enabling its movement to the cilium tip where it interacts with SUFU and GLI transcription factors, allowing GLI transportation to the cell nucleus.

Interestingly, cilia are not required for SHH signalling in Drosophila, as shown by mutations which block cilia formation (Han *et al.*, 2003). However, it is not clear at this time how many other signal transduction pathways in humans may require cilia, although there is evidence that cilia are also involved in Wnt and PDGFRα signalling (Eggenschwiler and Anderson., 2007).

Generally, one primary (non-motile) cilium is present on almost every interphase or non-dividing cell in the body (Satir and Christensen, 2007), but they are rarely present on immortalised cells (Strugnell *et al.*, 1996). Primary cilia were induced in a 3T3-L1 cell line by growing cells to high confluency and growth arresting them by serum starvation (Zhu *et al.*, 2009). It is thought that cilia are more easily induced in polarised cells and when the cells are confluent and growth arrested (Satir and Christensen, 2007). As shown by Bonnet and co-workers, polarisation of cells appears to be important in the normal development of primary cilia (Bonnet *et al.*, 2009). Thus, primary cilia on polarised cells can act as location markers and enable cell to orient themselves in relation to their surroundings (e.g. in the epidermal basal layer, cells are columnar in a vertical direction).

It was not known whether the cell lines used in this study (N/TERT1, HaCaT or HCA2) had primary cilia or not. The current studies with SHH and EGF included a growth arrest stage (24 hour culture minus FBS/BPE prior to SHH/EGF addition), which is thought to enable cilia formation. However, work had been carried out whilst the cells were still sub-confluent and therefore capable of proliferating on addition of EGF and it is not certain that primary cilia were present under these conditions, and if not, what conditions would be required to induce them. It had been previously shown that co-cultures at the air-liquid interface (keratinocytes not covered in culture medium but fed by medium from below) improved cell differentiation (Dickson *et al.*, 2000). Images of differentiated epidermis formed with HaCaT or N/TERT1 cells grown on a fibroblast containing collagen gel showed well organised, columnar basal cells (Bigelow *et al.*, 2005; Dickson *et al.*, 2000). An alternative method utilises a filter

124

insert so the medium level can be reduced once cells have adhered, to allow stratification at the air-liquid interface. In this method, fibroblasts may be grown in the well beneath to introduce additional paracrine effects.

Antibodies to cilia components such as acetylated-α-tubulin or IFT88 have been used to demonstrate the presence of cilia (immunofluorescence and confocal microscopy). Recently, it has been shown that cilia are present in the epidermis, dermis and hair follicles as well as BCCs. This method has also been used to show that cilia are present on hair follicle cells throughout their development and that structural proteins in cilia co-localise with SHH pathway proteins (Wilson *et al.*, 2009; Wong, 2009; Clement *et al.*, 2009; Lehman *et al.*, 2009). Transmission electron microscopy (TEM) has also been used to show ciliation of mesenchymal and ectodermal cells in the mouse limb bud and in pre-cystic collecting tubule cells of the kidney (Haycraft *et al.*, 2005; Bonnet *et al.*, 2009).

In conclusion, these studies suggest that fibroblasts may be needed to facilitate SHH pathway activation in keratinocytes by paracrine signalling and the presence of cilia may also be an important factor in enabling activation of SHH signalling.

3.1.3 Aims

- To determine whether SHH pathway signalling can be activated in co-cultures which allow epithelial-mesenchymal interactions.
- To determine by confocal microscopy and/or scanning electron microscopy, whether cilia are present on these cell lines under various culture conditions.

3.2 Methods

3.2.1 Cell lines

HCA2 fibroblasts (obtained from Professor David Kipling, Cardiff University, UK) are normal human diploid neonatal foreskin fibroblasts immortalised by the hTERT portion of telomerase. These have been shown to maintain normal

fibroblast characteristics with a long lifespan whilst maintaining more uniform populations than primary fibroblasts. Generally, primary cell change significantly with time and form variable populations which do not give reproducible experimental results (Bond *et al.*, 1999; McSharry *et al.*, 2001).

3.2.2 Maintaining cell lines

HCA2 fibroblasts were removed from liquid nitrogen and thawed at 37°C. The cells were transferred to a 50ml falcon tube and 20ml DMEM containing 10% FBS and 2mM L-glutamine (Gibco, Invitrogen, Paisley, UK) was carefully added and mixed. The cells in medium were transferred to a T75 culture flask (Corning, Fisher Scientific, Loughborough, UK) and incubated at 37°C in the presence of 5% CO_2. The medium was changed every 2-3 days and cells were subcultured when they reached 70-80% confluence. Subculture was achieved by aspirating the medium, washing the cells with 5ml dPBS, adding 5ml trypsin-EDTA (Gibco, Invitrogen, Paisley, UK) and incubating at 37°C with 5% CO_2 for approximately 5-12 minutes (or until cells were no longer adherent). An aliquot (5ml) of DMEM containing 10% FBS was then added to deactivate the trypsin-EDTA and the cell suspension was removed from the flask.. An aliquot of 2ml was added to a T75 flask containing 18ml DMEM with 10% FBS and the cells were then incubated at 37°C in the presence of 5% CO_2.

3.2.3 Cryo-preserving HCA2 for storage

A freezing mixture was prepared with 90% FBS and 10% DMSO, filter-sterilised (0.2μm) and stored in 1ml aliquots (in 2ml cryovials) at -80°C.

Medium was aspirated from a T75 flask when cells were 75-80% confluent. The cells were washed in 5ml dPBS and then treated with 5ml Trypsin-EDTA (incubate at 37°C in 5% CO_2 for 5-12 minutes). The trypsin was inhibited by

adding 5ml DMEM/F12 (1:1, vol:vol) containing 10% FBS and 2mM L-glutamine and the cells pelleted by centrifugation (1,200 rpm for 5 minutes at RT). The supernatant was aspirated and the cells re-suspended in 3-4ml DMEM/F12 (1:1, vol:vol) with 10% FBS and 2mM L-glutamine. Cells were counted by haemocytometer, adjusted to 1×10^5 cells per 1ml and added to cryovials containing 1ml of freezing mixture. The vials were wrapped in tissue, placed in a polystyrene tube box and frozen at -80°C overnight. They were transferred to liquid nitrogen for long term storage.

3.2.4 Co-culture of HaCaT and HCA2 cell lines

HaCaT cells at 80% confluence in a T75 flask, were released by incubating in 5ml trypsin-EDTA at 37°C with 5% CO_2 for 5-12 minutes (or until no longer adherent). Trypsin-EDTA was deactivated by addition of 5ml DMEM containing 10% FBS and 2mM L-glutamine and 300μl of the mixture was removed and applied to each of four 0.4μm filter inserts (Greiner Bio-One Ltd, Stonehouse, UK) in a 6 well plate. This was repeated for a second 6 well plate. HCA2 fibroblasts (80% confluent) were released from a T75 flask with trysin-EDTA and added to the wells beneath the filter inserts of one plate while the second plate had no fibroblasts added. 2ml DMEM containing 10% FBS and 2mM L-glutamine was added to each filter insert and the wells of both plates. The cells were incubated for 36 hours at 37°C with 5% CO_2. Growth medium was aspirated and the cells washed three times with dPBS, then 2ml DMEM with 2mM L-glutamine (but no FBS) was added to cells in each compartment. Cells were incubated at 37°C with 5% CO_2 to induce growth arrest. Keratinocytes and fibroblasts in both plates were incubated at 37°C in 5% CO_2 for 24 hours in the presence of either 10ng recombinant SHH, 10ng recombinant EGF, or both. Control cultures had no recombinant proteins added. The medium was aspirated, the cells washed three times with dPBS and RNA was extracted using Trizol (section 2.2.2.1).

3.2.5 Stratified Co-culture

The co-culture described in section 3.2.4 was also repeated in a modified form. In this case, 24 hours after plating, HaCaT cells were allowed to grow at the air-liquid interface by reducing the level of medium (DMEM with 10% FBS and 2mM L-glutamine) to the underside of the filter insert (to feed cells from below) and then incubating at 37°C with 5% CO_2 for 5 days (replacing the medium every 1-2 days) to allow stratification prior to inducing growth arrest (achieved in the same way as in **section 3.2.4**).

3.2.6 Samples for Scanning Electron Microscopy (SEM)

Scanning electron microscopy (SEM) was carried out by Chris Von Ruhland (Department of Medical Genetics, School of Medicine, Cardiff University). Co-cultures of HaCaT keratinocytes and HCA2 fibroblasts were prepared as before (see **section 3.2.5**) but with slight modification. HaCaT keratinocytes (150μl) from a 10ml subculture (5ml DMEM containing 10% FBS and 5ml trypsin added to a 30% confluent T75) were added to a 12 well plate containing filter inserts. The same number and volume of HCA2 fibroblasts were plated in 6 of the wells below the inserts. Another 2 wells remained submerged in the medium without growth at the air-liquid interface (see **section 3.2.4**) and 2 wells were grown at the air-liquid interface for 10 days (see **section 3.2.5**) to allow further stratification.

In addition, 300μl of HaCaT from a confluent T75 flask resuspended in 10mls were also added to each of two 3.3cm plates each containing 3 coverslips for examination of monolayer cultures (after 7 days of growth for the co-cultures). 2ml DMEM containing 10% FBS and 2Mm L-glutamine was added to each 3.3cm plate. The medium was aspirated and replaced with fresh medium after two days.

Co-cultured cells were serum starved after 10 days of growth at the air-liquid interface while monolayer cultures were serum starved after 36 hours. The medium was removed from the cells grown on coverslips or in filter inserts and they were washed with dPBS (3 times) and then fixed with 1% glutaraldehyde in

128

100mM phosphate buffer for 1 hour. HaCaT cells gown on cover slips were washed with H_2O for 10 minutes (twice), then 10 minutes each in 50%, 70% and 90% ethanol, followed by 10 minutes in 100% ethanol (twice). The cover slips were rinsed three times in hexamethyldisilazane for 10 minutes each (Nation, 1983) then allowed to air dry. The coverslips were attached to a 32mm diameter SEM stub with self adhesive carbon discs (TAAB Laboratories Equipment Ltd, BERKshire, UK). The cells were then coated with gold in an EMscope vacuum coater (EMScope, Ashford, UK) and examined in a JEOL 840A SEM at 5kV (Jeol UK Ltd, Welwyn Gardens City, UK.).

3.2.7 Samples for Confocal Microscopy

Confocal microscopy was carried out by Dr Chris George (Wales Heart Research Institute, School of Medicine, Cardiff University). HaCaT keratinocytes were subcultured from a 30% confluent T75 flask by addition of 5ml trypsin-EDTA and incubated at 37°C in 5% CO_2 for 10 minutes, before addition of 5ml DMEM plus 10% FBS to deactivate the trypsin. An aliquot (300µl) of HaCaT cells was removed and pipetted into three separate plates (3.3cm diameter) each containing 3 glass coverslips. 2ml DMEM containing 10% FBS and 2mM L-glutamine was added to each plate and mixed. The plates were incubated at 37°C in 5% CO_2 for 36 hours, after which, the medium was aspirated, the cells washed in dPBS (3 times), and serum-free DMEM plus 2mM L-glutamine was added (2ml/plate) and left for 24hours. The medium was aspirated, the cells were washed in dPBS (3 times) and ice-cold acetone-methanol (1:1 vol/vol) was applied for 5 minutes. Acetone-methanol was aspirated and cells were washed with dH_2O (3 times). Mouse acetylated α-tubulin antibody (T6074; Sigma-Aldrich Company Ltd, Gillingham, UK) in PBS (1:50 dilution) was applied for 1 hour. The cells were washed three times in dH_2O and donkey anti-mouse alexa 488 (Sigma-Aldrich Company Ltd, Gillingham, UK) in PBS (1:500) was applied for 30 minutes. Sections were mounted in hydromount plus 2.5% DABCO (Sigma-Aldrich Company Ltd, Gillingham, UK) to prevent photo-bleaching. Cover slips were

carefully placed onto microscope slide and digital images obtained using a Leica SP5 resonant scanning confocal microscope.

3.2.8 Real Time PCR (qPCR)

Real time PCR (qPCR) was carried out as previously described in Chapter 2 (see **Section 2.2.2.3**).

3.3 Results

3.3.1 Quantitative (Real Time) PCR on Cultured Keratinocytes

While HaCaT cells do not reflect the behaviour of normal keratinocytes as well as N/TERT1 cells (due to polyploidy), they are a commonly used keratinocyte cell line because they maintain "normal" epidermal differentiation in monolayer culture (Boukamp et al., 1988). HaCaT were chosen over N/TERT1 keratinocytes because they can be grown in the same culture medium as HCA2 fibroblasts, and HaCaT cells express more GLI1 than N/TERT1 (see **Figure 2.2**), which may lead to increased SHH pathway activation. The experiments depend on co-culture of keratinocytes with HCA2 fibroblasts in the same wells, so they must both grow in the same medium. N/TERT1 cells must be cultured in serum-free medium which does not favour the growth of HCA2 cells. This meant that primer optimisation (see **Table 2.4**) had to be repeated since gene expression may be different in HaCaT cells.

3.3.1.1 Optimising ACTB (β-actin) Primers on HaCaT Cell cDNA

ACTB (β-actin) primer optimisation was done with cDNA from control HaCaT cells which had not been treated with SHH or EGF (0.5, 1 and 1.5μg per reaction). ACTB primers were tested at three different levels: 0.05μg/μl, 0.1μg/μl and 0.15μg/μl. The reaction which gave the lowest Ct (cycle threshold) value was taken as the preferred combination of cDNA and primer (1.5μg cDNA and 0.15μg/μl ACTB primers in this case) because this is the earliest detectable point

of product above background levels. A low Ct level was obtained for ACTB primers and HaCaT cDNA as β-actin was an abundant cytoskeletal protein in these cells. The dissociation curves showed that the primers gave good results (**Figure 3.4a**) indicating that the reactions were not contaminated and the primers did not dimerize during the reaction. Serial dilutions of cDNA were made (neat, 1:10, 1:100, 1:1,000) and the qPCR fluorescence values plotted against the number of cycles for each dilution. For ACTB, the amplification plots were equally spaced (**Figure 3.4b**). The Ct values for each dilution were plotted against the dilution value to derive a standard curve, which showed a good R^2 value, slope and efficiency so the qPCR results appeared to be very accurate (**Figure 3.4c**).

(a) Dissociation Curve (b) Amplification Plot

(c) Standard Curve

$R^2 = 0.998$
Slope = -3.17
Eff = 106.6%
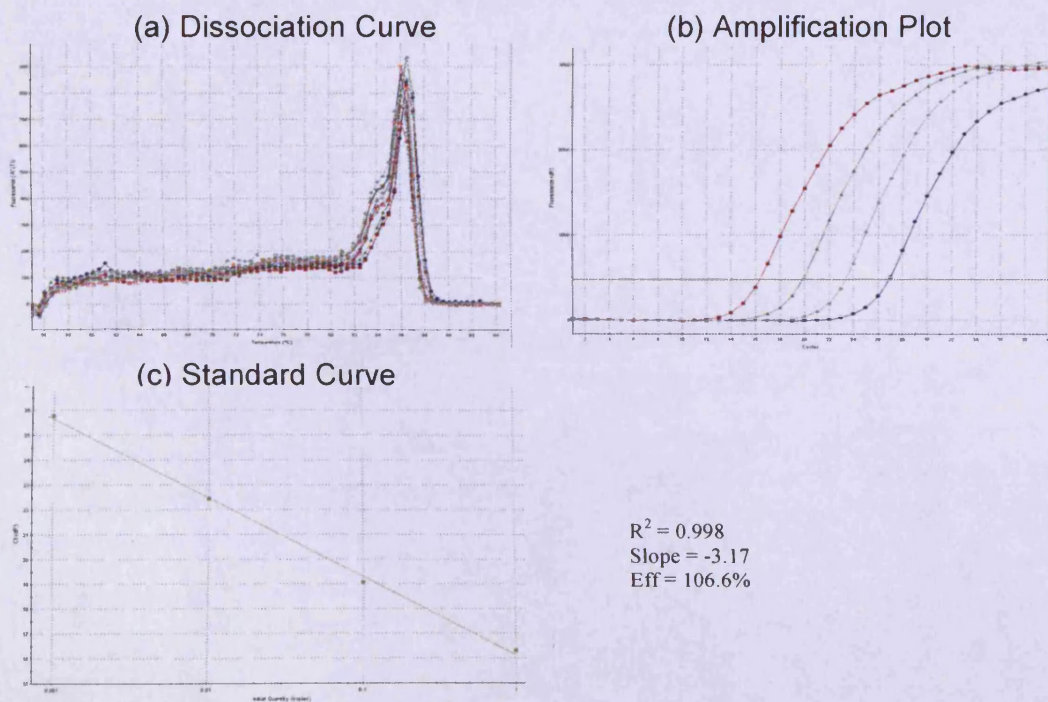
Figure 3.4: Optimisation of ACTB Primers and HaCaT Keratinocyte cDNA. (a) Dissociation curve for HaCaT cDNA with ACTB primers. (b) Dilution series of HaCaT cDNA using 1.5µg cDNA (red), 1:10 dilution (green), 1:100 dilution (grey) and 1:1,000 dilution (blue) with ACTB primers. (c) Standard curve for HaCaT cDNA dilution with ACTB primers.

3.3.1.2 Optimising EGR-3 primers

The primer and cDNA concentrations were optimised as detailed in **Chapter 2, Table 2.2**.

Control cDNA from HaCaT cells which were not treated with SHH or EGF was used for the optimisation (0.5, 1 and 1.5μg cDNA per reaction with four different primer amounts (0.5μg, 1μg, 1.5μg and 2μg). The reaction which gave the lowest Ct value used (1μg cDNA and 1μg EGR-3 primers) was used for all subsequent experiments. However, these Ct values were still relatively high and this is probably due to the low level of EGR-3 in these cells.

The dissociation curves (**Figure 3.5a**) showed a slight second peak and a slight shift in the main peak suggesting that there is more than one product and possibly some primer dimers. The qPCR reactions were repeated using serial dilutions of cDNA (neat, 1:10, 1:100, 1:1000) and the resulting fluorescence was plotted against the cycle number. The three dilutions showed equal spacing between the curves but one dilution was consistently out due to low EGR-3 levels (**Figure 3.5b**). This resulted in a standard curve with poor values for the slope and efficiency (slope should be between -3.2 and -3.5 and efficiency should be 90-110%). After repeating the optimisation with EGR-3 primers several times, good values for the slope and efficiency could not be achieved when all the serial dilutions were included, so the 1:1000 dilution was removed. This then produced a standard curve with good R^2 and slope values, but the efficiency was still slightly above recommended levels and might cause inaccuracies in the qPCR results.

(a) Dissociation Curve   (b) Amplification Plots

(c) Standard Curve

$R^2 = 1$
Slope = -3
Eff = 118%
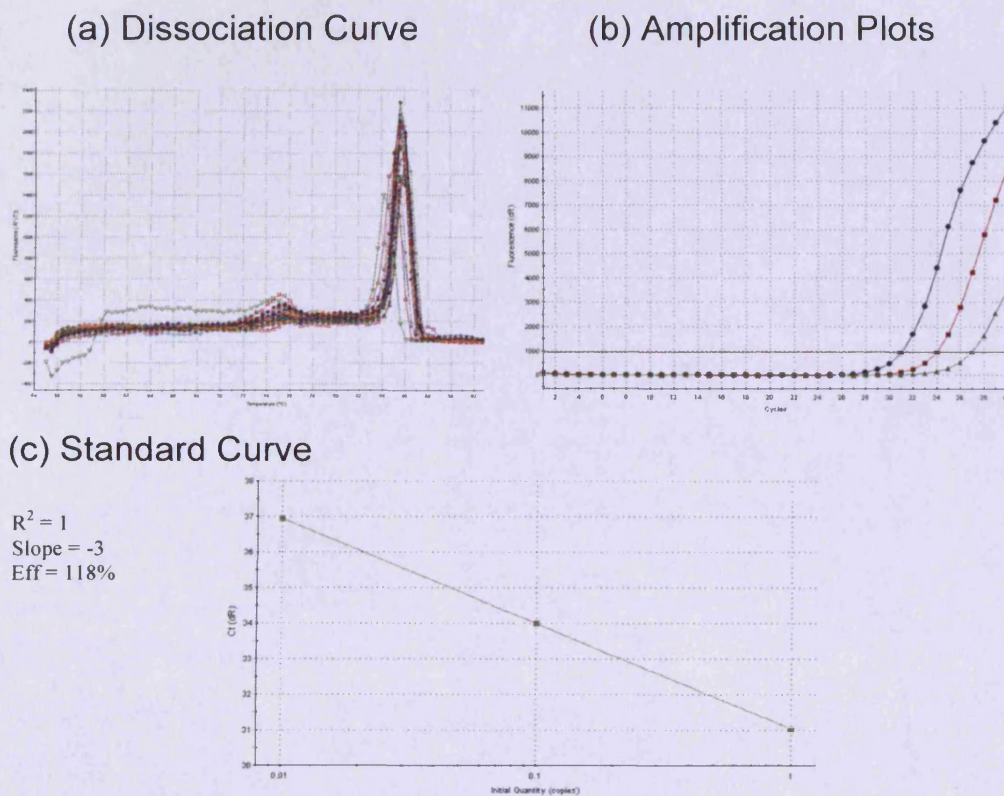
Figure 3.5: Optimisation of EGR-3 Primers and HaCaT Keratinocyte cDNA. (a) Dissociation curve for HaCaT cDNA with EGR-3 primers. (b) Dilution series of HaCaT cDNA using 1µg cDNA (blue), 1:10 dilution (red), 1:100 dilution (green) and a 1:1000 dilution (grey) and EGR-3 primers. (c) Standard curve for HaCaT cDNA dilution with EGR-3 primers.

3.3.1.3 Optimising PTCH primers

The primer and cDNA concentrations were also optimised as detailed in **Chapter 2, Table 2.2**. The lowest Ct values were obtained with 1µg PTCH primers with 2µg cDNA. There were no extra peaks in the dissociation curve showing that only one product was produced and there was no evidence for any primer dimers or contamination (**Figure 3.6a**). However, again the 1:1000 dilution was too low to achieve a good Ct value (ideally Ct should be at below 24 cycles) even after repeating the reactions several times, probably due low levels of PTCH expression in HaCaT cells (**Figure 3.6b**). The standard curve was plotted without the data for the 1:1000 dilution and reasonable values were obtained, with a good R^2 value but

133

slope and efficiency values slightly outside the guidelines (**Figure 3.6c**). Thus, the low levels of PTCH could lead to inaccurate data using these primer and cDNA concentrations.
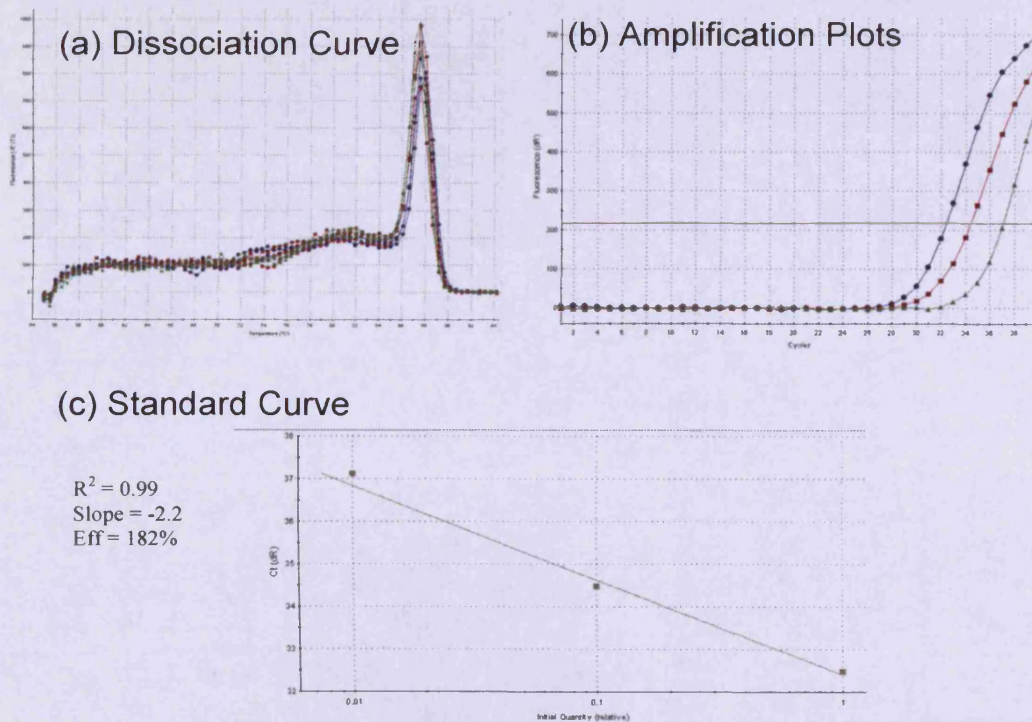
Figure 3.6: Optimisation of PTCH Primers and HaCaT Keratinocyte cDNA. (a) Dissociation curve for HaCaT cDNA with PTCH primers. (b) Dilution series of HaCaT cDNA using 1μg cDNA (blue), 1:10 dilution (red), 1:100 dilution (green) and a 1:1000 dilution (grey) and PTCH primers. (c) Standard curve for HaCaT cDNA dilution with PTCH primers.

3.3.1.3 Optimising IL-1R2 primers

Primer and cDNA concentrations were also optimised for IL-1R2 as detailed in **Chapter 2, Table 2.2**. The lowest Ct values were obtained with 1.5μg IL-1R2 primers and 1.5μg cDNA (**Figure 3.7**). The dissociation curves showed a slight second peak in front of the main peak suggesting that more than one product existed, possibly due to primer dimers (**Figure 3.7a**). The amplification plots show that the Ct values for each dilution were very late, again due to low level of IL-

134

1R2 expression in HaCaT cells. Thus, the qPCR results were the best possible with these cells but could still not be fully optimised even after several attempts (**Figure 3.7b**). The 1:1000 dilution came too late to fit on the plot and as a consequence the standard curve was drawn only with Ct values from the first three dilutions in the series. This provided R^2, slope and efficiency values that were reasonable so these conditions should give reliable qPCR results (**Figure 3.7c**).

(a) Dissociation Curve   (b) Amplification Plots

(c) Standard Curve

$R^2 = 0.99$
Slope = -3.37
Eff = 97.9%
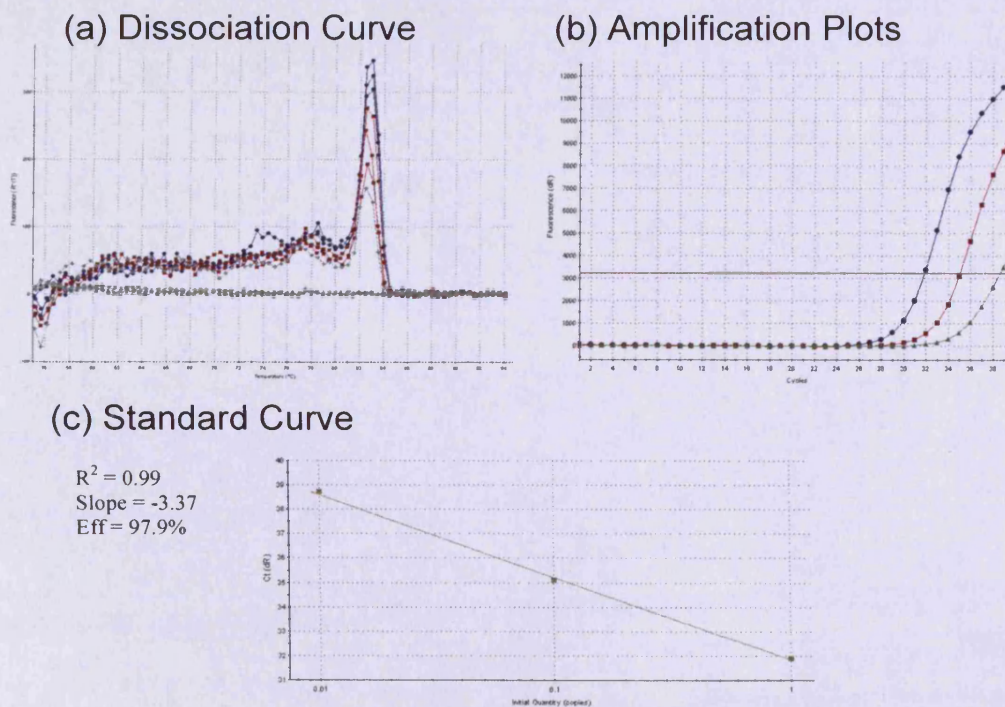
Figure 3.7: Optimisation of IL1R2 Primers and HaCaT Keratinocyte cDNA. (a) Dissociation curve for HaCaT cDNA with IL1R2 primers. (b) Dilution series of HaCaT cDNA using 1.5µg cDNA (red), 1:10 dilution (green), 1:100 dilution (blue) and a 1:1000 dilution (grey) and IL1R2 primers. (c) Standard curve for HaCaT cDNA dilution with IL1R2 primers.

3.3.1.5 Optimising S100A7 primers

The primer and cDNA concentrations were optimised for S100A7 using the same techniques (see **Chapter 2, Table 2.2**). The lowest Ct values were obtained with 1µg S100A7 primers and 2µg cDNA. The dissociation curve for these primers was very good, with only a small extra peak for one sample (**Figure 3.8a**), showing

that there was no contamination or primer dimers present. The amplification plots were equally spaced and the Ct values were reasonable (between 25 and 34 cycles). Lower Ct values (between 20 and 30) were not achieved even after the optimisation was repeated several times (**Figure 3.8b**). The standard curve values were within the recommended guidelines (**Figure 3.8c**). These primers appeared to be well optimised and should therefore provide accurate data from qPCR reactions.
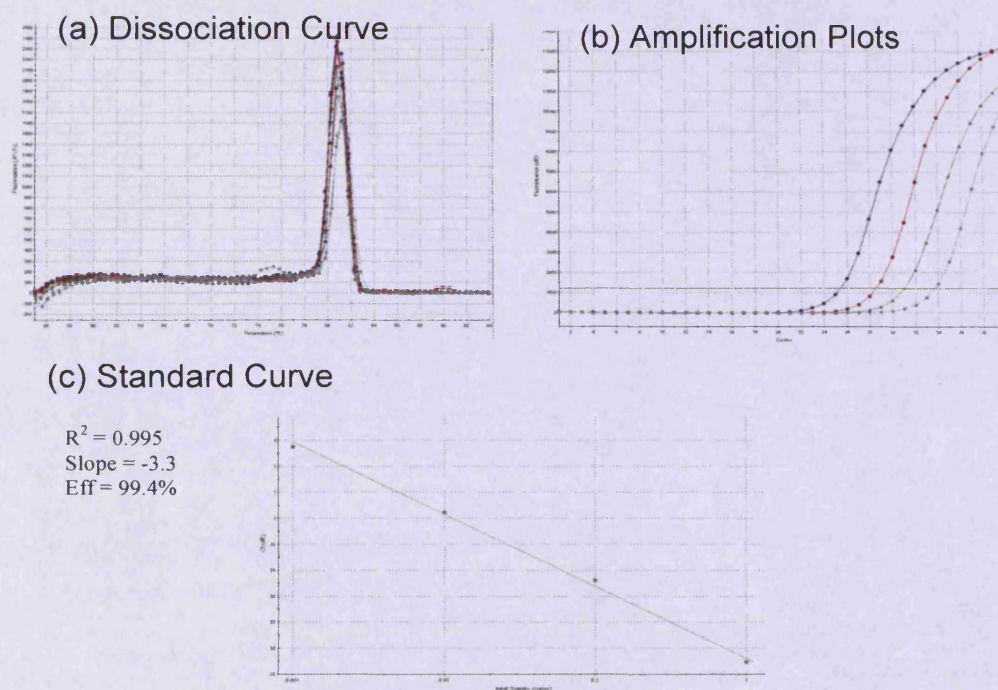
Figure 3.8: Optimisation of S100A7 Primers and HaCaT Keratinocyte cDNA. (a) Dissociation curve for HaCaT cDNA with S100A7 primers. (b) Dilution series with HaCaT cDNA: neat (1.5µg) cDNA (blue), 1:10 dilution cDNA (red), 1:100 dilution cDNA (green) and a 1:1000 dilution cDNA (grey) and S100A7 primers. (c) Standard curve for HaCaT cDNA dilution series with S100A7 primers.

3.3.1.6 SHH and EGF Signalling in Fibroblast: Keratinocyte Co-cultures.

HaCaT keratinocytes were cultured in a filter insert in the presence or absence of HCA2 fibroblasts. This allowed diffusion of growth factors between the HaCaT

136

keratinocyte and HCA2 fibroblast cell lines which facilitates paracrine interactions (**Figure 3.9**).
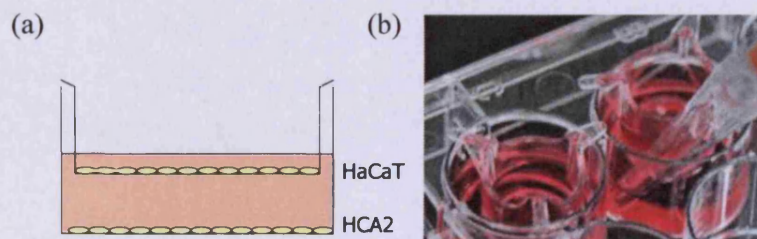
Figure 3.9: Co-culture of HaCaT Keratinocytes and HCA2 Fibroblasts. (a) HaCaT keratinocytes and HCA2 fibroblasts are both cultured in the same well but separated by a filter insert. (b) Photograph of an insert in the well of a tissue culture plate (adapted from Greiner Bio-One, Stonehouse, UK).

HaCaT keratinocytes were allowed to reach 80-100% confluency, and then treated with either recombinant SHH, recombinant EGF, both or neither. Keratinocyte RNA was extracted from the cells in each filter insert and the activity of SHH signalling was assessed by measuring expression levels of SHH-responsive genes (EGR-3, IL-1R2, S100A7 and PTCH) by RT-qPCR.

EGR-3 expression decreased slightly (0.2 fold) in the presence of SHH and more (0.6 fold) in the presence of EGF. In combination, the decrease (0.4 fold) was intermediate (**Figure 3.10a**). In the presence of HCA2 fibroblasts, EGR-3 expression increased 0.4 fold with SHH but decreased by 0.6 fold with EGF. When both were present, the EGF seemed to prevent the increase observed with SHH alone.

SHH increased IL-1R2 expression by 15 fold while EGF increased this by 140 fold in the absence of HCA2 fibroblasts (**Figure 3.10b**). When both SHH and EGF were present in the cell culture medium, the values were similar to EGF alone. In the presence of HCA2 fibroblasts, SHH has little or no effect but even higher levels of IL-1R2 were induced by EGF (210 fold) whether SHH was present or not.

There was little change in S100A7 expression when cells were treated with SHH alone (**Figure 3.10c**) but EGF reduced S100A7 levels about 10 fold (from 0.9 to 0.1). A similar reduction was seen in the presence of both SHH and EGF. The results obtained in the presence of HCA2 fibroblasts were similar.

The PTCH data was similar to EGF-3 and SHH appeared to have no effect on PTCH expression in the absence of HCA2 fibroblasts (**Figure 3.10d**). Again, EGF reduced PTCH levels compared to the control (no recombinant proteins), however EGF reduced PTCH by about 5 fold but SHH ameliorated this effect slightly. In the presence of HCA2 fibroblasts, SHH increased PTCH expression from 1 to 1.4 fold while EGF decreased PTCH levels 3 fold and inhibited the effect of SHH when both were applied.

(a) EGR-3 Expression

(b) IL-1R2 Expression

(c) S100A7 Expression
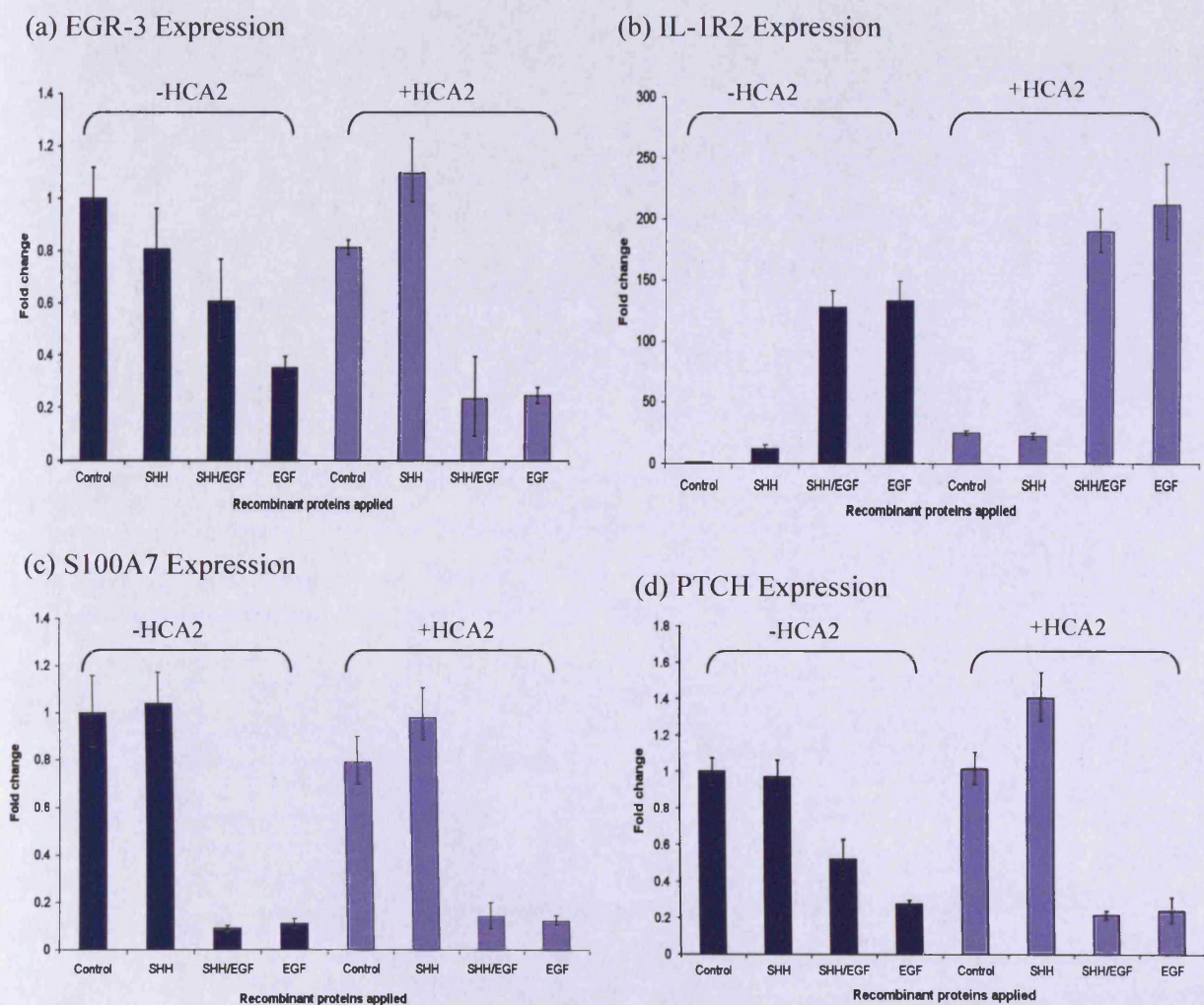
(d) PTCH Expression

Figure 3.10: Effects of Keratinocyte Co-culture with Fibroblasts on SHH Target Gene Expression. *Results show the effect of co-culture of HaCaT keratinocytes with HCA2 fibroblasts on expression of (a) EGR-3, (b) IL-1R2, (c) S100A7 and (d) PTCH. Dark blue boxes represent experiments carried out in the absence and light blue presence of HCA2 cells. Data expressed as a mean +/- SD for n=2 experiments.*

Thus, EGR-3, S100A7 and PTCH expression levels do not increase in the presence of SHH when fibroblasts are not present. However, expression is decreased in the presence of EGF. When fibroblasts were present, similar changes were apparent but there was only a slight increase in EGF-3 and PTCH when SHH was added. It

139

would be interesting to find out the reason for the unexpected down-regulation of these genes in the presence of EGF.

However, the response of IL-1R2 differed. The increased expression in the presence of EGF was more pronounced in the presence of fibroblasts. It seems that paracrine signalling may be enhancing the effect of EGF signalling already observed in the absence of fibroblasts. The up-regulation of IL-1R2 was more extensive than seen earlier (see **Figure 2.14**), where IL-1R2 expression was also increased with EGF but to a lesser extent. However, these experiments were done on two different cell lines (HaCaT and NTERT-1) which may explain the different levels of expression. It would be interesting to repeat the LY294002 and PD98059 inhibitor experiment (**Figure 2.14b, c**) to determine if PI3K and AKT are also controlling the expression of this gene in HaCaT cells.

The presence of HCA2 cells did not have a large effect on the expression of any of these genes. Also, there was no large fold increase when SHH and EGF were present in combination. This data shows that the presence of fibroblasts within a co-culture system does not contribute to SHH pathway activation, at least on its own.

There are some interesting differences and similarities between the results obtained with HaCaT calls (**Figure 3.10a-d**) and those obtained with N/TERT1 cells (see **Chapter 2**). Similar results may have been expected because HaCaT and N/TERT1 cells are essentially both keratinocyte cell lines grown in monolayer conditions. The major difference between HaCaT cells grown in the absence of fibroblasts in submerged cultures and N/TERT1 keratinocytes grown in monolayer cultures are: a decrease in expression of EGR-3, S100A7 and PTCH but a large increase of IL-1R2 in the presence of EGF (EGF or SHH/EGFs. This changes were not found with N/TERT1 cells. The results for IL-1R2 in HaCaT cells (**Figure 3.10b**) resembled those obtained for seen N/TERT1 cells (see **Figure 2.14a**) except the fold changes measured were much greater. For EGR-3 there was

little variance in expression when treated with SHH or EGF in N/TERT1 (**Figure 2.12a**), decreased expression in HaCaT caused by EGF (**Figure 3.10a**) was small (0.6 fold). The S100A7 results were quite different between the two keratinocyte cell lines, with small increases in expression in N/TERT1 in the presence of SHH or SHH plus EGF, and a larger increase in expression in the presence of EGF (**Figure 2.16a**) compared to no increased expression in the presence of SHH in HaCaT cells (**Figure 3.10c**). In N/TERT1 cells, PTCH showed no significant difference from the control in the presence of SHH, EGF or SHH/EGF (**Figure 2.18a**), not the same as found in HaCaT cells (**Figure 3.10d**).

3.3.1.7 Stratified Co-culture QPCR

Since paracrine signalling alone does not result in SHH pathway activation and cilia appear to be required for activation of SHH signalling, experiments were performed to determine whether SHH would become activated in conditions that favour polarisation (a requirement for cilia formation). Keratinocytes were cultured at the air-liquid interface by lowering the level of the culture medium to expose HaCaT keratinocytes to the air, whilst still reaching the underside of the filter insert to feed them from below (**Figure 3.11**). They were cultured for 5 days in filter inserts, allowing them to stratify (to enable polarisation of the cells) which should encourage cilia formation. HaCaT cells were also cultured in the presence and absence of HCA2 fibroblasts to determine whether paracrine signalling contributes to the polarisation. The filter inserts allow movement of growth factors between the two cell lines and may enable polarisation of HaCaT cells.
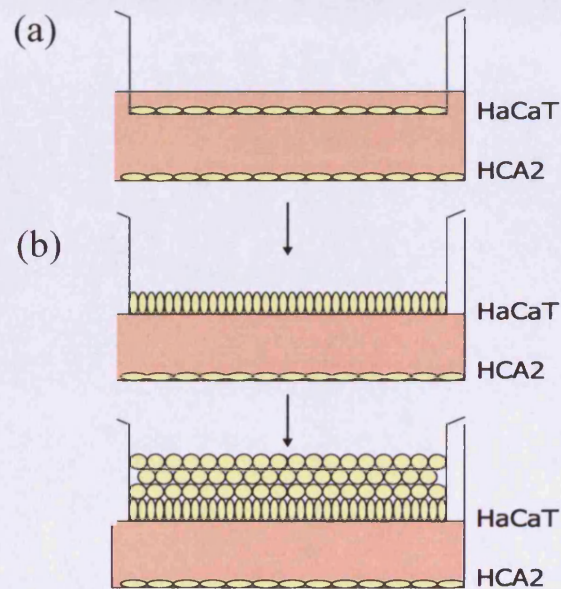
Figure 3.11: HaCaT Keratinocytes Cultured on a Filter Insert at the Air-Liquid Interface above HCA2 Fibroblasts. (a) HaCaT keratinocytes were covered in culture medium so that they could adhere to the filter insert. (b) After 24hours the culture medium level is reduced to feed the HaCaT keratinocytes from below the filter insert and leave them open to the air. (c) The cultures were then incubated for 5 days to allow stratification.

The expression of the same four SHH-responsive genes (EGR-3, IL-1R2, S100A7 and PTCH) was assessed by qPCR in HaCaT cells under these co-culture conditions. EGR-3 expression in HaCaT keratinocytes in the absence of HCA2 fibroblasts was increased slightly by recombinant SHH. IL-1R2 expression was decreased slightly, while S100A7 and PTCH expression remained unchanged.

In the presence of recombinant EGF (whether SHH was present or not), the expression of all four genes (EGR-3, IL-1R2, S100A7 and PTCH) was reduced. In

142

the presence of HCA2 fibroblasts, expression of EGR-3 remained unchanged compared to control HaCaT keratinocytes in the absence of HCA2 fibroblasts. IL-1R2, S100A7 and PTCH expression decreased compared to control levels for HaCaT keratinocytes grown in the absence of HCA2 fibroblasts.

In the presence of SHH, expression of EGR-3 levels remained unchanged, while levels of IL-1R2, S100A7 and PTCH levels decreased below control levels (when HCA2 were absent). EGF had no effect on EGR-3 expression, but expression of IL-1R2, S100A7 and PTCH did decrease. SHH and EGF applied to HaCaT cells in combination caused a further reduction in expression of EGR-3, IL-1R2, S100A7 and PTCH.

SHH increased EGR-3 expression compared to the control (no SHH protein). However, EGF decreased EGR-3 levels and inhibited the effect of SHH (**Figure 3.12a**). HCA2 fibroblasts had little effect on EGR-3 expression in control cells (no EGF or SHH) but the presence of fibroblasts altered the response in the presence of SHH and EGF. Thus, in the presence of HCA2 cells, EGR-3 levels decreased when both SHH and EGF were present together.

SHH halved IL-1R2 levels and EGF reduced IL-1R2 10 fold (**Figure 3.12b**). When both SHH and EGF were present in combination, the reduction was also 10 fold. In the absence of recombinant SHH and EGF, HCA2 cells inhibited IL-1R2 expression and the addition of SHH or EGF separately caused little change. However, when both were present, IL-1R2 levels dropped by half.

SHH had no effect on S100A7 expression levels, but EGF decreased S100A7 expression 10 fold. EGF also had the same effect when present in combination with SHH (**Figure 3.12c**). In the presence of HCA2 fibroblasts, S100A7 expression decreased 3 fold in the absence of the recombinant proteins and addition of SHH had no effect. However, EGF decreased S100A7 to the same level it did when HCA2 cells were not present.

SHH had no effect on PTCH expression but EGF reduced expression 10 fold. The same decrease was apparent (10 fold) when SHH and EGF were added to the cell medium in combination (**Figure 3.12d**). PTCH levels halved in the presence of HCA2 fibroblasts and SHH still had no effect. Interestingly, EGF alone had no effect on PTCH levels in the presence of HCA2 cells, but PTCH decreased 5 fold when both SHH and EGF were added in combination.

3.3.1.8 Scanning Electron Microscopy (SEM)

SEM was used to examine the surface of cells in order to determine the presence or absence of cilia in HaCaT keratinocytes under different conditions: co-culture where HaCaT were allowed to stratify at the air-liquid interface or monolayer culture with N/TERT1 keratinocytes.

(a) EGR-3 Expression

(b) IL1R2 Expression

(c) S100A7 Expression

(d) PTCH Expression
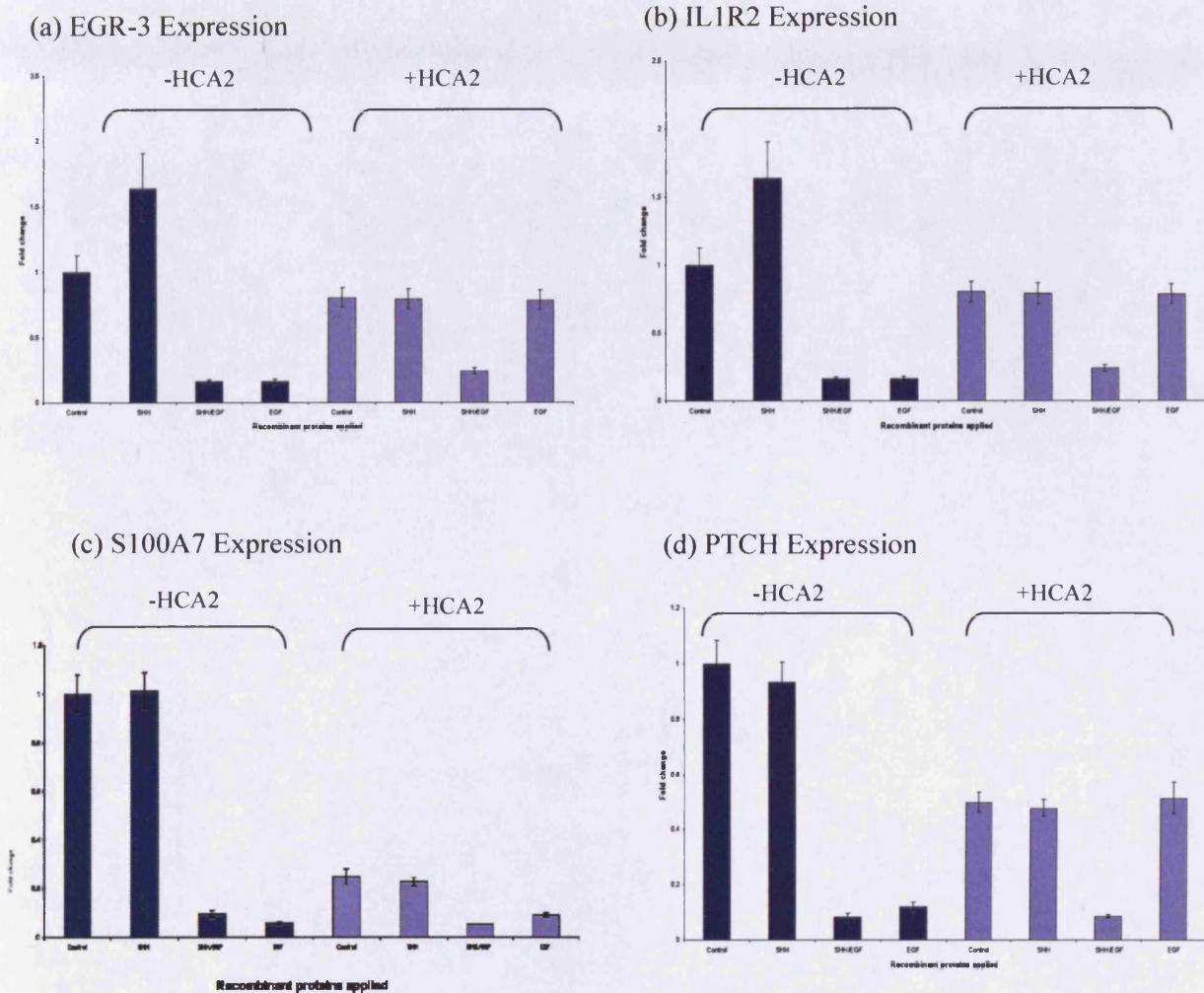
Figure 3.12: Effects of Keratinocyte Co-culture with HCA2 Fibroblasts (Stratified at Air-Liquid Interface for 5 days) on SHH Target Gene Expression. Co-cultures of HaCaT keratinocytes with HCA2 fibroblasts were allowed to stratify at the air-liquid interface for 5 days and the expression of (a) EGR-3, (b) IL-1R2, (c) S100A7 and (d) PTCH was measured in the presence and absence of SHH and/or EGF. Dark blue boxes represent experiments carried out in the absence of HCA2 cells and light blue boxes in the presence of HCA2 cells. Data expressed as a mean +/- SD for n=2 experiments.

There were no primary cilia found on HaCaT cells in monolayer culture (**Figure 3.13**). HaCaT cells cultured on filter inserts at the air-liquid interface did stratify and differentiate further but these cells did not have primary cilia either. The cells appeared flattened and gaps occurred between adjacent cells but this is an artefact caused by dehydration during SEM processing. Cilia-like surface structures could be seen on HaCaT keratinocytes cultured at the air-liquid interface for 10 days in the presence of HCA2 fibroblasts (**Figure 3.13c** and in **Figure 3.13d**). There also appeared to be some cell surface ruffling at the bottom of each image, structures that look similar to primary cilia. These cells were grown for a longer period in culture (10 days rather than 5 days) and this may have provided better conditions for cilia formation. Ideally, the experiment should be repeated under these conditions (HaCaT cultured for 10 days at the air-liquid interface) and qPCR used to determine whether SHH signalling was activated (increased) in the presence of primary cilia.
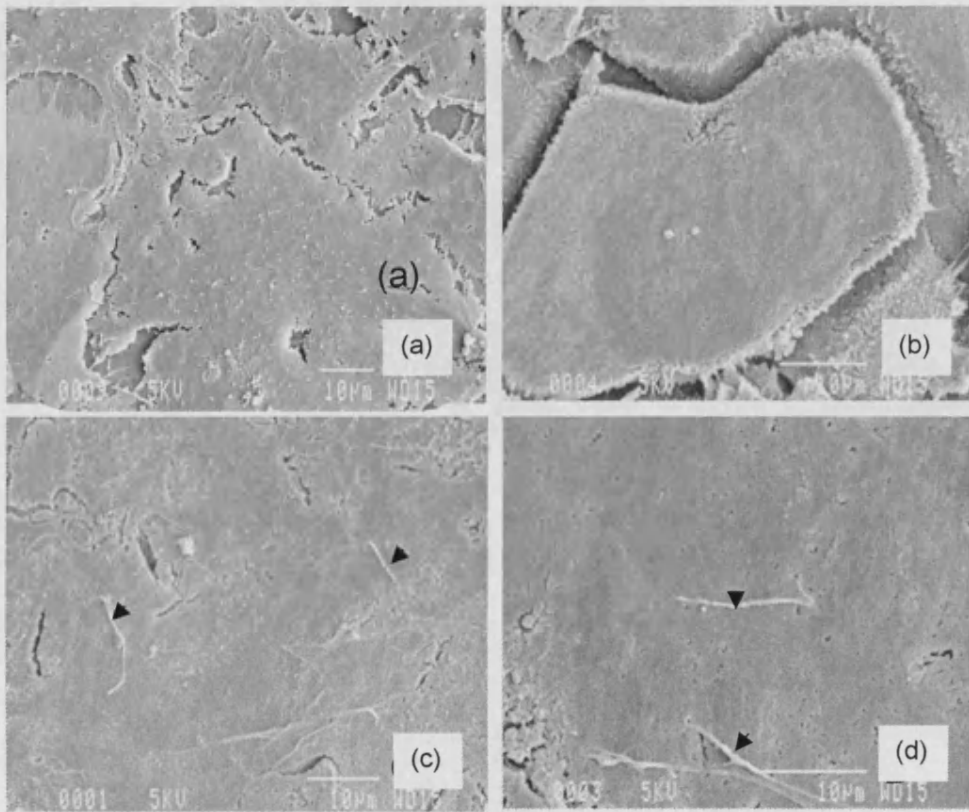
Figure 3.13: Scanning Electron Microscopy of HaCaT Cells Grown in Culture Conditions to Achieve Primary Ciliation. *(a) No cilia structures were observed in HaCaT cells grown in monolayer culture. (b) No cilia were observed in HaCaT keratinocytes grown on filter inserts at the air-liquid interface for 10 days (allowing stratification) in the absence of HCA2 fibroblasts. (c, d) Cilia were present in 10-15% of HaCaT cell cultures grown in filter inserts at the air-liquid interface for 10 days (allowing stratification) in the presence of HCA2 fibroblasts.*

In addition, it would be preferable to use immunofluorescence with an antibody to acetylated-α-tubulin detected by confocal microscopy to confirm that the cilia-like structures seen in SEM were cilia and not due to dehydration-induced surface ruffling.

Initial attempts to use confocal microscopy were carried out on monolayer cultures but primary cilia were not observed. No primary cilia were seen on the surface of any of the HaCaT cells grown in monolayer culture on glass coverslips (**Figure 3.14**). The acetylated-α-tubulin antibody localised to the cytoskeleton and was particularly intense at the junctions between cells (**Figure 3.14a, c**). The cytoskeleton was particularly visible in HaCaT cells due to strong antibody localisation (**Figure 3.14b, d**).

One major concern was the lack of specificity of the acetylated-α-tubulin antibody to the primary cilium since many microtubules were labelled. This would potentially make it hard to distinguish the primary cilia from other microtubule structures. At this time, confocal appeared to be a very time consuming method for the detection of primary cilia and a lack of positive control to confirm that the method would show primary cilia against the microtubule labelling led to the use of scanning electron microscopy (SEM) for more rapid results. However, the confocal microscopy did show a higher intensity of labelling at cell-cell junctions suggesting that if the conditions favouring cilia formation had been used it may have been possible to confirm the SEM results.
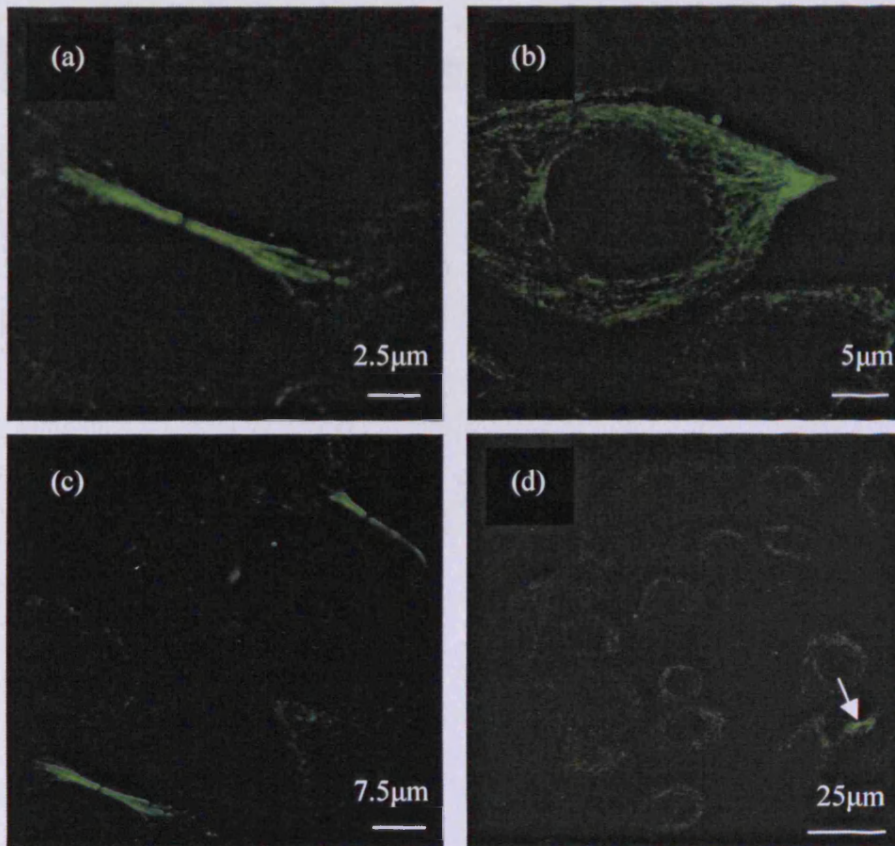
Figure 3.14: Immunofluorescence with Antibodies to Acetylated-α-Tubulin in HaCaT Keratinocytes Grown in Monolayer Culture on Glass Coverslips. *Confocal laser scanning microscopy (CLSM) with an acetylated-α-tubulin antibody linked to alexa 488 (green) showed no primary cilia present on the cells. However, high levels of acetylated tubulin were observed at intercellular junctions (a, b, c; arrow in d) and low levels immunolocalised to microtubules throughout the cytoplasm (b, d).*

3.4 Discussion

Optimisation of the qPCR experiments for each set of primers with the DNA was challenging due to the low levels of expression of these genes in the HaCaT cells under all conditions in the cell culture experiments. This meant that for all genes other than the housekeeping gene (ACTB), the amplification plots for the dilution series were at a high cycle number and for EGR-3 and PTCH the 1:1000 dilution gave a plot at a cycle number which was too high to include. However, standard curves for all genes except PTCH were still within recommended guidelines. A larger quantity of DNA may have resolved this problem.

The results of this study show differences in gene expression between the two keratinocyte cell lines (where N/TERT1 were used in Chapter 2 and HaCaT (in the absence of fibroblasts and not grown at the air: liquid interface) in this chapter. This might be expected as they are immortalised in different ways and N/TERT1 keratinocytes are thought to behave more like primary keratinocytes than the polyploidy HaCaT cell line.

It is very interesting that EGF has a large inhibitory effect on gene expression in HaCaT keratinocytes for EGR-3, S100A7 and PTCH but not for IL1-R2. This may have been caused by the presence of HCA2 fibroblasts. The abnormal phenotype of HaCaT cells may mean that there are slightly different signal transduction interactions compared to in N/TERT1 cells, removing their sensitivity to EGF. It would be expected that EGF inhibits PTCH expression, but the inhibition of EGR-3 and S100A7 expression is not continuous with N/TERT1 experimental results in chapter 2 or those published by Kasper et al., (2006). IL1R2 and PTCH results may have produced results as expected due to effects on expression caused by different arms of the EGF pathway compared to EGR-3 or S100A7. Paracrine signalling alone showed little effect on these results, showing that this was not enough to enable polarisation or cilia formation.

Downregulation of all expression when there was development of stratification in the presence of HCA2 fibroblasts confirms that paracrine signalling in combination with polarised cells caused changes in target gene expression. However, this still does not confirm that SHH signalling is activated since there was no increase expression in the presence of SHH. Strangely, in the presence of SHH/EGF expression was downregulated even though in the presence of EGF expression was close to that of the control. This was true for all genes (**Figure 3.10a-d**). This result of little change in expression from the control in the presence of SHH or EGF but a decrease in the presence of both proteins shows that there must be an interaction between SHH and EGF, this suggests that SHH signalling was activated, if only by a small amount. These results are encouraging and using this method with a longer stratification time (10 days rather than 5) for more cilia development would be the next step in moving towards a skin cell model with SHH pathway activation. With EGF signalling also activated, further qPCR studies could be carried out to find out more about augmentation of SHH signalling. This would be a good reproducible cell model for testing inhibitors for the treatment of BCC.

There may also be non-canonical SHH pathways that don't need cilia for activation. The SHH pathway in drosophila does not require cilia and non-canonical pathways are known in humans (Jenkins et al. 2009).

Unfortunately due to time restrictions, these experiments were only carried out twice each. But if they were to be repeated in future it would be beneficial to also repeat them on a more 'normal' keratinocyte cell line than HaCaT if possible. A means of carrying this out without the problems of N/TERT1 and HCA2 cells requiring separate culture media, would be to create organotypic cultures. This would use HCA2 fibroblasts suspended in a collagen matrix with N/TERT1 keratinocytes applied to the upper surface of the collagen. The collagen matrix would be lifted onto a steel mesh support so that the keratinocytes were allowed to grow at the air: liquid interface for stratification and the cells could be fed from the

underside of the collagen matrix. This means only one medium type would need to be used to feed the cells through the collagen and epithelial-mesenchymal interactions could occur (Dickson et al. 2000).

The results of the SEM experiments showed that HaCaT cells need to be grown at the air: liquid interface and allowed to stratify for 10 days (to encourage cilia formation) before SHH addition. This should be in the presence of fibroblasts to enable successful cilia formation, which may then lead to successful activation of SHH signalling. Interestingly, Strugnell et al. (1996) who found that addition of Ca^{2+} to keratinocyte culture medium was required to achieve differentiation of cells and enable cilia formation so this may be an avenue which could be followed to increase cilia formation (Strugnell et al., 1996). However, it had not previously been shown whether N/TERT1 keratinocytes form cilia in monolayer cultures or whether they also require the presence of fibroblasts and growth at the air: liquid interface. The results of chapter two which show little SHH pathway activation in monolayer cultures suggest a lack of primary cilia, but this needs to be confirmed by SEM in order to determine whether this genuinely is the cause of low pathway activation or whether it may be due to a lack of GLI1.

Primary cilia are only present under certain culture conditions, (they form when cells aren't dividing). It seems likely that cells that are committed to terminal differentiation that are truly growth arrested are more likely to produce primary cilia. This may be the reason for a lack of augmentation of GLI response genes by EGF in chapter 2. There were a small number of primary cilia formed in the presence of fibroblasts but none in their absence showing that fibroblasts are required for cilia formation. However, the time spent in culture at the air: liquid interface may increase stratification and polarisation leading to increased cilia formation. Keratinocytes appeared to be polarised (basal cells were columnar and well organised) in a complex culture study using HaCaT keratinocytes which were allowed to stratify at the air: liquid interface when they were grown on a collagen gel containing fibroblasts fed from the underside of the collagen by culture

152

medium, however cilia formation was not confirmed (Bigelow et al. 2005). Keratinocyte stratification in the presence of fibroblasts may increase the number of ciliated cells compared to in the absence of fibroblasts, thus increasing SHH activation. Cilia form when cells aren't dividing so it follows that they must be growth arrested. Therefore, serum starving for a greater length of time may be required to ensure growth arrest in order to induce a larger number of cilia (Pedersen et al. 2008). From the results of this chapter we could speculate that the number of cilia in the cell lines used may also be increased by direct contact with fibroblasts, by use of a fibroblast feeder layer for the keratinocytes; 3D complex cultures such as those used by Bigelow et al. (2005) or by growing keratinocytes and fibroblasts on either side of collagen coated porous nylon membranes.

Primary cilia have been found on primary mouse keratinocytes, therefore it seems likely that primary human cells would also have cilia and this could be tested by SEM. If cilia are found to be present then SHH pathway activation should be achievable. However, using immortalised cell lines has the advantage of experimental repeatability and reliability (Wong et al., 2009).

Although SEM showed the presence of cilia after 10 days of growth at the air: liquid interface, they may be abnormal or not polarised. There may not be SHH signalling in cells grown at the air: liquid interface in the presence of fibroblasts due to incomplete polarisation and/or abnormal protein behaviour within the cilia. If the IFT proteins do not behave normally the SHH pathway molecules cannot be transported to their sites of action so the GLIs may not be able to act as transcription factors. Tests are needed to show the ability to polarise and normal functionality of the cilia to confirm whether this is the reason that SHH signalling does not seem to be active even in the presence of fibroblasts. This may include further SEM to confirm the cilia alignment or confocal microscopy to confirm co-localisation of cilia proteins and the SHH pathway proteins, although confocal microscopy of cilia is very time consuming due to high levels of background fluorescence.

Despite the low numbers of cilia, the SHH pathway may still be active in this experiments carried out for this chapter. This could be shown by immunofluorescence with GLI antibodies to detect whether nuclear translocation indicating GLI activation has occurred or by western blotting to look for upregulated GLI expression. The reason this was not tested is that GLI antibodies tend to be of poor quality.

N/TERT1 keratinocyte cell lines or primary keratinocytes may form greater numbers of cilia when allowed to stratify in the presence of fibroblasts due to their more normal phenotype (they are not polyploid like HaCaT). Cilium formation requires the centrosome so there may be a problem with forming a primary cilium in polyploid cells, which would have more than one centrosome/centriole. HaCaT cells also have a P53 mutation, which N/TERT1 keratinocytes do not. Apart from P53 mutation frequency in cancers, P53 deactiviation is also known to cause polyploidy. (Lehman et al. 1993; (Dickson et al. 2000). The challenge here would be to find a culture medium in which either of these types of keratinocyte could grow in combination with fibroblasts as both N/TERT1 and primary keratinocytes tend to grow well in serum-free medium.

In this chapter, there has been a change in use of immortalised cell line from N/TERT1 keratinocytes used in the previous chapter to the HaCaT keratinocyte cell line. Unfortunately HaCaT cells are polyploidy and so are thought to behave less like 'normal' keratinocyte cells than N/TERT1 keratinocytes. Polyploidy may be caused by the p53 deactivating mutation, which is found in this cell line. Abherrent cilia formation may also occur due to formation of multiple centrosomes as a result of polyploidy (Oberringer et al. 1999; Dutertre et al. 2005). As explained in 3.1.2, the mother centrosome is required for cilia development. However, HaCaT are still a commonly used keratinocyte cell line due to their ability to differentiate (Boukamp et al. 1988). Another benefit of their use in this study was that in co-culture experiments the keratinocyte cells needed to be grown

154

in the same medium as HCA2 fibroblasts. HaCaT keratinocytes and the HCA2 fibroblast cell line were both cultured in DMEM plus 10% FBS, whereas N/TERT1 keratinocytes require serum-free medium. Although use of HaCaT was not ideal, due to time constraints, medium requirements and N/TERT1 keratinocyte infections at the time of experimentation, it was the most viable option. In future it would be very useful to try repeating these experiments with primary (more likely to have cilia than cell lines) or N/TERT1 keratinocytes, if a practical method could be found which could utilise both N/TERT1 and HCA2 cell lines in a co-culture. Co-culture experiments using filter inserts allowed diffusion of growth factors between the HaCaT and HCA2, therefore paracrine interactions could occur.

3.5 Conclusion

Primary cilia can be induced on HaCaT keratinocytes; however SHH pathway activation should next be confirmed under these culture conditions (10 days stratification at the air: liquid interface) and increased by optimisation of conditions to achieve maximum primary cilia numbers. This would make an extremely useful model for BCC.

Chapter 4

Epidermal Growth Factor Signalling
in Basal Cell Carcinomas

4.1 Introduction

Epidermal growth factor (EGF) signalling is thought to augment SHH signalling in the epidermis thus promoting tumorigenesis and BCC development (see **Figure 1.13** for details of pathways involved). EGF receptors are expressed throughout the epidermis, with prominent expression on cells of the basal layer, the postulated origin of BCCs (Nanney, 1984). EGF is also required in addition to SHH for hair follicle development which can be disrupted by loss of either signalling pathway (Chiang et al., 1999; Murillas et al., 1995).

Organotypic culture models (*in vitro* studies) have shown that HaCaT cells over-expressing SHH have the ability to invade a collagen matrix and inhibition of EGF signalling blocks this cellular infiltration (Bigelow et al., 2005). Furthermore, while eight GLI1/EGF-regulated genes were found to have GLI binding sites in their promoter regions, making them direct GLI targets, they also required EGF signalling for activation. Also, treatment of GLI1 expressing N/TERT1 cells with Gefitinib (EGFR inhibitor) caused a reduction in activation of GLI/EGF target genes but not GLI target genes inferring EGFR could augment the SHH pathway under some conditions.

MEK/ERK activation was found to modulate SHH signalling when UO126 (MEK1/2 inhibitor) abolished the synergistic effect of increased activation of GLI/EGF target genes, and LY294002 (PI3K/AKT inhibitor) had no effect (Kasper et al., 2006). However, EGFR signalling has not been directly compared in different BCC subtypes, so it is possible that not all BCC subtypes express EGFR equally or respond to EGF signalling in the same way. Since EGF can affect GLI responsive genes and SHH can also affect EGF signalling, the relative activity of the two pathways could lead to differential responses and individual effects on cell growth patterns *in vivo* (Bigelow et al., 2005; Kasper et al., 2006; Neill et al., 2008). Although PI3K/AKT pathway activity does not appear to modulate SHH signalling *in vitro*, it is important for actin cytoskeleton function and may still be involved in BCC growth or invasion (Jimenez et al., 2000).

157

The self-activating transcription factor c-Jun is a target of MEKK1/JNK signalling. In BCC, c-Jun may also be activated by the MEK/ERK arm of the EGF pathway (inhibition of MEK/ERK signalling has been shown to reduce c-Jun expression) and both of these arms of the EGF pathway are activated by RAS (see **Figure 1.12** for details; Neill et al., 2008). c-Jun is required for up-regulation of a subset of GLI target genes and is also a direct GLI1/2 target. However, while c-Jun and GLI2A interact, GLI1 and c-Jun do not. Since c-Jun is activated by EGF, it may have an important role as one of the transcription factors involved in EGF augmentation of GLI transduced genes (Neill et al., 2008).

The different growth patterns of the BCC subtypes (superficial, nodular and morpheaform) may be explained by differences in signal transduction. PTCH mutations activate SHH signalling which drives BCC formation. However, as the level of SHH signalling may vary due to different PTCH mutations or due to the activity of other signalling pathways such as EGF, different phenotypes may result. The location of cells harbouring mutations (e.g. stem cells of the hair follicle bulge or epidermis) may also have an effect on SHH signalling. There may also be some influence from paracrine signalling in the epidermis or from SHH signalling produced by adjacent hair follicles in the anagen growth phase.

Superficial subtypes are currently treatable with a topical formulation of the drug imiquimod (Aldara^{TM}), so this study has concentrated on the more invasive BCC types, morpheaform and nodular. A topical formulation would be particularly useful for eradicating or shrinking large BCCs (prior to surgery), for treating BCCs in areas such as the eyelid where surgery is not advisable, or for treating areas where tumours recur. Also, effective topical treatment is preferable to surgery for multiple tumours at one or more sites.

Since it is possible that EGF signalling is involved in causing the invasive subtypes of BCC (nodular and morpheaform), it is important to identify which genes encoding EGF pathway components are expressed in these BCC subtypes.

This information can then be used to confirm whether PD98059 and LY294002 are useful in a topical formulation in addition to SHH inhibitors.

SHH and EGF signalling pathways were proposed as targets for inhibitors within a topical formulation because published studies show that the EGF pathway can augment SHH signalling and that EGF causes invasion of SHH expressing keratinocytes (Bigelow et al., 2005). Therefore, it seems plausible that one or more components of EGF signalling may cause more invasive BCC subtypes, making these particularly useful therapeutic targets.

4.1.1 Aims

- To confirm whether there are any signalling pathway differences between BCC subtypes that might cause variation in response to the proposed formulation containing SHH and EGF signalling inhibitors.

- To determine whether EGF signalling through MEK/ERK or PI3K/AKT is likely to be involved in the invasion of morpheaform and nodular BCCs.

4.2 Methods

4.2.1 Immunohistochemistry

Biopsies were collected from patients only after ethical approval was obtained from the South East Wales Local Research Ethics Committee. Patients were given a Patient Information Sheet and asked to sign a Consent form. BCCs were removed by curettage and rapidly frozen in liquid nitrogen within 15 minutes. In total, 21 samples of six different morphologies were analysed: 11 Nodular, 2 combined Nodular-Micronodular, 3 Micronodular, 1 Morpheaform, 3 combined Micronodular-Morpheaform and 1 combined Morpheaform-Nodular.

4.2.1.1 Haematoxylin & Eosin Staining

Human BCC skin sections were cut at 5-10μm on a cryostat, air dried onto superfrost slides (Fisher Scientific, Loughborough, UK) and stored at -80°C until required.

Slides were brought to room temperature (RT), fixed in dried acetone (Fisher Scientific, Loughborough, UK) for 15 minutes at RT and washed 3 times in PBS (Phosphate Buffered Saline) for 5 minutes each. Sections were immersed in Mayer's haematoxylin (Fisher Scientific, Loughborough, UK) for 5 minutes, washed in running water for 5 minutes and then immersed in 1% eosin for 1 minute. The sections were washed quickly in water, dehydrated in graded alcohols for 5 minutes each (70%, 90%, 100% and 100%) and immersed in three consecutive baths of xylene (Genta Medical, York, UK) for 5 minutes each. Sections were then mounted in DPX (di-n-butyl phthalate in xylene) (Fisher Scientific, Loughborough, UK) and sealed with a cover slip.

4.2.1.2 Immunohistochemistry (IHC)

Slides were brought to RT, fixed in dried acetone at RT for 15 minutes and washed 3 times in PBS for 5 minutes each. The sections were blocked for non-specific binding of secondary antibody in 5% of appropriate serum relative to the species

160

in which the primary antibody was raised (donkey, rabbit or goat) diluted in 5% BSA (bovine serum albumin) and PBS (Sigma-Aldrich Company Ltd, Gillingham, UK) for 1 hour in a humidified chamber. This was followed by three 5 minute washes in PBS, blocking with avidin and biotin for 15 minutes each with a 5 minute PBS wash between (Avidin Biotin Blocking Kit, Vector Labs, Peterborough, UK).

Sections were washed 3 times in PBS (5 minutes each), and antibodies diluted in PBS containing 5% BSA (see **Table 4.1**) were applied to the sections and incubated for 1 hour. The sections were washed 3 times in PBS (5 minutes each) and the appropriate biotinylated antibody (anti-rabbit or anti-mouse immunoglobulins; see **Table 4.1**) diluted 1:200 in PBS plus 5% BSA was applied for 30 minutes and then washed 3 times in PBS (5 minutes each).

Streptavidin-conjugated to horseradish peroxidise (GE Healthcare Life Sciences, Little Chalfont, UK) in PBS plus 5% BSA (1:100) was applied for 30 minutes, followed by washing 3 times in PBS (5 minutes each) and then 200μl DAB (3, 3'-diaminobenzidine from Sigma-Aldrich Company Ltd, Gillingham, UK) solution (0.5ml in 4.5ml PBS/BSA and 6μl H_2O_2) was applied for about 10 minutes (until sections were sufficiently stained).

This was followed by three 5 minute washes in PBS, submersion in Mayer's haematoxylin (counter stain) for 5 minutes (or light green for 1 minute when using the c-Jun antibody) and a 5 minute wash under running tap water. Sections were dehydrated by submersing slides in 70%, 90%, 100% and 100% alcohol baths for 5 minutes each, followed by submersing slides in three consecutive xylene baths for 5 minutes each (clearing) and mounting in DPX with a cover slip. To test for non-specific binding of the secondary antibody and streptavidin-HRP, negative control sections were run without primary antibody.

161

Table 4.1: Antibodies for Immunohistochemistry and Immunofluorescence.

Antigen	Cat Code	Company	Species	Dilute	Store (°C)
EGFR	1005 Sc-03	Santa Cruz Biotechnology Inc, CA, USA	Rabbit	1:50	4
EGFR-P	Sc-12351-R	Santa Cruz Biotechnology Inc, CA, USA	Rabbit	1:50	4
p-AKT	193H12	Cell Signalling Technology Inc, Danvers, MA, USA	Rabbit	1:200	-20
ERK	9102	Cell Signalling Technology Inc, Danvers, MA, USA	Rabbit	1:200	-20
p-ERK	9106S	Cell Signalling Technology Inc, Danvers, MA, USA	Mouse	1:200	-20
c-Jun	Sc-1694	Santa Cruz Biotechnology Inc, CA, USA	Rabbit	1:50	4
K14 (LL002)		Gift from Prof E.B. Lane, University of Dundee	Mouse	1:10	4
Vimentin	M0725	Dako UK Ltd, Cambridge House, Cambridge, UK	Mouse	1:100	4
Biotinylated Anti-Mouse IgG	RPN1001V	GE Healthcare UK Ltd, Buckingham, UK.	Sheep	1:200	4
Biotinylated Anti-Rabbit IgG	RPN1004V	GE Healthcare UK Ltd, Buckingham, UK.	Donkey	1:200	4
Alexafluor 488 (green) conjugated anti-mouse or anti-rabbit IgG	A21206	Invitrogen, Paisley, UK	Donkey	1:500	-20
Alexafluor 594 (red) conjugated anti-mouse or anti-rabbit IgG	A21203	Invitrogen, Paisley, UK	Donkey	1:500	-20

4.2.1.3 Immunofluorescence Microscopy

Double immunofluorescence uses two different coloured fluorochromes, which allows images to be overlaid to show co-localisation of two different proteins. The above protocol (4.2.1.2) was followed until the addition of a biotinylated secondary antibody.

This was replaced by the appropriate goat anti-mouse or anti-rabbit IgG conjugated to alexafluor 488 (green) or 594 (red). These were added to sections at a 1:500 dilution in PBS plus 5% BSA (Invitrogen, Paisley, UK) and incubated for 30 minutes. The slides were washed three times in PBS (5 minutes each) and 200μl DAPI (4', 6-diamidino-2-phenylindole; Roche Applied Science, Mannheim, Germany) was applied to each section (1:5000 in PBS plus 5% BSA) to label the nuclei blue. This was immediately tapped off onto tissue and the sections were mounted in hydromount (Fisher Scientific, Loughborough, UK) containing 2.5% DABCO (Sigma-Aldrich Company Ltd, Gillingham, UK) to prevent photo bleaching. Cover slips were placed gently on top and the slides were allowed to stand for 30-60 minutes on the bench. Sections were then viewed using a Zeiss microscope with fluorescence optics and digital images obtained using an Axiocam HRc Zeiss camera with Axiovision software on an IBM PC.

4.3 Results

4.3.1 BCC Tumour Morphology

BCC tumours fit into three broad categories based on their morphology. It is important to remember that even the most infiltrative BCC grows slowly and they rarely metastasize. Superficial tumours grow across the epidermis, nodular tumours grow in large islands which may penetrate into the dermis (micronodular tumours are made up of lots of smaller tumour islands) and morpheaform tumours grow with finger-like projections down into the dermis. Often a tumour is a mixture of more than one subtype. The majority (20) of BCC samples collected for this study were nodular combined with micronodular although four of these were morpheaform combined with nodular or micronodular but only one was completely morpheaform (**Table 4.2**).

Typical examples of different tumour morphologies represented in the BCC samples collected show how variable they were within each type of BCC (**Figure 4.1**). This variability demonstrates how different the tumour environments may be between different patient samples or even within each sample. Haematoxylin and eosin staining showed tumour islands as blue/purple areas within a pink dermis (nuclei stain blue). Morpheaform tumours (**Figure 4.1 a, b**) have thin finger-like projections consisting of thin strands only 2 or 3 cells thick infiltrating into the dermis and some pieces of tumour can appear isolated from the main tumour islands. Nodular tumours (**Figure 4.1 c-e**) have large tumour islands that appear to be separated with larger dermal areas, where the bulk of the tumour is much larger. Some nodular tumours have a very different appearance (e), with the bulk of the tumour being a large but more complex in shape. Micronodular tumours have lots of tiny tumour nodules (**Figure 4.1 f**).

Table 4.2: Basal Cell Carcinoma Specimen Subtypes. BCC morphology according to visual analysis of haematoxylin and eosin stained sections. Variation was found between tumour samples within the same subtype.

Sample	Subtype	Description
1	Nodular	Nodules of BCC with several tumour islands.
2	Nodular	Two large nodular BCC tumour islands.
3	Morpheaform	Tumour strands (only 2 cells thick) weaving through dermis.
4	Nodular	Nodules of BCC with several tumour islands with epidermis present.
5	Nodular	Tumour nodules interlaced with stroma and epidermis present.
6	Nodular	Large tumour islands with little epidermis.
7	Nodular	One large tumour nodule.
8	Nodular	Small tumour islands.
9	Micronodular/ Morpheaform	Thick strands of tumour through the dermis with smaller tumour islands at the infiltrative edge.
10	Nodular/ Micronodular	Large nodular tumour islands with infiltrating regions of small tumour nodules.
11	Micronodular/ Morpheaform	Small tumour with some infiltrative regions.
12	Nodular	Large nodule with epidermis present.
13	Micronodular/ Morpheaform	Many small nodular tumour islands, some with lacy infiltrative appearance and the epidermis intact.
14	Micronodular	Many small tumour islands with some epidermis present.
15	Nodular/ Micronodular	Large nodular tumour island with small infiltrative islands at edge and little epidermis.
16	Micronodular	Many small nodular tumour islands with little epidermis.
17	Nodular	Large tumour islands.
18	Nodular	Small very separate tumour islands within the dermis.
19	Nodular	Both large and very small tumour islands with the epidermis present.
20	Micronodular	Many small nodular tumour islands with the epidermis present.
21	Morpheaform/ Nodular	Large tumour islands with very infiltrative edges.
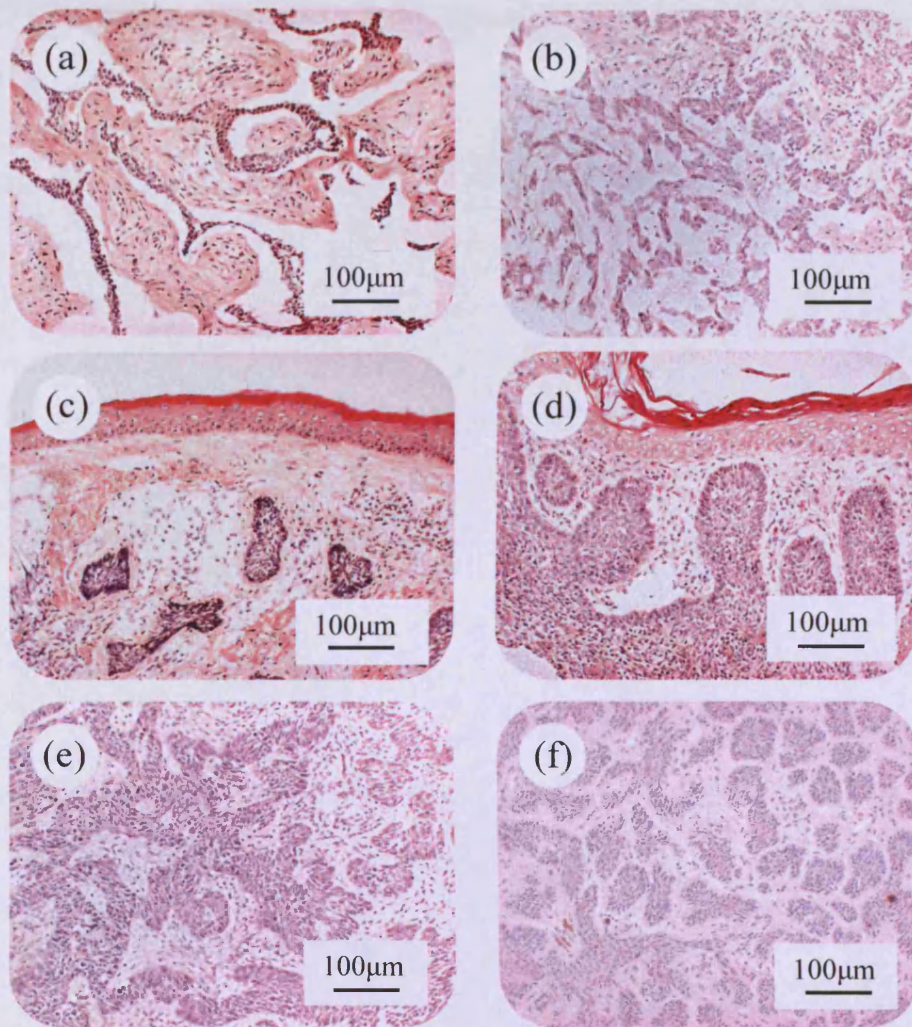
Figure 4.1: Haematoxylin and Eosin Stained BCC Tumour Sections showing the Range of Morphologies in this Study. Two were morpheaform: tumours #3 (a) and #9 (b). Three were nodular but had very different histology: tumour #8 had widely spaced tumour islands (c), #6 had large tumour islands (d) and #9 had large tumour islands which were 'infiltrative' (e). The other was micronodular with many closely spaced tumour islands, #20 (f). Scale bars (100μm) shown for each section.

4.3.2 EGF Pathway Components in Normal Human Skin

The expression and phosphorylation of proteins in the EGF signalling pathway have been examined in normal skin using antibodies to detect EGFR and three phosphorylated proteins (p-EGFR, p-ERK and p-AKT). Particular emphasis was placed on examining levels in the epidermis, sebaceous gland and hair follicle.

The EGFR antibody stained all the cells of the epidermis from the lower basal cells to the granular layer (**Figure 4.2a**). Staining was particularly intense in the periphery of some cells indicating an association with the plasma membrane. The use of a phospho-specific antibody to detect p-EGFR showed that not all of the EGFR present in the epidermis was phosphorylated (**Figure 4.2c**). Staining with the p-ERK antibody showed that phosphorylation of ERK occurred mainly in the upper layers of the epidermis with intense peripheral staining of granular cells (**Figure 4.2e**). Finally, the p-AKT antibody stained cells only in the lower epidermis (basal and immediate suprabasal cells) again with greater intensity at the cell periphery (**Figure 4.2g**).

The sebaceous gland was also examined in the sections stained with antibodies to EGFR, p-EGFR, p-ERK and p-AKT. The periphery of the individual sebocytes and the whole duct epithelium was stained with the EGFR antibody (**Figure 4.2b**). However, as with the epidermis, not all of the EGFR present was phosphorylated (**Figure 4.2d**). The staining with p-ERK (**Figure 4.2f**) was very similar to that with EGFR but p-AKT differed. This antibody stained the epithelial basal cells of the sebaceous duct and the epithelium between the sebocytes in the sebaceous gland (**Figure 4.2h**). The individual sebocytes remained unstained.

4.3.3 Immunoperoxidase Detection of EGFR in BCC Samples

Immunolocalisation of EGFR was variable in the group of BCC biopsy specimens examined (**Figure 4.3**).
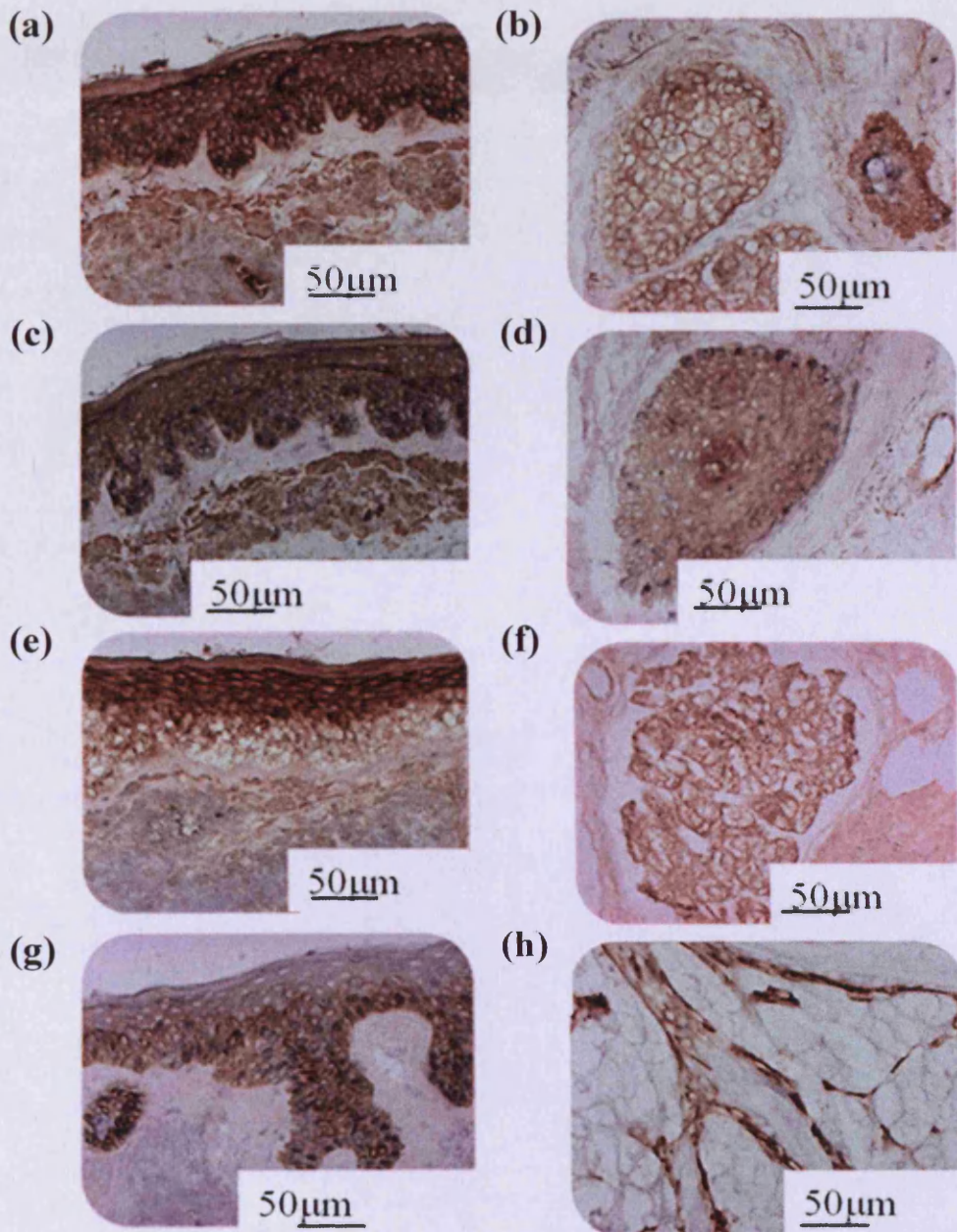
Figure 4.2: Immunoreactivity of EGF Pathway Components on Sections of Normal Human Skin. *EGFR (a, b) and p-EGFR (c, d) staining was positive throughout the cytoplasm of epidermal cells (a, c) and cells of the sebaceous gland (b, d). p-ERK staining (e, f) was cytoplasmic in the upper epidermal cell layers and throughout the sebaceous gland. p-AKT staining (g, h) was positive at the cell membrane in the basal layer and in some suprabasal cell layers, as well as in cells of the sebaceous gland and duct. Scale bars (50μm) shown for each section.*

In general, tumours showed cytoplasmic and/or membrane positive immunoreactivity throughout tumour islands or in patches within the islands. Cytoplasmic localisation of EGFR suggests activation by EGF ligand leading to transcription in the cell nucleus. Membranous localisation suggests no activation of EGFR. It is therefore likely that p-EGFR would be present if EGFR is located in the cytoplasm. In these experiments localisation was judged by visual appearance, with expression being judged as membranous if the margins of the cells were stained brown with the centre lighter in colour and cytoplasmic if the cell itself was stained brown.

EGFR staining in one nodular tumour (**Figure 4.3a**) showed a very strong cytoplasmic reaction throughout all tumour islands. A micronodular tumour (**Figure 4.3b**) also showed strong immunoreactivity which appears to be at the cell periphery in all tumour islands. However, one nodular tumour (**Figure 4.3c**) had patchy positive immunoreactivity in the cytoplasm of one large tumour island and another nodular tumour (**Figure 4.3d**) was positive for EGFR in the cytoplasm of one tumour island but was negative in the others. This shows a lack of correlation between EGFR location and the nodular subtype, although all these nodular tumours did vary histologically.
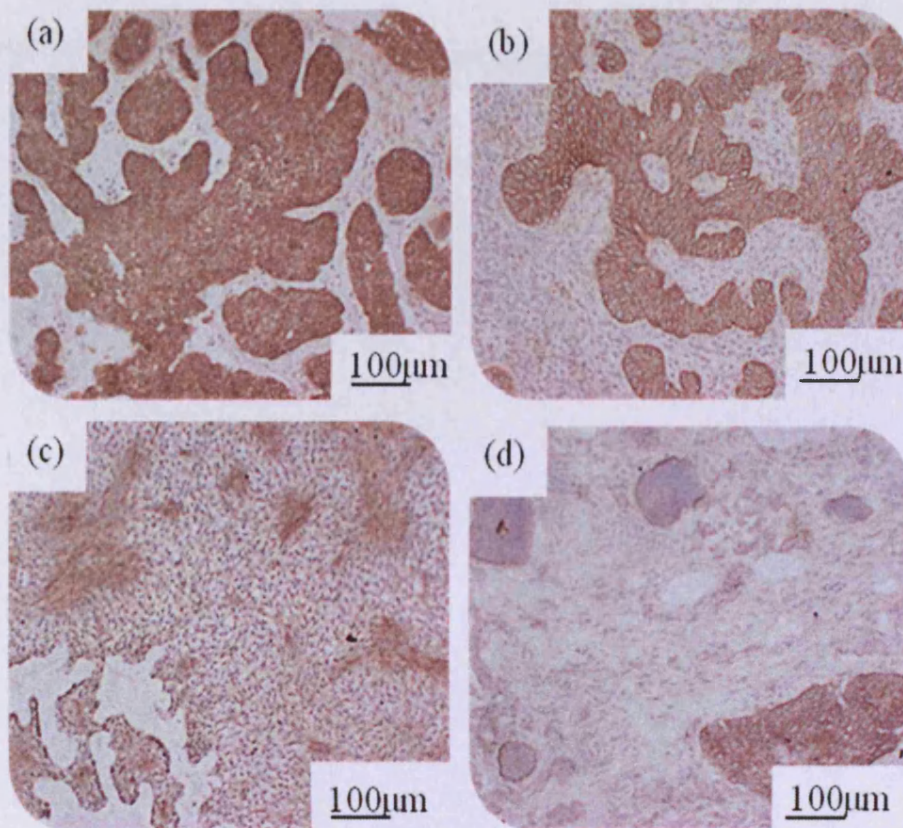
Figure 4.3: Immunohistochemistry of EGFR in Human BCC Samples from Four Different Patients. Nodular tumour #4 (a) with cytoplasmic EGFR expression throughout all tumour islands, Micronodular tumour #9 (b) with EGFR immunoreactivity throughout the tumour islands, Large nodular tumour #6 (c) showing patchy positive cytoplasmic immunoreactivity for EGFR and Nodular BCC #18 (d) showing EGFR immunoreactivity in one tumour island but not the others.

4.3.4 Immunoperoxidase Detection of p-EGFR in BCC Samples

Two different tumour samples were examined (#5 and #6). EGFR immunoreactivity was positive in the lower epidermis and was patchy in the tumour islands (**Figure 4.4a, c**). In general cells with a basal phenotype were stained. EGFR is autophosphorylated to p-EGFR when activated by its ligand and

this can be detected using a phospho-specific antibody. The same two tumour samples (#5 and #6) were examined for the presence of p-EGFR but immunoreactivity was very low and could be considered negative (**Figure 4.4b, d**).
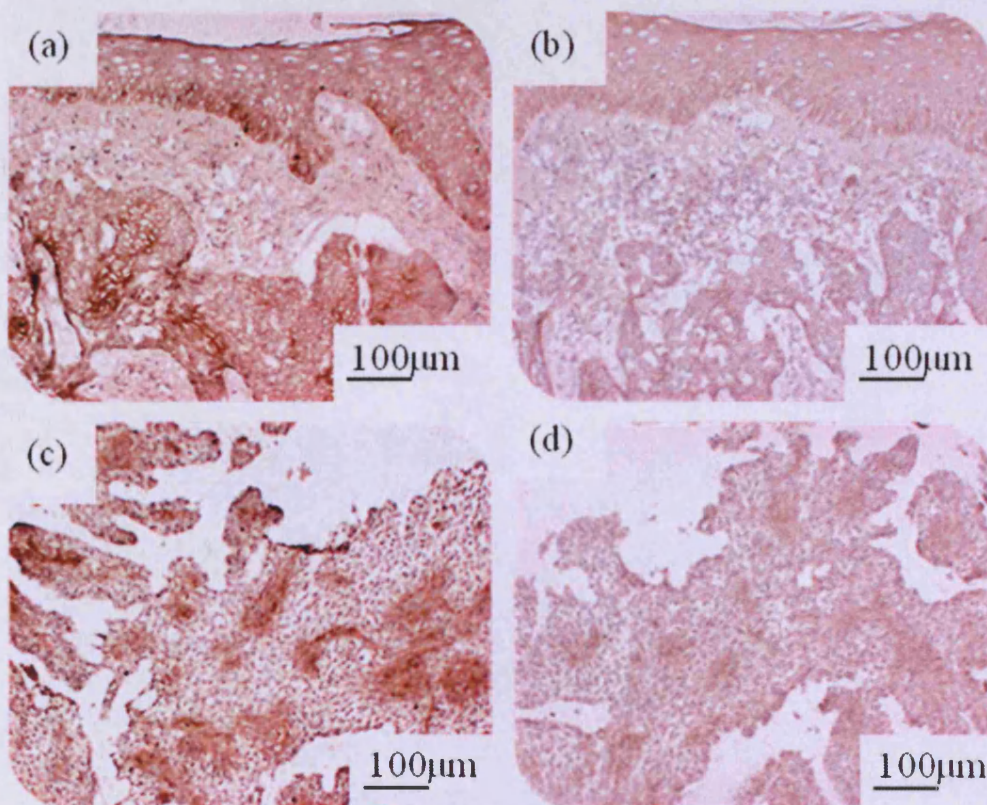
Figure 4.4: Immunohistochemistry (EGFR and p-EGFR) on two Human BCC Samples. Variable EGFR expression and little or no p-EGFR expression were observed in both samples. Tumour #5 showed patchy cytoplasmic expression of EGFR (a) but no staining was observed with p-EGFR (b). Tumour #5 was similar (c, d).Scale bars are shown for each sample (100μm).

EGFR immunoreactivity was variable in the 21 tumours examined and was considered to be low in 4, moderate in 11 and high in 6 (**Table 4.3**). There was also little correlation between the level of immunoreactivity and tumour subtype and the localisation was also variable with the majority (14 tumours) showing cytoplasmic staining, a few (4 tumours) showing membrane staining and the others (3 tumours) being stained at both locations.

Immunoreactivity to p-EGFR was cytoplasmic and only observed in 8 out of 21 tumour samples (low in 7 and moderate in 1). The 8 positive tumours were of all subtypes so there was no correlation between EGFR phosphorylation and subtype. The 6 tumours that showed high EGFR expression (**Table 4.3**) were either negative for p-EGFR (5) or only had very low levels of staining (1). This would be expected to lead to little or no activation of downstream pathways leading to reduced phosphorylation of ERK and/or AKT and therefore little c-Jun translocation to the nucleus in BCCs.

Table 4.3: EGFR and p-EGFR Immunoreactivity in BCC Tumour Samples. EGFR immunoreactivity is variable and unrelated to phenotype and p-EGFR immunoreactivity in BCC tumour samples is low or absent (* = low, ** = moderate and *** = high).

Sample	Subtype	EGFR		p-EGFR	
		Tissue level	Subcellular localisation	Tissue level	Subcellular localisation
1	Nodular	**	Cytoplasm	None	N/A
2	Nodular	**	Cytoplasm	*	Cytoplasm
3	Morpheaform	**	Cytoplasm	*	Cytoplasm
4	Nodular	***	Membrane	None	N/A
5	Nodular	**	Cytoplasm	None	N/A
6	Nodular	*	Cytoplasm	*	Cytoplasm
7	Nodular	**	Membrane	None	N/A
8	Nodular	**	Membrane	None	N/A
9	Micronodular/ Morpheaform	***	Membrane	None	N/A
10	Nodular/ Micronodular	*	Cytoplasm	None	N/A
11	Micronodular/ Morpheaform	**	Cytoplasm	*	Cytoplasm/ Nuclei
12	Nodular	**	Cytoplasm	*	Cytoplasm
13	Micronodular/ Morpheaform	***	Cytoplasm	*	Cytoplasm
14	Micronodular	***	Membrane/ Cytoplasm	None	N/A
15	Nodular/ Micronodular	**	Cytoplasm	None	N/A
16	Micronodular	**	Membrane/ Cytoplasm	None	N/A
17	Nodular	***	Cytoplasm	None	N/A
18	Nodular	***	Membrane/ Cytoplasm	None	N/A
19	Nodular	*	Cytoplasm	**	Cytoplasm
20	Micronodular	*	Cytoplasm	*	Cytoplasm
21	Morpheaform/ Nodular	**	Cytoplasm	None	N/A

4.3.5 Immunoperoxidase Detection of ERK and p-ERK in BCC

There was variable positive cytoplasmic ERK immunoreactivity in the tumour specimens examined, being weak in most tumours, patchy in some and positive throughout the tumour islands in others. ERK levels in micronodular tumours were

weak and patchy (**Figure 4.5a, b**) but in nodular tumours, ERK levels were more variable and ranged from high (**Figure 4.5c**) to little expression (**Figure 4.5d**).
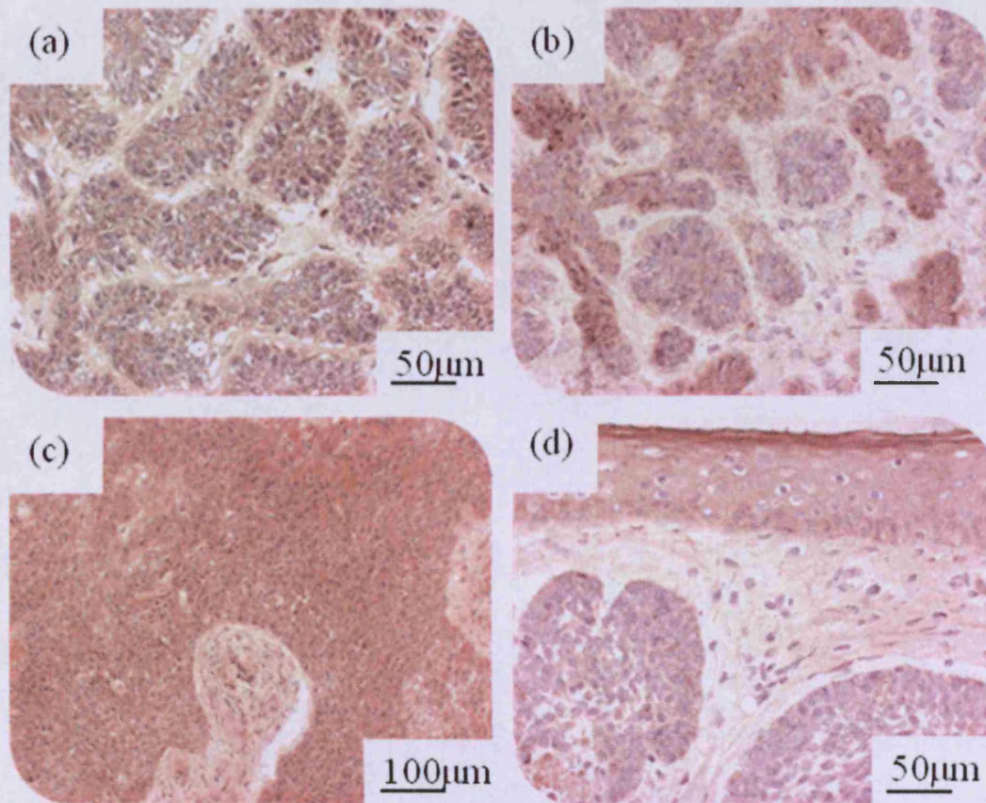
Figure 4.5: Immunohistochemistry of ERK in Human BCC Samples. ERK levels in BCC tumours were variable. Low levels of cytoplasmic ERK were found in micronodular tumours #16 (a) and #20 (b), high levels of expression in nodular tumour #17 (c) while nodular tumour #19 was negative (d).

Considering all 21 BCC tumour samples (**Table 4.4**), moderate ERK expression was localised to the cytoplasm and nuclei of 2 nodular tumours while low levels were found in the cytoplasm of 9 tumours (nodular, morpheaform, micronodular/morpheaform, micronodular) and ERK was absent in the other 10 tumours (nodular, micronodular, nodular/micronodular and micronodular/morpheaform). In some tumours, nuclear staining was also noted in addition to cytoplasmic staining. Thus, there was little correlation between tumour morphology and the level and localisation of ERK expression.

174

Table 4.4: Tumour Sample Morphology and Immunoreactivity (ERK and p-ERK) in Human BCC Samples. *Immunohistochemistry showed variable levels of ERK (* = low expression, ** = moderate expression). No samples were positive with the p-ERK antibody.*

Sample	BCC Subtype	ERK Tissue Level	ERK Subcellular Localisation	p-ERK Tissue Level	p-ERK Subcellular Localisation
1	Nodular	*	Cytoplasm/ Nuclei	None	N/A
2	Nodular	**	Cytoplasm	None	N/A
3	Morpheaform	*	Cytoplasm/ Nuclei	None	N/A
4	Nodular	**	Cytoplasm/ Nuclei	None	N/A
5	Nodular	None	N/A	None	N/A
6	Nodular	None	N/A	None	N/A
7	Nodular	*	Cytoplasm	None	N/A
8	Nodular	*	Cytoplasm	None	N/A
9	Micronodular/ Morpheaform	*	Cytoplasm	None	N/A
10	Nodular/ Micronodular	None	N/A	None	N/A
11	Micronodular/ Morpheaform	None	N/A	None	N/A
12	Nodular	None	N/A	None	N/A
13	Micronodular/ Morpheaform	None	N/A	None	N/A
14	Micronodular	None	N/A	None	N/A
15	Nodular/ Micronodular	None	N/A	None	N/A
16	Micronodular	*	Cytoplasm	None	N/A
17	Nodular	*	Cytoplasm/ Nuclei	None	N/A
18	Nodular	*	Cytoplasm/ Nuclei	None	N/A
19	Nodular	None	N/A	None	N/A
20	Micronodular	*	Cytoplasm	None	N/A
21	Morpheaform/ Nodular	None	N/A	None	N/A

No positive immunoreactivity was obtained using an antibody specific for the phosphorylated form of ERK (p-ERK) inferring that ERK activation was not apparent in any of these BCC samples (**Table 4.4**).

ERK cannot be activated by phosphorylation unless EGFR is phosphorylated leading to a series of protein activations downstream of the receptor, so p-ERK would not be expected in tumours that were p-EGFR negative. However, this does not explain the absence of p-ERK in p-EGFR positive tumours. Some samples showed patchy positive expression of both EGFR and ERK, and as ERK is downstream of EGFR, it might be expected that similar patterns of expression and location were observed in each sample. However, this did not seem to be the case because high EGFR expressing samples (4, 9, 17 and 18) showed low to moderate ERK expression and sample 13 showed no ERK expression at all. Also, no correlation by location was observed in sequential sections of tumour sample.

Thus, ERK was expressed at low level and was not activated by phosphorylation in the BCC samples examined. This infers that the MEK/ERK arm of the EGF pathway is unlikely to be involved in modulation of the SHH pathway at this stage of tumour growth or in promotion of an infiltrative phenotype.

4.3.6 Immunoperoxidase Detection of p-AKT in BCC Samples

Moderate p-AKT levels were observed in spindle shaped cells of nodular tumour #1, with staining of both the cytoplasm and plasma membrane (**Figure 4.6a**). Clusters of p-AKT positive cells were found in micronodular tumour #2 (**Figure 4.6b**) and another nodular tumour (#8) also showed small clusters of p-AKT positive cells (**Figure 4.6c**). Finally, a small epidermal down-growth above nodular tumour #19 also contained a cluster of p-AKT positive cells (**Figure 4.6d**).

Positive staining for p-AKT was found in 14 tumour samples (3 had moderate levels) while the other 7 tumour samples had no p-AKT immunoreactivity (**Table 4.5**). Generally, staining was cytoplasmic and localised at the centre and infiltrating edges of tumour islands.
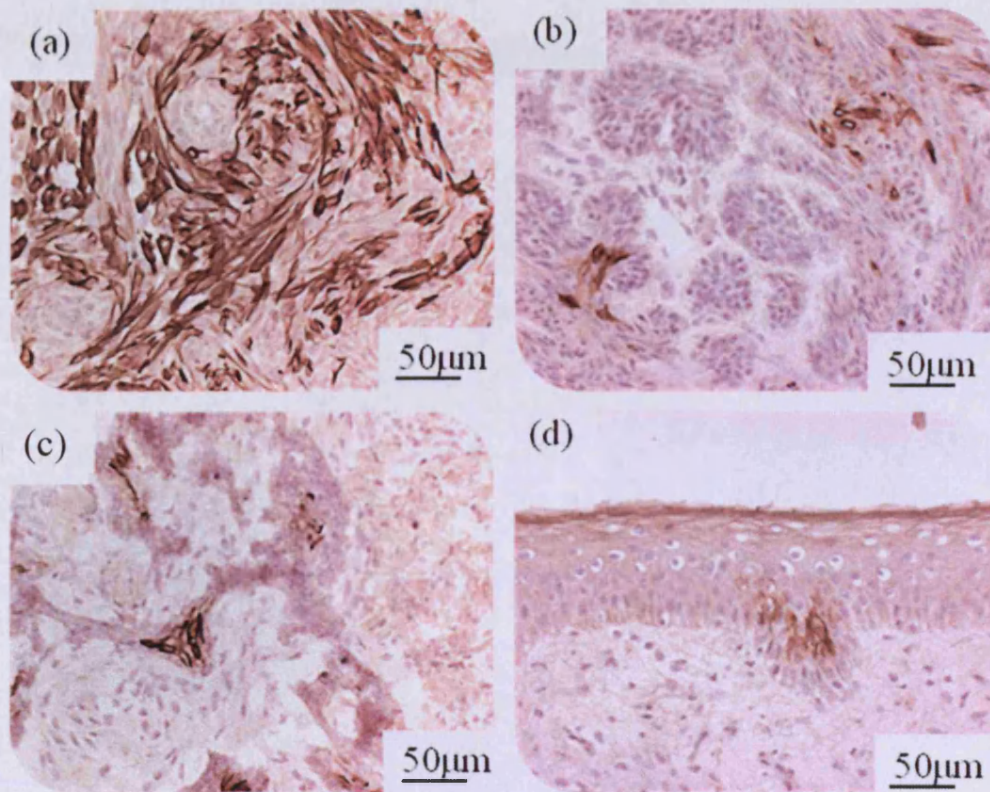
Figure 4.6: Immunohistochemistry of Human BCC Samples with p-AKT. *(a) nodular tumour #1 showed extensive strong p-AKT staining of spindle shaped cells. Smaller numbers of similar cells were positive in micronodular tumour #20 (b) and nodular tumour #8 (c). p-AKT positive cells were also observed in an epidermal down-growth above nodular tumour #19 (d).*

Again, there appeared to be very little correlation between p-AKT staining and tumour morphology. The morphology of the three samples that showed moderate levels of p-AKT all differed (nodular, nodular/morpheaform and micronodular/morpheaform). Tissue localisation in these moderately expressing samples did correlate to subtype, with micronodular and morpheaform being the most infiltrative or aggressive. No samples had high levels of p-AKT (**Table 4.5**).

Table 4.5: Levels and Sub-cellular Localisation of p-AKT in Human BCC Specimens.
Immunohistochemistry of p-AKT in all 21 BCC samples showed that moderate staining (**) was present in 3 specimens, low levels (*) in 11 specimens and no staining (None) in 7 samples. Where p-AKT was positive, only cytoplasmic staining was observed.

Sample	Subtype	p-AKT Tissue Level	p-AKT Subcellular Localisation
1	Nodular	**	Cytoplasm
2	Nodular	*	Cytoplasm
3	Morpheaform	None	N/A
4	Nodular	*	Cytoplasm
5	Nodular	*	Cytoplasm
6	Nodular	*	Cytoplasm
7	Nodular	None	N/A
8	Nodular/Morpheaform	**	Cytoplasm
9	Micronodular/Morpheaform	None	N/A
10	Nodular/Micronodular	*	Cytoplasm
11	Micronodular/Morpheaform	None	N/A
12	Nodular	None	N/A
13	Micronodular/Morpheaform	**	Cytoplasm
14	Micronodular	*	Cytoplasm
15	Nodular/Micronodular	*	Cytoplasm
16	Micronodular	*	Cytoplasm
17	Nodular	*	Cytoplasm
18	Nodular	None	N/A
19	Nodular	None	N/A
20	Micronodular	*	Cytoplasm
21	Morpheaform/nodular	*	Cytoplasm

If p-AKT positive cells were involved in infiltration and invasion, it would be expected that they would be located at the tumour margins. However, this pattern was not observed in the samples studied and p-AKT reactivity was found both at the margins and in the centre of tumour islands. This p-AKT immunoreactivity is unlikely to be due to a lack of antibody specificity, as western blotting analysis showed reactivity with a single protein band of the correct size (data not shown).

Interestingly, all cells positive for p-AKT were spindle shaped, more reminiscent of fibroblasts than keratinocytes. Tumour cells are known to undergo epithelial-

mesenchymal transition (EMT) and such altered cells grow more aggressively causing increased tumour down-growth into the dermis and subcutaneous tissues (Larue and Bellacosa, 2005). However, there was only one BCC with morpheaform characteristics (the most aggressive BCC subtype) in this study and this was only moderately positive.

4.3.7 Double Immunofluorescence Detection of p-AKT and Keratin (K14) or Vimentin

In order to ascertain whether the spindle shaped p-AKT expressing cells were due to EMT, the sections were treated with an antibody to vimentin (intermediate filament protein present in fibroblasts but not keratinocytes). Double immunofluorescence with the antibody to p-AKT would ascertain whether p-AKT positive tumour cells had converted to a fibroblast phenotype. In addition, a K14 antibody was used to identify keratinocyte characteristics that should be found throughout the tumour islands as these cells are of epidermal origin. However, if the p-AKT expressing cells had undergone EMT, they would express little or no K14 and should be vimentin positive. Tumour cells in the process of EMT might express both the fibroblast marker vimentin and the epidermal cell marker K14.

Staining sections of a nodular BCC tumour with both a K14 antibody (red fluorescent tag) and an p-AKT antibody (green fluorescent tag) showed that all cells expressed K14 in their cytoplasm but only a limited number of spindle shaped cells contained p-AKT (Figure 4.7a). However, it remains unclear as to whether the spindle cells express K14 or not. Staining a similar section with a vimentin antibody (red fluorescent tag) gave only background red fluorescence and the spindle cells again were stained bright green showing the presence of p-AKT (Figure 4.7b). A higher power view of the tumour stained with both p-AKT (green) and vimentin (red) showed that these two proteins appear to be mutually exclusive in terms of expression with the spindle shaped cells being p-AKT +ve

179

and vimentin –ve while the other cells in the section were p-AKT –ve and vimentin +ve (**Figure 4.7d**).
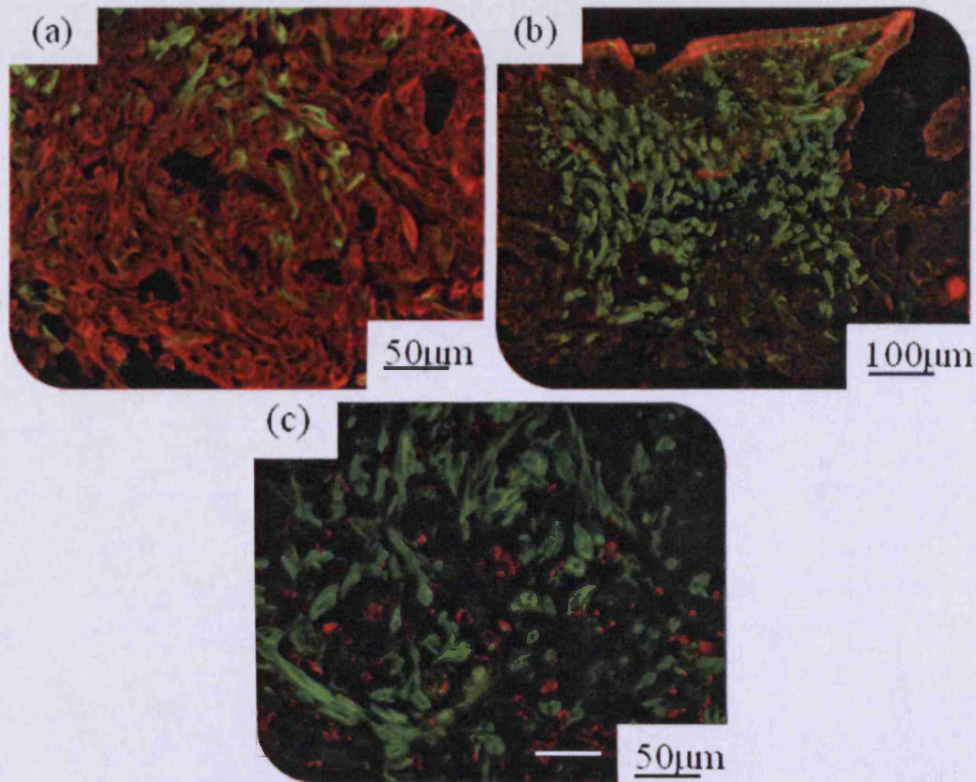
Figure 4.7: Double Immunofluorescence of p-AKT and an Epidermal Cell Marker (K14) or a Fibroblast Cell Marker (Vimentin) in Nodular Human BCC Sample (#15). Nodular BCC tumour islands (a, b, c) were stained with antibody to p-AKT (a-d) with a green fluorescent tag and either an antibody to K14 (a,) or an antibody to vimentin (b, c) with a red fluorescent tag. Combined images of both red and green fluorescence are shown with yellow indicating the presence of both antigens. Scale bars are indicated on each section.

4.3.8 Immunoperoxidase Detection of c-Jun in BCC Samples

Immunoreactivity for c-Jun was strongly positive and localised to the nucleus in virtually all tumour islands in all BCCs (**Figure 4.8**). Expression of c-Jun was

similar in tumours of different morphology (nodular, nodular/micronodular and morpheaform).

The transcription factor complex AP-1 is composed of c-Jun and c-Fos and nuclear localisation suggests that the AP-1 complex is active in the BCC samples examined.
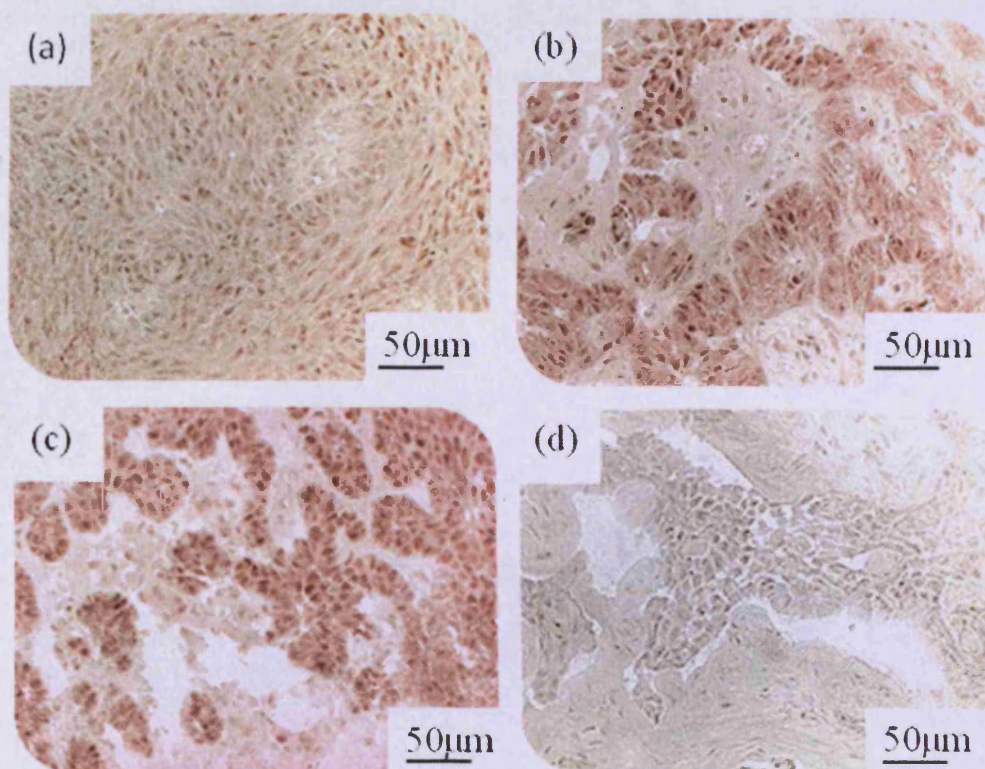
Figure 4.8: Immunohistochemistry Detection of c-Jun in Sections of Human BCC.
Immunoreactivity of c-Jun (with light green counter stain) showed strong nuclear
expression in most samples: nodular tumour #1 (a), micronodular/morpheaform tumour
#9 (b) and micronodular tumour #14 (c), but expression was low in some such as the
morpheaform tumour #3 (3).

All 21 tumour samples in this study expressed nuclear c-Jun and levels were high in 15 tumours and moderate in 6. There appeared little relationship between the level of c-Jun and tumour morphology (**Table 4.6**).

The AP-1 transcription complex is targeted by EGF signalling and interaction between c-Jun and GLI2 may lead to augmentation of SHH signalling. Augmentation was originally thought to occur via the MEK/ERK arm of the EGF pathway but the patchy expression of EGFR, p-EGFR, ERK and p-ERK found in this study suggests that the MEK/ERK pathway did not activate c-jun. Localisation of p-AKT to a few randomly spread tumour cells also suggests that activation of the PI3K/AKT arm of the EGF pathway cannot explain why all tumour cells are positive for c-jun. Thus, it seems likely that there is a different mechanism of activation in these tumours.

Table 4.6: Morphology, c-Jun Expression and Subcellular Localisation in Human BCC Specimens. *Immunoreactivity with the c-Jun antibody was found in the nuclei of all tumour island cells at a moderate (**) or high (***) level. Again there appeared little correlation between levels of c-Jun and tumour morphology.*

Sample	Subtype	c-Jun Expression Level	c-Jun Subcellular localisation
1	Nodular	***	Nuclear
2	Nodular	**	Nuclear
3	Morpheaform	**	Nuclear
4	Nodular	***	Nuclear
5	Nodular	**	Nuclear
6	Nodular	**	Nuclear
7	Nodular	***	Nuclear
8	Nodular	***	Nuclear
9	Micronodular/Morpheaform	***	Nuclear
10	Nodular/Micronodular	***	Nuclear
11	Micronodular/Morpheaform	***	Nuclear
12	Nodular	**	Nuclear
13	Micronodular/Morpheaform	***	Nuclear
14	Micronodular	***	Nuclear
15	Nodular/Micronodular	***	Nuclear
16	Micronodular	***	Nuclear
17	Nodular	***	Nuclear
18	Nodular	**	Nuclear
19	Nodular	***	Nuclear
20	Micronodular	***	Nuclear
21	Morpheaform/Nodular	***	Nuclear

4.5 Discussion

Signalling pathway differences between BCC subtypes were considered by comparison of a variety of nodular and morpheaform BCC samples.

Immunoreactivity for EGF signalling components EGFR, p-EGFR, p-ERK and p-AKT was confined to the dermis and to structures such as the sebaceous gland. In BCCs they would be expected to be found within tumour islands and particularly at the tumour island margins of the most aggressive phenotypes (nodular and morpheaform) if they were to be involved in augmenting SHH signalling causing a more aggressive phenotype as hypothesised.

Immunohistochemistry has shown a lack of EGFR auto-phosphorylation, which has led to reduced levels of ERK and AKT phosphorylation (in fact no p-ERK was found in any of the 21 samples) compared to levels expected in normal human skin.

EGFR was absent from BCCs in a study which used paraffin sections (Neill et al., 2008), but another group who also used frozen sections (better for maintaining antibody epitopes) found EGFR immunoreactivity in BCCs agreeing with the findings in this chapter (Rittie et al., 2007). Immunolocalisation of EGFR in this study was highly variable but neither location nor amount was linked to BCC subtypes of nodular, morpheaform or micronodular (**Table 4.2**). The different immunolocalisation of this protein between BCCs (membraneous or cytoplasmic) may be explained by internalisation and degradation of the protein caused by ligand binding. However, the lack of phosphorylation (only phosphorylation in 8 out of 21 tumours) suggests that this is not true and high EGFR levels also did not equate to phosphorylation. Lack of phosphorylation of this receptor in these samples meant that downstream signalling would not be activated by this pathway. Downstream proteins ERK and AKT may have been activated by a separate signalling pathway, which is quite possible as EGF-independent AKT activation

by p38MAPK (which was activated in the absence of EGFR by Her2) has been found previously in HER2 expressing human mammary epithelial cells (Diehl et al., 2006). In support of this hypothesis, Her2 expression was shown in 14 out of 16 BCCs using RT-PCR (Krahn et al., 2001).

EGFR was commonly expressed in the tumour samples used for this study, but downstream signalling component ERK was expressed only at low levels and in few tumours with variable localisation, whereas phosphorylation of ERK was absent in all of the samples. The low levels of ERK in BCCs in this study are continuous with previous observations using immunohistochemistry by Neil and co-workers. (Neil et al., 2008). This group also found a lack of p-ERK except in one sample where they found p-ERK localised to infiltrating cells, suggesting that phosphorylation of ERK may be involved in causing tumours to be more invasive. However, because this result was not repeated in any of the 21 samples analysed in this study, which were all nodular or morpheaform subtypes (the most invasive BCC subtypes) it seems unlikely that ERK phosphorylation would be involved in causing an invasive BCC phenotype. This is also at odds with the previously published observation that MEK1/2 inhibitor UO126 abolished the synergistic effect of increased activation of GLI/EGF target genes (Kasper et al., 2006). Activated ERK (p-ERK) is a target of MEK and thus MEK/ERK signalling is unlikely to promote an infiltrative BCC phenotype by modulation of the SHH signalling.

In order to confirm or deny Neill and colleagues interpretation of p-ERK expression in one tumour being the cause of an aggressive phenotype, this study would require extending to a larger sample number for immunohistochemistry with the p-ERK antibody to further compare the characteristics of the most and least aggressive BCCs. The same is true to confirm whether sub-cellular localisation of EGFR correlates to tumour subtype.

Reduced p-ERK and p-AKT in tumour islands and the overlying epidermis compared to normal human skin was found in BCCs but not in squamous cell carcinomas by immunohistochemistry (Rittié et al., 2007). However, p-AKT levels were not affected by GLI expression in HaCaT cell experiments suggesting that this branch of the EGF pathway is not affected by SHH signalling (Schnidar et al., 2009). The effects seen in tumour samples may be due to a paracrine effect or extracellular matrix interactions in BCCs which were not present in cultures of keratinocytes alone.

The spindle cell morphology of the few p-AKT positive cells shown by immunohistochemistry in two thirds of the samples in this study was particularly interesting because this morphology is associated with EMT. However, they were localised in the centre of tumour islands as well as the margins and in tumours of different morphologies, which does not correlate with an infiltrative phenotype, which EMT is associated with. In EMT there is a loss of cell to cell adhesions because AKT represses E-cadherin (cell junction protein), a loss of E-cadherin leads to epithelial-mesenchymal transition. In that situation, cell-cell adhesion is reduced and so the mesenchymal cells are more invasive, thus metastases are more likely to occur (Julien et al., 2007). However, EMT rarely occurs in BCCs, possibly explaining why there was little positive immunoreactivity for AKT in BCC tumour specimens. If the cells positive for AKT are indicators of EMT in the tumour specimens used for this study, then the low number of affected cells would correlate with the slow growth and poor invasive properties of BCCs. If this is the case, superficial BCC, the least aggressive subtype would likely express no p-AKT. However, immunofluorescence showed a lack of co-localisation of p-AKT with a fibroblast marker vimentin thus indicating that the p-AKT positive cells have not undergone EMT. Supporting this observation, it was shown that GLI1 repressed induction of the EMT marker vimentin in EGF-stimulated cells, making EMT unlikely in BCCs (Neill et al., 2008). The same group found that EGF/GLI expressing keratinocytes demonstrated an elongated morphology. Live cell-imaging confirmed that the cells could not detach or retract efficiently giving them

185

a stretched appearance (Neill et al., 2008). Again, a larger BCC sample number with a good variety of tumour invasiveness would be useful to repeat this immunohistochemistry in order to determine whether the more invasive or metastatic tumours have higher positive immunoreactivity for AKT and to find out why this would be related to a more aggressive phenotype.

The appearance of p-AKT immunoreactivity in cytoskeletal regions suggests that p-AKT may have migratory or a contraction function because it may be located on the stress fibres. In order to confirm or disprove the theory that p-AKT may be associated with EMT in BCC, double immunofluorescence with E-cadherin and p-AKT antibodies would be useful to confirm whether p-AKT positive cells express E-cadherin. If they do not express E-cadherin it is likely that they have undergone EMT. Unfortunately as yet we have not found a good E-cadherin antibody which is not the same species as the p-AKT antibody used in this study.

Previous publications have shown PI3K/AKT signalling enhanced remodelling of the actin cytoskeleton (Scita et al., 2000). It has also been shown that PI3K has multiple roles, including the strengthening of cell-cell adhesions; and in addition, p-AKT may indeed be involved in cell migration, as it has been shown to mediate lamellipodium formation (Cain and Ridley, 2009; Wennstrom et al., 1994). One report found evidence of p-AKT and β-actin co-localisation in neural growth cones (Zhou et al., 2004). PI3K signalling is required for axon growth, where it is activated at the leading edge of migrating neuronal cells. A PI3K regulatory subunit is involved in the control of actin organisation and cell migration. However, co-localisation with cytoskeletal filaments is not normally seen (Cain and Ridley, 2009; Jimenez et al., 2000). Together, the results of this study and these publications suggest that within those strangely spindle shaped cells there is p-AKT and β-actin co-localisation which may enable tumour cell migration deeper into the dermis or possibly even in the few moderately expressing tumours (3 out of 21 BCCs), leading to the rare event in BCC of metastasis. It is unlikely that the p-AKT antibody did in fact cross-react with a keratin or another protein because

186

this antibody has been used successfully for western blotting producing a single band of the correct molecular weight. For future work immunofluorescence could be used to label BCC biopsies with both actin and p-AKT to confirm that they are co-localised.

C-Jun was strongly expressed in all BCC nuclei in all tumour samples which supports previously published findings where immunohistochemistry and qPCR also showed c-Jun expression throughout tumour islands but not in the stroma (Laner-Plamberger, 2008). As c-Jun is required for the up-regulation of a subset of GLI target genes, it makes sense that it is present in all BCC nuclei. The presence of c-Jun but not upstream p-EGFR or p-ERK means that it is unlikely that it was activated by the MEK/ERK pathway in BCCs. Therefore c-Jun must be activated by another means, this could be another arm of the EGF signalling pathway, which is unlikely due to the lack of p-EGFR, but may be possible as one group have shown in prostate cancer cells (prostate cancer is an epithelial carcinoma like BCC) that EGF induced mitogenic signalling could be induced by grape seed extract, which at the same time activated JNK, which in turn activates c-Jun (Tyagi et al., 2003). Therefore, it is possible that c-Jun is activated by the MEKK1/JNK branch of the EGF pathway in BCCs. EGFR activation in the overlying epidermis is unlikely to be the cause of c-Jun expression in all the tumour samples because the epidermis is often disrupted in BCC and p-EGFR expression was not found in the overlying epidermis. In order to confirm why c-Jun is present in BCCs it would be useful to complete further immunohistochemistry using antibodies to proteins involved in MEKK1/JNK signalling. Other signalling pathways and the possibility of ligand independent activation of c-Jun may also need to be considered because signalling networks can be extremely complex.

The lack of correlation between BCC subtype and expression levels or sub-cellular localisation of all proteins considered in this study shows that MEK/ERK and PI3K/AKT EGF pathway components may not have any involvement in producing

the differing subtypes as originally hypothesised. Expression levels of other genes must therefore be involved in producing different tumour subtypes. One example which may be involved is bcl-2 (known to promote cell viability) which was found to be expressed in a greater number of cells within non-aggressive BCCs than in aggressive BCCs (Pratistadevi et al., 2000). The stroma surrounding the tumour cells is another possible cause of varying tumour morphology. In morpheaform BCCs the stroma may enable the 2-3 cell wide strands to infiltrate deeper into the normal tissue. This could be due to the structure of the stroma allowing tumour cells to infiltrate, or it could be caused by protein expression. For example, $\alpha v \beta 6$ integrin, which is normally up-regulated in wound healing as well as in carcinogenesis, was found to be increased in morpheaform BCCs compared to nodular BCCs (Marsh et al., 2008). In order to confirm whether altered stroma is the cause of more invasive subtypes, further immunohistochemistry would need to be carried out on proteins found in the stroma to confirm whether any of these are up-regulated in invasive subtypes compared to non-invasive BCCs. A further possibility is that signalling from the epidermis overlying the tumour may be involved in causing the different BCC subtypes, although, overlying epidermis is often disrupted. Low levels or no EGF pathway components, EGFR and p-EGFR, ERK and p-ERK, p-AKT were expressed in the overlying epidermis of BCCs in this study or in the BCCs themselves. Paracrine signalling has previously been shown in other epithelial carcinomas such as pancreatic cancer and was discussed as a possibility in BCCs in the previous chapter (Walter et al., 2010).

At this stage it is worth re-assessing the merit of a formulation that would inhibit both EGF and SHH signalling. The increased activity of EGFR in the overlying epidermis suggests that the keratinocytes may contribute to the tumour environment by paracrine signalling (Rittie et al., 2007). In chapter 3 of this study, a paracrine effect upon the expression of GLI target genes (expression was reduced in the presence of fibroblasts) was observed when keratinocytes were allowed to stratify at the air: liquid interface. The action of p-AKT needs to be confirmed in order to decide whether to include it in a topical formulation for

treatment of BCC. Immunohistochemistry and qPCR and/or western blotting would need to be carried out to look at the expression of proteins and cDNA on a larger sample of BCCs in order to eliminate possibilities and confirm the cause of invasive subtypes of BCC. Ideally a larger tumour sample would enable us to overcome the difficulty of making comparisons between levels of protein immunoreactivity and localisation between samples which have a large amount of morphological variability even within a single tumour.

Chapter 5

In Vitro Topical Delivery of Signal Transduction Inhibitors

5.1 Introduction

5.1.1 Basal Cell Carcinomas as Targets for Topical Drug Delivery

BCCs present an ostensibly accessible target for topically administered drugs. However, while these lesions are on the skin surface, problems developing topical formulations still exist due to the variable structure and depth of different types of BCC, as well as inherent variation from tumour to tumour. Penetration of drugs through the epidermis of superficial BCCs is more achievable than penetration into the deeper dermis, which would be essential to treat the more invasive BCCs such as the nodular and morpheaform subtypes.

5.1.2 Signal Transduction Pathways as Targets for Inhibition

As stated in the general introduction, constitutive activation of the SHH signalling pathway by deactivating mutations in the gene encoding PTCH, or occasionally activating mutations in the gene encoding SMO, are the principle causes of BCC. SMO inhibitors such as cyclopamine were considered useful in topical formulations to 'switch off' the SHH pathway. However, at the start of this research project, it was hypothesised that the MEK/ERK branch of the EGF pathway was involved in modulation of the SHH pathway in BCCs and may be a factor contributing to formation of the more invasive subtypes. It was also thought possible that the PI3K/AKT pathway had some involvement in tumour formation, so EGF pathway inhibitors might also prove to be useful therapeutic targets. Thus, a cocktail of drugs could be developed that would theoretically prevent further invasion whilst inhibiting tumour growth or even killing the tumour cells.

5.1.3 Inhibitors of EGF and SHH Signal Transduction Pathways

Many natural and synthetic compounds have now been reported as highly selective inhibitors of cellular signalling processes. These include LY294002 (derived from quercetin, a naturally occurring bioflavonoid), which is a selective PI3K inhibitor that can also affect AKT, a direct target of PI3K. Another flavonoid (PD98059) is a potent and selective inhibitor of MEK phosphorylation by cRAF or MEK kinase

and this causes inhibition of MAPK phosphorylation, directly downstream of MEK (Alessi et al., 1995; Dudley et al., 1995). Furthermore, cyclopamine binds directly to SMO, leading to reduced SHH signalling and known to inhibit tumorigenesis in BCCs (Chen et al., 2002a; Chen et al., 2002b; Taipale et al., 2000).

5.1.4 Routes for Topical Delivery

Generally, there are three main routes for topical drug delivery:

1. Dermatological: epidermis is the main target
2. Transdermal: dermal microvascular system is the main target
3. Transcutaneous: drugs bypass the dermal microvascular system and go into the underlying tissues

For effective transcutaneous delivery, drugs must permeate the lipophilic stratum corneum, followed by the more hydrophilic viable epidermis and then finally partition into the hydrophilic dermis. The nodular and morpheaform BCC subtypes, which go deep into the dermis, would require a combination of epidermal, dermal and subcutaneous targeting.

5.1.5 Skin Permeation

In order to maintain a fixed level of drug within the skin, the rate of permeation must not exceed the rate of clearance by the dermal vasculature. The permeation of compounds can be affected by numerous physiological factors: age, body site, race, pathological disorders, eruptions, infections, ichthyoses and tumours (such as eruptive BCCs). Other important factors are related to the delivery system and include concentration gradient, logP (lipophilicity), drug size (molecular weight) and type of vehicle (can increase or decrease speed of delivery).

The stratum corneum provides an effective skin barrier, and is very resistant to penetration, particularly for polar/hydrophilic compounds. It consists of 75-80% protein (mostly keratin) and 5-15% lipid. The lipid content is a complex mixture of

192

ceramides, fatty acids, cholesterol, cholesterol sulphate and sterol/wax esters (Benson, 2005; Hatfield and Fung, 1995). It varies depending on body site and also from person to person. Water is homeostatic and acts as a plasticizer for the stratum corneum to stop it from drying out and cracking, and natural moisturising factors (e.g. urea and urocanic acid) retain moisture and help to preserve suppleness (Benson, 2005).

5.1.6 Routes of Skin Permeation

There are three main routes of permeation through the outer layers of the skin (stratum corneum and epidermis). The trans-cellular route requires passage through both polar and lipophilic environments. Drugs must partition through the lipid membranes into corneocytes which contain highly hydrated keratin molecules (hydrophilic or polar environment). They must diffuse through the keratin matrix that fills the cell and then partition out of the cell via the lipid rich (hydrophobic) membranes into the lipid rich (lipophilic) intercellular spaces.

The intercellular route suits small uncharged molecules and involves passing through the stratum corneum by going around the epidermal cells rather than through them. This requires movement only through a hydrophobic (lipophilic) environment and it is likely that small molecule inhibitors (such as PD98059, LY294002 and cyclopamine) would be able to permeate the skin principally via this route due to their small size and lipophilicity.

The trans-appendageal route requires passage through skin appendages such as hair follicles and sweat ducts. However, while these structures only occupy about 0.1% of the skin's surface, it can provide a faster route for larger molecules to penetrate deeper into the skin.

There is no known active transport system to carry compounds through the skin. While it is likely that drugs may use one route preferentially, in reality, they will probably permeate via a combination of routes. It should also be noted when

delivering drugs to the skin that there are enzymes present (e.g. esterases, aryl hydrocarbon hydroxylases) which may be able metabolise drugs (Woolfson, 1990). These are localised in the stratum corneum, living epidermis, sebaceous glands and hair follicles, and can cause drugs to lose their efficacy as they pass through these structures.

5.1.7 Properties of Drugs that Permeate Skin

Physicochemical properties of compounds are important for their ability to permeate the skin. These properties include: lipophilicity, polarity, ionic state, molecular size, solubility and melting point. The compounds used in this project, (LY294002, PD98059 and cyclopamine) are all small lipophilic molecules. LY294002 and PD98059 are soluble in fish oil, DMSO and alcohol while cyclopamine is only soluble in DMSO and ethanol when heated to 50-60°C (Online source: LC Labs. (2004)). Due to their general lipophilicity, oil (with cyclopamine dissolved in DMSO or ethanol prior to addition), alcohols or DMSO would be the most useful vehicles for transporting these molecules into the skin.

5.1.8 Methods of Drug Delivery to the Skin

Drugs or other molecules may be transported through the stratum corneum by using creams, ointments, patches, nanogels or physically, eg microneedles. A cream, ointment or patch would be the most appropriate method for delivering drugs to the site of BCCs because they are the most cost effective mode of delivery and BCCs are likely to require repeated application to the skin.

5.1.9 Franz-type Diffusion Cell

In order to model the permeability of drugs *in vivo*, glass Franz-type diffusion cells (see **Figure 5.1**) can be used for *in vitro* permeation experiments on excised skin (Franz, 1975). The membrane (typically full thickness skin or heat separated epidermis) is sandwiched between the donor and receptor phases. The vehicle containing the dissolved drug is applied to the skin via the donor chamber. The

194

sampling arm can then be used to remove a receptor solution containing any drugs that had passed through the skin.
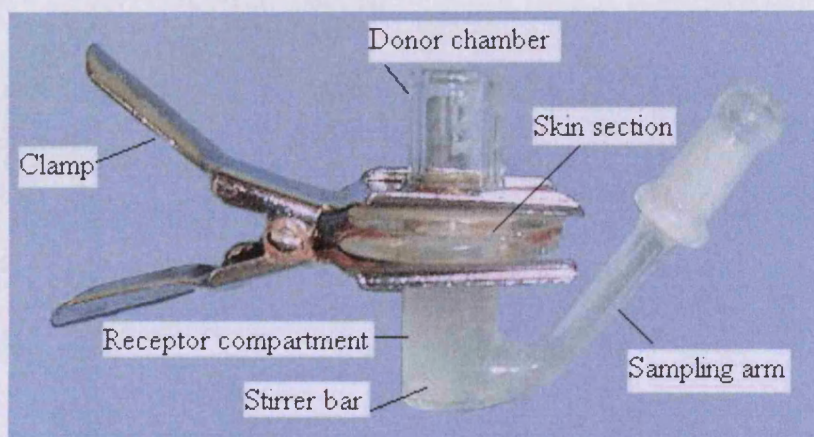
Figure 5.1: Franz-type Diffusion Cell. The diffusion cell consists of two glass sections clamped together with excised skin in the middle. Vehicle containing drug is applied to the skin surface via the donor chamber and permeants are removed from the receptor compartment below for analysis.

5.1.10 Vehicles for Topical Delivery

Vehicles are used to increase permeant flux across the stratum corneum barrier. They do this by partitioning into the stratum corneum and causing changes which allow increased permeability. Such changes should be reversible and not affect the lower layers of the skin. There are various options for vehicles of this type, depending on the lipophilicity of the drugs selected.

Sulfoxides such as DMSO (dimethyl sulfoxide), give maximal penetration but can be skin irritants. They act by denaturing skin proteins and partitioning with intercellular lipid domains. DMSO damages the stratum corneum, which increases permeation and is known as a 'Universal solvent' because both lipophilic and hydrophilic permeants are soluble in DMSO (Williams, A C, 2003).

Alcohols (such as ethanol) can be used as an enhancing vehicle. They are often used for maintenance of a concentration gradient to speed up penetration of a drug.

195

Alcohols penetrate the skin very quickly so this high solubility may need to be balanced with other vehicles to reduce the overall speed of penetration.

Fatty acids such as fish oil are skin friendly enhancing vehicles as they cause no damage and may in fact be beneficial in terms of moisturisation (Thomas and Heard, 2005). Their strong odour is a negative point from a patient perspective so these creams are often mixed with eucalyptol, which disguises the smell. Fish oil contains eicosapentaenoic acid, which reduces COX-2 expression and can also be used as a vehicle to deliver drugs through the skin. COX-2 activity leads to the formation of prostaglandins (Kim et al., 2006) and there is evidence of COX-2 over expression in morpheaform BCC (Jenkins, 2009; Yu et al., 2008). However, it is not entirely clear whether COX-2 has a positive or negative effect on BCC growth. Since inflammation is part of the innate immune response, any decrease in inflammation due to COX-2 inhibition, might also reduce the effectiveness of the immune system in carcinoma clearance. Although COX-2 inhibitors may cause an increased risk of cardiovascular disease and gastrointestinal disease, fish oil applied topically would carry a reduced risk, making this a potentially useful base for this formulation (Thomas et al., 2007).

Emulsifying ointment is a standard British Pharmacopaeia mixture of paraffin oils which reduces water loss from the skin. This is a skin friendly vehicle but may need other vehicles added such as sulfoxides, alcohols or oil to enhance drug penetration.

A series of vehicles can be tested to determine whether drugs permeate the skin sufficiently for effective BCC treatment and at what flux (speed). DMSO and ethanol represent maximal penetration for PD98059 and LY294002 due to their solubility in these solvents. These were therefore tested first to confirm that the drugs can permeate through full thickness skin. Once permeation had been demonstrated then a safe vehicle could be designed with the aim of delivering

drugs through the skin but minimising loss to the systemic circulation by slowing transit through the skin.

5.1.11 Flux and Dosing

Drug flux is the amount of drug delivered across the skin at steady state, as a function of application area and time. It may be increased by occlusion (increases stratum corneum water content by decreasing transepidermal water loss), an effect that has been seen for both hydrophilic and lipophilic permeants (Roberts et al., 1993; Wester et al., 1995).

The applied dose of drug can either be finite or infinite. A finite dose will be depleted over the course of a permeation study, but can mimic 'in-use' application. An infinite dose will not be depleted over the course of the permeation study or over the time of application and steady-state permeation should be achieved.

Fick's first law of diffusion states that the rate of transfer of a diffusing substance through a unit area of skin (flux) is proportional to the concentration gradient. This depends on the diffusion coefficient of the permeant as in the following equation:

$$J = -D \frac{dc}{dx}$$

J= flux of permeant

D= diffusion coefficient of permeant

dc/dx = the incremental change in concentration with distance (concentration gradient)

The pseudo-steady-state flux is the gradient of the linear portion of the permeation profile. The permeability coefficient (an estimate of the permeation rate of a solute across a membrane) can be determined from the concentration of the permeant in the applied vehicle.

5.1.12 Depth Profiling

Depth profiling is a method to quantify the amounts of drug localised within zones or layers of the stratum corneum and epidermis. The most common technique uses tape strips to repeatedly remove sequential skin tissue (layers) from the same surface area of dosed skin. Typically, this commences at the stratum corneum although it is possible to do this in reverse and commence at the basal layer of heat-separated epidermis.

The receptor solution must provide a suitable sink in which the permeants should be soluble, without modulating the barrier function. To ensure no retardation of the flux occurs due to imbalance of the concentration gradient, permeating species should not exceed 20% of their solubility in the receptor phase. The receptor phase should exert no effect on the membrane, which would alter their permeation, and should if possible mimic the *in vivo* situation.

5.1.13 Aims

- To determine the penetration of cyclopamine, LY294002 and PD98059 into the skin and whether the inhibitors affect each other's penetration.
- To probe which vehicles would be most appropriate for delivering these inhibitors to cutaneous BCCs *in vivo*.

5.2 Materials

PD98059, LY294002 and cyclopamine were all purchased from LC Labs (Woburn, MA, USA). All solvents were from Fisher Scientific (Loughborough, UK).

5.3 Methods

5.3.1 Solubility and Stability of LY294002, PD98059 and Cyclopamine

The stability of LY294002 and PD98059 over 48 hours at 37°C has been previously determined (Davison et al., 2008). However, the stability of cyclopamine is unknown, and due to the lack of a useable chromophore, this could not be measured by HPLC. Solubility (as determined by Davison et al., 2008) for LY294002, PD98059 and cyclopamine was repeated in this study (**Table 5.1**).

Table 5.1: Solubility of Cyclopamine, PD98059 and LY294002. Data for cyclopamine taken from LC Labs data sheets and data for PD98059, and LY294002 taken from Davison et al., 2008.

	Cetrimide mg mL^{-1}	Cetrimide 30% ethanol mg mL^{-1}	DMSO mg mL^{-1}	Fish Oil mg mL^{-1}	Ethanol mg mL^{-1}
Cyclopamine	0	11	4	0	20
PD98059	4.57	3	6.98	2.47	0.6
LY294002	9.42	15	14.76	5.16	25

5.3.2 In Vitro Skin Penetration and Permeation

Porcine ear skin was used as a model for normal human skin as it closely resembles human skin both enzymatically and structurally (Hawkins and Reifenrath, 1986; Dick and Scott, 1992; Schmook et al., 2001). The stratum corneum is similar in thickness and has similar permeation properties (Sekkat et al., 2002). Porcine ears were used throughout these experiments to maintain consistency in the permeability properties based on body site. Fresh ears were always used because it had been shown previously that frozen skin has different permeation properties, usually allowing compounds to permeate at an increased rate compared to fresh skin.

Cetrimide with 30% ethanol (necessary for cyclopamine solubility) was used as the receptor phase in the experiments (see **Figure 5.1**). Heard and co-workers showed that cetrimide does not give rise to any adverse affects on the skin and does not affect drug flux (Davison et al., 2008b; Heard et al., 2002). A micro stirrer was used to constantly agitate the receptor phase to mimic dermal clearance by the vasculature *in vivo*.

Porcine ears were obtained from an abattoir within an hour of slaughter and placed in ice-cold HEPES modified Hanks balanced buffered salt solution (Sigma-Aldrich Company Ltd, Gillingham, UK). Full thickness skin was excised by blunt dissection and continually bathed in Hank's buffer to maintain viability. The hairs were removed using clippers and the skin was cut into $2cm^2$ sections. In order to give a representation of BCC variation (some BCCs have disrupted stratum corneum, others do not), half of the skin sections had the stratum corneum disrupted by tape stripping to mimic morpheaform or superficial BCC. This was achieved by pressing firmly on the stratum corneum side with adhesive tape (Sellotape) and then rapidly removing it (repeated 25 times with clean tape). The skin sections were then placed between the greased flanges of a glass Franz type diffusion cell, stratum corneum side up, and the flanges were clamped together to form an airtight seal. A magnetic stirrer bar and the receptor phase (30 mg mL^{-1}

cetrimide with 30% ethanol, degassed) were added to the receptor compartment via the sampling arm, ensuring the receptor solution touched the underside of the skin and that there were no bubbles (can affect permeation by interfering with the concentration gradient). Parafilm (Fisher Scientific, Loughborough, UK) was placed over the sampling arm to prevent evaporation of the receptor phase. The Franz cell was then placed on a VarioMag Telesystem submersible stirrer plate (Camlab Ltd, Cambridge, UK) in a 37°C waterbath containing virkon to prevent microbial contamination of the skin (Nickel Electro Ltd, Weston-super-Mare, UK, Fisher Scientific, Loughborough, UK). The water just covered the receptor compartment and did not reach the skin. The Franz cell was allowed to equilibrate for half an hour after which 200µl of the donor phase (ethanol, DMSO, 200µl ethanol in fish oil) containing equimolar concentrations of LY294002 (1 mg mL^{-1}), PD98059 (0.8 mg mL^{-1}) or cyclopamine (1.34 mg mL^{-1}) was applied to the skin surface via the donor chamber. Parafilm was used to cover the donor chamber to mimic occlusion. Dosing of the donor phase (200µl aliquots) was repeated at 3 and 6 hour timepoints for half the Franz cells containing native skin and half the cells containing disrupted stratum corneum to mimic infinite dosing. The remainder of the cells mimicked finite dosing. This gave four dosing protocols: normal skin single dose, normal skin repeat dose, tape stripped skin single dose and tape stripped skin repeat dose. In addition, 4-6 replicates were used for each measurement.

The receptor phase was removed from the Franz cells via the sampling arm using a glass pasteur pipette (Fisher Scientific, Loughborough, UK) and 1ml samples were stored in autosampler vials at -20°C to await analysis. The receptor compartment was immediately replenished with fresh receptor phase and samples at various times (3, 6, 12, 24, 36 and 48 hours) over two days.

5.3.3 Standard Depth Profiling

Tape stripping is a method of depth profiling used to sequentially collect cell layers from the stratum corneum side of the epidermis. The cells are then removed from the tape and the quantity of drug which has penetrated to different cell layers measured by HPLC.

Franz-type cells were set up with porcine skin and LY294002 (1 mg mL^{-1}) added to 5 cells, PD98059 (1 mg mL^{-1}) to another 5 cells and a combination of LY294002 and PD98059 (0.5 mg mL^{-1} each) to another 5 cells. These inhibitors were dissolved in methanol and 300µl of this donor phase was applied to the skin surface in each Franz-type cell. A receptor phase of degassed cetrimide with 30% ethanol was added to the bottom of the Franz-type cell until the solution just touched the underside of the skin, taking care not to introduce any bubbles. The Franz-type cell was placed on a microstirrer in a 37°C waterbath containing Virkon to prevent microbial infection and agitated for 24 hours. The pig skin was removed from the Franz-type cells, a cotton bud was used to gently remove excess donor phase and tape strips were taken from the stratum corneum side of the skin. Three sequential strips were added to a vial of methanol until 30 strips had been removed (10 vials) and the final (11th) vial contained the remainder of the skin. The covered vials were left overnight on a rocker to wash off the cells, and then left uncovered until all the methanol had evaporated. Methanol (1ml) was added to each vial to re-dissolve the drugs and the concentration was measured by reverse phase HPLC.

5.3.4 Reverse Phase HPLC Method for Measuring LY294002 and PD98059

The quantity of LY294002 and PD98059 removed from the Franz-type cell receptor phase was measured by reverse phase HPLC (Agilent 1100 series automated system) using a Phenomenex Sphereclone 5µm particle size column with a flow rate of 0.5ml/minute. In order to quantitate the amount of each inhibitor separately, a mobile phase gradient was created to enable elution at

different time points. The mobile phase ratio started at zero with 80:20 methanol: dH_2O and changed over 8 minutes to 70:30 methanol: dH_2O, at 8:01 minutes the ratio changed to 90:10 methanol: dH_2O and remained at this ratio until 12 minutes. Using this protocol, PD98059 eluted at 7.3 minutes (retention time) and LY294002 eluted at 8.9 minutes.

The two inhibitors were detected by absorbance at 254nm and the peak areas under each trace (one for each Franz-type cell receptor phase removal timepoint) were calculated using Agilent ChemStation software. Microsoft excel was used to calculate the mass of permeant (PD98059 or LY294002) with the equation (mAU = milli-absorbance units):

Mass of permeant (mg cm^{-2}) = peak area (mAU)/gradient of calibration graph x receptor phase volume (ml)/area of application (mm^2)

The mean for 4-6 replicates was plotted. Steady state flux for the permeation of PD98059 and LY294002 was determined by plotting the cumulative permeation (μg cm^{-2}) against time. The linear portion of the resulting plot was taken as steady state flux. Calibration curves were plotted using known quantities of each inhibitor against the area under the peaks of the HPLC trace.

5.3.5 Reverse Depth Profiling

In order to clarify whether the drugs had reached the basal layer where BCCs reside, a different approach was used. The epidermis was heat separated from the dermis and then the underside of the epidermis was tape stripped (as previously explained), thus removing the basal layer first (reverse depth profiling).

Pieces of freshly excised porcine skin ($2cm^2$) were heated to 55°C for 30-60 seconds in a waterbath filled with distilled water. The epidermis was carefully separated from the dermis using forceps. The underside of the epidermis was sequentially tape stripped by applying pressure and then removing the tape. This

was repeated for several tape strip layers applying equal pressure with the thumb to each strip before removing. The cells were washed off the tape strip into 1.5ml eppendorf tubes using 0.9ml SDS sample buffer (4.12ml H_2O, 1ml 0.5M Tris, 0.8ml glycerol, 1.6ml 10% SDS, 0.08ml 1M DTT and 0.2ml bromophenol blue) and boiled for 5 minutes. The denatured protein solution was stored at -20°C until analyzed by SDS-PAGE and western blotting.

5.3.6 Polyacrylamide Gel Electrophoresis and Western Blotting

Total protein extracts were separated by electrophoresis (SDS-PAGE), transferred to membranes and analysed with a group of specific antibodies (western blotting).

5.3.6.1 Sodium Dodecyl Sulphate-Polyacrylamide Gel Electrophoresis (SDS-PAGE)

SDS-PAGE was carried out using the XCell Surelock mini-cell (Invitrogen, Paisley, UK). Proteins were separated on an SDS gel by electrophoresis and transferred to a membrane for western blotting using the XCell II Blot module. Immunochemistry was performed to detect the presence of proteins and to measure expression levels and the extent of phosphorylation in cells under different culture conditions.

Enough mixture for two 10% separating gels was made containing 0.1ml 10% SDS, 2.5ml 1.5M Tris, 3.3ml 30% acrylamide gel solution (Sigma-Aldrich Company Ltd, Gillingham, UK), 75μl APS (ammonium persulphate; Fisher Scientific, Loughborough, UK) and 7.5μl N,N,N',N'-tetramethylethylenediamine (TEMED; Sigma-Aldrich-Company Ltd, Gillingham, UK) and 4.1ml H_2O. This was pipetted into cassettes and overlaid with water. Once set, the water was removed and a 4% stacking gel (50μl 10% SDS, 1.25ml 0.5M Tris, 0.65ml 30% acrylamide gel solution, 3.05ml H_2O, 50μl 10% APS and 10μl TEMED) was added above the separating gel. A 12 prong comb was placed into the top of the cassette and after the stacking gel had set (about 5 minutes), the comb was

carefully removed and the wells washed with distilled water (dH$_2$O). The cassettes were placed into the apparatus and 1x running buffer (30g tris, 144g glycine and 10g SDS per litre of dH$_2$O) was poured into the apparatus, ensuring that the wells were full of buffer. The protein extracts (10μl) were loaded into the wells (volumes should give equal quantities of protein in each well for comparison) and molecular weight standards loaded on the gel (usually the end lanes). Three markers were used in combination: 10μl Precision Plus protein marker (Bio-rad, Hemel Hempstead, UK) or 5μl low molecular weight marker (Promega UK Ltd, Southampton, UK) together with 2μl Magicmark (Invitrogen, Paisley, UK). The outer and inner chambers were filled with running buffer and 125V at a starting current of 25mA per gel applied until the tracker dye reached the bottom of the separating gel. Cassettes were opened and the gel was stained with 0.25% Coomassie brilliant blue R250 (Sigma-Aldrich Company Ltd, Gillingham, UK) in 40% methanol (Fisher Scientific, Loughborough, UK) and 10% acetic acid (Fisher Scientific, Loughborough, UK) for one hour. The gel was then destained for 30 minutes in 40% methanol and 10% acetic acid. Duplicate gels were important as one was used for staining of the protein to check for even loading while the other gel remained unfixed and was used for western blotting.

5.3.6.2 Western Blotting

Immobilon membrane (PDVF from Millipore, UK) was immersed in methanol and then vigorously shaken in water to hydrate. Whatman paper and pads were soaked in western blot buffer (14.4g glycine, 3g Tris and 100ml methanol per litre dH$_2$O). Two pads were placed in the bottom of the western blot module, and then a gel/membrane sandwich was assembled (Whatman paper, gel, Immobilon membrane, Whatman paper) and placed on top of the pads. The module was then filled with further pads and the top locked. Buffer was added to the blotting module and the tank filled with dH$_2$O to keep the gel cool during transfer. Transfer continued for 1-2 hours at 25v with a starting current of approximately 100mA.

5.3.6.3 Protein Detection by Immunochemistry

Western blots on Immobilon membrane were rehydrated with methanol and washed in water, then placed in 5% skimmed milk (Marvel from Tesco, UK) in Tris-buffered saline with 0.1% Tween 20 (TBST from Sigma-Aldrich Company Ltd, Gillingham, UK) for 1 hour to block antigenic sites. Primary antibody (see **Chapter 2, Table 2.6** for dilutions of antibodies used) in 10ml 5% marvel was added and left for 1 hour, after which the membrane was washed (five times in TBST for 5 minutes each). Another 10ml 5% marvel containing the secondary antibody (see **Chapter 2** and **Table 2.6** for details) was added and left to incubate for 1 hour, then the membrane was washed in TBST (again five times for 5 minutes each).

The membrane was laid on Saran wrap in the dark room and covered with ECL reagent for 5 minutes. The reagent was made by combining 1ml solution 1 (1ml 250mM stock luminol (Sigma-Aldrich Company Ltd, Gillingham, UK) in DMSO, 0.44ml 90mM coumaric acid stock (Sigma-Aldrich Company Ltd, Gillingham, UK) in DMSO, 10ml Tris, pH 8.5 plus dH_2O to a total of 100ml) and 1ml solution 2 ($64\mu l$ 30% H_2O_2 and 10ml Tris, pH8.5 plus dH_2O to a total of 100ml). The reagent was poured off, the membrane enclosed in Saran wrap and placed in a cassette together with sensitive X-ray film (Amersham Biosciences, GE Healthcare Life Sciences, Little Chalfont, UK). This was left for 2 to 10 minutes (longest incubation carried out first) and then the X-ray film was placed in Kodak D-19 developer, rinsed in water and finally treated with Kodak Processing Chemical Fixer (Sigma-Aldrich Ltd, Gillingham, UK). Films were then left to dry.

5.3.7 Tissue Immunofluorescence

Stored slides containing frozen porcine skin ($7\mu m$ thick cryostat sections stored at -80°C) were thawed at room temperature (RT) for 10-15 minutes, fixed in acetone (Fisher Scientific, Loughborough, UK) for 15 minutes, dried for 5 minutes and washed in PBS three times for 5 minutes each. Undiluted primary antibody raised to K15 (sheep) or K10 (mouse) were applied to the sections, which were then

incubated for 1 hour in a humidified chamber and washed in PBS (three time for 5 minutes each). Biotinylated anti-sheep (GE Healthcare, Little Chalfont, UK) (1:200) or anti-mouse alexa 594 (1:500) were applied, incubated for 30 minutes and washed three times in PBS (5 minutes each). Slides were then incubated with avidin alexa 488 (Invitrogen, Paisley, UK) 1:500) for 30 minutes and washed in three times PBS (5 minutes each). Finally, sections were mounted with Hydromount (Fisher Scientific, Loughborough, UK) containing 2.5 % Dabco (Sigma-Aldrich Company Ltd, Gillingham, UK) and a cover slip added and allowed to dry for at least 1 hour before viewing under a microscope. The basal layer (stained by K15 antibody) and the suprabasal layers (stained by K10 antibody) of the epidermis could then be identified by fluorescence microscopy.

5.3.8 Derivatisation

Cyclopamine has an extremely low UV absorbance, because it lacks a chromaphore, and only absorbs at short wavelengths. Thus, traces of impurities with high UV absorbance can represent major contaminants, even though they were only 0.1% or less of the material present. Also, certain potential cyclopamine impurities such as acyl derivatives of the amino group are far more hydrophobic than cyclopamine itself, and these impurities would never elute from the column under the HPLC conditions typically used for cyclopamine analysis. HPLC can seriously under estimate and/or over estimate different types of impurities, and therefore cannot give reliable analytical results. Therefore, LCMS (liquid chromatography-mass spectrometry) is recommended for quantification of cyclopamine. However, due to the high cost of LCMS (and its lack of availability), three methods of cyclopamine derivatisation were tested as an alternative method of quantitation.

5.3.8.1 Dansylation (Bartzatt, 2001a; Bartzatt, 2001b)

An aliquot (250μl) of cyclopamine solution [1mg/ml in 17:3 acetonitrile: dH$_2$O] (LC Labs, Woburn, MA, USA; Fisher Scientific, Loughborough, UK) was added to 250μl 2M sodium carbonate solution, pH11 (Fisher Scientific, Loughborough,

UK) and 150µl dansyl chloride solution (1.54g/10mls H_2O from Sigma-Aldrich Company Ltd, Gillingham, UK). The tube was kept in the dark for 1.5 hours and mixed occasionally. Then, 600µl diethyl ether (Fisher Scientific, Loughborough, UK) was added and the solution mixed again. The top (organic layer) was removed for reverse phase HPLC analysis using a Phenomenex Sphereclone 5µm particle size column at 492nm, in a mobile phase of 70:30 acetonitrile: dH_2O run at 1ml/minute for 15 minutes.

5.3.8.2 Phenylisocyanate in Pyridine

This method was adapted from previously published work (Heard and Suedee, 1996). In brief, freeze dried cyclopamine (2mg) was reacted with an excess (1ml) of phenylisocyanate (Sigma-Aldrich Company Ltd, Gillingham, UK) in pyridine (10ml) at 120°C for 6 hours and then allowed to cool. The reaction mixture was then poured into 5ml methanol (Fisher Scientific, Loughborough, UK) to remove unreacted isocyanate and the quantity of derivatised cyclopamine was measured by reverse phase HPLC using a Phenomenex Sphereclone column with 5µm particle size at 254nm, with a mobile phase of 70:30 acetonitrile: dH_2O with 0.1% trifluoroacetic acid run at 1ml/minute for 15 minutes.

5.3.8.3 4'-bromophenacyl trifluoromethanesulfonate

This method was also adapted from published work (Ingalls, 1984). In brief, a 20µl aliquot of 0.1M 4'-bromophenacyl trifluoromethanesulfonate in acetonitrile (Sigma-Aldrich Company Ltd, Gillingham, UK) was added to a glass tube and 10µl 0.5M diisopropylethylamine in acetonitrile (Sigma-Aldrich Company Ltd, Gillingham, UK) was added to neutralise the acid. Then 1ml cyclopamine (5mg/ml dissolved in ethanol at 50-60°C) was added, mixed by vortex and the reaction kept at RT. The quantity of derivatised cyclopamine was measured at timepoints (5, 10, 30, 60, 120 and 180 minutes) after vortex mixing, by reverse phase HPLC analysis using a Phenomenex Sphereclone 5µm particle size column at 254nm, with a mobile phase of 70:30 acetonitrile:dH_2O run at 1ml/minute for 15 minutes.

5.3.9 Statistical Analysis

Flux was compared between each formulation and any differences were determined by using Ordinary ANOVA, Parametric, Tukey tests (Instat 3 for Macintosh, GraphPad Software, USA).

5.4 Results

5.4.1 *In Vitro* Dermal Delivery

The assessment of drug delivery through living epidermis is complex. However, tape stripping can be used to collect cells from skin surface and drug levels measured using methods such as HPLC to assess penetration. This works well for the stratum corneum and upper living layers of the skin but not so well for the lower epidermis due to the undulating nature of the dermal-epidermal junction. This makes it difficult to selectively remove cells from a specific layer. Thus, the reverse tape stripping method, where cells are removed from the underside of heat-separated epidermis (basal cells first) is particularly poor.

Other methods of separating skin such as EDTA or proteolytic enzymes would not work well, as the aqueous solutions would leach out the drugs being assayed. While tape stripping is commonly used for depth profiling to assess the penetration of drugs into the epidermis, satisfactory results are not always obtained. Removal of inhibitors from cells isolated by depth profiling (on tape strips) for measurement by high performance liquid chromatography (HPLC) may lead to inaccurate results because the drugs might not have permeated as far as the basal cells (**Figure 5.2**).
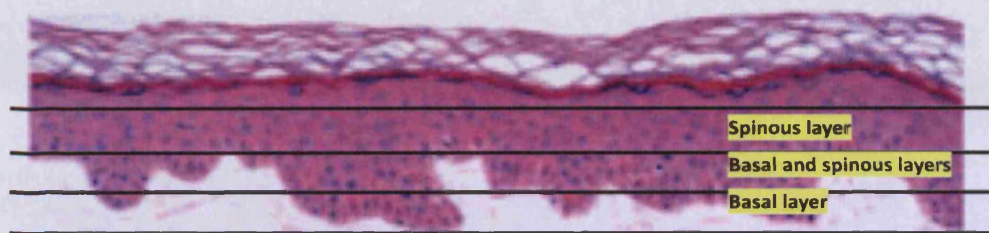
Figure 5.2: Depth Profiling of Heat-Separated Porcine Epidermis. This haematoxylin and eosin stained section of skin demonstrates the convoluted nature of the epidermis, showing that depth profiling removes cells from more than one layer in the lower epidermis (adapted from online source: Melanoma, A Skin Cancer Review).

5.4.1.1 Immunofluorescence and Western Blotting with Keratin Antisera to Define Epidermal Layers

Immunofluorescence confirmed that porcine skin was very similar to human skin in terms of keratin expression (Porter et al., 2004). K14 was immunolocalised to the basal layer and K10 was only present in suprabasal cell layers (**Figure 5.3**). K14 and K10 antibodies were therefore useful for determining the cells present in the tape stripped samples by western blotting (see section 2.2.4 for methods).

(a) K14 (Green)   (b) K10 (Red)   (c) Combined Image
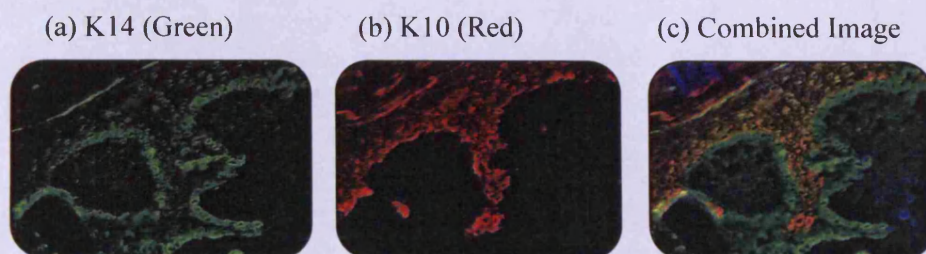
Figure 5.3: Immunofluorescence Detection of Keratins in Porcine Skin. K14 (green) staining was prominent in the basal layer (a) while K10 (red) was specifically localised to the suprabasal layers of the epidermis (b). The combined image (c) showed some dilution of the K10 signal by K14 in suprabasal cells (background staining) but not the reverse.

SDS-PAGE and western blotting of proteins extracted from reverse tape stripped epidermis at two different sites in porcine skin was carried out to show whether cells could be specifically removed from the basal layer. It could then be

210

determined whether the inhibitors (LY294002 and PD98059) could reach these cells.

Western blotting results showed high levels of K14 in the first strips (**Figure 5.4:** lanes 1, 2, 5, 6) as would be expected because these strips were taken from the basal layer side of the epidermis. However, K14 was still present in the protein extracted from cells removed on later tape strips (lanes 3, 4, 7, 8) although at a decreased level. This may be because the basal layer of the epidermis undulates, thus causing basal cells to be removed in later tape strips and it is probable that cells from the spinous layer of the epidermis were also present in the first tape strips. However, a K10 blot would have been more useful as this would show how much suprabasal contamination there was in the basal layer.
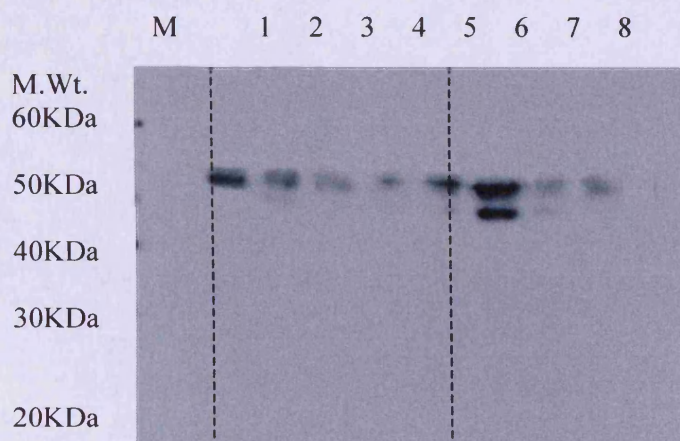
Figure 5.4: Western Blot of K14 in Reverse Tape Stripped Skin. K14 presence was shown in all tape strips. Lane M: low molecular weight marker (Promega UK Ltd, Southampton, UK), lanes 1 to 4: sequential tape strips starting at the basal layer and lanes 5-8: sequential tape strips starting at the basal layer but from a different region of skin. K14 levels are highest in early strips (basal layer) from both skin regions (lanes 1 and 2, lanes 5 and 6).

5.4.1.2 Depth Profiling Porcine Skin after Application of EGF Inhibitors (PD98059 and LY294002) in a Fish Oil Vehicle.

Depth profiling was carried out to demonstrate whether LY294002 (PI3K inhibitor) and PD98059 (MEK1/2 inhibitor) could successfully penetrate to the lower epidermis.

In order to determine the amount of inhibitor which had penetrated the epidermis by HPLC, standard curves were made for both inhibitors (LY294002 and PD98059). A range of standard solutions of each were made up using ethanol (at concentrations of 0.034, 0.068, 0.137 and 0.275 mg/ml). The inhibitors were separated by HPLC and detected at an absorbance of 254nm. The data was plotted using Agilent Chemstation software that showed a peak on the trace where the inhibitors had been detected. The area under each peak was measured using Agilent Chemstation software and a standard curve was plotted of area versus the concentration of each inhibitor solution (see **Figures 5.5 and 5.6**). The value of the gradient of the graph (m, where y = mx + c) was then used to calculate the amount of each inhibitor that had permeated through the skin (using the equation described in **section 5.3.4**). The R^2 values for each inhibitor were both very close to 1, which means that both calibration curves were accurate.

EGF inhibitors (LY294002 and PD98059 alone or in combination) in a methanol vehicle were then applied to porcine skin mounted in a Franz type diffusion cell. The inhibitors were allowed to permeate over 24 hours after which the skin was removed and depth profiling carried out using tape stripping (from the stratum corneum surface where the drugs were applied). Epidermal cells were washed off the tape strips and the inhibitors were extracted. For each drug applied, the level of drug that had permeated through different cell layers was measured by HPLC. Agilent Chemstation software was used to measure the area under each peak of the HPLC trace and the quantity of each inhibitor in the sequential tape strips was calculated using the equation described above (see **section 5.3.4**). The quantity and

212

percentage of each inhibitor in the sequential layers of epidermal cells was then plotted using Microsoft Excel.
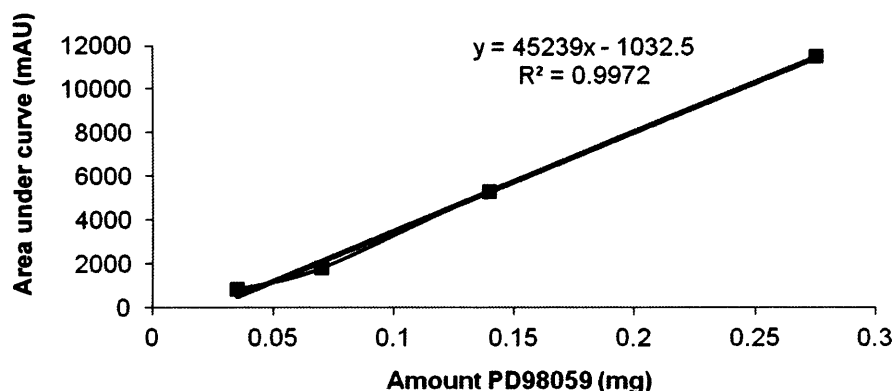
Figure 5.5: Standard Curve for PD98059 (n=3). Known concentrations of PD98059 (mg) in ethanol were plotted against the area under curve on the HPLC trace (in milli-absorbance units [mAU] at an absorbance of 254nm).
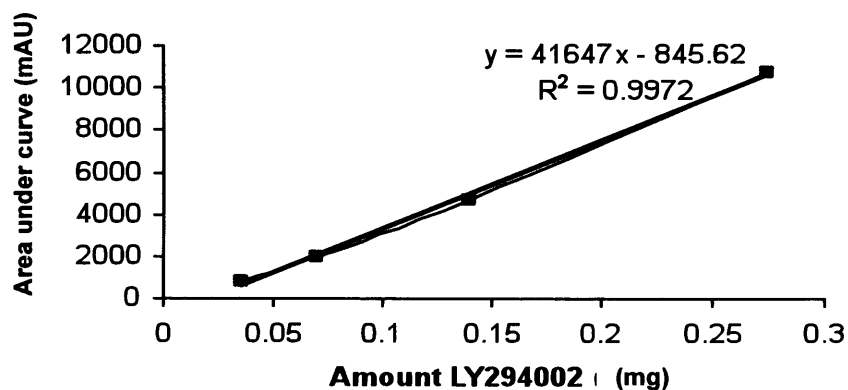
Figure 5.6: Standard Curve for LY294002 (n=3). Known concentrations of LY294002 (mg) in ethanol were plotted against the area under curve on the HPLC trace (in milli-absorbance units [mAU] at an absorbance of 254nm).

Depth profiling results obtained by measuring drug concentrations in ten consecutive tape strips showed that both drugs penetrated through the epidermis and into the living cells below (**Figure 5.7**). The profile of drug retention was typical, with 25-40% remaining on the skin surface (tape strip #1), about 36% being retained in the epidermis (tape strips #2-10) and 23-38% penetrating into the remaining epidermis and dermis (layer R).

When applied alone, there was approximately 7.0 pmol (40%) of PD98059 in the first tape strip (**Figure 4.7a**) and retention in the next two layers decreased rapidly (3 fold less in tape strip #2 and 2 fold less again in tape strip #3). Retention in tape strips #4-10 was similar (approximately 0.5 pmol per layer). Statistics showed there was a significant reduction in retained material in each of the early tape stripped layers but deeper layers were broadly similar. The epidermis as a whole (tape strips #2-10) retained a total of 6.4 pmol (36%) while the remainder (mainly dermis) contained about 4.0 pmol of PD98059 (23% of total) which represents the amount of drug that had penetrated the epidermal barrier.

The total amount of PD98059 retrieved when applied in the presence of LY294002 was reduced by about 30% (12.1 pmol compared to 17.4 pmol) compared to PD98059 applied alone (**Figure 4.7b**). However, more PD98059 penetrated into the dermis (layer R) in the presence of LY294002: 4.8 pmol (38% of total) compared to 4.1 pmol (23% of total) while retention by the epidermis was broadly similar (4.3 pmol or 36% of the total).

The amount of LY294002 retained in the epidermal tape strips was much less than for PD98059, with all layers containing less than 0.001μmol (1 pmol). The total LY294002 retrieved from tape strips 1-10 was almost 10 fold less: 1.5 pmol compared to 13.4 pmol for PD98059 (**Figure 4.7c**). The total LY294002 retrieved from the remaining skin was 0.7 pmol compared to 4.1 pmol of PD98059. However, this represented almost 50% of the drug retrieved compared to 23% for PD98059 alone. In overall terms, the permeation profile was similar and the

amount of drug was reduced in sequential layers. In the presence of PD98059, the profile and quantity of LY294002 uptake and retention in the epidermis was reduced slightly but appeared broadly similar (**Figure 4.7d**).
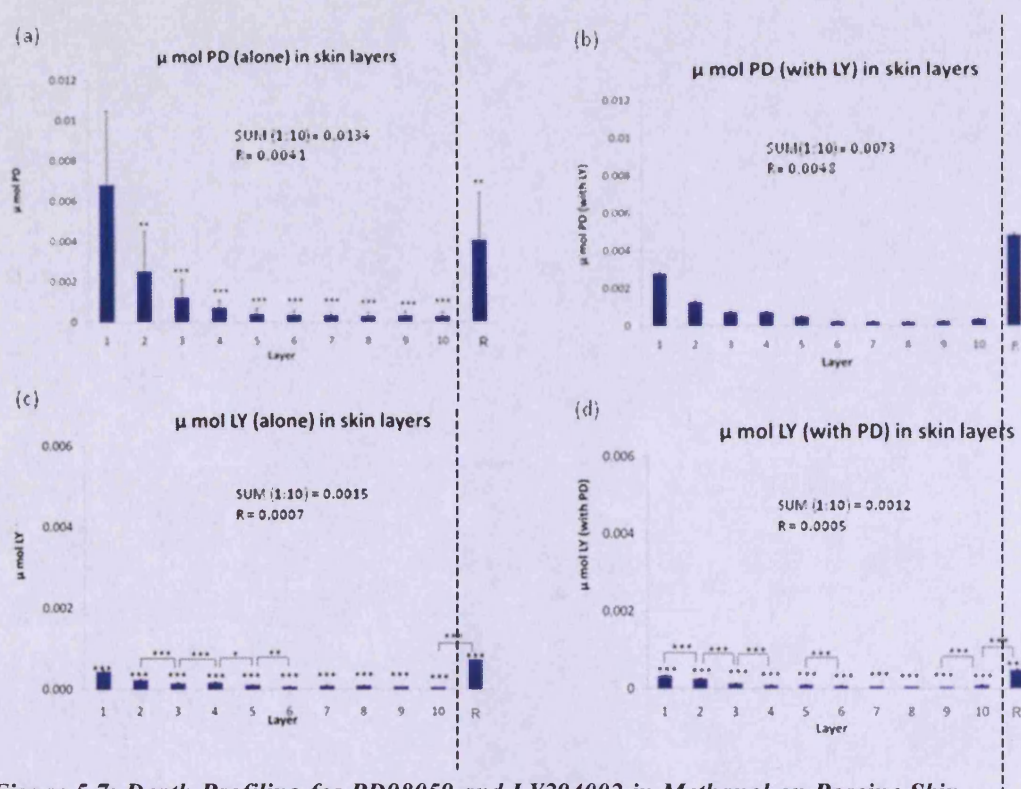
Figure 5.7: Depth Profiling for PD98059 and LY294002 in Methanol on Porcine Skin. *Layers 1 to 10 were tape stripped from the epidermal surface of porcine skin and layer R was the remaining skin after stripping. (a) PD98059 alone, (b) PD98059 with LY294002 present, (c) LY294002 alone and (d) LY294002 with PD98059 present. Statistical analysis using Ordinary ANOVA Tukey Test: * P=<0.05, ** P= <0.005, *** P= <0.001. Data expressed as the mean +/- SD for n=3 experiments with 6 replicates for each experiment. Statistical data has been included to compare each layer to layer 1 and to the previous layer. The lowest rows of stars were compared to layer 1.*

In total, less than 1% of each of the applied inhibitors was retrieved from full thickness skin (layers 1 to 10 and R, the skin remainder). A total of 150µg of each inhibitor was applied to the skin surface. The percentage of total drug applied that was then retrieved from sequential layers (1 to 10 plus the remainder, R) of tape

215

stripped skin followed a typical pattern of drug retention. These percentage values were plotted separately for each inhibitor (**Figure 5.8**) under conditions where both were applied simultaneously (allows for any inhibition or increase in uptake into the skin layers caused by the presence of both inhibitors). The values obtained were 0.38% for PD98059 and 0.07% for LY294002. The first layer contained the highest percentage of applied drug (0.072% for PD98059 and 0.011% for LY294002) compared to the lower epidermal layers (#2-10). There was also a significant decrease in the percentage of PD98059 retained in deeper epidermal layers when compared to layer 1 (P = <0.001), but the decrease was not significant for LY294002. The percentage of PD98059 retained in the epidermis as a whole (#2-10) was 0.173% (0.026 mg) compared to 0.0344% (0.0052 mg) for LY294002. The remainder of the skin (dermis) retained 0.1287% (0.019 mg) of the applied PD98059 and 0.0227% (0.0034 mg) LY294002.
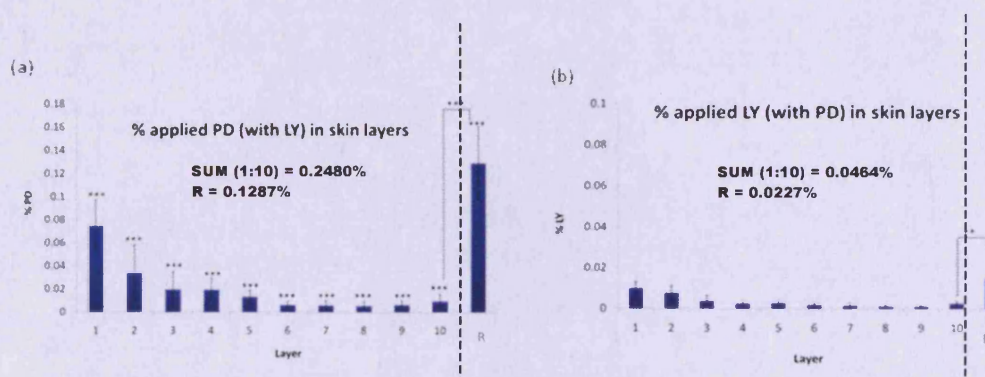
Figure 5.8: Depth Profiling for PD98059 and LY294002 in Methanol on Porcine Skin. *(a) The percentage of applied PD98059 (in the presence of LY294002) permeated. (b) The percentage of applied LY294002 (in the presence of PD98059) permeated. Statistical analysis was done by Ordinary ANOVA, Tukey test. * P=<0.05, ** P= <0.005, *** P= <0.001. Data expressed as the mean +/- SD for n=3 experiments with 6 replicates for each experiment. Statistical data has been included to compare each layer to layer 1 and to the previous layer. The lowest rows of stars were compared to layer 1.*

5.4.1.3 *In Vitro* Skin Permeation Tests

Intact stratum corneum is the main barrier to skin permeation and disrupted stratum corneum enables easier penetration of inhibitors into the skin. Some BCCs have a disrupted stratum corneum (especially nodular subtypes, which often have an ulcerated centre) but this is extremely variable between subtypes and individual BCCs (e.g. morpheaform BCCs rarely show ulceration). Thus, experiments were carried out on both native (intact) skin, and on skin which had been taped stripped (to cause disruption to the stratum corneum). This should mimic the best and worst case scenarios for permeation into BCCs.

Penetration of LY294002 (PI3K inhibitor) and PD98059 (MEK inhibitor) through porcine skin using a selection of vehicles including fish oil, DMSO and ethanol was carried out using Franz cells. The receptor phase was removed and replaced at 3, 6, 12, 24, 36 and 48 hour time points. A typical HPLC trace (**Figure 5.9**) of the receptor phase removed from a Franz cell showed separate column elution times for LY294002 (7.3 minutes) and PD98059 (8.9 minutes) in fish oil even though both compounds are of similar size and lipophilicity (clogP: 2.57 and 3.03 respectively). The area under each peak increased with time and was largest at the later time points (24, 36 and 48 hours). The peaks with elution times between 2.5 and 5.5 minutes were due to the solvent front and skin debris.

A small shift in retention time was found for both LY294002 and PD98059 when individual traces for each experimental time point were overlaid (**Figure 5.10**). However, both inhibitors were clearly separated from each other at all times so peak areas could be accurately measured.

5.4.1.3.1 DMSO Vehicle

Tests using Franz-type diffusion cells enabled measurement (by HPLC) of LY294002 and PD98059 permeation through full thickness porcine skin into the receptor phase. Thus, the cumulative amount of drug permeating in a given time

could be measured. The steady-state flux for each skin sample was also measured and the standard deviation between skin sample-Franz cell replicates was assessed.
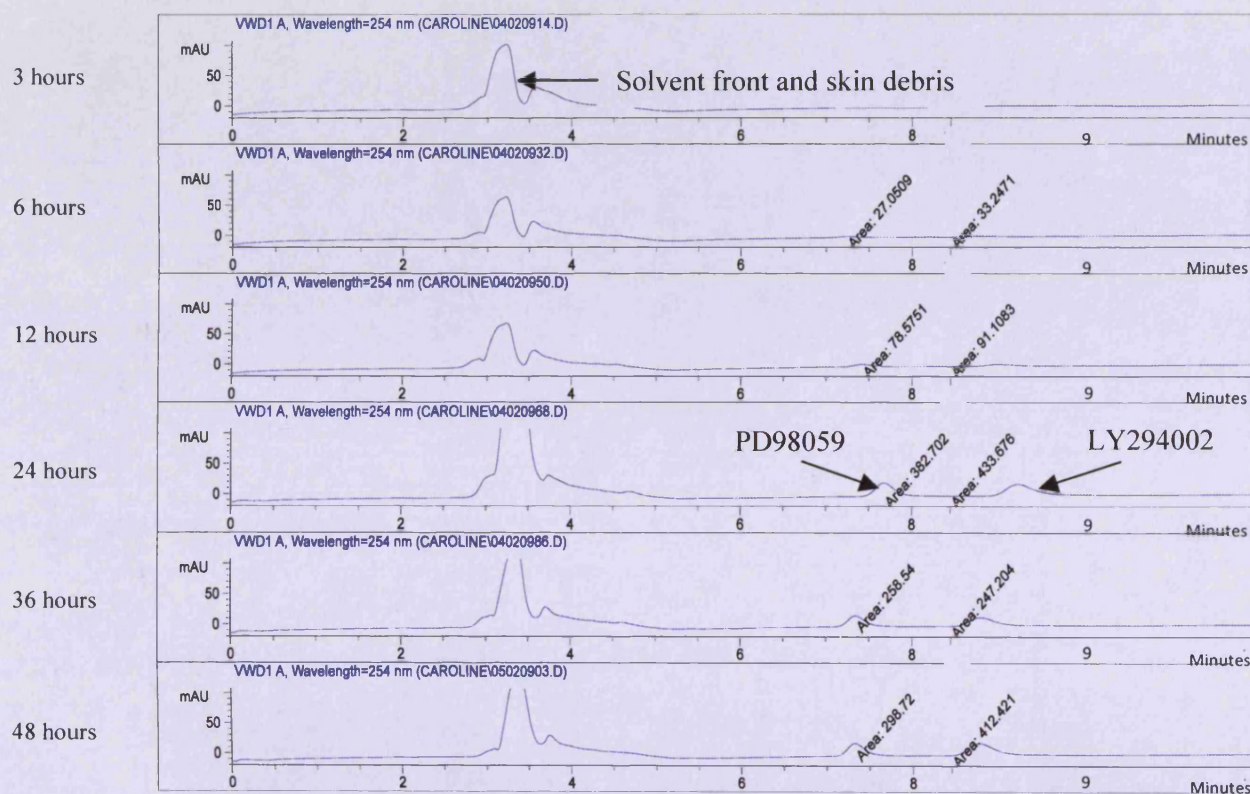
Figure 5.9: HPLC Elution Profile for LY294002 and PD98059 in a Fish Oil Vehicle. *HPLC traces for the receptor phases from one Franz cell taken at different time points (3, 6, 12, 24, 36 and 48 hours) showing elution of PD98059 (~7.3 minutes) and LY294002 (~8.9 minutes). The peak height (milli-absorbance units [mAU]) increased with time after permeation of a single dose through tape stripped porcine skin. Peaks between 2.5 and 5.5 minutes were caused by the solvent front and skin debris.*

218
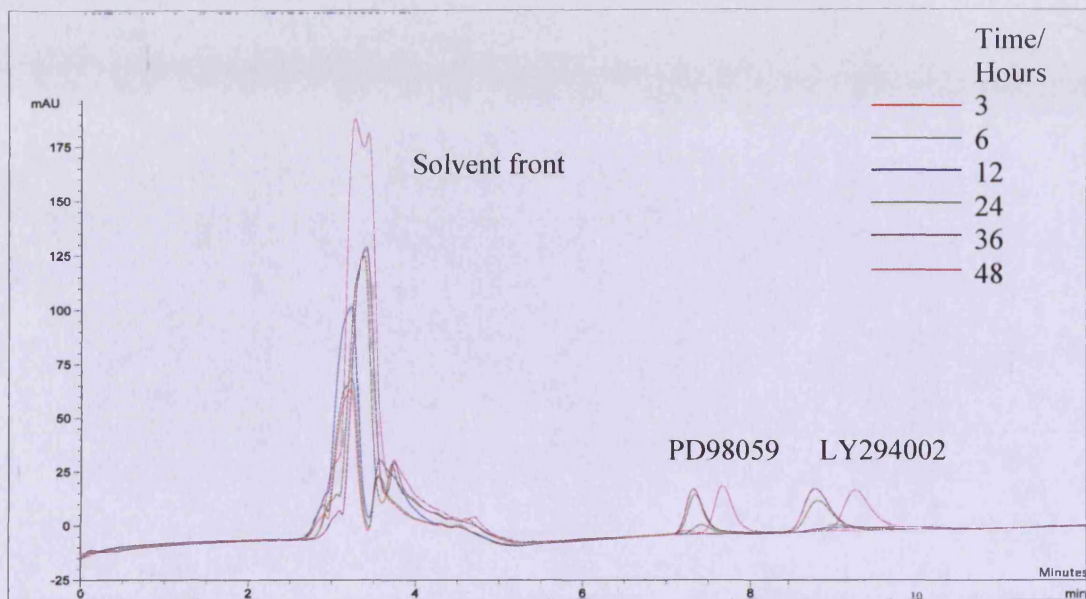
Figure 5.10: HPLC Traces for LY294002 and PD98059 in a Fish Oil Vehicle. Overlaid traces for the receptor phase of one Franz cell at different time points (3, 6, 12, 24, 36 and 48 hours) showing some peak shift but peak separation for PD98059 (7.3-7.7 minutes) and LY294002 (8.8-9.4 minutes) was maintained. Absorbance was measured in milli-absorbance units (mAU) at a wavelength of 254nm.

Tape stripped skin with repeat dosing in a DMSO vehicle enabled the largest cumulative amount of PD98059 (MEK1/2 inhibitor) to permeate through full thickness skin (**Figure 5.11**). Tape stripped skin with a single dose of PD98059 achieved almost the same cumulative amount of inhibitor to permeate the skin. In fact, the inhibitor permeated the skin slightly faster at earlier time points (12 and 24 hours) but the cumulative amount did not increase as much between 24 and 36 hours (not statistically significant). Native (intact) skin allowed a lower cumulative amount to permeate the skin at 48 hours (approximately 25% or 0.05mg cm^{-2} less than tape stripped skin with repeat dosing) and with a single dose of PD98059 applied to the skin this was even less (0.08mg cm^{-2} less with native skin single dose than tape stripped single dose, not statistically significant).

219

Cumulative amount of PD98059 in a DMSO vehicle permeated through Porcine Skin
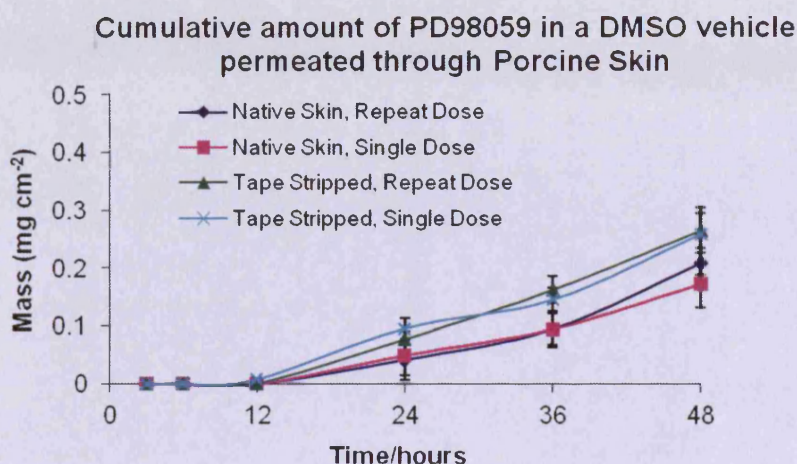
Figure 5.11: Cumulative Permeation of PD98059 in a DMSO Vehicle through Porcine Skin. Cumulative amounts of inhibitor permeated over 48 hours through tape stripped or intact (native) porcine skin with single or repeat dosing. Statistical analysis was done by Ordinary ANOVA, Tukey test and data was expressed as the mean +/- SD for n=3 experiments with 6 replicates for each experiment.

Tape stripped skin had a greater flux than native skin for PD98059 and repeat dosing gave increased flux over a single dose (**Table 5.2**).

Table 5.2: Mean Flux and Standard Deviation (SD) for Permeation of PD98059 in a DMSO vehicle through Porcine Skin

	Mean Flux $(mg/cm^2/hr)$	SD
Normal (Native) Skin (Repeat Dose)	0.00455	0.00146
Normal (Native) Skin (Single Dose)	0.00390	0.00249
Tape Stripped Skin (Repeat Dose)	0.00678	0.00172
Tape Stripped Skin (Single Dose)	0.00590	0.00161

Tape stripped full thickness porcine skin with repeat dosing allowed the greatest permeation of LY294002 (**Figure 5.12**). Tape stripped skin with a single dose enabled 0.05mg/cm^{-2} less LY294002 to permeate, which was the second greatest cumulative amount after 48 hours. However, there was no significant difference between a single dose of LY294002 and a repeat dose. Native skin with repeat

220

dosing allowed less permeation of the inhibitor (P<0.05 when compared to tape stripped repeat dose) and native skin with single dosing showed the least permeation (P<0.05 when compared to tape stripped skin repeat dose). Tape stripped skin had a slightly higher flux than native skin, but repeat dosing had little effect on the flux for this inhibitor (**Table 5.3**).

Cumulative amount of LY294002 in a DMSO vehicle permeated through Porcine Skin
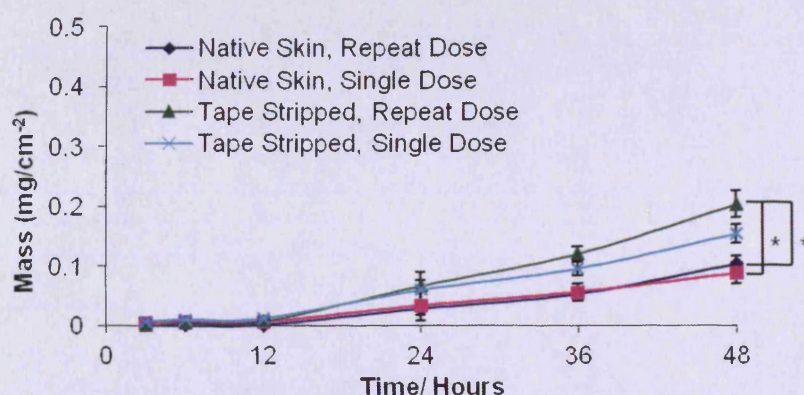
Figure 5.12: Cumulative Permeation of LY294002 in a DMSO vehicle through Porcine Skin. Increased permeation of LY294002 was found with Tape stripped skin compared to native skin. Increased permeation was achieved for both tape stripped and native skin by repeat dosing. Statistical analysis was done by Ordinary ANOVA, Tukey test (* P<0.05). Data expressed as the mean +/- SD for n=3 experiments with 6 replicates for each experiment.

Table 5.3: Mean Flux and Standard Deviation for Permeation of LY294002 in DMSO through Porcine Skin.

	Mean Flux ($\times 10^{-3}$ mg/cm^2/hr)	SD ($\times 10^{-3}$)
Normal (Native) Skin (Repeat Dose)	3.17	0.67
Normal (Native) Skin (Single Dose)	3.45	1.69
Tape Stripped Skin (Repeat Dose)	3.97	0.25
Tape Stripped Skin (Single Dose)	3.97	0.25

221

5.4.1.3.2 Ethanol Vehicle

Tape stripped skin with repeat dosing gave a higher cumulative amount of PD98059 penetration through full thickness porcine skin when using an ethanol vehicle compared to DMSO or fish oil.

Tape stripped skin with a single dose of the inhibitor gave a lower cumulative amount of drug penetration at 48 hours than repeat dosing (**Figure 5.13**). However, at earlier time points the cumulative amount which had permeated the skin was actually higher with a single dose of inhibitor than with repeat dosing. The increase in cumulative amount was greatest at between 12 and 24 hours but then did not seem to increase further between 24 and 48 hours.

Native (intact) skin gave the lowest cumulative amounts of PD98059 penetration at 48 hours with single dosing being 0.1mg cm^{-2} less than for tape stripped skin. The cumulative amount of PD98059 permeation with repeat dosing was also reduced compared to tape stripped skin (0.2 mg cm^{-2} less). Repeat dosing on native skin gave a lower cumulative amount of inhibitor permeation than a single dose after 48 hours (P<0.05 for native skin with single or repeat dosing when compared to tape stripped skin with repeat dosing). Tape stripped skin with repeat dosing gave a higher cumulative amount of LY294002 penetration through full thickness porcine skin when using an ethanol vehicle compared to DMSO or Fish Oil.

Tape stripped skin had nearly twice the flux of native skin and repeat dosing increased the flux over a single dose of PD98059 (**Table 5.4**).

Figure 5.13: Cumulative Permeation of PD98059 in an Ethanol vehicle through Porcine Skin. Tape stripped skin, native skin and single dosing or repeat dosing were compared. Statistical analysis was done by Ordinary ANOVA, Tukey test. * P<0.05. Data expressed as the mean +/- SD for n=3 experiments with 6 replicates for each experiment.

Table 5.4: Mean Flux and Standard Deviation for Permeation of PD98059 in an Ethanol vehicle through Pig Skin

	Mean Flux (x10^{-3} mg/cm^2/hr)	SD (x10^{-3})
Normal (Native) Skin (Repeat Dose)	6.40	1.20
Normal (Native) Skin (Single Dose)	5.60	325
Tape Stripped Skin (Repeat Dose)	10.15	3.96
Tape Stripped Skin (Single Dose)	17.05	1.83

Tape stripped skin with a single dose of LY294002 gave a slightly lower cumulative amount of penetration at 48 hours than repeat dosing (**Figure 5.14**). Single dosing on native skin also gave a lower cumulative amount of penetration than repeat dosing on native skin. Native skin with a single dose of LY294002 gave lower cumulative penetration of the inhibitor than tape stripped (0.2 mg cm^{-2} less) at 48 hours. LY294002 cumulative permeation with repeat dosing was also 0.2mg cm^{-2} less at 48 hours through native skin compared to tape stripped skin.

223

Cumulative amount of LY294002 in an Ethanol vehicle permeated through Porcine Skin
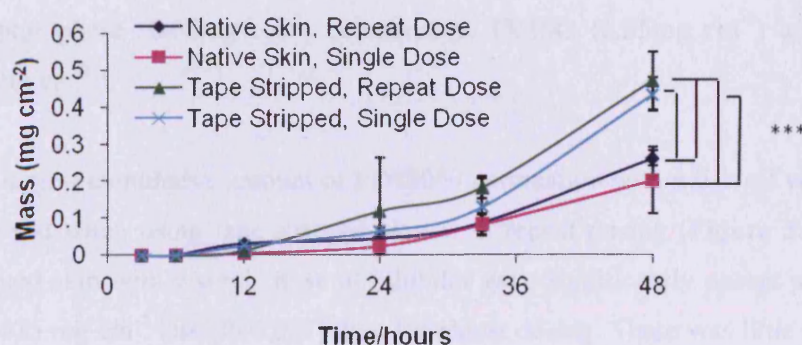
Figure 5.14: Cumulative Permeation of LY294002 in an Ethanol Vehicle through Porcine Skin. Tape stripped skin enabled increased penetration of LY294002 compared to native skin. Repeat dosing gave an increase in penetration for both tape stripped and native skin. Statistical analysis was done by Ordinary ANOVA, Tukey test. *** P<0.001. Data expressed as the mean +/- SD for n=3 experiments with 6 replicates for each experiment.

The rate of transfer of LY294002 diffusing through a unit area of skin (flux) was higher through tape stripped skin than native skin and repeat dosing provided little increase in flux (**Table 5.5**).

Table 5.5: Mean Flux and Standard Deviation for Permeation of LY294002 in an Ethanol vehicle through Porcine Skin.

	Mean Flux ($\times 10^{-3}$ mg/cm^2/hr)	SD ($\times 10^{-3}$)
Normal (Native) Skin (Repeat Dose)	6.23	1.55
Normal (Native) Skin (Single Dose)	9.70	5.90
Tape Stripped Skin (Repeat Dose)	15.13	2.60
Tape Stripped Skin (Single Dose)	15.13	2.61

224

5.4.1.3.3 Fish Oil Vehicle

Fish oil was a much less effective vehicle compared to both DMSO and ethanol, with more than ten times less cumulative amount of PD98059 recovered from the receptor phase (0.06mg cm^{-2}) compared to DMSO (0.25mg cm^{-2}) and ethanol (0.4mg cm^{-2}).

The largest cumulative amount of PD98059 permeation with a fish oil vehicle was achieved when using tape stripped skin with repeat dosing **(Figure 5.15)**. Tape stripped skin with a single dose of inhibitor gave significantly poorer permeation at 0.025 mg cm^{-2} less (P<0.001) than for repeat dosing. There was little difference in cumulative inhibitor permeation between tape stripped and native skin.

Cumulative amount of PD98059 in a Fish Oil vehicle permeated through Porcine Skin
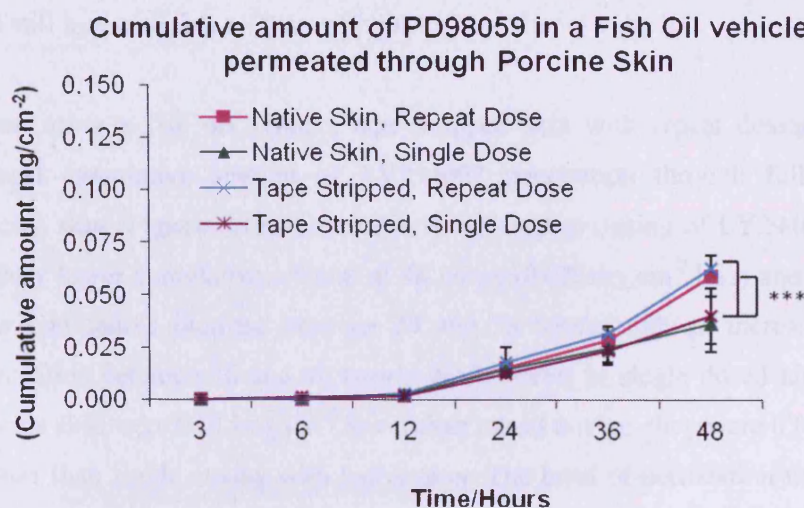
*Figure 5.15: Cumulative Permeation of PD98059 in a Fish Oil Vehicle through Porcine Skin. An increase in permeation was achieved with repeat dosing on both tape stripped and native skin compared to single dosing on both tape stripped and native skin. Statistical analysis was done by Ordinary ANOVA, Tukey test. *** P<0.001. Data expressed as the mean +/- SD for n=3 experiments with 6 replicates for each experiment.*

Tape stripped skin with a single dose of PD98059 had a slightly higher flux than native skin treated with repeat dosing, while tape stripped skin with repeat dosing

225

had a similar flux (**Table 5.6**). Native skin treated with only a single dose of PD98059 had the lowest flux (standard deviation low for this experiment).

Table 5.6: Mean Flux and Standard Deviation for Permeation of PD98059 in a Fish Oil Vehicle through Porcine Skin.

	Mean Flux $(\times 10^{-3}$ mg/cm^2/hr)	SD $(\times 10^{-3})$
Normal (Native) Skin (Repeat Dose)	1.68	0.22
Normal (Native) Skin (Single Dose)	1.00	0.59
Tape Stripped Skin (Repeat Dose)	1.65	0.33
Tape Stripped Skin (Single Dose)	2.20	0.18

LY294002 permeated to a greater extent than PD98059 with a fish oil vehicle (tape stripped, repeat dosing), with a greater flux although its permeation and flux was still less with fish oil than with DMSO or ethanol vehicles.

When using a fish oil vehicle, tape stripped skin with repeat dosing gave the highest cumulative amount of LY294002 penetration through full thickness porcine skin (**Figure 5.16**). Normal skin with repeat dosing of LY294002 gave a slightly lower cumulative amount at 48 hours (0.025mg cm^{-2} less) and also had a slow cumulative increase between 24 and 36 hours, with an increased rate of permeation between 36 and 48 hours. While levels in single dosed tape stripped porcine skin were 0.015mg cm^{-2} lower than repeat dosing, they were 0.050mg cm^{-2} greater than single dosing with native skin. The level of permeation through tape stripped skin treated with a single dose or repeat dosing was significantly higher than single dosing of native (intact) skin (P<0.05).

The greatest cumulative amount of LY294002 (0.125 mg cm^{-2}) permeated through porcine skin with a fish oil vehicle after 48 hours was larger than the cumulative amount of PD98059 (0.062 mg cm^{-2}).
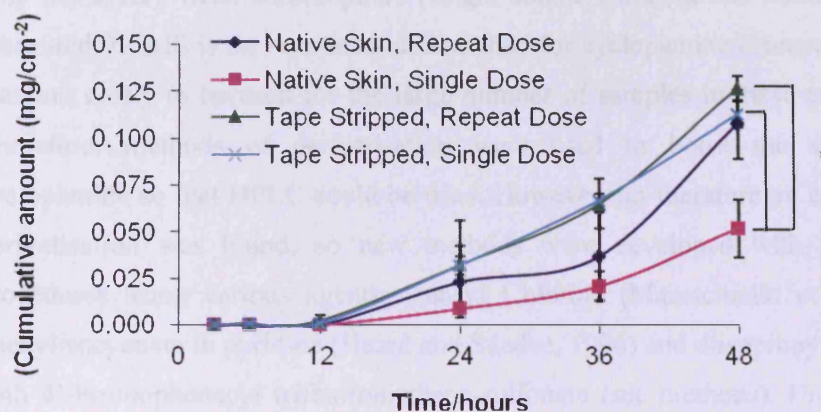
Figure 5.16: Cumulative Permeation of LY294002 in a Fish Oil Vehicle through Porcine Skin. *An increase in penetration was achieved on repeat dosing with both tape stripped and native skin and single dosing on tape stripped skin compared to native skin with a single dose of inhibitors. Statistical analysis was done by Ordinary ANOVA, Tukey test. * P<0.05. Data expressed as the mean +/- SD for n=3 experiments with 6 replicates for each experiment.*

The lowest flux for LY294002 was on normal intact skin with a single dose and both repeat dosing and tape stripping almost doubled the flux (**Table 5.7**). The standard deviation was also low for these experiments. There was a reduction in penetration when using a fish oil vehicle compared to with DMSO or ethanol vehicles.

Table 5.7: Mean Flux and Standard Deviation for Permeation of LY294002 in a Fish Oil vehicle through Porcine Skin.

	Mean Flux (x10^{-3} mg/cm^2/hr)	SD (x10^{-3})
Normal (Native) Skin (Repeat Dose)	4.80	0.35
Normal (Native) Skin (Single Dose)	2.85	0.08
Tape Stripped Skin (Repeat Dose)	4.08	0.070
Tape Stripped Skin (Single Dose)	5.93	0.094

5.4.1.3.4 Cyclopamine

HPLC estimation of drug molecules requires UV detection and as cyclopamine only has a very weak chromophore (single double bond), levels cannot easily be measured. LCMS is the recommended method for cyclopamine estimation but this was too costly to be used for the large number of samples in these experiments. Therefore, methods of derivatisation were used to boost the signal from cyclopamine so that HPLC could be used. However, no literature on cyclopamine derivatisation was found, so new methods were developed with a series of procedures using various agents: Dansyl Chloride (Maraschiello et al., 2003), phenylisocyanate in pyridine (Heard and Suedee, 1996) and diisopropylethylamine with 4'-bromophenacyl trifluoromethane-sulfonate (see methods). Unfortunately, none of these methods were successful in facilitating the UV detection of cyclopamine during HPLC analysis.

This was almost certainly due to unsuccessful conversion of the hydroxyl group present in the structure of cyclopamine by the derivatising moieties. The reasons for this remain unclear, as the secondary OH would have been expected to react with the OH-specific reagents. However, on the grounds of time constraints, no further analysis of cyclopamine was carried out.

5.5 Discussion

The key finding from this study was that both PD98059 and LY294002 successfully permeate through full thickness porcine skin (depth profiling using fish oil, ethanol or DMSO vehicles). This means that permeation-wise these inhibitors would be useful to target aggressive subtypes of BCC which grow down into the dermis. Immunohistochemistry had already been used by Davison and co-workers (2010) to show that PD98059 and LY294002 maintain their activity after penetration of the stratum corneum. These inhibitors have also been found to be compatible and the depth profiling experiments in this study confirmed that they do not inhibit each other's permeation.

Tape stripping as a method of depth profiling has its drawbacks as demonstrated by the keratin distribution in **Figure 5.3** and in the diagram of the skin which shows that the lower epidermal layers follow the line of the rete ridges so tape strips would remove cells from various epidermal layers at once (**Figure 5.2**). It would have been interesting to qualitatively measure the levels of Keratin 10 and Keratin 14 by western blotting when conventional tape stripping was performed in order to confirm the depth of the cells collected on the strips.

As an alternative to tape stripping laser capture micro-dissection was considered. This enables selection of specific cells or areas of cells and removing them by a cutting laser and then a second laser catapults these cells into a tube. Traditionally, these cells would be used for RNA extraction, but it seemed reasonable that this application could be adapted for capturing cells to quantify the amount of drug which had permeated into them, as long as a large enough number of cells could be collected to measure the drugs. This method would allow detailed analysis of penetration into the epidermis, dermis and hair follicle. However, the equipment available was not able to select these specific regions, so traditional tape stripping methods of depth profiling were continued. Although it can be argued that tape stripping is a relatively crude technique, several replicates (6 Franz-type cells for

each sample and 3 repeats for each experiment) were used and this is still the gold-standard experiment for depth-profiling probably because alternatives such as laser dissection are more costly and time consuming.

Depth profiling was carried out using a methanol vehicle for the inhibitors (LY294002 and PD98059) because this represents maximal penetration to show whether these inhibitors were capable of penetrating through the epidermis into the living cells below. The results showed that approximately one third of each inhibitor retrieved remained on the top layer of skin after the excess was gently removed with a cotton bud. The inhibitors remaining on the surface were unable to penetrate the stratum corneum possibly due to saturation but also because the stratum corneum is the protective upper layer of the skin which prevents penetration. Approximately one third of the inhibitors were retained within the epidermis and one third penetrated the remaining epidermis and dermis where they were then retained. This is a very positive result because LY294002 and PD98059 are able to penetrate to the site of aggressive BCCs (throughout full thickness skin), but they were also retained in the skin so they would be able to act on BCC as long as MEK/ERK and PI3K/AKT signalling is activated. However, less than 1% of each inhibitor applied was retrieved from full thickness skin, this may be problematic in terms of side effects such as irritation on the skin surface where the inhibitor remained, but this depends on the required quantities of each inhibitor, which would be determined by tests on BCC cell culture models such as those discussed in Chapter 3. The inhibitors penetrated the full thickness of the skin and into the receptor phase below, so the levels reaching the systemic circulation are equally important because they may cause side effects. LY294002 penetrated to a lesser extent than PD98059 and LY294002 also retarded penetration of PD98059 and PD98059 slightly retarded penetration of LY294002. This means that the quantity of inhibitors to be used in a topical formulation would require further consideration after testing their efficacy on cell culture models.

DMSO and ethanol represented the maximal possible penetration of LY294002 and PD98059 through intact skin because they are potent penetration enhancers. However, as shown by Davison and co-workers DMSO causes delamination of the stratum corneum and denucleation in the epidermis (Davison et al., 2008a). Ethanol also permeated full thickness skin quickly, with the risk of partitioning the drugs into the systemic circulation. Fish oil gave a much lower flux for permeation of both inhibitors with a steady state flux of 0.00168 for PD98059 compared to 0.00455 for DMSO (normal skin repeat dose), but would be useful as a vehicle due to its safety. Fish oil permeation characteristics as a vehicle could be improved by the addition of enhancers such as 1, 8-cineole, ethanol or DMSO (in small amounts to reduce the deleterious effect on the stratum corneum). As cyclopamine is most soluble in ethanol and DMSO, one or both of these in combination with fish oil would make a useful vehicle. The concentrations of PD98059 and LY294002 can be increased in this sort of vehicle because they are very soluble in fish oil, although cyclopamine is not. The quantity of each drug needed would rely upon testing on a cell model.

It is clear from this study that ethanol and DMSO both disrupt the stratum corneum (the skin's main barrier) enabling increased penetration of the inhibitors, as shown in published data (Oh et al., 2003; Williams, 2003). According to the results of this study, ethanol doesn't have such a disruptive effect on the stratum corneum barrier as DMSO but still behaves as an enhancing vehicle. Tape stripping the upper surface of the skin also disrupted the stratum corneum, increasing the flux of inhibitors and the cumulative amount of permeation, particularly for fish oil which does not damage the stratum corneum. Increased percutaneous absorption through damaged stratum corneum has already been demonstrated (Bronaugh and Stewart. 1985). These results are important because inhibitor penetration into BCCs, which already have disrupted barrier function, will be increased compared to BCCs with an intact stratum corneum. Where the stratum corneum is intact enhancers will be required in the formulation (such as ethanol or DMSO) to increase drug permeation. Also, an increased mass of drug or

repeat dosing (which was shown to increase cumulative amount of inhibitors permeated) will be required to increase the mass of inhibitors that permeate.

Due to the skin drying effect of ethanol and the toxicity of DMSO, only very small amounts should be used or alternative enhancers which cause fewer side effects should be sought. Occlusion (by use of a patch) may also be used to increase permeation by reducing transepidermal water loss. Water has been shown to increase permeation of hydrophilic and lipophilic molecules through the skin by increasing stratum corneum water content, although the mechanism of action for lipophilic molecules remains unclear. This would also protect the area from contact which may rub the formulation off the skin. Commercial examples of successful occlusion include nicotine patches and occlusive dressings for Lignocaine and Prilocane cream for increased speed of anaesthesia (Williams, 2004; Benson, 2005). Alternatively, to avoid too much PD98059 and LY294002 reaching the systemic circulation, penetration retarders such as some DMSO derivatives (not all DMSO derivatives act as permeation enhancers, some are in fact retarders to skin permeation) may be added to the topical formulation (Benson, 2005).

Research groups have focussed on designing methods to bypass the stratum corneum in order to increase penetration. These include using microneedles to make holes in the stratum corneum but reaching nerves in the living epidermis must be avoided to prevent and causing pain (Haq et al., 2009). These holes in the stratum corneum enable increased permeation in a similar way to the tape stripping method used in this study. Therefore, microneedles may be a useful method for delivery of drugs to BCCs in order to enable the same formulation to be used on all BCCs regardless of the level of stratum corneum disruption. This is may be unnecessary for the EGF signalling inhibitors, LY294002 and PD98059 which penetrated the skin well. However, only a small percentage of PD98059 or LY294002 (MEK and PI3K inhibitors) penetrated the skin, so a large amount would remain in the topical formulation on top of the stratum corneum rather than

entering the skin, smaller amounts of inhibitor could be applied using microneedles. If an excess of these inhibitors is left on the skin surface there may be side effects (such as irritation) caused because EGF signalling affects healthy keratinocytes as well as carcinoma cells. Microneedles would be a useful method of delivery for cyclopamine or its derivatives which suffer from poorer solubility and therefore only poorly penetrate the intact stratum corneum.

Various studies for transcutaneous drug delivery have been carried out using assorted skin types and even skin equivalents such as graftskin™, a human living skin equivalent and Skinethic™, a human reconstructed epidermis. Pig skin has been shown to be a good model for human skin, is cost effective and easy to obtain (Schmook et al., 2001). A major problem is maintenance of skin viability for the duration of drug permeation experiments. The skin was less viable towards the end of the experiments, so to overcome this it would be useful to use a growth medium as the receptor phase in the Franz type cells. However, the inhibitors would need to be soluble in growth medium. It would also be beneficial eventually to confirm the findings on porcine skin by testing the penetration of inhibitors for this study in an appropriate formulation on human skin, which can be obtained from surgery after ethical approval has been obtained.

PD98059 was chosen because it inhibits MEK1 phosphorylation, activation of the MEK/ERK branch of the EGF pathway (Chapter 3). An alternative would be UO126, which could be used in parallel for cell experiments on a BCC culture model to confirm the results of PD98059. LY294002 is specific for PI3K, an alternative inhibitor of PI3K would be Wortmannin. However, Wortmannin is a less specific inhibitor, but could be used to confirm experimental data in cell culture prior to development of a topical formulation for LY294002.

Cyclopamine is a teratogen and possible carcinogen so it is desirable to use an alternative to reduce toxicity. Several dietary alkaloids with structural similarity to cyclopamine have been identified as weak inhibitors of SHH signalling (Lipinski

et al., 2007). It has been shown that solanidine, solasodine and tomatidine are all able to reduce PTCH expression to unstimulated levels in cells treated with recombinant SHH. Although cyclopamine is more potent, tomatidine was the most potent of these derivatives (100 times less potent than cyclopamine; Lipinski et al., 2007). During this study alternative cyclopamine derivatives became available which have more suitable characteristics for use in a topical formulation including reduced toxicity and increased solubility. GDC-0449, BMS-833923/XL139, CUR-61414 and IPI-926 are currently in clinical trials for the treatment of BCC or other carcinomas which have activated SHH signalling. Furthermore, GDC-0449 has been shown to induce tumour regression in medulloblastoma (Robarge et al., 2009; Toftgard and Tegund, 2010).

Cyclopamine (SMO inhibitor) has a weak chromophore and is also very hard to measure by HPLC so alternatives such as BODIPY-cyclopamine (a fluorescent derivative) would be useful for future studies, although alternative SMO inhibitors may also be easier to assess (Chen et al., 2002b). A SMO inhibitor would be useful in a topical formulation for treating BCCs, because this would inhibit the majority of the signalling pathway (there may be important interactions with other signalling pathways between SMO and the GLIs which we are currently not aware of). GLI inhibitors such as GANT61 and HPI-1, 2, 3, 4 would only be useful if we could be sure that the SHH pathway has no upstream interactions with other signalling pathways such as the EGF pathways (Toftgard and Tegund, 2010).

In future, it may also be useful to conduct drug permeation through full thickness skin using a BCC cell model such as that described in Chapter 3. This would confirm that the inhibitors could successfully penetrate full thickness skin and still inhibit invasive tumour growth deeper in the subcutaneous layer. This is important because although the amount of permeated drug in the receptor phase is measurable, it may not all be active due to the damaging effects of skin enzymes. Although Davison et al. (2010) did previously show maintenance of activity, it is not known whether the total amount of permeants remain active. A foreseeable difficulty with this method is that porcine skin, although cleaned with the transport

234

buffer solution, before permeation experiments, would still be colonised by micro-organisms. Furthermore, microbial contamination must be avoided in any cell culture experiments. Harsher cleaning methods (with alcohols) would disrupt the stratum corneum thus artificially increasing permeation. To overcome this, 0.22µm cyclopore track etched membrane or a filter insert would be used to separate the skin from the cell culture medium beneath. A benefit of this approach is that the cell culture medium should maintain porcine skin viability for longer than the cetrimide receptor phase used in this study. Another option to prevent microbial infection would be to include antibiotics (penicillin and/or streptomycin) in the cell culture medium.

The cells could be grown on a glass coverslip in the base of a Franz type diffusion cell or in a multi-well plate using a filter insert to separate the skin from the cells. This would be simple if only a monolayer of keratinocytes were required but to do this using a co-culture of keratinocytes (at the air liquid interface) and fibroblasts would be much more complex. Fibroblasts could be grown on a glass coverslip in the base of the receptor phase of a Franz type cell, with keratinocytes in a filter insert (also in the receptor compartment), but grown at the air: liquid interface for 10 days to allow stratification and cilia formation. Then the skin (on top of a 0.22 µm cyclopore track etched membrane) and donor compartment could be clamped on top and the medium in the receptor phase increased to cover the keratinocytes and reach the underside of the skin. Finally the inhibitors would be applied to the donor phase. However, there are lots of potential problems that could arise so this method would require rigorous optimisation. This idea was developed from work previously carried out in the laboratory, where it has was shown that MCF-7 breast cancer cells could be grown successfully in the base of the receptor phase of a Franz-type diffusion cell (Davison et al., 2010). Treated plastic flasks are usually used for growing cells *in vitro*. However, the keratinocytes and fibroblast cell lines used were successfully grown on glass coverslips for immunofluoresence work. In a previous study using MCF-7 cells, it is thought that cleaning the Franz-type

diffusion cells with Decon 90 caused etching of the glass surface making the glass rough, enabling the cells to successfully adhere.

Additional experiments are needed to ascertain the mass of each inhibitor required for an efficacious BCC treatment and to determine the therapeutic window for safe administration prior to further development of the delivery formulation. Initially, this would involve further development of the *in vitro* BCC cell model with keratinocytes able to stratify in which SHH and EGF signalling could both be successfully activated enabling tumour down-growth to be visualised. Inhibitors to the SHH and EGF pathways would be added to the cell growth medium to discover whether they prevent growth of the SHH expressing 'tumour' cells or cause them to regress. If SHH-expressing cell death occurred, further permeation studies could be carried out leading to the development of a formulation which could be applied topically to carry these drugs to their site of action without permeating into the systemic circulation.

Conclusions

- PD98059 and LY294002 successfully penetrate and permeate full thickness skin.
- Ethanol and DMSO vehicles enable the fastest permeation for PD98059 and LY294002 because they disrupt the stratum corneum, retardation may be required to prevent these inhibitors entering the systemic circulation.
- An alternative to cyclopamine is required to inhibit the SHH pathway due to its toxicity, lack of solubility and the challenges it presented in its analysis.

Chapter 6

General Discussion

6.1 General Discussion

The original hypothesis stated that EGF signalling might interact with SHH signalling and cause augmentation of some SHH target genes. This could have occurred via either branch (MEK/ERK or PI3K/AKT) of the EGF signalling pathway. It was hypothesised that the interaction between EGF and SHH signalling might increase the invasiveness of BCCs and therefore contribute directly to the more invasive subtypes (nodular and morpheaform). These types of BCC are currently treated by surgical removal, which is both costly and time consuming, so any efficacious therapy that could reduce the onset of these types of BCC would be beneficial.

In order to test a combination therapy using an inhibitor of the EGF pathway and together with an inhibitor of SHH signalling (at the level of smoothened), both pathways needed to be active in keratinocyte cell lines. Attempts to activate the SHH signalling pathway by the addition of recombinant SHH protein to the cells or by insertion of an SHH gene into the nucleus of the cells was not very successful. The current research identified that SHH pathway activation required culture conditions that would allow primary cilium formation and this required paracrine signalling. Primary cilia can be induced in cultured cells by growth arrest (induced by starvation due to an absence of serum in the medium). The SEM data presented showed that approximately 10% of cultured cells had cilia under the conditions used, a positive step forward towards achieving SHH signalling in keratinocyte cell lines. However, higher levels of ciliation is required and further efforts should be made to increase the levels of cilia (possibly by longer growth arrest) in order to achieve improved SHH signalling in culture. Testing the original hypothesis requires that SHH and EGF signalling operate at reasonable levels simultaneously and this would allow comparison of the levels of downstream gene expression in the presence and absence of EGF.

If the lack of a cellular response to SHH is due partially or fully to the absence or reduction in numbers of cilia on cultured cells, it could be proposed that primary cilia would be a particularly good target option for therapy. However, it is likely that this is a general mechanism so targeted therapies may well affect other signal transduction pathways that rely on this structure (widespread in the epidermis and hair follicle). This would potentially cause side effects due to a more widespread action than intended so systemic affects cannot be ruled out. In addition, when BCCs were examined directly, only 3 out of 8 had primary cilia (Wong et al, 2009) so these structures may not be as widespread as indicated, which may limit the effectiveness of cilia inhibitors. It was also suggested that mutations in RAS, an effector molecule in the EGF pathway, might somehow facilitates SHH signalling in the absence of cilia, so GLI inhibitors may be more useful in such cases (see Wong et al., 2009). Development of GLI inhibitors is currently in progress (Teglund and Toftgard, 2010) but this also has the disadvantage of targeting a downstream molecule and therefore upstream effects which would not be inhibited (Jenkins, 2009).

Thus, at his point in time, the role of EGF signalling in the development of BCCs is still unclear. Immunohistochemistry comparison of EGF signalling in nodular, micronodular, morpheaform and mixed morphology BCCs concluded that EGFR signalling was not responsible for the differences between nodular and morpheaform subtypes. Also the reduced levels of p-ERK and p-AKT expression found in BCCs does not agree with previous work that has already demonstrated that components of the EGF pathway are important for augmentation of SHH signalling (Bigelow et al., 2005; Kasper et al., 2006). In addition, other cancers that involve SHH pathway activation (such as squamous cell carcinoma and medulloblastoma) also have highly active EGF pathway signalling. In particular, medulloblastomas have increased expression of PI3K/AKT and MEK/ERK indicating that both arms of the EGF pathway are active (Baryawno et al., 2010; Wlodarski et al., 2008). Thus, EGF pathway inhibitors such as PD98059 and LY294002 might be useful for treating these cancers. However, further work

should be carried out to confirm that the low levels of EGF pathway components in BCCs are not contributing to tumour growth. Work in this thesis has shown that PD98059 and LY294002 are able to permeate the skin and are reasonable EGF pathway inhibitors but if levels of EGF signalling are low in BCC, it may not be necessary to combine them with a SMO inhibitor for treating BCCs.

Published microarray data has suggested that RAS (downstream part of the EGF signalling pathway) is activated in BCCs, which agrees with previously published work (Wong et al., 2009; Yu et al., 2008). It is also apparent form the work done by this group that other signalling pathways may be involved in BCC development. In particular, Wnt and Bcl-2 expression, which are important in apoptosis and increased β-catenin levels that have been found to be increased in the nuclei of morpheaform cells (Yu et al., 2008). Thus, further research into the influence of other signalling pathways on BCC development would be very important in order to develop the most appropriate topical formulations.

Finally, inhibitors of the MEK/ERK and PI3K/AKT arms of the EGF pathway were tested for their ability to permeate full thickness skin. Both PD98059 and LY294002 successfully penetrated the skin and were retrieved from the receptor phase in laboratory experiments. As small molecule inhibitors easily penetrate the skin, they make ideal candidates for treating BCC, but this depends upon the action of EGF signalling (particularly PI3K/AKT and MEK/ERK pathways) in these tumours. Although cyclopamine inhibits SHH signalling, it is toxic and not easy to measure so it would not be useful in a topical formulation. However, more soluble and less toxic derivatives are now becoming available and should be considered for future development of a topical formulation for BCCs. These would have to be tested for their ability to permeate full thickness skin, and for their effects on a BCC cell line in which SHH signalling can successfully be activated.

In conclusion, while it seems that EGF is capable of modulating SHH signalling, this pathway may not be important in BCC development, although further work

240

should be done to confirm this. A cyclopamine derivative or another inhibitor of smoothened is likely to be useful for a formulation to treat most BCCs. Further work needs to be carried out in order to determine whether combination treatments blocking other signalling pathways would have an added benefit in BCCs. It would also be useful to develop a BCC cell model that can be activated by recombinant SHH would be ideal to test these therapeutic options.

Another alternative to topical formulations for the treatment of BCCs which does not directly involve inhibition of signalling pathways is photodynamic therapy. It has been shown to be a useful non-invasive treatment for BCC. This therapy uses light sensitive cream, which in the presence of intense visible laser light causes cancer cells to die by the creation of reactive oxygen species. Until recently this therapy has only been effective on superficial BCC due to the limited penetration of the active chemical (aminolevulinate). However, now that alternatives such as methyl aminolevulinate are available, which are thought to penetrate through the skin much further, this type of therapy is generating a lot of interest (Foley *et al.*, 2009). Currently, photodynamic therapy is being tested in clinical trials, but even if found to be effective, this requires patients to undergo treatment in a clinical setting whereas the development of an effective topical formulation that could inhibit cellular signalling would be a useful alternative as treatment could be easily carried out at home and without the need of a health professional to administer.

References

Adolphe, C., Hetherington, R., Ellis, T., and Wainwright, B. (2006). Patched1 functions as a gatekeeper by promoting cell cycle progression. Cancer Res *66*, 2081-2088.

Adolphe, C., Narang, M., Ellis, T., Wicking, C., Kaur, P., and Wainwright, B. (2004). An in vivo comparative study of sonic, desert and Indian hedgehog reveals that hedgehog pathway activity regulates epidermal stem cell homeostasis. Development *131*, 5009-5019.

Ahmadian, A., Ren, Z., Williams, C., Ponten, F., Odeberg, J., Ponten, J., Uhlen, M., and Lundeberg, J. (1998). Genetic instability in the 9q22.3 region is a late event in the development of squamous cell carcinoma. Oncogene *17*, 1837-1843.

Alessi, D., Cuenda, A., Cohen, P., Dudley, D., and Saltiel, A. (1995). PD 098059 is a specific inhibitor of the activation of mitogen-activated protein kinase kinase in vitro and in vivo. J Biol Chem. *270*, 27489-27494.

Alonso, L., and Fuchs, E. (2006). The hair cycle. J Cell Sci *119*, 391-393.

American Academy of Family Physicians. (2004). Diagnosis and treatment of basal cell and squamous cell carcinomas. <http:www.aafp.org/afp/2004/1015/p1481.html.> (accessed 2004).

Ansarin, H., Daliri, M and Soltani-Arabchahi, R (2006) Expression of p53 in aggressive and non-aggressive histologic variants of basal cell carcinoma. Eur J Dermatol. *16*, 543-7.

Aszterbaum M, Rothman, A., Johnson, L. Fisher, M., Jingwu Xie, Bonifas, J., Xioli Zhang, Scott, M. Epstein Jr, E (1998). Identification of mutations in the human *PATCHED* gene in sporadic basal cell carcinomas and in patients with the basal cell nevus syndrome. J Invest Dermatol. *110*, 885 - 887.

Athar, M., Tang, X., Lee, J. L., Kopelovich, L., and Kim, A. L. (2006). Hedgehog signalling in skin development and cancer. Exp Dermatol. *15*, 667-677.

Bai, C., Auerbach, W., Lee, J., Stephen, D and Joyner, A. (2002). Gli2, but not Gli1, is required for initial Shh signaling and ectopic activation of the Shh pathway. Development *129*, 4753-61.

Bailey, J., Mohr, M and Hollingsworth.M. (2009). Sonic hedgehog paracrine signaling regulates metastasis and lymphangiogenesis in pancreatic cancer. Oncogene *28*, 3513-25.

Bartzatt, R. (2001a). Dansylation of hydroxyl and carboxylic acid functional groups. J Biochem Biophys Methods *47*, 189-195.

Bartzatt, R. (2001b). Fluorescent labeling of drugs and simple organic compounds containing amine functional groups, utilizing dansyl chloride in Na(2)CO(3) buffer. J Pharmacol Toxicol Methods *45*, 247-253.

Baryawno, N., Sveinbjornsson, B., Eksborg, S., Chen, C.S., Kogner, P., and Johnsen, J.I. (2010) Small-molecule inhibitors of phosphatidylinositol 3-kinase/AKT signaling inhibit Wnt/beta-catenin pathway cross-talk and suppress medulloblastoma growth. Cancer Res. *70*, 266-276.

Bastiaens, M.T., Hoefnagel, J.J., Bruijn, J.A., Westendorp, R.G., Vermeer, B.J., and Bouwes Bavinck, J.N. (1998). Differences in age, site distribution, and sex between nodular and superficial basal cell carcinoma indicate different types of tumors. J Invest Dermatol. *110*, 880-884.

Beddis, I.R., Mott, M.G., and Bullimore, J. (1983). Case report: nasopharyngeal rhabdomyosarcoma and Gorlin's naevoid basal cell carcinoma syndrome. Med Pediatr Oncol. *11*, 178-179.

Benson, H.A.E. (2005). Transdermal Drug Delivery: Penetration Enhancement Techniques. Current Drug Delivery *2*, 23-33.

Biesecker, L.G. (1997). Strike three for GLI3. Nat Genet *17*, 259-260.

Bigelow, R.L., Jen, E.Y., Delehedde, M., Chari, N.S., and McDonnell, T.J. (2005). Sonic hedgehog induces epidermal growth factor dependent matrix infiltration in HaCaT keratinocytes. J Invest Dermatol. *124*, 457-465.

Blanpain, C., and Fuchs, E. (2006). Epidermal stem cells of the skin. Annu Rev Cell Dev Biol. *22*, 339-373.

Bodak, N., Quielle, S., Avril, M, Bouadar, B., Drougard, C., Sarasin, A and Daya-Grosjean, L. (1999). High levels of patched gene mutations in basal-cell carcinomas from patients with xeroderma pigmentosum. Proc Natl Acad Sci U S A. *96*, 5117-22.

Bonnet, C.S., Aldred, M., von Ruhland, C., Harris, R., Sandford, R., and Cheadle, J.P. (2009). Defects in cell polarity underlie TSC and ADPKD-associated cystogenesis. Hum Mol Genet. *18*, 2166-2176.

Boukamp, P., Petrussevska, R.T., Breitkreutz, D., Hornung, J., Markham, A., and Fusenig, N.E. (1988). Normal keratinization in a spontaneously immortalized aneuploid human keratinocyte cell line. J Cell Biol. *106*, 761-771.

Bowden, P.E., Stark, H., Breitkreutz, D and Fusenig, N. (1987) Expression and modification of keratins during terminal differentiation of mammalian epidermis. Curr Top Dev Biol. *22*, 35-68.

Bowden, P.E. (1993). Characterization of a human type-I keratin gene-cluster. J Invest Dermatol. *100*, 441-441.

Boylan, M., van den Berg, H.W., and Lynch, M. (1998). The anti-proliferative effect of suramin towards tamoxifen-sensitive and resistant human breast cancer cell lines in relation to expression of receptors for epidermal growth factor and insulin-like growth factor-I: growth stimulation in the presence of tamoxifen. Ann Oncol. *9*, 205-211.

Bronaugh, R.L., Stewart, R.F. (1985). Methods for in vitro percutaneous absorption studies V: Permeation through damaged skin. J Pharm Sci. *74*, 1062-6

Burke, R., Nellen, D., Bellotto, M., Hafen, E., Senti, K.A., Dickson, B.J., and Basler, K. (1999). Dispatched, a novel sterol-sensing domain protein dedicated to the release of cholesterol-modified hedgehog from signaling cells. Cell *99*, 803-815.

Cain, R. J., and Ridley, A. J. (2009). Phosphoinositide 3-kinases in cell migration. Biol Cell. *101*, 13-29.

Candi, E., Schmidt, R., and Melino, G. (2005). The cornified envelope: a model of cell death in the skin. Nat Rev Mol Cell Biol. *6*, 328-340.

Chang, Y. C., Madkan, V., Cook-Norris, R., Sra, K., and Tyring, S. (2005). Current and potential uses of imiquimod. South Med J. *98*, 914-920.

Chen, J. K., Taipale, J., Cooper, M. K., and Beachy, P. A. (2002a). Inhibition of Hedgehog signaling by direct binding of cyclopamine to Smoothened. Genes Dev. *16*, 2743-2748.

Chen, J. K., Taipale, J., Young, K. E., Maiti, T., and Beachy, P. A. (2002b). Small molecule modulation of Smoothened activity. Proc Natl Acad Sci USA. *99*, 14071-14076.

Chiang, C., Swan, R. Z., Grachtchouk, M., Bolinger, M., Litingtung, Y., Robertson, E. K., Cooper, M. K., Gaffield, W., Westphal, H., Beachy, P. A., and Dlugosz, A. A. (1999). Essential role for Sonic hedgehog during hair follicle morphogenesis. Dev Biol. *205*, 1-9.

Cho, K. H., Baek, S., and Sung, M. H. (2006). Wnt pathway mutations selected by optimal beta-catenin signaling for tumorigenesis. FEBS Lett. *580*, 3665-3670.

245

Clement, C., Kristensen, S., Mollgard, K., Pazour, G., Yoder, B., Larsen, L and Christensen, S. (2009). The primary cilium coordinates early cardiogenesis and hedgehog signaling in cardiomyocyte differentiation. J Cell Sci. *122*, 3070-82.

Cohen, M. M., Jr. (2003). The hedgehog signaling network. Am J Med Genet A. *123A*, 5-28.

Cooper and Hausman (1998) Cooper, G and Hausman, R. (2006). The Cell: A Molecular Approach 4th ed. Amer. Soc. Microbiol., Washington and Sinauer Assoc., Sunderland, MA.

Couvet-Privat, S., Bouadjar, B., Avril, M., Sarasin, A and Daya-Grosjean, L. (2002). Significantly high levels of ultraviolet-specific mutations in the smoothened gene in basal cell carcinomas from DNA repair-deficient xeroderma pigmentosum patients. Cancer Res. *62*, 7186-9.

Crowson et al. (2006). Basal cell carcinoma: biology, morphology and clinical implications. Review Modern Pathology *19*, 127-47.

Dahmane, N., Lee, J., Robins, P., Heller, P., and Ruiz i Altaba, A. (1997). Activation of the transcription factor Gli1 and the Sonic hedgehog signalling pathway in skin tumours. Nature *389*, 876-881.

Davies, J., Chen, F,W., and Ioannou,Y. (2000). Transmembrane molecular pump activity of Niemann-Pick C1 protein. Science *5500*, 2295–2298.

Davison, Z. (2008) Transcutaneous delivery of anti-breast cancer agents, PhD thesis, Cardiff University, Cardiff.

Davison, Z., Dutkowski, C., Gee, J. M., Nicholson, R. I., and Heard, C. M. (2008). In vitro effects on MCF-7 breast cancer cells of signal transduction inhibitor/tamoxifen/eicosapentaenoic acid combinations and their simultaneous delivery across skin. Pharm Res. *25*, 2516-2525.

Daya-Grosjean, L and Sarasin, A. (2000). UV-specific mutations of the human patched gene in basal cell carcinomas from normal individuals and xeroderma pigmentosum patients. Mutat Res. *450*, 193-9.

Daya-Grosjean, L., and Couve-Privat, S. (2005). Sonic hedgehog signaling in basal cell carcinomas. Cancer Lett. *225*, 181-192.

Dessaud, E., Yang, L., Hill, K., Cox, B., Ulloa, F., Ribeiro, A., Mynett, A., Novitch, B and Briscoe, J. (2007). Interpretation of the sonic hedgehog morphogen gradient by a temporal adaptation mechanism. Nature *450*, 717-20.

Diagnosis and Treatment of basal cell and squamous cell carcinomas. (www.aafp.org/afp/2004/1015/p1481.html, diagnosis and treatment of basal cell and squamous carcinomas, American academy of family physicians. (accessed 2004).

Dick, I. P. and Scott, R. C. (1992). Pig ear skin as an in-vitro model for human skin permeability. J. Pharm. Pharmacol. *44*, 640-645.

Dickson, M. A., Hahn, W. C., Ino, Y., Ronfard, V., Wu, J. Y., Weinberg, R. A., Louis, D. N., Li, F. P., and Rheinwald, J. G. (2000). Human keratinocytes that express hTERT and also bypass a p16(INK4a)-enforced mechanism that limits life span become immortal yet retain normal growth and differentiation characteristics. Mol Cell Biol. *20*, 1436-1447.

DiSanto, S., Abt, A. B., Boal, D. K., and Krummel, T. M. (1992). Fetal rhabdomyoma and nevoid basal cell carcinoma syndrome. Pediatr Pathol. *12*, 441-447.

Dudley, D. T., Pang, L., Decker, S. J., Bridges, A. J., and Saltiel, A. R. (1995). A synthetic inhibitor of the mitogen-activated protein kinase cascade. Proc Natl Acad Sci USA. *92*, 7686-7689.

Eggenschwiler, J and Anderson, K (2007). Cilia and developmental signaling. Annu Rev Cell Dev Biol. *23*, 345-73.

Ellis, M. (2004). Overcoming endocrine therapy resistance by signal transduction inhibition. Oncologist *9*, 20-26.

Erez, A., Ilan, T., Amariglio, N., Muler, I., Brok-Simoni, F., Rechavi, G., and Izraeli, S. (2002). GLI3 is not mutated commonly in sporadic medulloblastomas. Cancer *95*, 28-31.

Fan, H., and Khavari, P. A. (1999). Sonic hedgehog opposes epithelial cell cycle arrest. J Cell Biol. *147*, 71-76.

Fan, H., Oro, A. E., Scott, M. P., and Khavari, P. A. (1997). Induction of basal cell carcinoma features in transgenic human skin expressing sonic hedgehog. Nat Med. *3*, 788-792.

Feldman, J. Geimer, S and Marshall, W. (2007). The mother centriole plays an instructive role in defining cell geometry. PLoS Biol. *6*, 149.

Franklin, C and Kraft, A. (1992). Protein kinase C-independent activation of c-jun and c-fos transcription by epidermal growth factor. Biochim Biophys Acta. 1134, 137-42.

Filippakopoulos, P., Müller, S and Knapp, S. SH2 domains: modulators of nonreceptor tyrosine kinase activity. Curr Opin Struct Biol. *19*, 643-9.

Foley, P., Freeman, M., Menter, A., Siller, G., El-Azhary, R. A., Gebauer, K., Lowe, N. J., Jarratt, M. T., Murrell, D. F., Rich, P., *et al.* (2009). Photodynamic therapy with methyl aminolevulinate for primary nodular basal cell carcinoma: results of two randomized studies. Int J Dermatol. *48*, 1236-1245.

Franz, T. J. (1975). Percutaneous absorption-on the relevance of in vitro data. J Invest Dermatol. *64*, 190–195.

Fuchs E (2008) Skin Stem Cells: rising to the surface. J Cell Biology Bol. *180*, 273

Gailani, M and Bale, A. (1997). Developmental genes and cancer: role of patched in basal cell carcinoma of the skin. J Natl Cancer Inst. *89*, 1103-9.

Gailani, M., Stahle-Backdahl, M., Leffell, DJ., Glynn, M., Zaphiropoulos, PG., Pressman, C., Unden, AB., Dean, M., Brash, DE., Bale, AE., Toftgard, R. The role of the human homologue of Drosophila patched in sporadic basal cell carcinomas. Nature Genetics *14*.

Goodrich, L., Milenkovic, L, Higgins, K and Scott, M. (1997). Altered neural cell fates and medulloblastoma in mouse patched mutants. Science *277*, 1109-13.

Grachtchouk, M., Mo, R., Yu, S., Zhang, X., Sasaki, H, Hui, C and Dlugosz, A. (2000). Basal cell carcinomas in mice overexpressing Gli2 in skin. Nat Genet. *24*, 216-7.

Graham-Brown, R.A.C. and Burns, D.A. (2007). Lecture Notes on Dermatology. 4th ed. Blackwell Publishing.

Hahn, H., Wicking, C., Zaphiropoulous, P., Gailani, M., Shanley, S., Chidambaram, A., Vorechovsky, I., Holmberg, E., Unden, A., Gillies, S., *et al.* (1996). Mutations of the human homolog of Drosophila patched in the nevoid basal cell carcinoma syndrome. Cell *85*, 841-851.

Han, Y., Kwok, B and Kernan, M. (2003). Intraflagellar transport is required in Drosophila to differentiate sensory cilia but not sperm. Curr Biol. *13*, 1679-86.

248

Haq, MI., Smith, E., John, D. N., Kalavala, M., Edwards, C., Anstey, A., Morrissey, A. and Birchall, J. C. (2009). Clinical administration of microneedles: skin puncture, pain and sensation. Biomed Microdevices *11*, 35-47.

Hardy, M (1992). The Secret Life of the Hair Follicle. Trends in Genetics. *8*, 55-56.

Hardy,K., Booth, B., Hendrix, M., Salomon, D and Strizzi, L.(2010). ErbB/EGF signaling and EMT in mammary development and breast cancer. J Mammary Gland Biol Neoplasia. *15*, 191-9

Harries, M., and Smith, I. (2002). The development and clinical use of trastuzumab (Herceptin). Endocr Relat Cancer *9*, 75-85.

Hatfield, R. M. and Fung, L. W. M. (1995). Molecular Properties of a Stratum Corneum Model Lipid System:Large Unilamellar Vesicles. Biophysical Journal *68*, 196-207.

Hausman, C.A. (2004). The Cell: A Molecular Approach: ASM Press).

Hawkins, G. S and Reifenrath, W. G. (1986). Influence of skin source, penetration cell fluid, and partition coefficient on in vitro skin penetration. J. Pharm. Sci. *75*, 378-381.

Haycraft, C., Banizs, B., Aydin-Son, Y., Zhang, Q., Michaud, E and Yoder, B. (2005) Gli2 and Gli3 localize to cilia and require the intraflagellar transport protein polaris for processing and function. PLoS Genet. *1(4)*.

Heard, C. M., and Suedee, R. (1996). Stereoselective adsorption and trans-membrane transfer of propranolol enantiomers using cellulose derivatives. International Journal of Pharmaceutics *139*, 15-23.

Heard, C. M., Harwood, J. L., Maguire, P., McNaughton, G., and Pugh, W. J. (2002). Simultaneous penetration of NSAID and essential fatty acid esters as a dual-action anti-arthritis therapy. In: Perspectives in Percutaneous Penetration, Vol 8a (Cardiff: STS Publishing).

Henson, E., Johnston, J., Los. M and Gibson, S. (2007) Clinical activities of the epidermal growth factor receptor family inhibitors in breast cancer. Biologics. *1*, 229-39.

Henson, E. S., and Gibson, S. B. (2006). Surviving cell death through epidermal growth factor (EGF) signal transduction pathways: implications for cancer therapy. Cell Signal *18*, 2089-2097.

Hu, Z., Bonifas, J. M., Aragon, G., Kopelovich, L., Liang, Y., Ohta, S., Israel, M. A., Bickers, D. R., Aszterbaum, M., and Epstein, E. H., Jr. (2003). Evidence for lack of enhanced hedgehog target gene expression in common extracutaneous tumors. Cancer Res. *63*, 923-928.

Huangfu, D., Liu, A., Rakeman, A. S., Murcia, N. S., Niswander, L., and Anderson, K. V. (2003). Hedgehog signalling in the mouse requires intraflagellar transport proteins. Nature *426*, 83-87.

Huntzicker, E., Estay, I., Zhen, H., Lokteva, L., Jackson, P and, Oro, A. (2006) Dual degradation signals control Gli protein stability and tumor formation. Genes Dev. *20*, 276-81.

Hutchin, M. E., Kariapper, M. S., Grachtchouk, M., Wang, A., Wei, L., Cummings, D., Liu, J., Michael, L. E., Glick, A., and Dlugosz, A. A. (2005). Sustained Hedgehog signaling is required for basal cell carcinoma proliferation and survival: conditional skin tumorigenesis recapitulates the hair growth cycle. Genes Dev *19*, 214-223.

Incardona, J. P., and Eaton, S. (2000). Cholesterol in signal transduction. Curr Opin Cell Biol *12*, 193-203.

Ingham, P. W., and McMahon, A. P. (2001). Hedgehog signaling in animal development: paradigms and principles. Genes Dev *15*, 3059-3087.

Ingalls, T (1984). Derivatisation of carboxylic acids by reaction with 4'-bromophenacyl trifluoromethanesulfonate prior to determination by high-performance liquid chromatography. Journal of Chromatography *299*, 365-376.

Jenkins, D. (2009). Hedgehog signalling: emerging evidence for non-canonical pathways. Cell Signal. *21*, 1023-1034.

Jimenez, C., Portela, R. A., Mellado, M., Rodriguez-Frade, J. M., Collard, J., Serrano, A., Martinez, A. C., Avila, J., and Carrera, A. C. (2000). Role of the PI3K regulatory subunit in the control of actin organization and cell migration. J Cell Biol. *151*, 249-262.

Jin, Z., El-Deiry, W. S. (2005). Overview of cell death signaling pathways. Cancer Biology & Therapy *4*, 139-163.

Johnson et al. (1996). Human homolog of patched, a candidate gene for the basal cell nevus syndrome. Science *272*, 1668-1671.

Julien, S., Puig, I., Caretti, E., Bonaventure, J., Nelles, L., van Roy, F., Dargemont, C., de Herreros, A. G., Bellacosa, A., and Larue, L. (2007). Activation of NF-kappaB by AKT upregulates Snail expression and induces epithelium mesenchyme transition. Oncogene 26, 7445-7456.

Kalli, K. R., Bradley, S. V., Fuchshuber, S., and Conover, C. A. (2004). Estrogen receptor-positive human epithelial ovarian carcinoma cells respond to the antitumor drug suramin with increased proliferation: possible insight into ER and epidermal growth factor signaling interactions in ovarian cancer. Gynecol Oncol. 94, 705-712.

Kameda et al. (2001). Acceleration of the formation of cultured epithelium using the sonic hedgehog expressing feeder cells. Tissue Eng. 5, 545-55.

Karhadkar, S.S., Bova, G.S., Abdallah, N., Dhara, S., Gardner, D., Maitra, A., Isaacs, J. T., Berman, D. M., Beachy, P. A. (2004). Hedgehog signalling in prostate regeneration, neoplasia and metastasis. Nature 431, 707-12.

Kasper, M., Schnidar, H., Neill, G. W., Hanneder, M., Klingler, S., Blaas, L., Schmid, C., Hauser-Kronberger, C., Regl, G., Philpott, M. P., and Aberger, F. (2006). Selective modulation of Hedgehog/GLI target gene expression by epidermal growth factor signaling in human keratinocytes. Mol Cell Biol. 26, 6283-6298.

Kiguchi, K., Beltrán, L., Rupp, T and DiGiovanni, J. (1998) Altered expression of epidermal growth factor receptor ligands in tumor promoter-treated mouse epidermis and in primary mouse skin tumors induced by an initiation-promotion protocol. Mol Carcinog. 22, 73-83.

Kim, K. H., Park, E. J., Seo, Y. J., Cho, H. S., Kim, C. W., Kim, K. J., and Park, H. R. (2006). Immunohistochemical study of cyclooxygenase-2 and p53 expression in skin tumors. J Dermatol. 33, 319-325.

King, R. J. B., and Robins, M. W. (2006). Cancer Biology: Pearson Prentice Hall).

Klijanienko, J., Caillaud, J. M., Micheau, C., Flamant, F., Schwaab, G., Avril, M. F., and Ponzio-Prion, A. (1988). [Basal-cell nevomatosis associated with multifocal fetal rhabdomyoma. A case]. Presse Med. 17, 2247-2250.

Kruger, K., Blume-Peytavi, U and Orfanos, C. (1999). Basal cell carcinoma possibly originates from the outer root sheath and/or the bulge region of the vellus hair follicle. Arch Dermatol Res. 291, 253-9.

Lacina, L., Smetana, K., Jr., Dvorankova, B., Pytlik, R., Kideryova, L., Kucerova, L., Plzakova, Z., Stork, J., Gabius, H. J., and Andre, S. (2007). Stromal fibroblasts from basal cell carcinoma affect phenotype of normal keratinocytes. Br J Dermatol. *156*, 819-829.

Lancour et al. (2002). Carcinogenesis of basal cell carcinomas: genetics and molecular mechanisms. Review Br J Dermatol. *146*, 17-9.

Laner-Plamberger, S., Kaser, A., Paulischta, M., Hauser-Kronberger, C., Eichberger, T., and Frischauf, A. M. (2009). Cooperation between GLI and JUN enhances transcription of JUN and selected GLI target genes. Oncogene *28*, 1639-1651.

Lavrijsen Lavrijsen AP, Tieben LM, Ponec M, van der Schroeff JG, Van Muijen GN. (1989). Expression of EGF receptor, involucrin, and cytokeratins in basal cell carcinomas and squamous cell carcinomas of the skin. Arch Dermatol Res. *281(2)*:83-8.

Larue, L., and Bellacosa, A. (2005). Epithelial-mesenchymal transition in development and cancer: role of phosphatidylinositol 3' kinase/AKT pathways. Oncogene *24*, 7443-7454.

LC Laboratories, PD98059 data sheet (2004). <http://www.lclabs.com/PRODFILE/L-P/P-4313.php4> (accessed 2004).

Lehman Lehman JM, Laag E, Michaud EJ, Yoder BK. (2009) An essential role for dermal primary cilia in hair follicle morphogenesis. J Invest Dermatol. *129*, 438-48.

Ling et al. (2001). PATCHED and p53 gene alterations in sporadic and hereditary basal cell cancer. Oncogene *53*, 7770-8.

Lipinski, R. J., Dengler, E., Kiehn, M., Peterson, R. E., and Bushman, W. (2007). Identification and characterization of several dietary alkaloids as weak inhibitors of hedgehog signaling. Toxicol Sci. *100*, 456-463.

Liu MS, Yang PY, Yeh TS. (2007). Sonic hedgehog signaling pathway in pancreatic cystic neoplasms and ductal adenocarcinoma. Pancreas *34*, 340-6.

Loyola University: Medical Education Network. (2004) www.meddean.luc.edu/.../melton/bccmor2.htm Histology-morpheaform basal cell carcinoma, Loyola University Medical Education network. (accessed 2004).

Lupi, O. (2007). Correlations between the Sonic Hedgehog pathway and basal cell carcinoma. Int J Dermatol. *46*, 1113-1117.

252

Maesawa, C., Tamura, G., Iwaya, T., Ogasawara, S., Ishida, K., Sato, N., Nishizuka, S., Suzuki, Y., Ikeda, K., Aoki, K., *et al.* (1998). Mutations in the human homologue of the Drosophila patched gene in esophageal squamous cell carcinoma. Genes Chromosomes Cancer *21*, 276-279.

Mancuso, M., Leonardi, S., Tanori, M., Pasquali, E., Pierdomenico, M., Rebessi, S., Di Majo, V., Covelli, V., Pazzaglia, S., Saran, A. (2006). Hair cycle-dependent basal cell carcinoma tumorigenesis in Ptc1neo67/+ mice exposed to radiation. Cancer Res. *66*, 6606-14.

Medicine, Medscape, Basal cell carcinoma, Robert S Bader. (2004). <http:emedicine.medscape.com/article/871111-overview> (accessed 2004).

Melanoma, A skin cancer Rreview, healthy skin reflectance model. (2004). <http://melanoma.blogsome.com/category/skin-structure/.> (accessed 2004).

Mill, P., Mo, R., Fu, H., Grachtchouk, M., Kim, P., Dlugosz, A and Hui, Chi-chung (2003). Sonic hedgehog-dependent activation of Gli2 is essential for embryonic hair follicle development. Genes & Development 282-294

Millar, S (2002). Molecular mechanisms regulating hair follicle development. J Invest Dermatol. *118*, 216-225.

Ming, J. E., Kaupas, M. E., Roessler, E., Brunner, H. G., Golabi, M., Tekin, M., Stratton, R. F., Sujansky, E., Bale, S. J., and Muenke, M. (2002). Mutations in patched-1, the receptor for sonic hedgehog, are associated with holoprosencephaly. Hum Genet. *110*, 297-301.

Morton, J, Lewis, B. (2007). Cell Cycle. Shh signaling and pancreatic cancer: implications for therapy? Cell Cycle *6*, 1553-7.

Murcia, N., Sweeney, W Jr and Avner, E. (2000) New insights into the molecular pathophysiology of polycystic kidney disease. Kidney Int. *55*, 1187-97.

Murillas, R., Larcher, F., Conti, C. J., Santos, M., Ullrich, A., and Jorcano, J. L. (1995). Expression of a dominant negative mutant of epidermal growth factor receptor in the epidermis of transgenic mice elicits striking alterations in hair follicle development and skin structure. Embo J. *14*, 5216-5223.

Nanney LB, M. M., Stoscheck CM, King JLB   (1984). Comparison of epidermal growth factor binding and receptor distribution in normal human epidermis and epidermal appendages. J Invest Dermatol. *83*, 385-393.

253

Neill, G. W., Harrison, W. J., Ikram, M. S., Williams, T. D., Bianchi, L. S., Nadendla, S. K., Green, J. L., Ghali, L., Frischauf, A. M., O'Toole, E. A., et al. (2008). GLI1 repression of ERK activity correlates with colony formation and impaired migration in human epidermal keratinocytes. Carcinogenesis 29, 738-746.

Nievers, M. G., Schaapveld, R. Q., and Sonnenberg, A. (1999). Biology and function of hemidesmosomes. Matrix Biol. 18, 5-17.

Nilsson, M., Undèn, A., Krause, D., Malmqwist, U., Raza, K., Zaphiropoulos, P and Toftgård, R. (2000). Induction of basal cell carcinomas and trichoepitheliomas in mice overexpressing GLI-1. Proc Natl Acad Sci USA. 97, 3438-43.

Normanno, N., Bianco, C., Strizzi, L., Mancino, M., Maiello, M., De Luca, A., Caponigro, F and Salomon, D. (2005). The ErbB receptors and their ligands in cancer: an overview. Curr Drug Targets 6, 243-57.

Nusslein-Volhard, C., and Wieschaus, E. (1980). Mutations affecting segment number and polarity in Drosophila. Nature 287, 795-801.

Oh, S. Y., Kim, K. Y., Kim, Y. G., Kim, H. G. (2003). High-performance liquid chromatographic analysis of nitrendipine in human plasma using ultraviolet detection and single-step solid-phase sample preparation. J Pharm Biomed Anal. 32, 387-92.

Oro, A.E., and Higgins, K. (2003). Hair cycle regulation of Hedgehog signal reception. Dev Biol. 255, 238-248.

Oro, A.E., Higgins, K.M., Hu, Z., Bonifas, J.M., Epstein, E.H., Jr., and Scott, M.P. (1997). Basal cell carcinomas in mice overexpressing sonic hedgehog. Science 276, 817-821.

Owens and Watt. (2003). Contribution of stem cells and differentiated cells to epidermal tumours. Nat Rev Cancer. 6, 44-51.

Paladini, R.D., Saleh, J., Qian, C., Xu, G.X., and Rubin, L.L. (2005). Modulation of hair growth with small molecule agonists of the hedgehog signaling pathway. J Invest Dermatol. 125, 638-646.

Palma, V., Lim, D.A., Dahmane, N., Sanchez, P., Brionne, T.C., Herzberg, C.D., Gitton, Y., Carleton, A., Alvarez-Buylla, A., and Ruiz i Altaba, A. (2005). Sonic hedgehog controls stem cell behavior in the postnatal and adult brain. Development 132, 335-344.

Parisi, M and Lin, H. (1998). The role of the hedgehog/patched signaling pathway in epithelial stem cell proliferation: from fly to human. Cell Res. *8*, 15-21.

Pasternak (1999). An Introduction to Human Molecular Genetics: Fitzgerald Science Press.

Pathology of basal cell carcinoma. (2004) <emedicine.medscape.com/article/ 871111-overview> (accessed 2004).

Pearse, R., Collier, L., Scott, M and Tabin, C. (1999). Vertebrate homologs of Drosophila suppressor of fused interact with the gli family of transcriptional regulators. Dev Biol. *212*, 323.

Pedersen, L., Veland, I., Schrøder, J and Christensen, S. (2008). Assembly of primary cilia. Dev Dyn. *237*, 1993-2006.

Pepinsky, R. B., Zeng, C., Wen, D., Rayhorn, P., Baker, D. P., Williams, K. P., Bixler, S. A., Ambrose, C. M., Garber, E. A., Miatkowski, K., et al. (1998). Identification of a palmitic acid-modified form of human Sonic hedgehog. J Biol Chem. *273*, 14037-14045.

Ping, X. L., Ratner, D., Zhang, H., Wu, X. L., Zhang, M. J., Chen, F. F., Silvers, D. N., Peacocke, M., and Tsou, H. C. (2001). PTCH mutations in squamous cell carcinoma of the skin. J Invest Dermatol. *116*, 614-616.

Porter, J. A., Ekker, S. C., Park, W. J., von Kessler, D. P., Young, K. E., Chen, C. H., Ma, Y., Woods, A. S., Cotter, R. J., Koonin, E. V., and Beachy, P. A. (1996). Hedgehog patterning activity: role of a lipophilic modification mediated by the carboxy-terminal autoprocessing domain. Cell *86*, 21-34.

Porter, R. M., Gandhi, M., Wilson, N. J., Wood, P., McLean, W. H., and Lane, E. B. (2004). Functional analysis of keratin components in the mouse hair follicle inner root sheath. Br J Dermatol. *150*, 195-204.

Quirk, C., Gebauer, K., Owens, M., and Stampone, P. (2006). Two-year interim results from a 5-year study evaluating clinical recurrence of superficial basal cell carcinoma after treatment with imiquimod 5% cream daily for 6 weeks. Australas J Dermatol. *47*, 258-265.

Ramsey, ML., Sewell LD. (2010). Basal cell carcinoma. In: James WD, Elston D. (Chief Eds.); eMedicine Dermatology. St. Petersburg, FL: eMedicine Corporation,.

Rang, H.P., Dale, M.M, Ritter, J.M, Moore, P.K. (2003) Pharmacology (5th Ed.)

Reifenberger, J., Wolter, M., Weber, R., Megahed, M., Ruzicka, T., Lichter, P and Reifenberger, G. (1998) Missense mutations in SMOH in sporadic basal cell carcinomas of the skin and primitive neuroectodermal tumors of the central nervous system. Cancer Res. *58*, 1798-803.

Reifenberger, J., Wolter, M., Knobbe, C., Köhler, B., Schönicke, A., Scharwächter, C., Kumar, K., Blaschke, B., Ruzicka, T and Reifenberger, G. (2005). Somatic mutations in the PTCH, SMOH, SUFUH and TP53 genes in sporadic basal cell carcinomas. Br J Dermatol. *152*, 43-51.

Reis-Filho, J., Torio, B., Albergaria, A and Schmitt, F. (2002) p63 expression in normal skin and usual cutaneous carcinomas. J Cutan Pathol. *29*, 517-23.

Rittie, L., Kansra, S., Stoll, S. W., Li, Y., Gudjonsson, J. E., Shao, Y., Michael, L. E., Fisher, G. J., Johnson, T. M., and Elder, J. T. (2007). Differential ErbB1 signaling in squamous cell versus basal cell carcinoma of the skin. Am J Pathol. *170*, 2089-2099.

Robarge, K. D., Brunton, S. A., Castanedo, G. M., Cui, Y., Dina, M. S., Goldsmith, R., Gould, S. E., Guichert, O., Gunzner, J. L., Halladay, J., *et al.* (2009). GDC-0449-a potent inhibitor of the hedgehog pathway. Bioorg Med Chem Lett. *19*, 5576-5581.

Roberts, M.S., and Walker, M. S. (1993). Transdermal drug delivery: Penetration enhancement techniques. In Walters, K. A. and Hadgraft, J. Eds, Pharmaceutical skin penetration enhancement. Marcel Decker, New York, pp1-30.

Satir, P., and Christensen, S. T. (2007). Overview of structure and function of mammalian cilia. Annu Rev Physiol. *69*, 377-400.

Sato, N., Leopold, P. L., and Crystal, R. G. (1999). Induction of the hair growth phase in postnatal mice by localized transient expression of sonic hedgehog. J Clin Invest. *104*, 855-864.

Scales, S and Sauvage, F. (2009) Mechanisms of Hedgehog pathway activation in cancer and implications for therapy. Trends Pharmacol Sci. *30*, 303-12.

Schmidt-Ulrich, R and Paus, R (2005). Molecular Principles of Hair Follicle Induction and Morphogenesis. BioEssays, 27, 247-261.

Schmook, F. P., Meingassner, J. G., Billich, A. (2001). Comparison of human skin or epidermis models with human and animal skin in in-vitro percutaneous absorption. International Journal of Pharmaceutics. *215*, 51-56.

Schnidar, H., Eberl, M., Klingler, S., Mangelberger, D., Kasper, M., Hauser-Kronberger, C., Regl, G., Kroismayr, R., Moriggl, R., Sibilia, M., and Aberger, F. (2009). Epidermal growth factor receptor signaling synergizes with Hedgehog/GLI in oncogenic transformation via activation of the MEK/ERK/JUN pathway. Cancer Res. *69*, 1284-1292.

Scita, G., Tenca, P., Frittoli, E., Tocchetti, A., Innocenti, M., Giardina, G., and Di Fiore, P. P. (2000). Signaling from Ras to Rac and beyond: not just a matter of GEFs. Embo J. *19*, 2393-2398.

Sekkat, N., Kalia, Y. N., and Guy, R. H. (2002). Biophysical study of porcine ear skin in vitro and its comparison to human skin in vivo. J Pharm Sci. *91*, 2376-2381.

Shaw, A., Gipp, J and Bushman, W. (2009) The Sonic Hedgehog pathway stimulates prostate tumor growth by paracrine signaling and recapitulates embryonic gene expression in tumor myofibroblasts. Oncogene. *28*, 4480-90.

Sheng et al. (2002). Dissecting the oncogenic potential of Gli2: deletion of an NH(2)-terminal fragment alters skin tumor phenotype. Cancer Res. *18*, 5308-16.

Silva-Vargas, V., Lo Celso, C., Giangreco, A., Ofstad, T., Prowse, D. M., Braun, K. M., and Watt, F. M. (2005). Beta-catenin and Hedgehog signal strength can specify number and location of hair follicles in adult epidermis without recruitment of bulge stem cells. Dev Cell. *9*, 121-131.

Singla, V., and Reiter, J. F. (2006). The primary cilium as the cell's antenna: signaling at a sensory organelle. Science *313*, 629-633.

Skin Cancer Guide, Prevention of skin cancer (2004) <www.skincancerguide.com/images/content/reddish_02.jpg&imgrefurl> (accessed 2004).

Smyth, I., Narang, M. A., Evans, T., Heimann, C., Nakamura, Y., Chenevix-Trench, G., Pietsch, T., Wicking, C., and Wainwright, B. J. (1999). Isolation and characterization of human patched 2 (PTCH2), a putative tumour suppressor gene inbasal cell carcinoma and medulloblastoma on chromosome 1p32. Hum Mol Genet. *8*, 291-297.

Soehnge, H., Ouhtit, A and Ananthaswamy, O. (1997) Mechanisms of induction of skin cancer by UV radiation. Front Biosci. *2*, 538-51.

St-Jacques, B., Dassule, H. R., Karavanova, I., Botchkarev, V. A., Li, J., Danielian, P. S., McMahon, J. A., Lewis, P. M., Paus, R., and McMahon, A. P. (1998). Sonic hedgehog signaling is essential for hair development. Curr Biol. *8*, 1058-1068.

257

Stone, D., Murone, M., Luoh, S., Ye, W., Armanini, M., Gurney, A., Phillips, H., Brush, J., Goddard, A., de Sauvage. F and Rosenthal, A. (1999) Characterization of the human suppressor of fused, a negative regulator of the zinc-finger transcription factor Gli. J Cell Sci. *112*, 4437-48.

Strugnell, G., Wang, A., and Wheatley, D. (1996). Primary cilium expression in cells from normal and aberrant human skin. J Submicrosc Cytol Pathol. *28*, 215-225.

Svärd J, Heby-Henricson K, Persson-Lek M, Rozell B, Lauth M, Bergström A, Ericson J, Toftgård R, Teglund S. (2006) Genetic elimination of Suppressor of fused reveals an essential repressor function in the mammalian Hedgehog signaling pathway. Dev Cell. *10*, 187-97.

Taipale, J., Chen, J. K., Cooper, M. K., Wang, B., Mann, R. K., Milenkovic, L., Scott, M. P., and Beachy, P. A. (2000). Effects of oncogenic mutations in Smoothened and Patched can be reversed by cyclopamine. Nature *406*, 1005-1009.

Teglund, S., and Toftgard, R. (2010). Hedgehog beyond medulloblastoma and basal cell carcinoma. Biochim Biophys Acta *1805*, 181-208.

Teh, M., Blaydon, D., Chaplin, T., Foot, N., Skoulakis, S., Raghavan, M., Harwood, C., Proby, C., Philpott, M., Young, B and Kelsell, D. (2005) Genomewide single nucleotide polymorphism microarray mapping in basal cell carcinomas unveils uniparental disomy as a key somatic event. Cancer Res. *65*, 8597-603.

Thayer, S., di Magliano, M., Heiser, P., Nielsen, C., Roberts, D., Lauwers, G., Qi, Y., Gysin, S., Fernández-del Castillo, C., Yajnik, V., Antoniu, B., McMahon, M., Warshaw, A and Hebrok, M. (2003) Hedgehog is an early and late mediator of pancreatic cancer tumorigenesis. Nature. *425*, 851-6.

Thomas, C. P., Davison, Z., and Heard, C. M. (2007). Probing the skin permeation of fish oil/EPA and ketoprofen-3. Effects on epidermal COX-2 and LOX. Prostaglandins Leukot Essent Fatty Acids. *76*, 357-362.

Thomas, C. P., and Heard, C. M. (2005). In vitro transcutaneous delivery of ketoprofen and essential polyunsaturated fatty acids from a fish oil vehicle incorporating 1,8-cineole. Drug Deliv. *12*, 7-14.

Tian, H., Callahan, C., DuPree, K., Darbonne, W., Ahn, C., Scales, S and de Sauvage, F. (2009) Hedgehog signaling is restricted to the stromal compartment during pancreatic carcinogenesis. Proc Natl Acad Sci USA. *106*, 4254-9.

258

Toftgard, S and Tegund, R. (2010) Hedgehog beyond medulloblastoma and basal cell carcinoma. Biochim Biophys Acta. *1805*, 181-208.

Treat Skin Cancer. Basal Cell Carcinoma treatment options. Galderma, Australia. (2004) <www.treatskincancer.com/Basal_Cell_Carcinoma.> (accessed 2004).

Tumbar, T., Guasch, G., Greco, V., Blanpain, C., Lowry, W., Rendl, M and Fuchs, E. (2004) Defining the epithelial stem cell niche in skin. Science *303*, 359-63.

Unden, A. B., Zaphiropoulos, P. G., Bruce, K., Toftgard, R., and Stahle-Backdahl, M. (1997). Human patched (PTCH) mRNA is overexpressed consistently in tumor cells of both familial and sporadic basal cell carcinoma. Cancer Res. *57*, 2336-2340.

Unden, A., Gailani, M., Ståhle-Bäckdahl, M., Leffell, D., Glynn, M., Zaphiropoulos, P., Pressman, C., Dean, M., Brash, D., Bale, A and Toftgård, R. (1996) The role of the human homologue of Drosophila patched in sporadic basal cell carcinomas. Nat Genet. *14*, 78-81.

University of Virginia, Cell Biology Handouts, Skin. (2004) <http://www.med-ed.virginia.edu/public/CourseSitesDocs/HistologyCellBiologyThread/handouts/un restricted/original/MMHndt_Skin.html.> (accessed 2004).

Vidal, D., and Alomar, A. (2004). Efficacy of imiquimod 5% cream for basal cell carcinoma in transplant patients. Clin Exp Dermatol. *29*, 237-239.

Vlahos, C. J., Matter, W. F., Hui, K. Y., and Brown, R. F. (1994). A specific inhibitor of phosphatidylinositol 3-kinase, 2-(4-morpholinyl)-8-phenyl-4H-1-benzopyran-4-one (LY294002). J Biol Chem. *269*, 5241-5248.

Vorechovsky, I., Tingby, O., Hartman, M., Stromberg, B., Nister, M., Collins, V. P., and Toftgard, R. (1997). Somatic mutations in the human homologue of Drosophila patched in primitive neuroectodermal tumours. Oncogene *15*, 361-366.

Vortkamp, Gessler, M and Grzeschik, K. (1991) GLI3 zinc-finger gene interrupted by translocations in Greig syndrome families. Nature *352(6335)*, 539-40.

Walter, K., Omura, N., Hong, S-M., Griffith, M., Vincent, A., Borges, M and Goggins, M. (2010). Overexpression of Smoothened Activates the Sonic Hedgehog Signaling Pathway in Pancreatic Cancer-Associated Fibroblasts. Clinical Cancer Research. *16*, 1781

Wang, L., Liu, Z-Y., Gambardella, L., Delacour, A., Shapiro, R., Yang, I., Sizing, I., Rayhorn, P., Garger, E., Benjamin, C., Williams, K., Taylor, F., Barrandon, Y., Ling, L and Burkly, L. (2000) Conditional disruption of hedgehog signaling pathway defines its critical role in hair development and regeneration. Journal of Investigative Dermatology *114*, 901-908.

Watkins, D. N., Berman, D. M., Burkholder, S. G., Wang, B., Beachy, P. A., Baylin, S. B. (2003). Hedgehog signalling within airway epithelial progenitors and in small-cell lung cancer. Nature *20*, 313-7.

Wennstrom, S., Hawkins, P., Cooke, F., Hara, K., Yonezawa, K., Kasuga, M., Jackson, T., Claesson-Welsh, L., and Stephens, L. (1994). Activation of phosphoinositide 3-kinase is required for PDGF-stimulated membrane ruffling. Curr Biol. *4*, 385-393.

Wester, R.C., Maibach, H.I., (1995) In Smith, E. W., Maibach, H. I eds Percutaneous Penetration Enhancers, RC Press, Boca Raton, pp 21-28.

Wicking, C., Shanley, S., Smyth, I., Gillies, S., Negus, K., Graham, S., Suthers, G., Haites, N., Edwards, M., Wainwright, B., and Chenevix-Trench, G. (1997). Most germ-line mutations in the nevoid basal cell carcinoma syndrome lead to a premature termination of the patched protein, and no genotype-phenotype correlations are evident. Am J Hum Genet. *60*, 21-26.

Williams, A. C. (2003). Transdermal and Topical Drug delivery: Pharmaceutical Press, London.

Wilson, C. W., Chen, M. H., and Chuang, P. T. (2009). Smoothened adopts multiple active and inactive conformations capable of trafficking to the primary cilium. PLoS One *4*, e5182.

Wlodarski, P. K., Boszczyk, A., Grajkowska, W., Roszkowski, M., and Jozwiak, J. (2008). Implication of active ERK in the classic type of human medulloblastoma. Folia Neuropathol. *46*, 117-122.

Woolfson, A.D. (1990). The metabolism of amethocaine by porcine and human skin extracts: influence on percutaneous anaesthesia. International Journal of Pharmaceutics *62*, 9-14.

Wong, S.Y., Seol, A.D., So, P.L., Ermilov, A.N., Bichakjian, C.K., Epstein, E.H., Jr., Dlugosz, A.A., and Reiter, J.F. (2009). Primary cilia can both mediate and suppress Hedgehog pathway-dependent tumorigenesis. Nat Med. *15*, 1055-1061.

Xie, J., Johnson, R.L., Zhang, X., Bare, J.W., Waldman, F.M., Cogen, P.H., Menon, A.G., Warren, R.S., Chen, L.C., Scott, M.P., and Epstein, E.H., Jr. (1997). Mutations of the PATCHED gene in several types of sporadic extracutaneous tumors. Cancer Res. *57*, 2369-2372.

Xie, J., Murone, M., Luoh, S.M., Ryan, A., Gu, Q., Zhang, C., Bonifas, J.M., Lam, C.W., Hynes, M., Goddard, A., *et al.* (1998). Activating smoothened mutations in sporadic basal-cell carcinoma. Nature *391*, 90-92.

Yauch, R.L., Gould, S.E., Scales, S.J., Tang, T., Tian, H., Ahn, C.P., Marshall, D., Fu, L., Januario, T., Kallop, D., *et al.* (2008). A paracrine requirement for hedgehog signalling in cancer. Nature *455*, 406-10.

Young, L., Stevens and Heath (2006). Functional Histology: Churchill Livingstone.

Youssef, K. K., Van Keymeulen, A., Lapouge, G., Beck, B., Michaux, C., Achouri, Y., Sotiropoulou, P and Blanpain, C. (2010). Identification of the cell lineage at the origin of basal cell carcinoma. Nat Cell Biol. *12*, 299-305.

Yu, M., Zloty, D., Cowan, B., Shapiro, J., Haegert, A., Bell, R. H., Warshawski, L., Carr, N., and McElwee, K. J. (2008). Superficial, nodular, and morpheiform basal-cell carcinomas exhibit distinct gene expression profiles. J Invest Dermatol. *128*, 1797-1805.

Zeng, X., Goetz, J. A., Suber, L. M., Scott, W. J., Jr., Schreiner, C. M., and Robbins, D. J. (2001). A freely diffusible form of Sonic hedgehog mediates long-range signalling. Nature *411*, 716-720.

Zenz, R., Scheuch, H., Martin, P., Frank, C., Eferl, R., Kenner, L., Sibilia, M and Wagner, E. (2003) c-Jun regulates eyelid closure and skin tumor development through EGFR signaling. Dev Cell. *4*, 879-89.

Zhang, Y and Kalderon, D. (2001). Hedgehog acts as a somatic stem cell factor in the Drosophila ovary. Nature. *410*, 599-604.

Zhang, J., Lipinski, R., Shaw, A., Gipp, J and Bushman, W. (2007) Lack of demonstrable autocrine hedgehog signaling in human prostate cancer cell lines. J Urol. *177*, 1179-85.

Zhou, F. Q., Zhou, J., Dedhar, S., Wu, Y. H., and Snider, W. D. (2004). NGF-induced axon growth is mediated by localized inactivation of GSK-3beta and functions of the microtubule plus end binding protein APC. Neuron *42*, 897-912.

Zhu, D., Shi, S., Wang, H., and Liao, K. (2009). Growth arrest induces primary-cilium formation and sensitizes IGF-1-receptor signaling during differentiation induction of 3T3-L1 preadipocytes. J Cell Sci. *122*, 2760-2768.